HUNGARIAN UNIVERSITY OF AGRICULTURE AND LIFE SCIENCE

Performance and power quality evaluation of grid-connected solar photovoltaic systems

PhD Dissertation

by

Divine Kafui Atsu

Gödöllő
2021

Doctoral school

Denomination: Doctoral School of Mechanical Engineering

Science: Mechanical Engineering

Leader: Prof. Dr. István Farkas, DSc
Institute of Technology
Hungarian University of Agriculture and Life Science, Gödöllő, Hungary

Supervisor: Prof. Dr. István Farkas, DSc
Institute of Technology
Hungarian University of Agriculture and Life Science, Gödöllő, Hungary

Co-Supervisor: Dr. István Seres, PhD
Institute of Mathematics and Basic Science
Hungarian University of Agriculture and Life Science, Gödöllő, Hungary

…… ……

Affirmation of supervisor Affirmation of head of school

CONTENTS

NOMENCLATURE AND ABBREVIATION

AC	Alternating current
AGC	Automatic Generation Control
a-Si	amorphous silicon
Av	Average
AVR	Automatic Voltage Regulator
BOS	Balance of system
CAES	Compressed Air Energy Storage
CEE	Central Eastern European
CIHD	Current individual harmonic distortion
CMV	Common mode voltage
CTHD	Current total harmonic distortion
CWS	China microinverter with Solarex module
DC	Direct current
DG	Distributed generation
DHPF	Decoupled harmonic power flow
DN	Distribution network
DS	Distribution system
DSI	Demand side integration
EMC	Electromagnetic compatibility
EMI	Electromagnetic interference
ES	Energy Storage
EV	Electric vehicle
EVA	Ethyl vinyl acetate
FACTS	Flexible alternating current transmission system
FiT	Feed-in tariff
GCPV	Grid-connected photovoltaic
G-G	Glass to glass
GHI	Global Horizontal Irradiation
G-T	Glass to Tedlar
GUNT	Geräte Unterricht Naturwissenschaft Technik
HC	Hosting capacity
HCAC	Hill climbing algorithm controls
HEA	Hungarian Energy and Public Utility Regulatory Authority
HERIC	Highly efficient and reliable inverter concept
HV	High voltage
HWJ	Holland microinverter with Juta module
IEC	International Electrotechnical Commission
IEEE	Institute of Electrical and Electronics Engineers
IGBT	Insulated gate bipolar transistors

IHD	Individual harmonic distortion
Impp	Maximum power point current
InCon	Incremental conductance
Isc	Short circuit current
KÁT	Kötelező átvételi tarifa (Energy control programme)
LTC	Load tap changer
LV	Low voltage
LVUF	Line voltage unbalance factor
MAVIR	Magyar Villamosenergia-ipari Átviteli Rendszerirányító
Max	Maximum
mc-Si	Monocrystalline silicon
METÁR	Hungarian Renewable Energy Support System Scheme
MFB	Hungarian Development Bank
Min	Minimum
MOSFET	Metal–oxide–semiconductor field-effect transistor
MPP	Maximum power point
MPPT	Maximum power point tracker
MV	Medium voltage
NiCr-Ni(K)	Nickel chromium-Nickel (type K)
NPC	Neutral point clamped
OLTC	On-load tap changer
P&O	Perturb and observe
PCC	Point of common coupling
PCOMP	Compensation power output
pc-Si	Polycrystalline silicon
PDC	DC power output
PF	Power factor
PF_{dist}	Distributed power factor
PF_{true}	True power factor
PHEV	Plug-in hybrid electric vehicle
PINV	Inverter power output
Plt	Long term voltage flickers
PoA	Plane of array
PQ	Power quality
PSO	Particle swarm optimisation
Pst	Short term voltage flickers
Pt	Platinum
pu	Point unit
PV	Photovoltaic
PVUF	Phase voltage unbalance factor
PWHD	Partial Weighted Harmonic Distortion

RG	Renewable generation
RMS	Root mean square
RTD	Resistance temperature detector
RVC	Rapid voltage change
SEE	South Eastern European
SG	Smart Grid
SMES	Superconducting Magnetic Energy Storage
STATCOM	Static Synchronous Compensation
STC	Standard test conditions
Stdev	Standard deviation
SVR	Step voltage regulators
THD	Total harmonic distortion
VDE	Verband der Elektrotechnik
VFD	Variable frequency drives
VIHD	Voltage individual harmonic distortion
Vmpp	Maximum power point voltage
Voc	Open circuit voltage
VSI	Voltage source inverter
VTHD	Voltage total harmonic distortion
VUF	Voltage unbalance factor
VUR	Voltage unbalance ratio

1. INTRODUCTION, OBJECTIVES

This chapter presents the background and the importance of the study as well as the objectives of the research.

1.2. Introduction

The energy received from the sun by the earth is clean, enormous and available in all parts of the world. This energy is more than enough to meet the world's energy demand if it is well exploited. The conversion of solar light into electrical energy is one option for the use of solar energy. With the life expectancy of the source of radiation amounting to another 4.5 billion years, the reservoir of solar radiation is virtually inexhaustible in the middle and long-term future (Aliman et al., 2007).

However, the global demand for primary energy continues to rise with the increasing population and economic growth. To meet the energy demand, various countries, regional and international organizations have prioritized the exploitation of distributed energy sources due to their role in solving the issues of environmental pollution caused by the use of fossil fuels and the future uncertainty of the conventional energy sources (Mancarella and Chicco, 2009). Consequently, solar PV has experienced unprecedented growth over the last decade, recording annual additions consistently above 100 GW for the past three years and the highest among all the renewable energy sources. The current installed capacity of solar PV stands at 627 GW (REN21, 2020). This growth in solar PV is focused exclusively on grid-connected PV systems (REN21, 2020).

However, the rising penetration rate of solar PV and other distributed generated systems onto the grid significantly impacts the electric grid because of the variability of these distributed generation (DG) energy sources and the bidirectional power flow effect they introduce into the power network. The challenges become more severe, especially in low voltage systems with low demand levels having high penetration levels of grid-tied systems. Determining the impact of the penetration of DG systems onto the grid is still unclear. This is because it depends on the existing grid infrastructure and the utility regulations that vary for each country (Obi and Bass, 2016). Utility providers have become skeptical in allowing the continuous connection of PV systems onto the grid. This has heightened the awareness of power quality, and consequently, new power quality regulations and standards are being imposed by different countries and sub-regions to regulate power fed into the grid from distributed sources to ensure the power grid's efficiency and stability.

To meet the growing global energy demands and make room for modernization, different types of PV system models and schemes at various scales are being applied by various governments and subregional organizations to cater for the requirements of various consumers. This has led to the introduction of advanced semiconductor power electronic products, both linear and nonlinear, as part of the grid-connected PV system's BOS to meet their goal. The cumulative effect of all these factors has aggravated the power output quality issues introduced into the grid. Significant harmonic distortions are currently introduced into the grid at the input stage of the modern electronic power converters (Darvishi et al., 2011).

This current research seeks to investigate the performance of microinverter systems under steady irradiation supply (solar PV simulator) and outdoor ambient conditions. The power quality characteristic measurements for different scenarios will be analyzed and the results compared with other studies on microinverters and their compliance with available standards for grid-connected PV systems. The harmonic current's dependence on the system harmonic voltage will also be investigated.

Similarly, the performance of various grid-connected string inverters will be studied under different working conditions. The power quality characteristic measurements for different scenarios will be analyzed and compared with other studies on large scale inverters and their compliance with available standards for grid-connected PV systems. The influence of varying PV technologies and setups on the different inverters' power quality output will also be investigated.

1.2. Objectives

The main aim of the research is to conduct a comprehensive investigation of the technical challenges and the impacts of integrating solar PV into the low voltage power distribution network. Emphasis will be laid on assessing the different systems' outputs by applying various inverters and working scenarios. Specific consideration will be given to the Hungarian grid operational conditions. The detailed research objectives are as follows:

- Determine the performance output of microinverters under constant indoor conditions and outdoor real operation condition.
- Investigate the performance output and compliance of microinverters under different outdoor working conditions and with varying solar PV technologies.
- Assess the performance output of different grid-connected string inverters under varying ambient conditions and determine their compliance with specified grid-connection standards in the Hungarian low voltage power network.
- Determine the correlation between the harmonic current and the system harmonic voltage for the different inverter systems.

2. LITERATURE REVIEW

In this chapter, the related studies on the subject are reviewed, laying bare the existing knowledge gaps in terms of the challenges encountered by previous researchers and their recommendations for removing these barriers. The intensions of this study in filling the knowledge gaps are also enumerated.

2.1. Grid-connected PV systems

Grid-connected or Grid-tied PV systems, also known as utility-interactive PV systems, are designed to operate with and interconnected to the electrical utility grid. In grid-connected systems, the inverter is the primary component. The inverter converts the PV array's DC power into AC power consistent with the utility grid's voltage and power quality requirements. The inverter also stops the PV system from supplying power when the utility is not energized or synchronized. This safety feature is required in all grid-connected PV systems. It ensures that the PV system will not continue to operate and feed power into the utility grid when the grid is down for service or maintenance (Green Rhino Energy, 2018).

PV generators have been classified into micro, small, medium and large scale generators. Microscale PV systems have a capacity ranging from 1 to 5kWp, small-scale solar PV generators range from 5 kWp to 5 MWp, medium scale 5 MWp–50 MWp and large scale >50 MWp. Commonly described scales at which solar PV is connected to the electric network are defined in Table 2.1 (Ackermann et al., 2001).

Table 2.1. Definition of scales of grid-connected solar PV

Identifier	**Connection point**
Small scale	230/400 V (or 240/415 V) Low Voltage Distribution Network
Utility scale	> 230/400 V (or 240/415 V) Distribution Network
Large scale	≥ 66 kV Transmission and sub-transmission Network

Grid-connected PV systems are getting very common in countries where policy support systems have been put in place, and the excessive PV power generated is injected into the grid. Fig. 2.1 shows the balance of system of a grid-connected PV system.

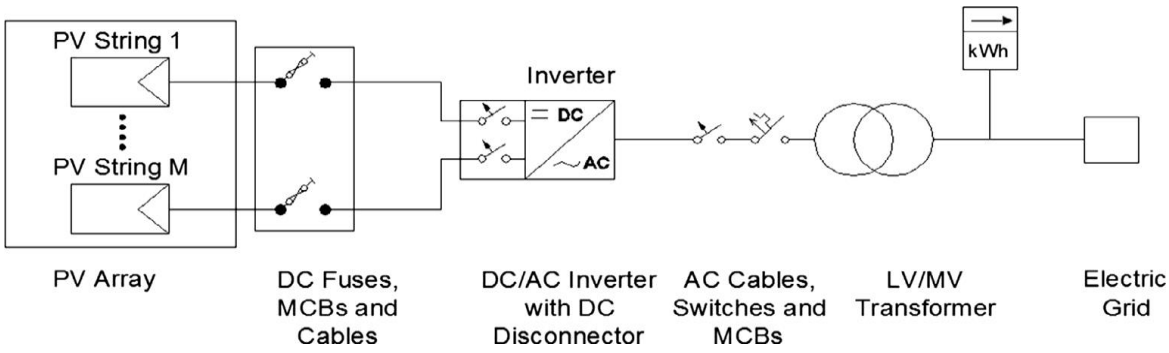

Fig. 2.1. Single-line diagram of an on-grid PV system (Senol et al., 2016)

Due to the varying nature of the solar resource, power output from PV plants may change from time to time. Any drop in power supply from the solar PV plant must be compensated for by increased generation from other available sources to meet consumers' power demand. This presents many challenges to power system planners and operators as sufficient reserves, with quick ramping up capabilities, should be available to make up for the sudden shortages in power. This calls for a deep understanding of the possible temporal variations in PV systems' output to manage distribution networks integrated with solar PV power plants (Femin et al., 2016). Fig. 2.2 presents the definition of distributed generating units.

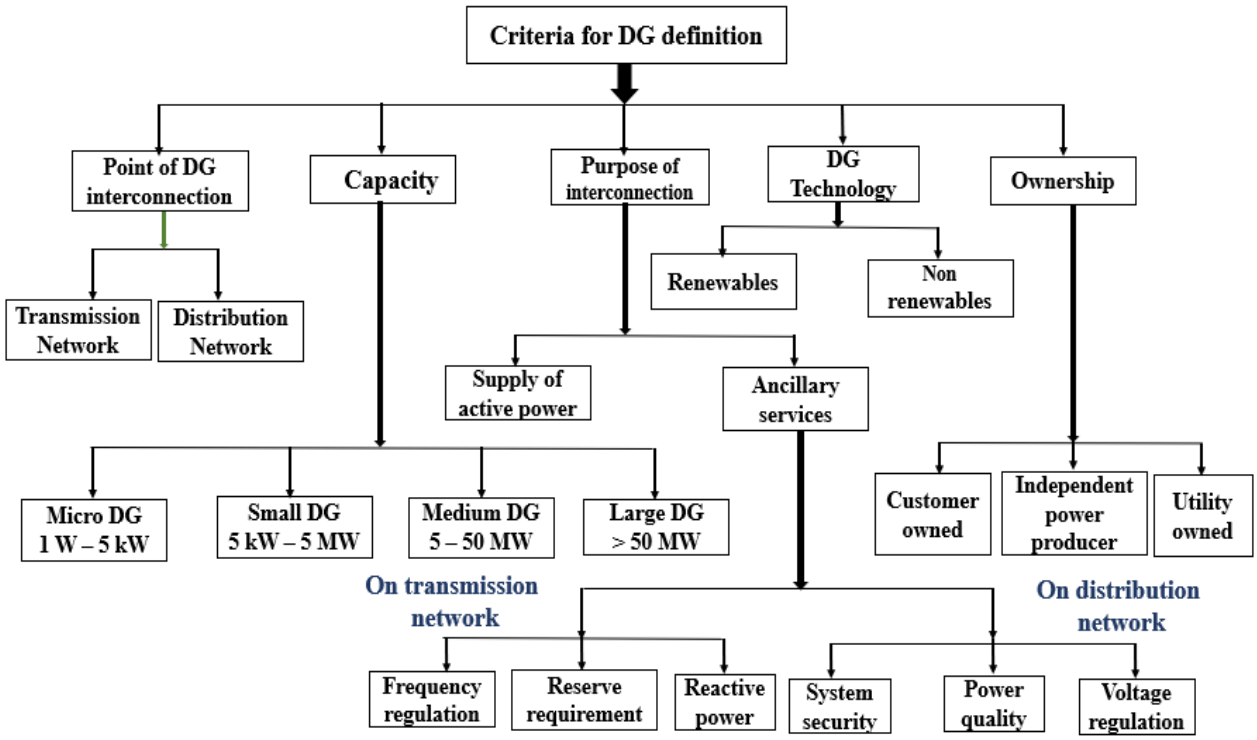

Fig. 2.2. Definition of distributed generation units (Ackermann et al., 2001)

2.2. Configuration of grid-connected PV systems

The efficiency and proper operation of photovoltaic systems are dependent on several factors. Prominent among them are environmental conditions and system design. These can significantly impact the whole system's efficiency and power quality (Aktas et al., 2013).

Different configurations of grid-connected PV systems can be classified into four categories. The centralized configuration, as shown in Fig. 2.3a, is made up of series and parallel connections of PV modules supplying power to a line commutated inverter. The centralized configuration represents an old configuration with problems such as high harmonic injection into the grid. Fig. 2.3b demonstrates the String configuration in which each string supplies the grid through a dedicated inverter. The next configuration called the Multi-string is illustrated in Fig. 2.3c. Each string is equipped with a DC-DC converter in this system, which performs the maximum power point tracking (MPPT) operation. The strings then share their power through a DC-link with an inverter that controls the DC link's voltage by transferring extra power to the grid. The last configuration is the AC-module shown in Fig. 2.3d, where a complex power electronic interface is used for each module (Mirhassani et al., 2015).

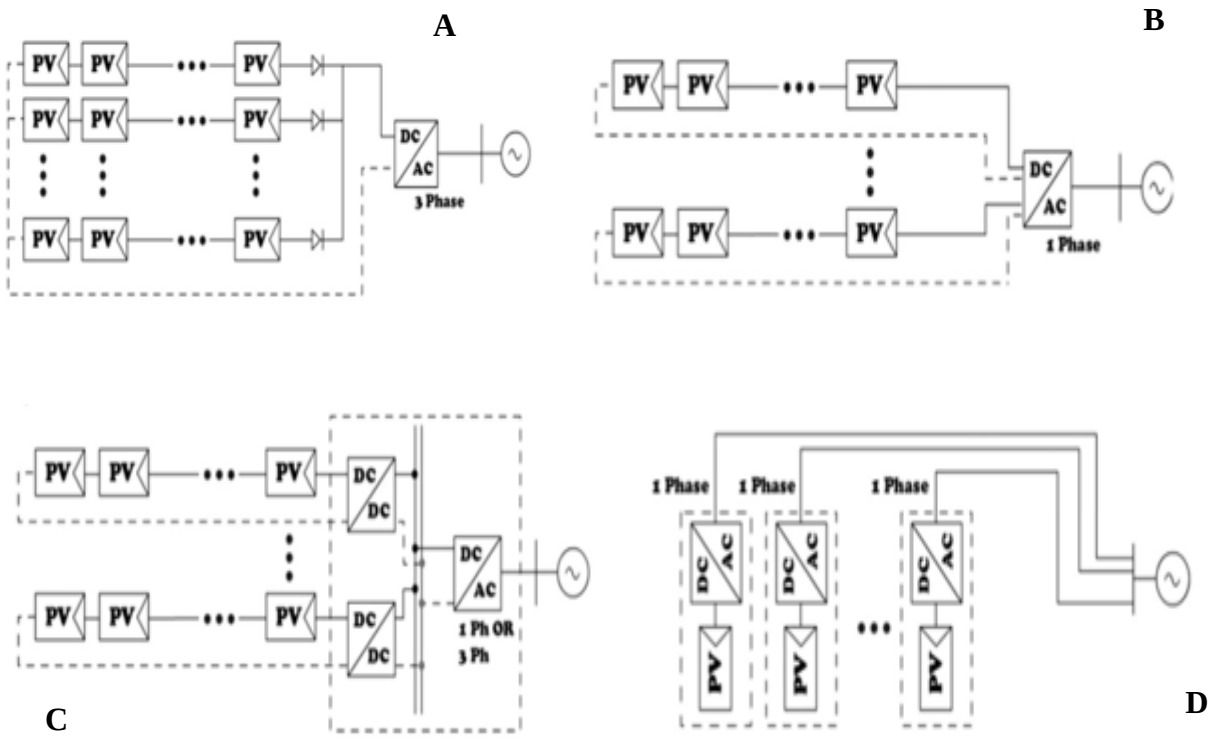

Fig. 2.3. Different configurations of grid-connected PV systems. (a) Centralized approach (b) String approach (c) Multi-string approach (d) AC- module approach

Comparing the four configurations of grid-connected PV (GCPV) in terms of efficiency, reliability, power mismatch possibility and expandability has shown that the centralized approach was the weakest strategy. However, for medium and utility-scale GCPV systems, the most efficient and reliable configuration was suggested to be the multi-string inverter (Mirhassani et al., 2015)

2.3. Smart grid

The development of a more intelligent electricity network called smart grid (SG) has complexities in balancing all the variables associated with dynamic load control powered from high penetration of non-dispatchable RG. Energy storage is the most crucial SG advanced component to provide reliable energy supplies whenever intermittent power sources reach high grid penetration levels. Energy storage offers significant contributions in overcoming the difficulty of random fluctuation created by RG balancing the difference and reduces the mismatch between supply and demand (Paatero and Lund, 2006).

Energy storage devices consist of electric vehicles (EV) (Linse and Kuhn, 2015), Plug-in hybrid electric vehicle (PHEV) (Fathabadi, 2018), pumped hydro storage (Kougias and Szabó, 2017), lead-acid batteries (Dathu and Hariharan, 2020), compressed air energy storage (CAES) (Dooner and Wang, 2020), flywheel, superconducting magnetic energy storage (SMES) (Olabi, 2017), and capacitors are expected to be widespread in RG integrated to distribution systems. Energy storage devices utilize a power conversion system to integrate into the distribution network; they can inject or absorb both active and reactive power to compensate for voltage variations in the short or medium term. Energy storage integration to the distribution systems

can be used to improve local power quality and reliability, voltage support, provide ancillary services and backup power, reduce losses, and help defer the upgrade of distribution systems (Martinez et al., 2011).

Approximately, 1 MWh storage per MW of wind power is enough to reduce at least 10% of the local voltage rise in weak networks. Energy storage can serve either as a load or generator. Energy storage devices with power electronic interfaces provide ancillary services to improve PQ and reliability and increase RGs integration into the DS (Juan A Martinez and Martin-arnedo, 2011), (Paatero and Lund, 2006) and (McGranaghan, 2009).
Benefits for distributed energy storage system are:

- Storage of off-peak PV/wind energy.
- Power smoothing for large solar arrays;
- Peak-load deduction (peak shaving) at substation;
- Distribution and transmission feeder reliability improvement;
- Customer feeder load management;
- Ancillary services (frequent regulation, black start capability)
  (Juan A Martinez and Martin-arnedo, 2011)

2.4. Grid-connected PV technology associated problems

The tying of distributed and intermittent sources of power onto the grid presents a lot of challenges. This section reviews works related to the negative impacts of integrating PV as distributed power generation source onto the transmission grid and the mitigation strategies proposed in the literature.

High penetration of solar PV into the grid distribution system introduces various challenges onto the DN such as voltage rise, reverse power flow, transformer, and cable rating, increase power losses, voltage unbalance, malfunctioning of onload tap changers (OLTC) and automatic voltage regulator (AVR) (Agüero et al., 2011). The negative impact of PV systems tends to affect the operation, control, and security of the traditional distribution feeders. The low voltage grid originally was not designed to integrate external power sources like PV systems which have impacted the behaviour of the distribution network.

The integration of distributed generators into the distribution network impacts both the steady-state and the transient or dynamic power systems' stabilities. The steady-state impacts on the distribution system include voltage fluctuation, reverse power flow, high electrical losses, transformer and cable rating issues, low power quality, poor power balancing, reactive power management, malfunction of the protection scheme, the operation of OLTC, reliability and regulation issues. The dynamic impacts include islanding effect and transient changes due to the variability of irradiation. The severity of the effects is dependent on the degree of DG penetration, at the point of connection of the DG in the distribution feeder and the technology of distributed generators (Turitsyn et al., 2010).

2.4.1. Effects on voltage

2.4.1.1. Voltage rise and fluctuation

Voltage rise in the grid system is caused by the high penetration of solar PV into the utility grid. This occurs when there is an increase in voltage at the inverter side relative to the utility voltage. Grid impedance and inverter output-circuit conductors cause the rise in voltage which is a negative voltage drop on the circuit between the inverter and the point of common coupling (Cobben et al., 2007).

Traditionally, low voltage distribution networks are defined radially and are for one-way power flow from a high voltage sub-station to low voltage customer loads. Voltage settings at the secondary side of the controllable transformer, before the load, are usually set at ± (5 –10) % greater than the customer end-use voltage to accommodate the distribution network line losses. The violation of this limit undermines the security of the network. To keep the voltage at the distribution level within the statutory limits, on-load tap changer transformers (OLTC) coupled with the automatic voltage regulator (AVR) are used to control the transformer output voltage to keep the voltage magnitude within limits (Tengku Hashim et al., 2012). The introduction of distributed generators (DG) distorts this order with sudden voltage rise and reverse power flow.

As an acceptable practice, voltage must be supplied at the consumer's terminals within certain limits specified by the utility provider. The condition of voltage rise and fluctuation gets worse with the increase in the penetration levels. The impact is significant and unbearable when large RGs are integrated close to lightly loaded feeders. The RG location, configuration of each feeder, and capacitor banks determine the magnitude of voltage rise (Katiraei and Agüero, 2011). Voltage fluctuation arises from changes in the load situation at a system node or point of common coupling regarding the system perturbation.

The source voltage and the voltage drop along the feeder determine the voltage at the end of a feeder. Voltage drop in the feeder is due to the impedance of the feeder conductor and current flow, load, and the transformer. To determine the voltage drop along a feeder line, the line diagram and its corresponding phasor diagram as depicted in Fig. 2.4 and Fig. 2.5 respectively were used (Viawan et al., 2007).

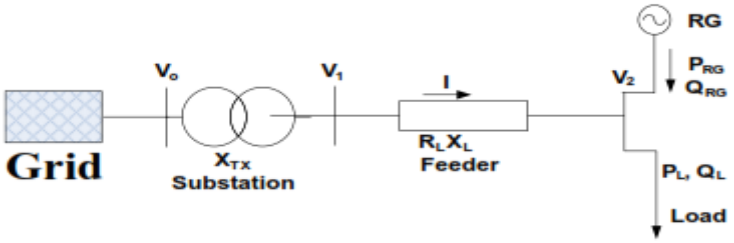

Fig. 2.4. Distribution system with load and RG (Viawan et al., 2007)

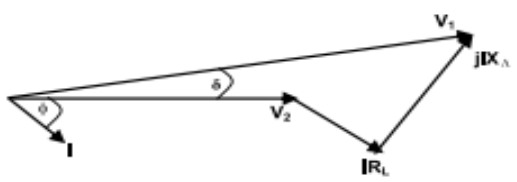

Fig. 2.5. Voltage drop in a distribution system (Viawan et al., 2007)

The current *I* is a function of the load; $S = P_L - jQ_L$ and the voltage $V_2 = \frac{S}{I}$

$$V_2 = \frac{S}{I} = \frac{P_L - jQ_L}{I}, \quad (2.1)$$

Assuming V_1 and V_2 represent the voltages in buses 1 and 2 respectively, and *I* is the line current. The voltage drop along the feeder line will be given by,

$$\Delta V = V_1 - V_2 = \frac{R_{LN}(P_L - P_G) + X_{LN}(Q_L - Q_G)}{V_2}. \quad (2.2)$$

2.4.1.2. Voltage control strategies

Several methods exist for the control of voltage and voltage fluctuations in DN. Some of them apply active management of transformers which helps maintain the voltage within the permissible limits, demand-side integration (DSI), electrical energy storage (ES), the interconnection of adjacent lines, and reinforcing the distribution system. Others include network management system, on-load tap changer, power curtailment and generator power. The commonly suggested strategies used for voltage control include OLTC transformer, shunt capacitor and reactor, Storage device approach, Reactive power control, Reactive power compensation (flexible alternating current transmission system (FACTS) devices; STATCOM, SVC and Active power curtailment approach (Petinrin and Shaabanb, 2016).

Storage of power from solar PV systems is seen as one of the approaches to regulating distribution feeders' voltage profile. Various storage devices like lead-acid batteries, lithium-ion batteries and electric double-layer capacitors can be used to control the voltage at the connection point. It can also regulate the power between the PV generation and the utility grid to improve power quality in the grid (X. Liu et al., 2012).

Reactive power support can also be employed to bring down the voltage rise at the PCC. This could be achieved by coordinating reactive power injection through individual PV based inverters or centralized control of the reactive power. This method can be used to increase the number of PV integration so that the individual PV inverters will absorb or inject reactive power into the network (Tengku Hashim et al., 2012). Reactive power compensation devices like STATCOM, SVC and shunt capacitor banks are used to provide voltage regulation in the distribution network (Degner et al., 2011). Curtailment of the PV active power is also a mitigation approach to prevent overvoltage on the feeder with high PV integration (Tengku Hashim et al., 2012).

The AVR relay ensures that the voltage at a local or remote location is controlled within the acceptable requirements. As the penetration of PV systems on the low voltage network increase, the AVR operation becomes complicated and ineffective due to the reverse power flow accompanied by high voltage and current on the network. The negative impact of PV systems on low voltage networks has led to the development of different voltage mitigation measures in recent years (Madzonga et al., 2009).

Vovos et al. (2007) compared the distributed and centralized techniques for controlling distributed network voltages regarding the distributed generator capacity. Consequent losses increased substantially in the centralized control approach and required additional cost to establish the control center and communication network. An algorithm for using tap changing transformer in distribution systems and inverters interfaced with distribution generators was developed by (Oshiro et al., 2011). Information on the voltage and power received from the network was used to determine the control centre's optimal reference value, which is transferred to transformers and inverters.

A control procedure for the shunt capacitor to mitigate voltage rise in the distribution network was developed by Kabemura et al., (2004). The average value of the voltage at the PCC was used to operate the shunt capacitor switching to avoid frequent operation loss. With this method, operation relied largely on only local information without considering the overall optimal voltage profile.

Ausavanop and Chaitusaney, (2011) propounded a method of coordination between the renewable generators and voltage regulator devices applying Tabu Search algorithm and probabilistic load flow computation based on Monte Carlo simulations to evaluate the intermittency from RGs and Loads. Investigations done using the proposed algorithm on IEEE 34-bus feeder revealed that voltage fluctuation could be maintained within the acceptable limit when the constraints are satisfied. Petinrin and Shaabanb, (2016) concluded that the mitigation of voltage imbalances resulting from voltage fluctuation and intermittency could be offered if the voltage and reactive power control equipment are operated based on smart grid technologies, especially at the demand side integration and energy storage. They further proposed that the combination of electrical energy storage and demand-side measures operating from the supply side (Energy Storage), the other from the demand side integration (DSI), will potentially allow generation plants, both traditional and renewable, to operate more cost-effectively. They recommended that the coordination of voltage control devices and RG for voltage profile improvement should be further investigated.

Shivashankar et al., (2016), in their studies, revealed that research focusing on grid-connected power quality issues created when PV output varies are limited and thus recommends more work should be done on voltage flicker, the voltage at grid side, reverse power flow and frequency deviation. And that, the effectiveness of the mitigation methods depends on the forecast of solar radiation from which PV output power is estimated. Demand response has a great potential to increase the distribution system voltage at nearly all the critical nodes. It postpones the need for network upgrades and reduces overall plant and capital cost investments (Venkatesan et al., 2012).

A Genetic Algorithm based-optimization approach was used to optimise customers' energy consumption to reduce voltage deviation and feeder losses. The proposed method's effectiveness was demonstrated from the case studies using time-sequence analysis, over a 24-h period on the IEEE 123 bus test feeder. Test results show that the proposed algorithm causes a reduction in peak load, energy losses and enhances system capability to maintain voltages within the permissible limits (Petinrin and Shaaban, 2014). It is also observed that the voltages at the point of common coupling (PCC) are usually unbalanced due to the unbalanced loads in

the system. To keep the system healthy, the limits around 5% for voltage rise and 2% for voltage unbalance are required. One popular method to solve the voltage rise problem is by injection of reactive power in a positive sequence. However, this is uneconomic because the PV owner may be charged for the injected reactive power (Liu et al., 2014)

2.4.2. Voltage stability and voltage unbalance

Voltage stability is the phenomenon where the voltages at the buses in the grid are maintained at a steady-state after they have been subjected to a disturbance from a given initial operating condition. Voltage stability depends on the ability to maintain or restore equilibrium between load demand and load supply of a power system. Voltage stability could be achieved when reactive power needs in a power network system are met (Chidi et al., 2012).

Grid-tied inverters are responsible for keeping the power factor of the output signal at unity. When the power factor is at unity, there is no reactive power exchange between the inverter and the grid. This becomes problematic when solar PV is connected to a weak grid, and the capacity is large. Voltage instability problems will occur since the PV system will draw reactive power (Kundur et al., 2004). Unequal line voltage magnitudes in a three-phase electric system are known as voltage unbalance (Von Jouanne and Banerjee, 2001). The use of single-phase distributed generators and unbalanced phase loads in the electric system are also other sources of voltage unbalance. In a PV-DG system, increased penetration of residential rooftop PV into the grid with random installation across the distribution system is another reason for increasing or decreasing the network voltage imbalance index (Shahnia et al., 2011).

Voltage unbalance has a negative impact on the distribution system causing overheating of equipment such as induction motors, power electronic converters and adjustable speed drives, in addition to causing power and energy losses in the distribution grid. Network problems such as the malfunction of relays and voltage regulators and the generation of non-characteristic harmonics from power electronic loads could also be introduced by voltage unbalance in the network (Meersman et al., 2011).

Voltage unbalance mitigation strategies proposed include reactive power compensation, distributed energy storage technology, and DG unit connection topologies to the system. An energy storage system using fuzzy control and Park's transformation to mitigate voltage unbalance in a highly intermittent PV interconnected distribution system (Wong et al., 2016).

2.4.3. Reactive power fluctuation

Reactive power fluctuation occurs because of the frequent operation of load tap changer (LTC) transformers, voltage-controlled capacitor banks and step voltage regulators (SVRs). The transmission line would need to supply reactive power when the capacitor bank is in the off mode. Since transmitting reactive power is more expensive than local supply, the large penetration level of RG has a significant economic impact on the DS (Petinrin and Shaabanb, 2016).

In power systems, shunt capacitor banks are usually employed for Power Factor correction and voltage support. However, it has been established that they may result in amplification of voltage and current harmonics caused by the non-linear loads due to electrical resonance.

Therefore, passive and active harmonic filters are preferred for harmonic mitigation and power factor correction under distorted voltage and current conditions (Singh and Singh, 2014).

2.4.4. Harmonic distortion

Acceptable quality of electricity supply to customers should show a perfect sinusoidal voltage waveform at all customer locations. The deviation of the voltage and current waveforms from sinusoidal is described as harmonic distortion. The harmonic component in an AC power system can be defined as the sinusoidal component of a periodic waveform with a frequency equal to an integer multiple of the system's fundamental frequency. Harmonics in voltage or current waveforms can then be conceived as perfectly sinusoidal components of frequencies multiple of the fundamental frequency (De La Rosa, 2006).

Harmonic distortion occurs as a result of nonlinear loads drawing non-sinusoidal current when they are even connected through a pure sine wave voltage source. Non-sinusoidal current contains harmonic current that interacts with the impedance of distribution lines and causes voltage harmonics. The connection of converter units also introduces additional total harmonic distortions (THD) at the point of common coupling and in other buses. In grid-connected PV systems, the occurrence of harmonic distortions is dependent on the power converter technology used. Power electronics switching devices also inject high-frequency components rather than the desired current (Huda and Živanović, 2017).

The point of connection of PV systems into a power distribution network influences the harmonic distortion level introduced into the DN. Relative to low voltage connection points, PV systems connected at high voltage points in the network produces less harmonic distortion. In cases where there is an impedance mismatch between the grid and the inverter of the DG units at the points of common coupling, harmonic resonance also occurs (Pandi et al., 2013).

The inverter interface between the Solar PV and the grid works by converting DC to AC through the inverter, which is a semiconductor switching circuit, but the AC waves obtained from these devices may not be perfect sinusoidal waves. As a result, harmonics are introduced into the power network. The total harmonic distortion permissible varies from country to country and regularly updated depending on the existing grid infrastructure and the hosting capacity. The specified values range from < 5% to < 8% and for inverter current up to the 50th harmonic (Jayasekara and Wolfs, 2010).

Effects of harmonic distortion

- Excesssive loading of consumers' electrical installation and power system elements by higher-order frequencies of currents and voltages.
- Overheating of neutral conductors as a result of higher current harmonics whose frequency is the multiplier of number.
- Increased 3rd harmonics in the neutral conductor can damage and even cause fire because the neutral conductor is not usually overload protected.
- Increased transformer heating and saturation effects in the core of the conductor.
- Higher harmonic occurrence in the power grid can cause interferences on telecommunication lines.

- Causes overloading and resonant condition on the capacitors bank (Stojkov et al., 2009).

2.4.4.1. Mitigation of harmonic distortion

Particle swarm optimization method was used to design passive filters for three different types of loads: constant – torque –variable speed loads, constant –speed –variable torque loads and variable – speed - variable torque loads. The obtained results showed a reduction in the total harmonic distortion in the current, voltage at AC mains, supply current, and improved power factor (Singh and Singh, 2014).

2.4.4.2. Types of electrical loads

Electrical loads can be classified into two main groups: Linear loads and nonlinear loads. In linear loads, voltage and current signals follow one another very closely, such that the voltage drop that develops across a constant resistance varies as a direct function of the current that passes through it. It is a relation that can be described by Ohm's law. Examples of linear loads are shown in Table 2.2 (De La Rosa, 2006).

Table 2.2. Examples of linear loads

Resistive elements	**Inductive elements**	**Capacitive elements**
Incandescent lighting	Induction motors	Power factor correction capacitor banks
Electric heaters	Current limiting reactors	Underground cables
	Induction generators (windmills)	Insulated cables
	Damping reactors used to attenuate harmonics	Capacitors used in harmonic filters
	Tuning reactors in harmonic filters	

Loads in which the current waveforms do not resemble the applied voltage waveform due to the use of electronic switches which conduct load current only during a fraction of the power frequency period are known as nonlinear loads. Nonlinear loads are those in which Ohm's law cannot describe the relation between voltage and current. Examples of nonlinear loads are shown in Table 2.3 (De La Rosa, 2006).

Table 2.3. Examples of nonlinear loads

Power electronics	**Arc devices**
Power converters	Fluorescent lighting
Variable frequency drives	Arc furnaces
DC motor controllers	Welding machines
Cycloconverters	
Cranes	
Elevators	
Steel mills	
Power supplies	
UPS	
Battery chargers	
Inverters	

2.4.5. Power quality

Electricity generation from solar energy depends mainly on irradiance. Change in climate conditions such as cloud cover may cause voltage flickers. In high penetration levels of PV systems, the impact is more elevated, affecting the quality of power supply to the grid (Fan et al., 2010).

The changing power flow as a result of the fluctuation in solar irradiance, temperature and the type of semiconductor components are some sources of power quality issues with grid-connected PV systems. Quality power translates into pure sinusoidal voltage and current output from a PV system, which prevents the occurrence of harmonics, inter harmonics and voltage distortions (Patsalides et al., 2007).

Kow et al. (2016)(Jordan et al., 2012) while comparing the performance of artificial intelligence and the conventional methods in mitigating power quality events, it was found that power system monitoring, the grid inverter, the dynamic voltage regulator, the static synchronous compensator, the unified power quality conditioner, and energy storage systems are some options which can compensate for power quality events. And that, these methods outperform the conventional methods in terms of response time and controllability. However, they require memory to achieve these objectives (Kow et al., 2016).

2.4.6. Frequency deviation

Frequency deviation from the nominal frequency in a distribution network occurs when there is an imbalance between power generation and consumption. The maximum permissible frequency deviation in a generator is 1%; beyond which there could be a loss of synchronism (Taha Attya and Hartkopf, 2013). The effect of frequency deviation is observed in the change of electromotor winding speed and damage to generators. Fewer DG units limit the capacity of

the system to mitigate frequency deviation during disturbances. The inertia of the rotating masses of synchronous generators SG(s) determines the system's immediate frequency response during a major imbalance between generation and consumption. Replacement of large-scale conventional power plants by DG systems can also affect the system's frequency stability due to the decreases in the number of generators participating in frequency control and reduction in the overall inertia of the system (Rahmann and Castillo, 2014).

2.4.7. Effects of intermittency

The intermittency in PV generation output caused by the shading effect of moving clouds has been noted as one of the challenges posed by grid-connected PV systems which results from the sudden covering of the entire array or part array by a moving cloud (Chalmers et al., 1985).

The control measures to handle PV generation sudden changes include:

i. Automatic Generation Control (AGC),
ii. regulating conventional generation,
iii. scheduling of more units to regulating duty, and
iv. use of combustion turbines or combined cycle generating units with very responsive gas or oil firing systems, making these specific generators easily controllable.

The challenges in handling PV generation sudden changes are listed as,

- the ramping rate imbalance - the rate at which the PV generation drops (e.g., MW/min) may be faster than the rate at which the conventional generation is ramped up,
- conventional generation entrusted with compensating for the loss of PV generation may reach peak generation output before attaining desired load-generation balance,
- cost of fuel (oil or gas) in combustion generators and the scheduling aspect. (Nghitevelekwa and Bansal, 2018).

Alam et al. (2014) proposed using the ramp-rate control technique for limiting PV output fluctuations caused by passing cloud cover. The setup involves an inverter power output (PINV) obtained from the combined PV panel DC power output (PDC) and compensation power output (PCOMP) from a storage device.

2.4.8. Islanding and malfunction of protection system

Unintended islanding is an electrical phenomenon where an on-grid solar PV system continues to supply power to the grid even when the utility side is disconnected. This energizes the utility feeders, posing a danger to personnel working on the feeders (Velasco et al., 2011). However, grid-tied solar PV inverters have been embedded with special anti-islanding protection features to arrest such situations when they occur.

The existing protection schemes in distribution networks are designed according to the unidirectional power flow. Bidirectional power flow as a result of the high penetration of DG into the existing DN may lead to overvoltage, increased fault current levels and malfunctioning of relays, reclosers, fuses, voltage regulators due to the lack of directional sensing and adequate sensitivity to detect the reverse faults (Conti, 2009). Coordination of protective devices helps to isolate faulted equipment without halting the whole power system. However, increased DG

penetration into the DN may lead to wrong coordination due to the bidirectional flow of fault current (Girgis and Brahma, 2001).

2.5. Hosting capacity

The PV hosting capacity is the maximum PV penetration at which no technical or legal constraints in the grid are violated. Determination of hosting capacity (HC) enables stakeholders to quantify the impact of the DG units on the performance of the power system by using a set of assessment indicators (Yang and Bollen, 2008). The selection of these sets of indicators depends on the points of interest, including voltage profile, current of the various lines, steady-state voltage violations, harmonic distortion levels, power quality, low frequency and high frequency, mains protection etc. (Bertini et al., 2011).

The installation of inverter-based distributed generation units, particularly solar photovoltaic (PV) systems, if not correctly sized, may give rise to problems such as over and under voltages, excessive line losses, overloading of transformers and feeders, protection failure, and high harmonic distortion levels exceeding the international standards' limits in the distribution systems. These problems occur when the amount of distributed generation units exceed the maximum permissible penetration level, that is when the system (or the feeder) exceeds its hosting capacity (HC) limit (Paliwal et al., 2014).

For HC determination, the DG penetration level is increased in intervals of 0–100%, and for each penetration level, the selected performance indices are calculated. If any of them exceeds its limits, then the DG penetration level is determined as the system's HC. Besides, a feeder's HC is not a single value, but a range of values; therefore, many HC values can be calculated (Bollen and Hassan, 2011). The flowchart in Fig. 2.6 demonstrates the assessment of the HC of distribution systems to distributed generators.

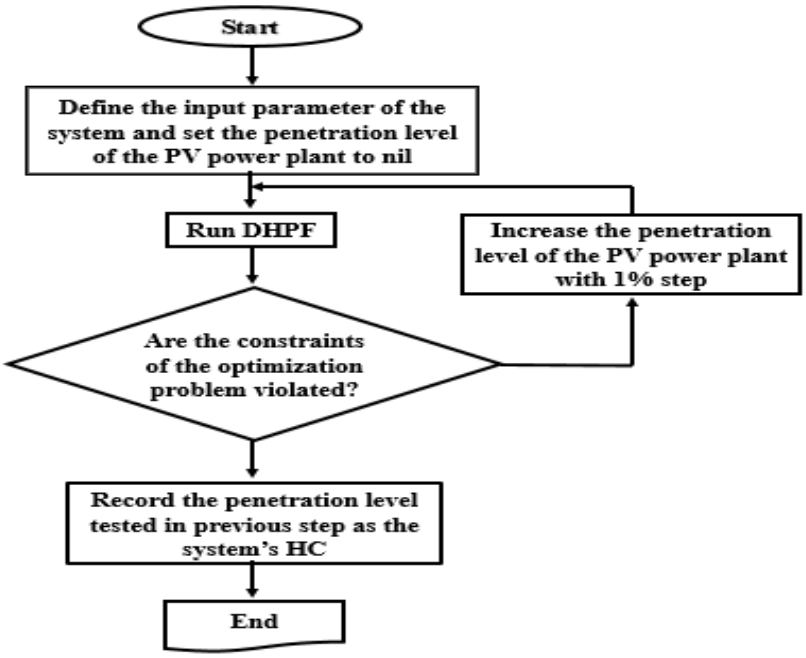

Fig. 2.6. Hosting capacity assessment for distribution networks (Sakar et al., 2018).
(DHPF = Decoupled harmonic power flow)

Different methodological choices have been realized to enhance the grid-HC such as reactive power control (Ho et al., 2016), voltage control active power curtailment, energy storage technologies (Jayasekara et al., 2016), network reconfiguration and reinforcement and harmonic mitigation techniques (Capitanescu et al., 2015).

Stetz and Braun (2011) investigated the technical and economic strategies for increasing the hosting capacity of a real LV grid for PV integration. The methods were made up of four different autonomous PV inverter control strategies and a distribution transformer with on-load tap changers (OLTC) and traditional grid reinforcement measures. The results were obtained by using 12-month RMS simulations with a step-size of 1 min. They concluded that the hosting capacity of the LV grid could be increased by applying autonomous inverter control strategies in an economically efficient manner. It was also found out that the autonomous provision of reactive power by PV inverters turned out to be a reasonable approach to lower the overall PV grid integration costs sufficiently. However, their study was limited to LV systems; hence, the recommendation for further studies to be done on MV grid simulation and the combination of different control strategies for both LV and MV grid systems.

2.6. Model for harmonics in power systems

A harmonic component in an AC power system is defined as a sinusoidal component of a periodic waveform with a frequency equal to an integer multiple of the system's fundamental frequency. Harmonics of the original waveform can be obtained by Fourier analysis shown in Eq. 2.3, to 2.7 (Fekete et al., 2012). Any periodic signal with the period *T* can be represented by a Fourier series per the following equation.

$$f(t)=\frac{a_o}{2}+\sum_{h=1}^{\infty}\left(a_h\cos(h\omega t)+b_h\sin(h\omega t)\right), \tag{2.3}$$

The content where *h=1* forms the fundamental component and the content where *h>1* forms the harmonics. The coefficients a_h and b_h can be determined by:

$$a_h=\frac{1}{\pi}\int_0^{2\pi} f(t)\cos(h\omega t)dt, \tag{2.4}$$

$$b_h=\frac{1}{\pi}\int_{\mathbf{0}}^{\mathbf{2\pi}} \mathbf{f(t)}\sin(h\omega t)dt. \tag{2.5}$$

When a signal is sampled periodically in 2π the Fourier coefficients can be calculated approximately by summation. The waveform distortion is evaluated at the harmonic orders $h = 2, H_{max}$, where $H_{max} = 40$ is a typical value. For instance, a current waveform can be characterized by individual harmonics: $X_h = I_h/I_1$ *for* $h = 1, H_{max}$.

In order to describe harmonic distortion of the signal, the well-known Total Harmonic Distortion (THD) index is used (example for current):

$$THD_1 = \sqrt{\sum_{h=2}^{40} \left(\frac{I_h}{I_1}\right)^2 \times 100.} \quad (2.6)$$

THD weighting factors can be introduced into the calculation of the harmonic distortion to assess the harmonics of the individual orders. The characteristics determined in this way are known as the Partial Weighted Harmonic Distortion (PWHD):

$$PWHD_1 = \sqrt{\sum_{h=14}^{40} h\left(\frac{I_h}{I_1}\right)^2 \times 100.} \quad (2.7)$$

2.7. Grid inverters

PV systems serve several purposes when connected to the grid. The priority is to generate power to meet the load requirements of customers. The generated power can also be used for ancillary purposes, such as supporting the voltage and the grid's reactive power, improving the quality of the network power, solving the issues of power loss, and active power filtering of the grid (Zeb et al., 2018). Broadly, inverters can be classified into these main groups (a). centralized, string and multi-string inverters (b). the single and multi-stage solar inverters, and the isolated and transformerless circuit inverters, (Zeb et al., 2018). These inverter configurations are shown in Fig. 2.7.

The centralised configuration of the inverter is mostly used to interface the large PV plants with the grid. The two-level (2L) full bridges and the three-level (3L) configurations are most often used for the central inverter topologies. These are made up of the neutral point clamped (NPC), conventional H-bridge (H4), the emerging voltage source inverter (VSI) topologies (T-type) (Kabalcı, 2020). Initially, thyristors were employed in the switching devices of central inverters, however, with time, converters such as the metal–oxide–semiconductor field-effect transistor (MOSFET) and the insulated gate bipolar transistors (IGBT) are now being employed. These applications are intended to solve the grid-connected issues of power quality and high total harmonic distortion (THD). According to (Ankit et al., 2018; Goroohi Sardou et al., 2018), even with the introduction of these high switching frequency processes, the central inverters up to date have not achieved the intended desired efficiency neither have the power quality issues been eliminated. A single MPPT algorithm is mostly applied in the central inverters, and that is the major disadvantage of this type of inverters (Kabalcı, 2020)

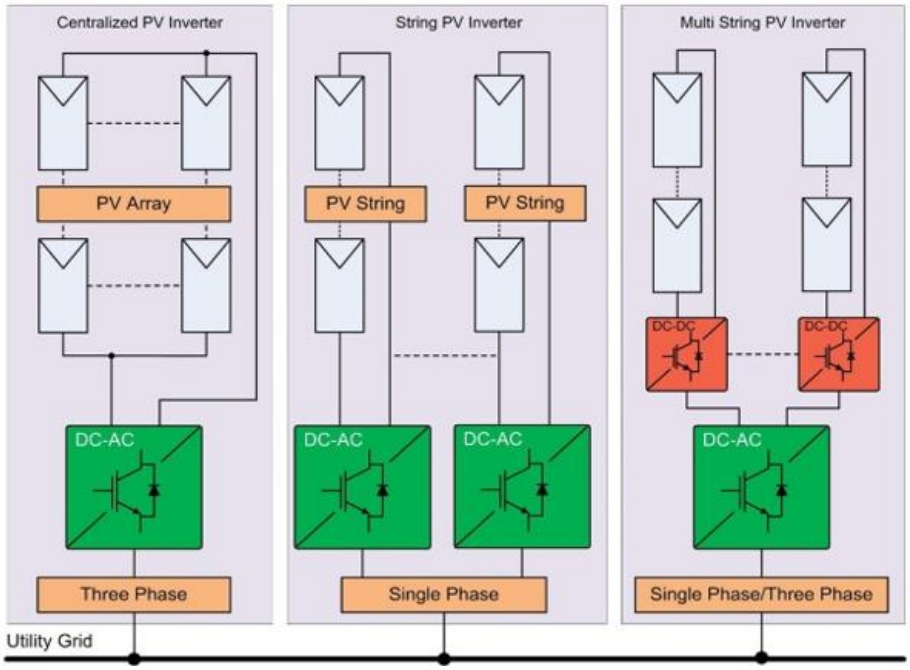

Fig. 2.7. Inverter topologies of grid-connected PV systems (Kabalcı, 2020)

The multi-string inverter, however, has each string of modules connected to one inverter. In the case of increasing the system's power capacity, additional inverters with strings of modules are coupled together. In the string inverter configuration, a transformer or dc-dc converter is required to boost the string voltage if it does not meet the expected voltage (E. Hossain et al., 2014). Different topologies such as the H4 topology, H5 topology, H6 topology and the highly efficient and reliable inverter concept (HERIC) are employed in string inverters (Zeb et al., 2018). The primary role of the H4, H6 topologies is to make stable the common-mode voltage (CMV) whiles in use. The second group of topologies which include the H5 and HERIC are exploited to minimize the leakage of current as the inverters are inbuilt with faster switching abilities which possess networks that generate zero voltages to cancel the filter and the dc bus capacitor's reactive power (Rizzoli et al., 2016; Zeb et al., 2018). Dutta et al. (2018) found that the inverter topology with the most capability to reduce current leakage without compromising its efficiency is the transformerless inverters.

Inverters can either have transformers embedded at the output stage or without an inverter which are termed transformerless inverters. A review of commercial inverters by (Kerekes et al., 2011) reveals that the transformerless inverters produce an increment in the efficiency of about 3% beyond the other topologies of inverters. Aside from the higher efficiency, the transformerless inverters also have as an advantage, a comparatively lower cost, smaller weight and size. Furthermore, transformerless inverters eliminate losses that may occur as a result of the presence of a transformer.

The replacement of central inverters for the string inverters is as a result of the deficiency of central inverters caused by the fact that they possess a single MPPT. However, the string inverters are unable to overcome the adverse effects when one or more modules in the string are shaded. This situation has led to the introduction of microinverters which are mounted on each module (Meneses et al., 2013). With this arrangement of microinverters, the total

efficiency of the whole system, therefore, increases compared to the string and central inverters. The topology of microinverters is utilised mostly in household PV installations with small power requirements.

Notwithstanding the abovementioned characteristics, transformerless inverters present their peculiar issues and are unable to solve some critical problems such as getting rid of the leakage current that occurs from parasitic capacitance, which pertain to the interfacing of solar PV systems with grid networks. The adverse effects of the leakage current is the creation of noise resulting from electromagnetic interference (EMI), higher THD, and losses in the power output (Tofigh Azary et al., 2018).

Several methods have been employed to eliminate current leakages such as disconnecting the PV module or PV array from the grid when in the flywheel mode by creating a link between the negative terminal of the PV module and the grid's neutral (Xiao et al., 2011). In order to eliminate the problems with the inverters as earlier mentioned, a single-stage bidirectional inverter is applied (Xia et al., 2017). The most widely utilised topology for current leakage elimination by decoupling the PV module from the grid and at the same time employing the switches to control the freewheeling through the common-mode operation is the two-stage HERIC topology (Chen et al., 2015). The least switching losses are experienced using the HERIC topology, which can produce performance efficiencies of 99% (Chen et al., 2015). Stages of inverter topologies are executed with or without galvanic isolation depending on the use of the line transformer at the final stage. Isolated inverter topologies are introduced to curtail the issues faced by transformerless inverters and also present galvanic isolation between the grid and the PV system. Galvanic isolation is an approach that isolates electrical circuits to remove stray currents. Even though signals can still go across the separated circuits, drifting currents induced by AC power are blocked. The introduction of the high-frequency transformer establishes the isolation (Öztürk et al., 2018).

Grid-connected inverters are embedded with dc-dc converters to match the voltage generated by the PV array to the inverter using the MPPT algorithm control. To solve the problems of leakage inductance, EMI noise associated with inverter topologies, a combination of the hard-switching topology and the resonant tank is applied (Kabalcı, 2020).

Several challenges encountered by the inverter are as a result of the varying of the solar radiation causing an extensive range of generated voltage and power and the accompanying wide range of temperature. To solve the problems mentioned above, a storage mechanism usually an electrolytic capacitor is chosen because of its longevity and embedded between the inverter and the dc-dc converter (Zhang et al., 2014).

Inverters can also be either line commutated inverters or self-commutated inverters. The line commutated inverters employ the switching device to control the turn-on time but cannot control the turn-off switch. A supplementary switch thus controls the turn-off switch. However, the self-commutated inverter employs the switching system to control the turn-on state and the turn off state. Examples are the MOSFET and the IGBT. They have several capabilities such as controlling both the voltage and current waveforms, power factor and the harmonic distortions. The self -commutated inverters are currently used for PV power (Ishikawa, 2002).

Grid-connected Solar PV inverters can also be a current type or voltage type. In the current-type inverter system, the dc side consists of the current source. A sinusoidal current waveform output is also obtained at the ac side of the inverter. Its main purpose is to supply into the grid. The voltage type inverter has the dc side as the voltage source. A sinusoidal voltage waveform output is thus obtained at the ac side of the inverter. Changing the control scheme can also serve as both the voltage and current source when seen from the inverter's ac side. The voltage scheme inverter cannot be employed in standalone PV systems operation (Ishikawa, 2002).

2.8. Microinverters

With the introduction of various policies by different countries to enhance the dissemination and utilization of solar PV, diverse models and schemes at various scales are being initiated to meet consumers' demands. The recent introduction is the microinverter unit. The microinverter can be employed as a standalone unit, which is usually installed close to the load or (grid meter) to generate AC power using mainly one or two modules connected to meet the low input voltage of the microinverter. The microinverter offers the opportunity to monitor each module's performance, making troubleshooting straightforward to undertake. The small and compacted nature of microinverters allows their use at the back of PV modules. Microinverters' primary role is to extract the maximum power of a module and inject the AC component into the grid while meeting the standards set by the utility regulators for grid-connected PV systems.

Microinverters are usually applied to systems with nominal power ranging from 200 *Wp* to about 600 *Wp* and are incorporated with maximum power point trackers (MPPT) for stable operation. Microinverters generate less internal temperatures and devoid of bulky electrolytic capacitors for input power decoupling. These make them have an average lifespan of 25 years, regardless of the weather conditions (Sher and Addoweesh, 2012). Studies have shown the advantages of microinverters over string inverters (Petreuş et al., 2013). Since each module has a dedicated MPPT, module mismatch is eliminated. There is also a minimal shading occurrence, a common issue with residential or rooftop PV systems (Deline et al., 2012). Microinverters also possess the edge of being compact, with low maintenance requirements, and easy to install and operate, hence gaining attention in recent years. Microinverters are composed of either the single-stage with the implementation of the maximum power point tracker or double stage conversion topology, which uses the DC to DC converter in the absence of MPPTs (Sher and Addoweesh, 2012). To further enhance the acceptance and dissemination of microinverters, they are constructed less bucky and easy to self-install with signal outputs close to the grid (Kjaer et al., 2005; Myrzik and Calais, 2003).

Galvanic isolation is required in interfacing the inverter with the grid to help resolve the problem of grounding (Kjaer et al., 2005). The presence of the galvanic isolation determines the essence of a transformer in the inverter. This is because the galvanic isolation is obtained with the company of the transformer. In case a transformer is present in the microinverter, they are situated at the DC side with a high-frequency operation because of their small sizes. It has been found that microinverters without transformers improve efficiency by 2% and enhance the power density (Cavalcanti et al., 2010; Kerekes et al., 2011).

However, there is also the fear of high leakage current (Islam and Mekhilef, 2014), which occurs due to stray capacitance between the module terminal and the ground. High leakage current could significantly affect the PV system's output power and its reliability if it is not resolved by using the right means such as adding switches or acting on the pulse width modulation or applying passive filters (Khan et al., 2017). These parasitic capacitances can reach as high as 150 μF/kWp or 1 μF/kWp for crystalline silicon cells and amorphous silicon cells, respectively, and depends on the temperature and other climatic factors present at the site (Araújo et al., 2008). Studies have shown that stray current could be bypassed by creating an alternative conducting channel without incorporating more switches to the microinverter (Tang et al., 2016).

Several researchers have listed many microinverters having power output ranging from 90 Wp to 600 Wp with power density ranging from 0.09 W/cm^2 to 0.41 W/cm^2. The listed microinverters possess maximum power point voltage ranging between 15 and 37.8 V whiles the power factor and total harmonic distortion ranges from 0.95 to 1 and ≤ 2.9% to ≤ 5%, respectively (Islam and Mekhilef, 2014; Kjaer et al., 2002). Different designs of microinverters have been propounded in various studies and are in operation. However, regardless of the microinverter's topology, technically, it is made up of the following units: DC-DC converter, the inverter, the control unit, a protection circuit, and an interface that links it with the grid. A typical outlook of a microinverter with the essential components is presented in Fig. 2.8 (Meinhardt et al., 1999).

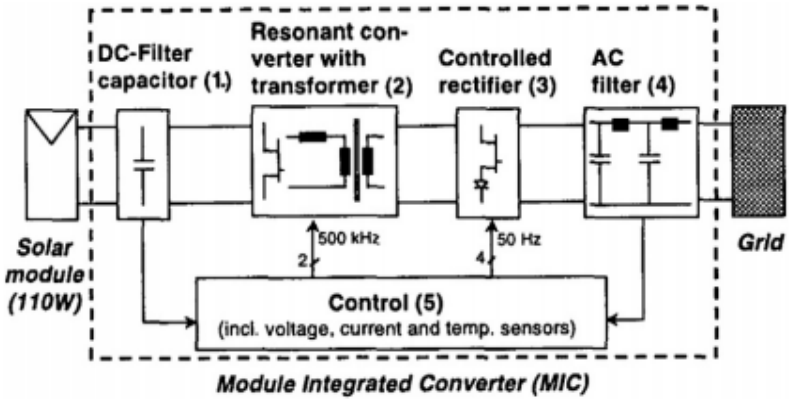

Fig. 2.8. A classic example of a microinverter (Meinhardt et al., 1999)

A study by (M. A. Hossain et al., 2015) on microinverters' thermal performance revealed a strong correlation between the degree of the temperature of the microinverter with irradiation, the temperature of the PV module, temperature of the surrounding, and the nominal AC power out of the module.

2.9. Maximum power point tracking methods

The fluctuation of solar radiation causes the corresponding variation in current and voltage and consequently the fluctuating power. In order to extract the most power from the solar cell or module, the maximum power point depending on the fluctuation must be detected by a control system. This control mechanism is the maximum power point tracker (MPPT). The objective of these control systems is to achieve the highest efficiency. The algorithm for these systems

works by tracking both output parameters based on the fluctuations and the load demand (Kabalci, 2017).

There are two main classes of MPPT controllers, the direct and the indirect MPPT techniques. The direct method detects and measures the performance parameters such as voltage, current, and power whiles in operation to generate signals for the tracking process (Sera et al., 2013). The indirect technique dwells on the calculation results made for current, voltage, and power to detect the maximum power point rather than measurement. The direct MPPTs work faster and more efficiently as they determine the varying parameters based on operation conditions (Romero-Cadaval et al., 2013).

Commercially, the direct methods are the preferred options because of their swiftness and effectiveness and guaranteed efficiency. The most extensively used direct MPPTs are the perturb and observe (P&O), the incremental conductance (InCon) and the Hill climbing algorithm controls (HCAC). The direct methods have also been enhanced by incorporating computational intelligence techniques such as the genetic algorithm, artificial neural network, fuzzy logic control and particle swarm optimisation (PSO) (Romero-Cadaval et al., 2013). Direct MPPTs usually apply online information to determine the maximum power point (MPP). However, the indirect method involves an offline analysis of the PV system to determine the MPP for the tracking process (Salas et al., 2006). The PSO technique has been specially designed to solve the issues with partial shading of solar modules (Ishaque et al., 2012). The PSO controls have significant cost constraints for its commercial use because of the introduction of improved microprocessors, sensors and other circuit components that are of higher performance (Li et al., 2018). (Çelik et al., 2018) outlined the different MPPT control methods that are commonly used, as shown in Table 2.4.

Table 2.4. Online, offline and hybrid MPPT control methods (Çelik et al., 2018)

Online MPPT control methods	**Offline MPPT control methods**	**Hybrid MPPT control methods**
Perturb-and-Observe (P&O	Fuzzy Logic Control (FLC)	P&O and ANN
Incremental Conductance (InCon)	Artificial Neural Network (ANN)	Analytical Calculation and P&O
Capacitor Control	Genetic Algorithm (GA)	Particle Swarm Optimization (PSO)
Forced Oscillation	Short Circuit Current (Isc)	Optimized FLC
Sliding Mode	Open-Circuit Voltage (Voc)	Differential Evolution
Load I-V Control	Temperature Based Method	Direct Prediction Method (DPM)

The advantage of the computational MPPT control methods is their ability to deal with the issues of prediction and imprecision under rapidly changing solar radiation (Salam et al., 2013). In assessing how close an inverter's performance is to the maximum power point, the applied parameter is the maximum power point tracker efficiency (ηMPPT). ηMPPT is the ratio of the

inverter's operating energy to the rated energy of the same inverter under ideal conditions. The parameter generally used to evaluate the functioning of the inverter close to the MPP is the MPPT efficiency, (ηMPPT). This parameter could be defined as the ratio between the energy obtained by the inverter of a given PV generator, and the energy that could be obtained from the same generator if the inverter were provided with an MPPT ideal system (Çelik et al., 2018).

There are stipulated standards that must be met when interfacing the inverters with the grid. These include frequency deviation limits, voltage deviation limits, meet the power factor requirements, anti-islanding, grounding and leakage current limits, total harmonic distortion (THD), independent harmonic distortion (IHD) and synchronization (Kabalcı, 2020). Several standards exist that are mostly determined by the national utility operators of various countries or international or regional organisations. Countries without standards are forced to adopt the standards of other nations' or standards by international organisations. These include EMC Limits for harmonic current emission, IEEE 1547.1 IEEE Standard Conformance Test Procedures for Equipment connecting Distributed Resources to the Electric Power Systems, IEEE 929-2000 Recommended Practice for Utility Interface of Photovoltaic (PV) Systems, UL 1741 Standard for Safety Inverters, Converters, Controllers and Interconnection System Equipment for Use with Distributed Energy Resources, IEC 60364 2005 Electrical Installations of Buildings. The standards for the connection of microinverters on to the grid are presented in Table 2.5 TO 2.10. (DeBlasio, 2009; Hasan et al., 2017; Kabalcı, 2020; Meneses et al., 2013; Oruganti, 2014).

Table 2.5. Various standards for the voltage and current harmonics in grid-connected systems

Requirement	**IEEE 1547-2008**	
Nominal Power	10 kW	
	Order (h)	**Limit**
Harmonic Content	3–9	4.0%
	11–15	2.0%
	17–21	1.5%
	23–33	0.6%
Even harmonics are limited to 25% of the odd harmonic limits		
THD < 5%	-	-
DC Current Injection	<1% of rated output current	
Voltage Deviations	**Range (%)**	**Time (s)**
	V < 50	0.1
	50 ≤ V < 88	2
	110 ≤ V < 120	2
	V ≥ 120	0.05
Frequency Deviation	**Range (Hz)**	**Time (s)**
	49 < f < 51	0.2

Requirement	**IEEE 1547-2008**	
Nominal Power	30 kW	
	Order (h)	**Limit**
Harmonic Content	3–9	4.0%
	11–15	2.0%
	17–21	1.5%
	23–33	0.6%
	> 35	0.3%
Even harmonics are limited to 25% of the odd harmonic limits		
DC Current Injection	<0.5% of rated output current	
Voltage Deviations	**Range (%)**	**Time (s)**
	V < 50	0.16
	50 ≤ V < 88	2
	110 ≤ V < 120	1
	V ≥ 120	0.16
Frequency Deviation	**Range (Hz)**	**Time (s)**
	59.3 < f < 60.5	**0.16**

Table 2.6. Voltage flicker limits at different voltage levels

The Standards	Network	Plt	Pst
IEEE Std. 1547	MV HV-EHV	0.7 0.6	0.9 0.8
UK IEC61000	MV-HV	0.65 08	1.0 1.0
Malaysian GC	LV (less than 11 kV) MV (11 - 33) kV HV (above 33 kV)	0.8 0.7 0.6	1.0 0.9 0.8
USA	LV MV – HV	0.7 0.6	0.9 0.8

Table 2.7. Various standards for the voltage and current harmonics in grid-connected systems

Requirement	**EN61000-3-2**	
Nominal Power	16A 230 V	
	Order (h)	**Limit (A)**
Harmonic Content	3	2.31
	5	1.14
	7	0.77
	9	0.4
	11	0.33
	13	0.21
	15 - 36	2.25/h
	2	1.08
	4	0.43
	6	0.3
THD < 5%	(8–40)	1.84/h
DC Current Injection	<0.22 A	
Voltage Deviations	Range (%)	Time (s)
Frequency Deviation	Range (Hz)	Time (s)

Requirement	**VDE**	
Nominal Power	—	
	Order (h)	**Limit (A/MVA)**
Harmonic Content	3	3
	5	1.5
	7	1
	9	0.7
	11	0.5
	13	0.4
	17	0.3
	19	0.25
	23	0.2
	25	0.15
	25 - 40	3.75/h
THD < 5%	Even	1.5/h
	greater than 40	4.5/h
DC Current Injection	<1 A, max. trip time	= 0.2 s
Voltage Deviations	Range (%)	Time (s)
	V < 85	0.2
	V≥ 110	0.2
Frequency Deviation	Range (Hz)	Time (s)
	47.5 < f < 50.2	0.2

Table 2.8. Current harmonic distortion limits for grid-connected PV systems

The standards	Type	Harmonic order (h)	Distortion limit	THD (%)
IEEE 1547 AS 4777.2	Odd	33 < h	< 0.3%	< 5%
		23 ≤ h ≤ 33	< 0.6%	
		17 ≤ h ≤ 21	< 1.5%	
		11 ≤ h ≤ 15	< 2%	
		3 ≤ h ≤ 9	< 4%	
	Even	10 ≤ h ≤ 32	< 0.5%	
		2 ≤ h ≤ 8	< 1%	
IEC 61000-3-2	Odd	h = 3, 5 and 7	< (3.45, 1.71, and 1.15) %	< 5%
		h = 9, 11 and 13	< (0.6, 0.5, and 0.3) %	
		15 ≤ h ≤ 39	< 0.225%	
	Even	h = 2, 4 and 6	< (1.6, 0.65, and 0.45) %	
		8 ≤ h ≤ 40	< 0.345%	

Table 2.9. Voltage harmonic distortion limits of PV systems

Standard	Voltage Bus	Individual harmonic limit (%)	THD (%)
IEEE 519	(V ≤ 1) kV	5%	8%
	(1≤V ≤ 69) kV	3%	5%
	(69≤V ≤ 161) kV	1.5%	2.5%
	(V > 161) kV	1%	1.5%
IEC 61000-3-2	(2.3≤V ≤ 69) kV	3%	5%
	(69≤V ≤ 161) kV	1.5%	2.5%
	(V > 161) kV	1%	1.5%

Table 2.10. Power factor range at the PCC in different grid codes

Country	Power factor range at the point of common coupling	
	Lead	Lag
Germany	0.95	0.95
Italy	0.90	0.90
China	0.95	0.95
Spain	0.85	0.85
Australia	0.9	0.95
South Africa	0.95	0.95

Inverters are usually embedded with two controllers. At the side close to the array is the controller meant to track the maximum operating point of the modules for high power extraction, while near the grid at the point of common coupling is the controller which ties the power from the array to the grid. The controller at the grid side is required to improve the quality of the output power to meet the grid's standards. The control topologies are of three classes, the single-stage, two-stage and the power control shifting phase, which has an added feature to control the reactive power (Mahela and Shaik, 2017). The crucial power quality issues are the THD, voltage and frequency fluctuations, injection of dc current-rated to the current ratio of the inverter, islanding and grounding control (Meneses et al., 2013).

The commercial topologies of central inverters work at efficiencies at about 85–90%, and they are bulky and heavy because of the incorporation of transformers and coolers. Besides, the 2L inverter topologies the other topologies cause a higher THD ratio and lesser power factor compared to the 3L topologies (Jana et al., 2016; Kouro et al., 2015). The central inverters used originally were based on thyristors as switching devices, they have now been developed into power converters using MOSFET and insulated gate bipolar transistors (IGBT). The increased switching frequency has tackled some of the deficiencies mentioned above, such as low power quality and higher total harmonic distortions. However, they are still far from ensuring the desired overall efficiency (Ankit et al., 2018; Goroohi Sardou et al., 2018; Jana et al., 2016).

The centralized inverter configurations of 3L-NPC or 3L T-type inverter topologies are illustrated in Fig 2.9a and b, respectively (Kouro et al., 2015).

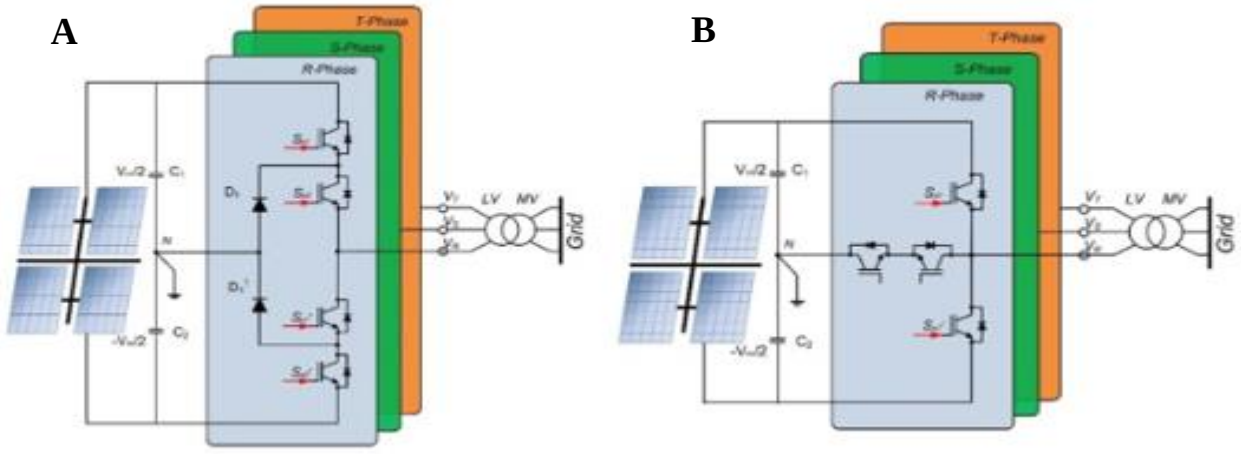

Fig 2.9. Centralized inverter configurations a) 3L-NPC inverter topology b) 3L T-type inverter topology (Kouro et al., 2015)

The 3L-NPC generates a constant common-mode voltage (CMV) and comparably low THD ratio compared to the conventional inverter topologies. However, it requires higher isolation and an increased number of switching capacity for the inverter configuration. The constant CMV supplied by the neutral point of 3L-NPC DC bus increases its edge over the conventional H4 inverter topology. The operation of transformerless inverters does not cause leakage current problems or modulation deficiencies in the 3L-NPC topology. Thus, 3L T-type inverter operates devoid of any transformer at the output as 3L-NPC topology does (Ahmad and Singh, 2018; Faraji et al., 2017; Kouro et al., 2015).

2.10. The Hungarian electricity system and solar energy potential

Hungary practices the free choice of energy supply to the consumer after the liberalization of the electricity market in 2008. However, electricity prices in some segments are still regulated within the system called the universal supply with the government regulating the end-user prices (IAEA, 2019).

The Hungarian Energy and Public Utility Regulatory Authority (HEA) is responsible for regulating electricity among other utility services. They issue decrees, issue permits for performing any activity concerning electricity in the country. They are also responsible for approving operational network and commercial codes. The HEA also oversees the compliance of obligations in licenses and electricity transmission across the county's borders (IAEA, 2019).

Hungary imports about 28.6% of electricity and other fuels out of which electricity is generated from neighbouring countries like Slovakia, Austria, Ukraine (MAVIR, 2018). The main electricity export destinations are Croatia and Serbia (Businesswire, 2019b). The other sources of electricity consumption include 35.7% Nuclear Energy, 18% Oil and Gas, 10.6% Hydrocarbons and 7.1% composed of Renewables, which sums up the gross electricity consumption as of 2017 (MAVIR, 2018). The installed domestic power plant capacity as of the end of 2018 was 9212 MW. This is made up of 23% of gas, 50% from nuclear, 15% from coal and 12% from renewables. The peak energy demand was 6869 MW. 58% of the energy supplied in Hungary is imported from neighbouring countries (IAEA, 2019).

Table 2.11. Hungarian transmission network (Mavir, 2019)

Transmission network length (km)			
		Route	**Circuit**
Overhead	750 kV	268.10	268.10
	400 kV	2 287.16	2 982.91
	220 kV	1 099.32	1 393.65
	132 kV	142.04	199.24
Cable	132 kV	16.64	16.64
Total		**3 813.26**	**4 860.54**

Table 2.12. Hungarian transmission network and substations owned by MAVIR and voltage levels (2018) (Mavir, 2019)

Substation	**Voltage level (kV)**	**Substation**	**Voltage level (kV)**
Albertfalva	220/132	Litér	400/132
Albertirsa	750/400	Martonvásár	400/220
Békéscsaba	400/132	Ócsa	220/132
Bicske Dél	400/132	Oroszlány	220/132

Debrecen	220/132/35/20/10	Paks	400/132
Detk	220/132	Pécs	400/132
Dunamenti	220/132	Perkáta	400/132
Dunaújváros	220/132	Sajóivánka	400/132
Felsőzsolca	400/132/35/20	Sajószöged	400/220/132
Göd	400/220/132	Sándorfalva	400/132
Gönyű	400	Szeged	220/132/35/20
Győr	400/220/132	Szigetcsép	400/132
Hévíz	400/132	Szolnok	400/220/132/20
Józsa	400/132	Szombathely	400/132
Kerepes	400/132	Tiszalök	220/132
Kisvárda	220/132		

Regarding solar energy resource potential, the sunshine hours in Hungary range from 1,950-2,150 kWh/m^2 annually, with the annual solar radiation received on the horizontal surface being 1280 kW/m^2. These values characterize Hungary as having a comparatively high potential for solar energy exploitation, as shown in Fig. 2.10 and 2.11. Fig. 2.10 and 2.11 present the Global solar radiation (GHI) intensity of Hungary and the solar PV potential of Europe, respectively.

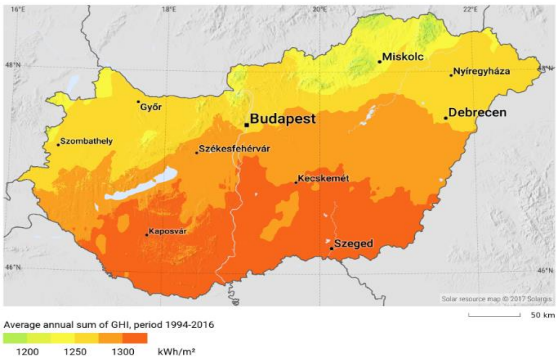

Fig. 2.10. Global solar radiation (GHI) intensity Hungary (Solargis, 2019)

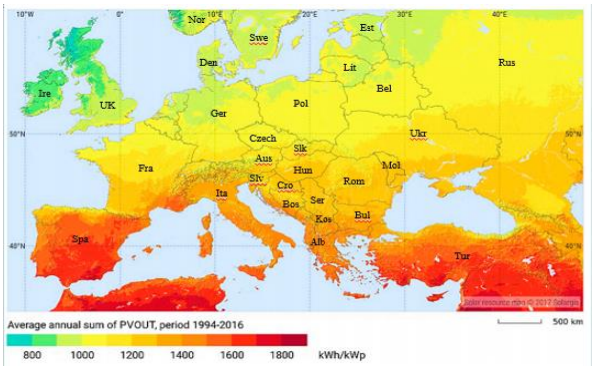

Fig. 2.11. Solar photovoltaic power potential of of Europe (Solargis, 2019) and current research

Fig 2.11 shows an annual average PV energy potential of Hungary to range between 700–1900 kWh/kWp depending on the geographical location. The yearly average PV energy potential ranges between 1050–1450 kWh/kWp, as shown in Fig. 2.11. Hungary's PV energy potential ranks her as a country having relatively an average PV power potential in Europe.

In terms of favourable conditions for investment in solar PV systems development, Hungary was ranked among the top ten most attractive countries among the Central Eastern European and South-Eastern European countries (CEE & SEE) in the "Attractiveness index for solar photovoltaic (PV) energy investments by the Renewable Market Watch (Businesswire, 2019a).

Solar PV experienced unprecedented growth in the last few years as a result of the government's policy support and PV regulation and PV investment attractiveness of the country. The total installed capacity at the end of 2018 was 700 MWp (Bellini, 2019).

The primary key driver for the rapidly increasing growth in installed capacity experienced in Hungary over the past few years, is the net-metering programme, for PV installations up to 50 KWp. The net metering programme is supported by a subsidized loan facility offered by the Hungarian Development Bank (MFB). Another PV support programme is the METÁR programme. This was a reformation of the FiT programme (KÁT system), which existed at the initialization stage of the support programme. Both programmes run concurrently, but new entrants can only be admitted to the METÁR programme (Leal-Arcas, R. et al., 2020). The FiT and the premium facility were some other facilities that have been introduced at diverse scales to enhance the dissemination of solar PV and meeting various customers' demands (Szabo, 2019). These facilities have increased the pressure on the grid with the injection of significant power quality issues from the use of several advanced electronic gadgets.

2.10. Summary of literature review

The study of the literature has revealed that there has been an unprecedented growth in Solar PV as a result of the favourable policies that have been put in place by the various countries to enhance its use.

- The growth in solar PV has been observed in the area of grid-connected systems. New and complex semiconductor electronics are being introduced into the market to meet the power demands of diverse consumers. These complex semiconductor electronics, however, draw non-sinusoidal waveforms of current thus introducing harmonics into the grid.
- The impact of the introduced harmonics on the grid depends on the grid's existing structure at the study location and the penetration levels of the distributed generated systems. This points to the fact that a study location's results could not be the same for other sites.
- It was also evident that the inverter type and system infrastructure influenced the power quality issues injected into the grid. However, the degree of impact of each system varies and not yet ascertained.
- The harmonic current depended on the system's harmonic voltage. However, the correlation between the two has not been thoroughly investigated.
- The review has revealed that research focusing on power quality issues created by grid-connected solar PV output varies and is limited. However, most of the studies conducted in this area focused on harmonic distortions. Thus, it recommends more work be done on voltage flicker, the voltage at the grid side, reverse power flow and frequency deviation.
- The hosting capacity of a low voltage (LV) power grid could be increased by applying inverter control strategies. It was realized that the independent provision of reactive power by PV inverters could be a reasonable approach to lower the power quality issues hence increasing the hosting capacity of the grid.

- Numerous power quality issues faced by grid inverters result from the intermittency of solar radiation, causing a wide range of generated voltage and power and the accompanying wide range of temperature. The influence of these factors varies based on the grid-connected PV system components.
- Most of the earliest inverters were based on thyristors as switching devices, which have now been evolved to power converters using metal oxide semiconductor field-effect transistors (MOSFET) and insulated gate bipolar transistors (IGBT). The resultant effect is the increased switching frequency that has resolved some of the power quality issues, especially, total harmonic distortions. The inference is that the inverter plays a major in dealing with power quality issues in grid-connected PV systems.

From the literature analysis, it could be concluded that the grid-connected inverters have evolved over the years with the incorporation of complex semiconductor electronics to increase efficiency and overcome the numerous limitations. Thus, the gap in knowledge in the performance of the different grid-connected inverters under various settings and operating conditions have been observed. Therefore, this has provided the current study with the desired objectives to offer answers to the knowledge gap.

3. MATERIALS AND METHODS

This chapter presents the materials, procedures, and processes used in the research, including the scientific methods involved in the experimental measurements and the description of the test systems to obtain the set research objectives.

3.1 Measurements on the microinverter applying the photovoltaic simulator

This section presents the materials and methods of the assessment of the performance of microinverters under a steady irradiation source (solar PV simulator) and outdoor ambient conditions employing the same inverter and setup. The power quality characteristic measurements for the different scenarios will be analysed, and their compliance with available standards for grid-connected PV systems assessed while comparing the results with other scenarios and studies on microinverters.

3.1.1. Materials and methods for measurements with the solar PV simulator

Microinverters' primary function with the incorporation of MPPTs is to extract the maximum power possible of a module and inject the AC component into the grid while complying with the utility regulators' standards for distributed energy sources connected to the grid and notwithstanding the loads hooked onto the network.

This section of the study sought to analyse the quality of microinverters' power output by employing a solar PV simulator, and modules of different technologies and make (structure) that meet the microinverter's requirements. The Geräte Unterricht Naturwissenschaft Technik (GUNT) ET255 set up was retrofitted to conduct the experiment, as described below. An additional socket or measuring point was created to enable the simultaneous measurement of the AC voltage and current using the power quality analyser. The setup was made up of a photovoltaic simulator, connecting sockets for solar photovoltaic modules, a toggle switch to change between either operating the photovoltaic simulator or the real photovoltaic modules. A combiner box with terminals for the integration of extra PV module strings depending on the size of the PV system. The combiner box comprises an overvoltage protection system to protect the components of the setup. The setup has the DC switch disconnector, which isolates the PV generator from the other parts should a failure occur. The voltage and the current limits of the DC switch disconnector are set at the maximum Voc and Isc values of the PV generators and the PV simulator. The grid-connected microinverter employed is (module inverter) designed for small outputs of about 180 Wp. It has an in-built maximum power point tracking (MPPT) function. The switch-on voltage of the inverter is 35 V, and the MPP voltage tracking range lies between 28 V and 50 V. The specifications of the module inverter are presented in Table 3.1. The retrofitted setup (GUNT ET255) enables the measurement of AC voltage and current simultaneously and evaluates the power quality characteristics of the various waveforms generated under the different scenarios.

3.1.2. Measurements with the PV simulator

The initial test was conducted using the PV simulator as the PV power source to feed the inverter. Two scenarios were considered. Firstly, constant PV generation at fixed irradiation and temperature of 1000 Wm^{-2} and 25 °C, respectively. This selection generates a steady nominal power of 146 Wp, Voc of 41.3 V, Isc equals 5 A, Vmpp of 31.4 V, and Impp 4.65 A. The second scenario with the PV simulator as the PV power source applied irradiation of 400 Wm^{-2} at a constant module temperature of 25 °C, generating Voc of 39.6 V, Isc of 2 A Vmpp 32.3 V and Impp of 1.87 A. The peak power for the second scenario is 45 Wp. These two conditions are to assess the system's power quality performance at the two extreme states of PV generation under steady irradiation.

3.1.3. Measurements with PV modules in real outdoor operation

The second investigation with the GUNT ET 255 employed PV modules in actual outdoor operation as the DC power source. In this case, different technologies and structures of PV modules were used to assess the quality of the power output of the system/microinverter. The microinverter and the PV generator specifications are presented in Table 3.1 and Table 3.2, respectively.

Table 3.1. Characteristics of the 2E inverter

Parameter	**Value**
Maximum input power	150 W
Grid feed-in from	2.5 W
Maximum input voltage	55 V
Output voltage	230 V
Switch-on voltage	35 V

Table 3.2. Characteristics of PV generator

Parameter	**Value**
Power output	150 W
Current at maximum output	4.7 A
Voltage maximum output	31.4 V
Maximum short circuit current	5.1 A
Maximum open circuit voltage	41.3 V

In order to measure both AC voltage and current output simultaneously and obtain the power quality characteristics of the inverter output, additional measurement points have been created on the ET 255 for connection to the power analyzer. The experimental setup and schematic diagram are shown in Fig. 3.1. and 3.2, respectively. Measurements were done for a duration of eight hours.

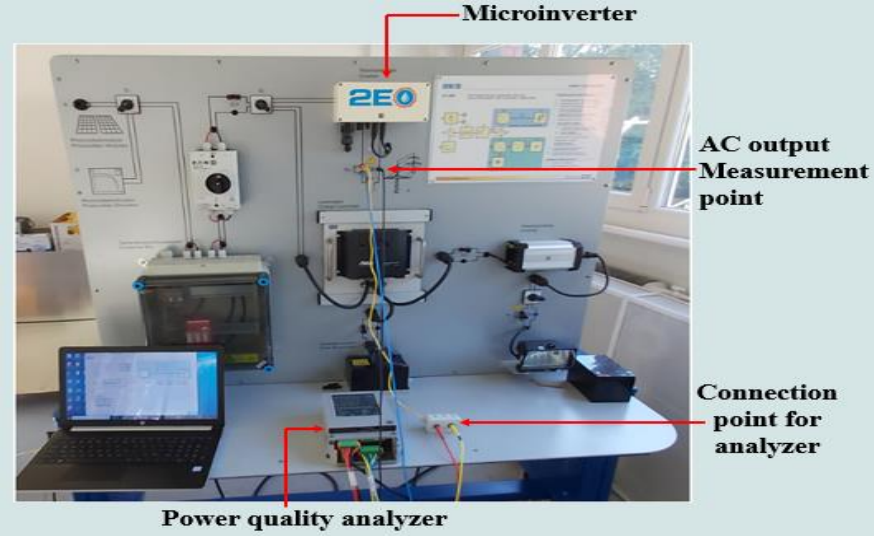

Fig. 3.1. Experimental setup

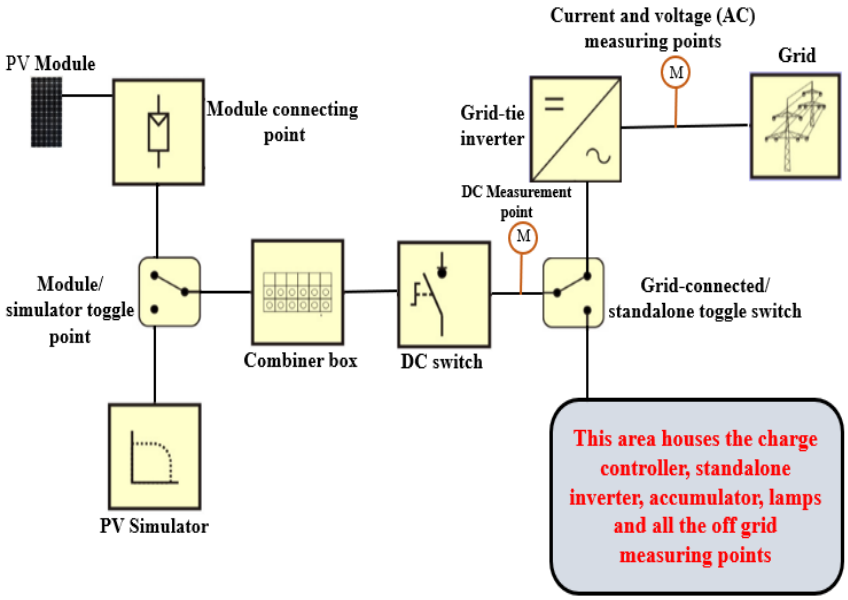

Fig. 3.2. Schematic diagram of the setup

The Wally A3 electric power quality analyzer with an in-built data logging capability was used to measure and store the AC output waveform characteristics. Table 3.3 presents the specifications of the Wally A3 power analyzer.

Table 3.3. Specifications of Wally A3 power analyzer

Ranges	**Voltage**	**0-400 Vac**
		0-100 Vac
	Current	5 Arms (direct insertion)
		3 Vac/dc (from current clamps with voltage)
		3KA/300 A (from flexible clamps Rogowski)
	Frequency	DC or 42.5 – 69 Hz
Accuracy	Voltage	±0.1% U_{din} from 10% to 150% of U_{din}
	Current	±0.1% I_{din} from 10% to 150% of I_{din}
	Frequency	±10 mHz
	Harmonics	Meet EN 61000-4-7 class 1
	Flicker	Meet EN 61000-4-15
	Power quality	Meet EN 61000-4-30 Class A

The measurements are computed over 10 to 12 cycles of consecutive windows, according to IEC 61000-4-30 standard. Sampling is done synchronously with phase-locking at 512 samples/cycle with a range of 42.5 ÷ 69 Hz (25.6 kHz @50 Hz). Solar radiation data was measured at the plane of the module or array (PoA) using the Delta – T SPN1 Pyranometer. The ADAMS 4018 interface is used to extract the measured irradiation and then converted into a digital signal and stored in the computer. The pyrometer has an accuracy of ±0.1 $W.m^{-2}$, spectral sensitivity of 400 nm – 2700 nm in W/m^2, a resolution of 1 W/cm^2, signal output and temperature of 0 V-2 V and ± 0.02 %/°C, respectively. The Almemo 2290-4 multimeter with a data logger option was used to acquire the ambient temperature and the temperature of the rear of the modules. A measuring module NiCr-Ni (K), Pt 1000, with the range –200.0 to +1370.0 °C having a resolution of 0.1 *K* was used. Temperature sensors (resistance temperature detector, RTD) 1 kΩ Platinum (Pt 1000) with accuracy ±0.001%, ±3850 ppm/°C, 2-SIP was applied for the temperature measurement.

3.1.4. Performance evaluation of microinverter systems in outdoor operation

The study was undertaken at the forecourt of the Solar Energy and Environmental Engineering Laboratory in Szent Istvan University, Godollo, Hungary, which has geographical coordinates of 47°35’39” N, 19°22’0” E. The modules used for the research had no predefined criteria for selection, but available modules which have two distinct makes and structure were used. The two main technologies used are glass-cell-glass structure and glass-cell-Tedlar structure. The modules are the Dunasolar, Solarex, and Juta modules. Dunasolar is a hydrogenated-amorphous silicon thin film double glassed solar panel. Solarex module is a polycrystalline silicon module, with glass to Tedlar structure. Juta is made up of monocrystalline silicon technology with Tedlar to glass structure. The variety of the module assembly allows for the

comparison of the power quality of the technologies. Module specifications, as given by the manufacturer, are presented in Table 3.4. The modules were fixed to an inclined support facing true south having an angle to the horizontal equal to the site's latitude. The installation of the modules is shown in Fig. 3.3. The experiments were conducted on bright sunny days in order that the modules voltage output meets the kick start voltage of the microinverters. Measurements for each scenario were taken for ten hours (8 am-6 pm) in the second week of August 2020.

Table 3.4. Module characteristics at standard test conditions (STC)

	DUNA SOLAR	**SOLAREX**	**JUTA**
Parameters	a-Si (G-G)	pc-Si (G-T) (60Wp)	mc-Si (G-T)
P_{mpp} (W_p)	40	60	20
V_{oc} (V)	62.5	21.3	22
I_{sc} (A)	1.15	3.8	
V_{mpp} (V)	44.0	17.1	17
I_{mpp} (A)	0.90	3.5	1.18
Module Area/ (m^2)	0.791	0.564	0.36
Temp. coeff. of power	-0.47%/C	-0.47%/°C	-0.4 %/°C

Fig. 3.3. Installation of 1st set of PV modules

Fig. 3.4. Installation of 2nd set of PV modules

3.2. Performance of GMI 300 and MaySun-600W-B microinverters

The study to analyse the power quality output of commercial microinverters used in outdoor conditions was conducted by employing different technology modules and make (structure).

The study was undertaken at the forecourt of the Solar Energy and Environmental Engineering Laboratory in Szent Istvan University, Godollo, Hungary, which has geographical coordinates of 47°35’39” N, 19°22’0” E. The modules used for this study had no predefined criteria for selection, but available modules that met the microinverters' input requirements have been used. The two main types of modules applied were the polycrystalline module (Solarex), and the monocrystalline modules (Juta) with specifications presented in 3.5. The MaySun-600W-B (China inverter) and the GMI 300 (Holland inverter) microinverters with specifications provided in Table 3.6 were used for the study. Modules were fixed to an inclined support facing true south and having an angle to the horizontal equal to the site’s latitude. The installation of the modules is shown in Fig. 3.4.

The experiments were conducted on bright sunny days in order that the modules voltage output meets the kick start voltage of the microinverters. Measurements for each scenario were taken for seven hours (9 am - 4 pm) in the first week of October 2020. An extra measurement socket was built to connect the analyser to the microinverter to enable the simultaneous measurement of both current and voltage with the power quality analyser. The setup is shown in Fig. 3.5. The Wally power quality analyser with specifications and certifications presented in Table 3.3 was used to measure the power output characteristics. The various parameters were measured at intervals ranging from 200 ms to 3 s.

Table 3.5. Module characteristics at standard test conditions (STC)

	SOLAREX	**JUTA**
Parameters	pc-Si (G-T) (60Wp)	mc-Si
P_{mpp} ($W_{p)}$	60	20
V_{oc} (V)	21.3	22
I_{sc} (A)	3.8	
V_{mpp} (V)	17.1	17
I_{mpp} (A)	3.5	1.18
Module Area/ (m^2)	0.564	0.36
Temp. coeff. of power	-0.47%/°C	-0.4 %/°C
Stratigraphy	Glass-EVA-CELL-EVA-Tedlar (With frame) (G-T)	Glass-EVA-CELL-EVA-Tedlar (With frame) (G-T)

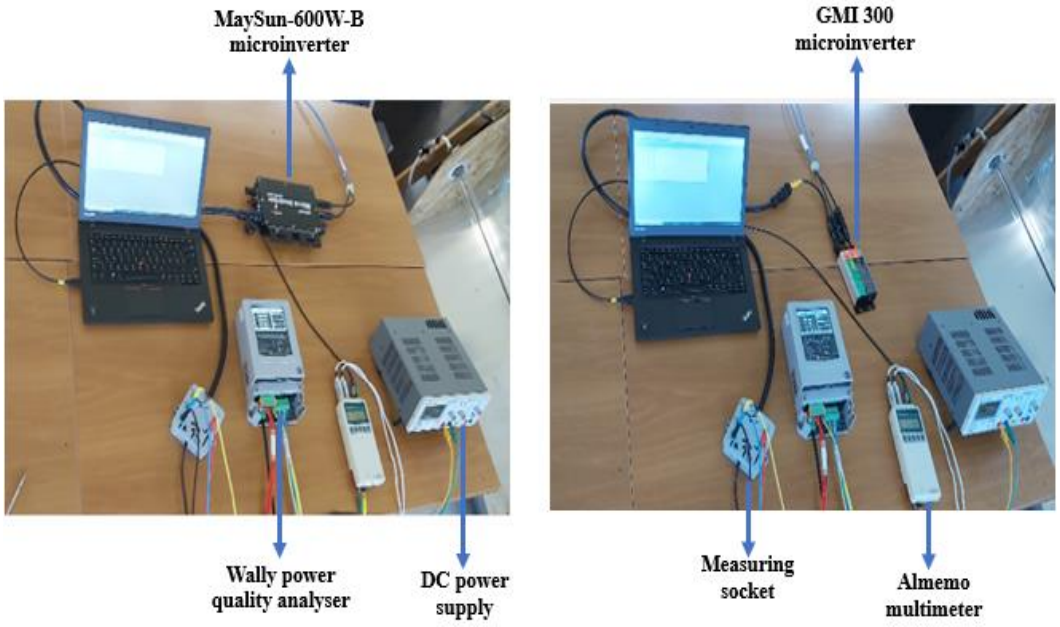

Fig. 3.5. Data acquisition setup showing the Power quality analyser and the microinverter

Table 3.6. Characteristics of the different microinverters

Parameters	**MaySun-600W-B (China inverter)**	**GMI 300 (Holland inverter)**
Max. DC input voltage	50 V	50 V
MPPT voltage range	25-40 V	24-40 V
Operation voltage range	22-50 V	18-50 V
Maximum input current	20 A	12A
Rated voltage range	@230V:180-260 V	@230VAC: 180-280 V
Rated output current	5 A	1.21 A
Rated frequency range	50Hz/60HzAuto	50 Hz/60 Hz Auto
Power factor	>98%	>0.99
MPPT efficiency	99.5%	99.9%
Maximum output efficiency	92%	92.5%
Grid detection	DIN VDE 1026UL1741	

3.3. Power quality performance of grid-connected string inverter systems

Power quality assessment was conducted on the rooftop grid-connected solar PV system installed at Szent István University, Gödöllő, Hungary. This system has been in operation since 2005 when it was commissioned as one of the first grid-connected systems in the country. The system is made up of two different PV technologies: Polycrystalline silicon (pc-Si) PV technology (ASE-100) and amorphous silicon (a-Si) PV technology (DS-40). It is divided into three sub-structures and installed on the flat roof of the student dormitory ‘C’ (47°35'45.4"N 19°21'51.7"E), as shown in Fig. 3.7. Sub-system 1 comprises 32 pieces of the pc-Si modules

(RWE Schott Solar). Sixteen (16) modules are connected in series and two modules connected in parallel. Sub-systems 2 and 3 are made up of seventy-seven (77) pieces each of the a-Si modules (Dunasolar). Seven (7) of these modules are connected in series and eleven (11) connected in parallel (Seres and Farkas, 2007).

The entire system has an array area of 152.5 m^2 and mounted at a fixed inclination of 30° facing true south with each sub-system connected to a separate inverter. Sub-system 1 is connected to the SunPower SP3100-600 inverter, while sub-systems 2 and 3 are connected to the SunPower SP2800-550 inverter. The modules' characteristics at standard test conditions (STC) and the inverter characteristics are presented in Tables 3.7 and Table 3.8, respectively. To enable the measurement of the power output for the three systems simultaneously, a measuring socket containing multiple measuring points was built and connected to the input of the energy meter. Fig 3.6 and 3.7 show the photographic presentation of the measurement setup and the installed PV array, respectively. Data on the various characteristics of the output signal was measured at intervals ranging from 200 ms to 3 s. Data for three different days with unique irradiation figures were selected out from the several days of measurement for the analysis purposes. These days had the following characteristics: 1) high solar radiation for the larger period of the day with no intermittency or fluctuation; 2) high level of irradiation with high intermittency and periods of very low solar radiation and 3) low solar radiation with high intermittency.

Table 3.7. Characteristics of PV modules at STC

Parameters	**pc-Si (ASE 100)**	**a-Si (DS40) 1**	**a-Si (DS40) 2**
Peak power (Wp)	105	40	40
Voltage at maximum power point (V)	35	44.8	44.8
Current at maximum power point (A)	3	0.8	0.8
Short circuit current (Isc) (A)	3.3	1.15	1.15
Open circuit voltage (Voc) (V)	42.6	62.2	62.2
Surface area of module (m^2)	0.845	0.813	0.813
Temp. coeff. of Voc (%/^{o}C)	-0.38	-0.2797	-0.2797
Temp. coeff. of Isc (%/^{o}C)	0.10	0.0897	0.0897
Temp. coeff. of power (%/^{o}C)	-0.47	-0.190	-0.190
Nominal operating cell temperature/NOCT (^{o}C)	45	50	50

Table 3.8. Inverter characteristics

Model	SP 3100-600	SP 2800-550
Peak power of PV generator	4.2 kWp	3.8 kWp
Rated output power	3.1 kW	3.0 kW
Maximum no-load voltage	600 V	500 V
Rated voltage (MPPT)	280 – 600 V	210 – 550 V
Efficiency max	94%	94%
Euro efficiency	92%	92%
Number of phases	1	1
Rated mains voltage	400±10%	400±10%
Input current max	15.0 A	10.8 A
Output frequency	50±2%	50±2%
Cos ϕ	1	1

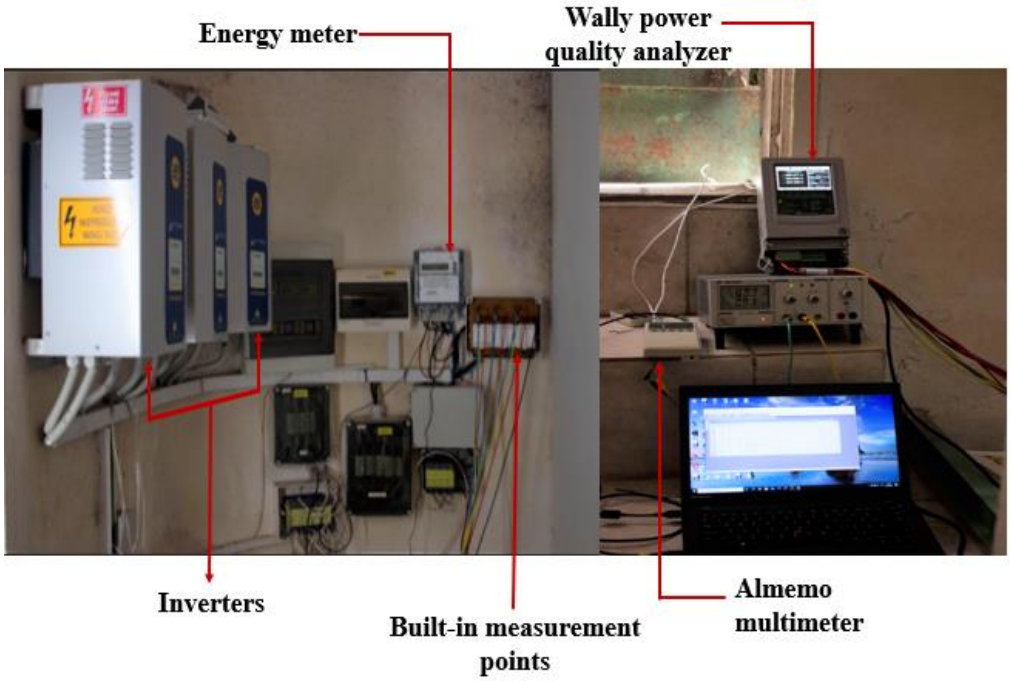

Fig 3.6. Measurement setup of the rooftop grid-connected system

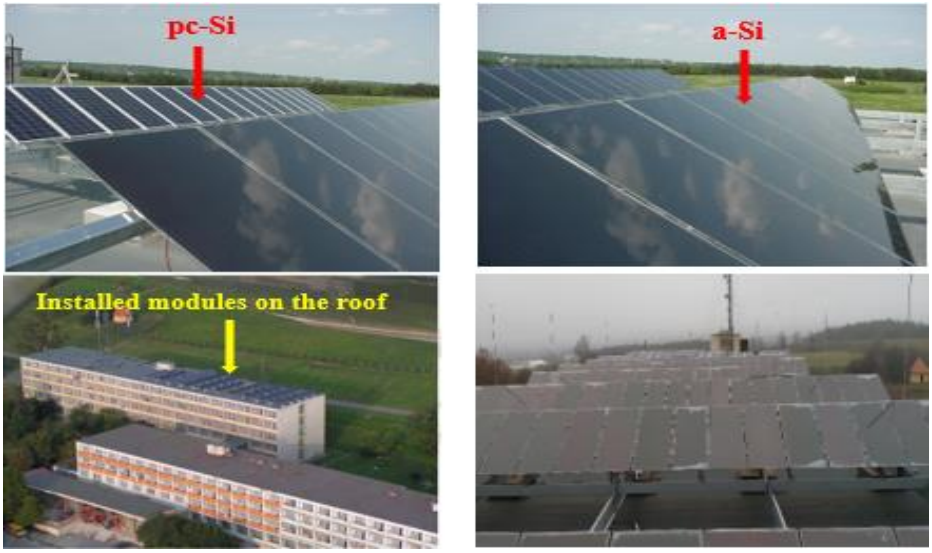

Fig. 3.7. Installed PV array

3.4. Power quality output of a single-phase inverter system

Power quality assessment of the grid-connected PV system in front of the Aula building at the Szent Istvan University on the coordinates 47°35′40.7″N and 19°21′42.3″E was performed in November 2020. Measurements were taken at the point of common coupling of the PV system with the grid. The PV system is made up of transparent glass modules of the monocrystalline Si technology with specifications presented in Table 3.9. The modules have been inclined at an angle of 40° to the horizontal facing south with an azimuth of 180°. However, the system is shaded from the sun by the Aula building for most of the morning. The system is tied to the grid through the Solaredge inverter with specification presented in Table 3.10. The total production capacity of the system is 3.3kWp. Figure 3.8 shows the layout of the system. The Wally 'A' power quality analyser with specifications and standard compliance qualifications outlined in Table 3.3 in section 3.1.3.

The measurements were taken from 9 am to 4 pm, and 9 am to 3:30 pm depending on the sunset. The intervals for measurement varied for each parameter ranging from 200 ms to 3 s. The measurements were taken over several days; however, results for 1st, 6th and 7th Nov were chosen for analysis purposes because of the trend of irradiation profiles for these days. These were three days with contrasting irradiation; one with smooth non-intermittent high solar radiation, the second with high but intermittent solar radiation and the third with low and intermittent solar radiation. The choice is to enable the assessment of the impact of the different shapes of solar radiation profiles on the power quality output of the installed PV system. The setup for the measurement is shown in Fig. 3.8. To be able to measure the output of the system and accommodate the current which was greater than the standard limit of the Wally power analyser, an improvised current and voltage measurement points constructed and attached to the wally equipment had the current output divided using a set of ten resistors each of magnitude 1 MΩ. Solar radiation was measured at the plane of the PV array using the Kimo solarimeter LSL 200 (resolution 1 Wm-2, accuracy 5%). Radiation data was taken at the interval of 1-minute.

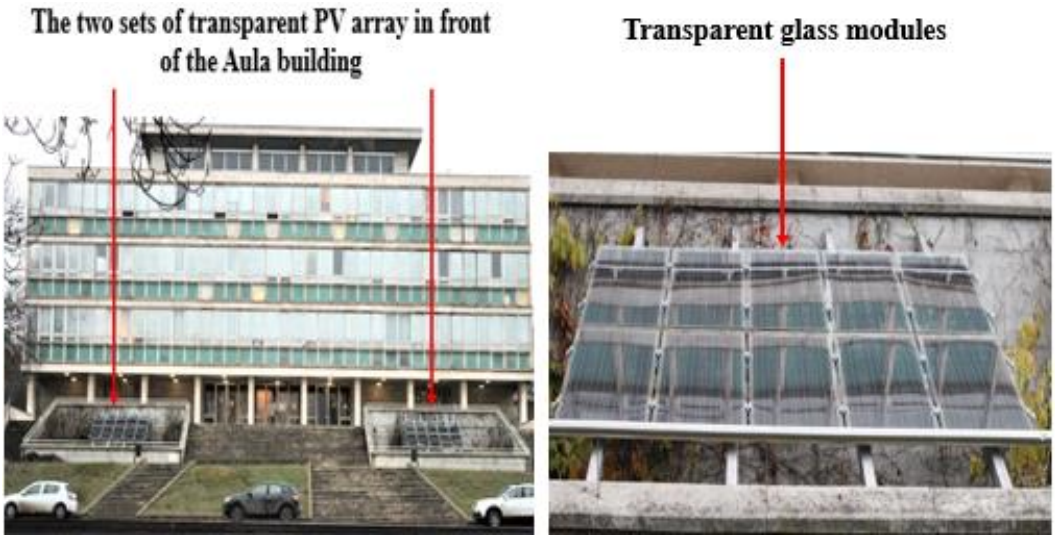

Fig. 3.8. Installed transparent glass PV modules of the Aula system

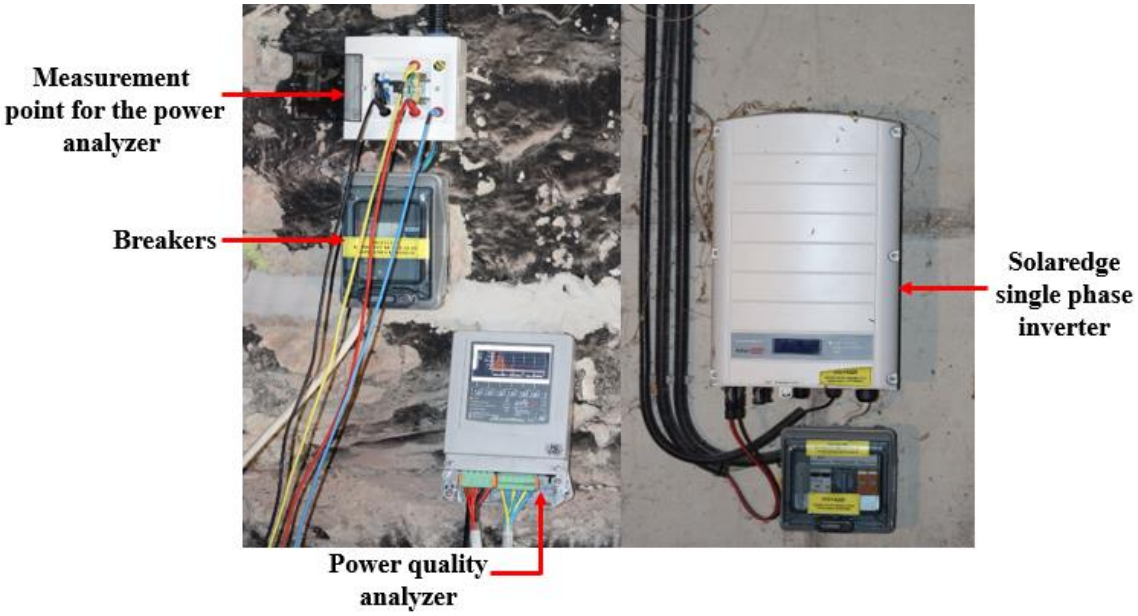

Fig. 3.9. Measurement setup at the Aula system

Measurements were taken from 9 am to 3:00 pm, 9 am to 3:30 pm, and 9 am to 4 pm for 1st, 6th and 7th November. The period of measurement varied due to the sunset time for the various days. The three days were selected from the lot, to present contrasting outputs for low irradiation, steady and high irradiation, and intermittent solar radiation profiles. These solar radiation profiles were chosen to assess their impact on the grid-connected PV system's power quality performance.

Table 3.9. Specifications of PV modules

Type of the collector modules	**SolarWatt Vision 36M Glass**
Technology	Monocrystalline
Covering material	Partly tempered high transparent float glass, 4 mm
Transparency	20%
Open Circuit Voltage	23.4 V
Short Circuit Current	9 A
Nominal Voltage (under STC)	19.2 V
Nominal current (under STC)	8.7 A
Nominal power	165 Wp
Total system capacity	3.3 kWp
Maximal system voltage	1000 V

Table 3.10. Specifications of inverter

Inverter type	**SE 3500-ER-01-ITA**
Phases	Single-phase
Operating voltage range	270 – 500 Vdc
Maximum input current	13.5 Adc
Maximum output power	3500 VAac
Operating voltage	220/230 Vac
Maximum output current	19.5 Aac
AC Nominal frequency	50/60 Hz
Power factor range	+/- 0.9 to 1
Transformerless ungrounded	Yes
Maximum inverter efficiency	97.6%
European weighted efficiency	97.5%

4. RESULTS

This chapter presents the results obtained from the experimentation and the discussions highlighting the new scientific findings. These include the power output characteristics for various commercial microinverters and string inverters.

4.1. Results and discussion on the investigations with the laboratory setup

The growth of solar PV has been so quick and has overgrown what the development of grid codes could cope with. As a result, there are relatively different grid connection specifications for various countries depending on the robustness of the grid system. There are diverse views as to whether PV systems should be passive or perform actively in grid control. Therefore, there is the need for harmonization of codes taking into account the reliability of the various power networks (Braun et al., 2012). In this section, the measured data of the investigations on the GUNT system (indoor and outdoor) is analyzed, comparing the results of each setup and scenario to each other and various assessments carried out on the compliance with available standards in the subregion of the experimental study.

4.1.1. Measurements with the solar PV simulator

In this subsection, the results obtained from the solar PV simulator measurements are discussed, considering the various standards for grid-connected systems.

4.1.1.1. Voltage profiles during the use of the solar simulator

Fig. 4.1 presents the voltage profiles of both scenarios of 400 Wm^{-2} and 1000 Wm^{-2} for the solar PV simulator with the 2E GUNT microinverter. Voltage measurements were done at an interval of 200 ms. The voltage output for the 400 Wm^{-2} recorded maximum and minimum values of 240.8 V and 230. 3 V, respectively, during the period of the experiment. The mean voltage and the standard deviations were 236.3 V and 1.9934 V, respectively. It was observed that there were no dips during the period of the study; all the recorded voltages were above the nominal voltage of 230 V. The measured voltages were all within the standard operating range as specified by the EMC standards, EN 50160, EN 61000 as ±10% for low voltage and medium voltage power systems (CENELEC, 2007). On the other hand, the voltage profile for the 1000 Wm^{-2} recorded some values below the nominal voltage, even though they were minimal (less than 0.5 % of the total recorded values). The average voltage and the standard deviations were 235.9 V and 1.545 V, respectively. The range of disparity was about 10 V. The high value of standard deviation for the 400 Wm^{-2} shows how significant the disparities in the recorded voltages were as compared to the values recorded for the 1000 Wm^{-2}. It was observed that for two-thirds of the measurement period, the voltages for the 400 Wm^{-2} were higher than the figures for the 1000 Wm^{-2}, except in the middle one third, where the values for both scenarios had insignificant differences as shown in Fig. 4.1.

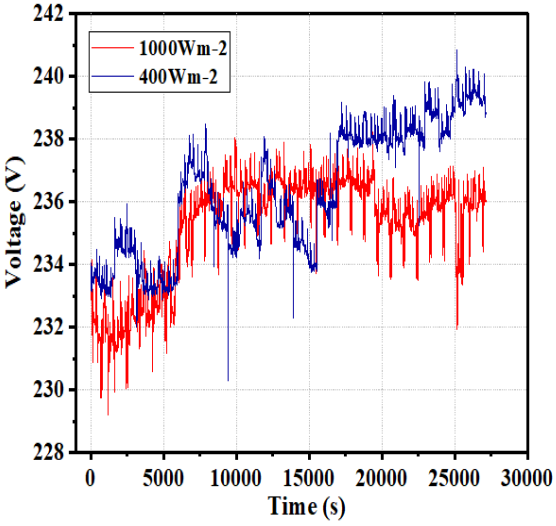

Fig 4.1. Voltage profile with the solar simulator (400 Wm^{-2} and 1000 Wm^{-2})

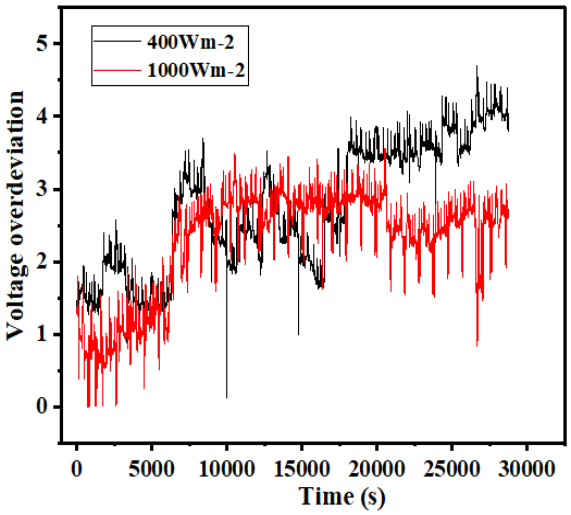

Fig 4.2. Voltage deviations when the solar simulator was used (400 Wm^{-2} and 1000 Wm^{-2})

The 400 Wm^{-2} showed higher positive deviations during the early stage and latter stages of the measurement, as shown in Fig. 4.2. The highest voltage deviation of 4.712% was recorded by the 400 Wm^{-2} whiles the 1000 Wm^{-2} recorded the highest and minimum deviations of 3.5% and 0.009%, respectively.

4.1.1.2. Voltage flickers

Due to the varying nature of solar irradiation, the penetration of solar PV systems in the grid can cause voltage flickers to occur. Voltage flickers are perceptible changes in lamp output due to sudden changes in voltage. Voltage flickers are assessed based on the frequency of occurrence and deviation from the nominal voltage over a stated period according to the IEEE 1453 standard. To enable the proper management of voltage flickers, they have been classified as short-term probability flicker severity (Pst) and long-term probability flicker severity (Plt). The occurrence of flickers is observed in the sudden changes in the brightness of lamps with the noticeable flicking of the lights (Ferdowsi et al., 2020). According to lower voltage characteristics, the EMC standard of EN 6100 prescribes Pst < 1.0 and Plt < 0.8. The IEEE 1547, IEC 61000-3-3 standards also specify that voltage flickers be between 0.6 and 0.9 pu for Plt and Pst, respectively (Tagare, 2011). The measured short-term voltage flickers for 400 Wm^{-2} and 1000 Wm^{-2} scenarios are presented in Figs. 4.3, and 4.4. Voltage flickers were recorded at intervals of 3 s. There were no Plt flickers registered for any of the test scenarios with the solar simulator. The 400 Wm^{-2} had higher magnitude flickers compared to the 1000 Wm^{-2}. The highest and minimum flickers recorded were 2.248 and 0.1and 1.552 and 0.088 for 400 Wm^{-2} and 1000 Wm^{-2}, respectively. 15.5% of the recorded flickers for 400 Wm^{-2} were outside the standard range whiles for 1000 Wm^{-2}, it was 5%. This, therefore, indicates that comparably, there was a higher level of quality issues under low irradiation (low PV generation) conditions even under a constant irradiation source using the solar simulator. The points of occurrence of the Pst have no peculiarity but occurred throughout the period of experimentation especially for the 400 Wm^{-2}.

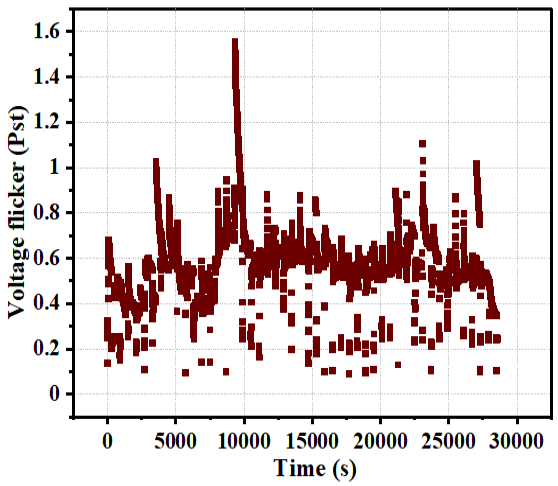

Fig. 4.3. Voltage flickers - Pst (400 Wm^{-2})

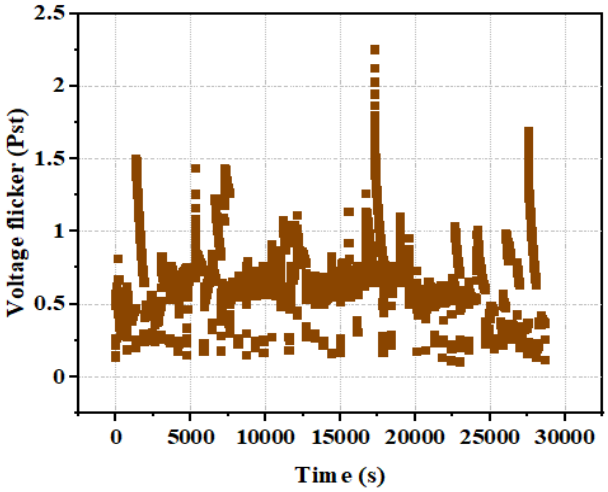

Fig. 4.4. Voltage flickers - Pst (1000 Wm^{-2})

4.1.1.3. Harmonic distortion

Harmonic distortions have been measured for both 400 Wm^{-2} and 1000 Wm^{-2} scenarios, and the results shown in Fig. 4.4 and Fig. 4.5, respectively. The presence of harmonics in power systems distorts the AC current and voltage waveforms. The awareness of harmonic distortions in power systems has increased in recent years with the high penetration of distributed energy sources, especially regarding variable power sources. The use of grid inverters, which are mainly incorporated with power electronics, are the significant sources of harmonic distortion at the point of common coupling with the grid, consequently affecting the grid's healthy performance and causing the grid protection devices to malfunction and fail. The limits for harmonic current emission as specified in the IEC 61000-3-2, IEEE 1547, AS 4777.2 standards and the voltage harmonic standards listed in Tables 2.5 – 2.7.

Results show that the individual harmonic distortions for both 400 Wm^{-2} and 1000 Wm^{-2} scenarios were within the limit specified by the IEEE 519 and the IEC 61000-3-2 standards. The individual harmonic distortions for both scenarios were all below 0.5%. The highest for the 400 Wm^{-2} was 0.32% and 0.46% for the 1000 Wm^{-2} scenario. However, the total harmonic distortions far exceeded the standard limit of 5%. The current total harmonic distortion (CTHD) for 400 Wm^{-2} and 1000 Wm^{-2} were 13% and 6.93%, respectively. The CTHD decreased with increasing irradiation (high PV power) levels at the same temperature from the solar simulator as shown by the results. The extent of the harmonic content of the output signal is dependent on the carrier frequency and the switching function. In order to obtain an efficient output from the solar PV system, the operational range of the amplitude modulation index is usually fixed from 0.5 to 1.0 (Alexander, 2016). The harmonics decrease with a higher modulation index, thus, approaching 1 (Al-Shetwi et al., 2020). This could be seen in the high harmonic presence in the 400 Wm^{-2} compared to the 1000 Wm^{-2}. This implies that PV systems operating at comparably lower irradiation levels will inject higher harmonics into the grid because of the contrary relationship that exists between the irradiation and harmonic distortion generation.

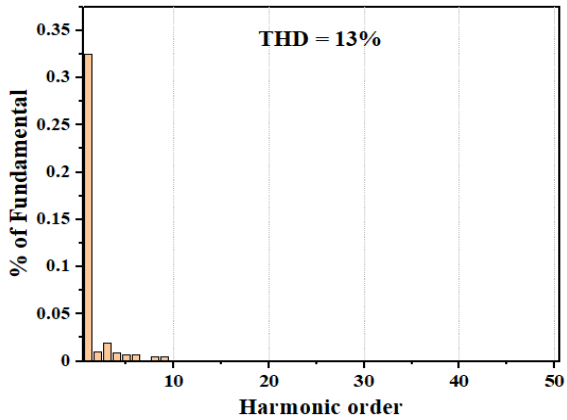

Fig. 4.4. Current harmonic for 400 Wm^{-2}

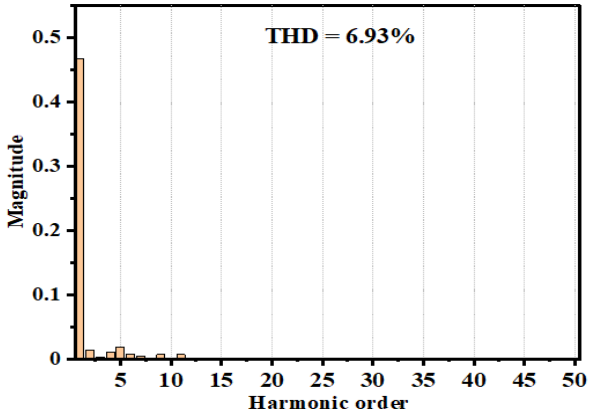

Fig. 4.5. Current harmonics for 1000 Wm^{-2}

Figs. 4.6 and 4.7 present the voltage harmonic distortions recorded for the 400 Wm^{-2} and 1000 Wm^{-2} scenarios. The individual harmonic distortions and the total harmonic distortions for both scenarios were within the limits specified by the standards. Distortions for both cases were similar in magnitude. The voltage total harmonic distortions were 2.24% and 2.27% respectively for 400 Wm^{-2} and 1000 Wm^{-2}, which were within limits prescribed by the standards. The 5^{th} harmonics of both scenarios had total harmonic distortions of 3.545% and 3.47%, respectively, for 1000 Wm^{-2} and 400 Wm^{-2}. Apart from the 5^{th} harmonic, all the other harmonics recorded distortions that were lower than 3% and within the limit of the standards for both cases under the solar simulator.

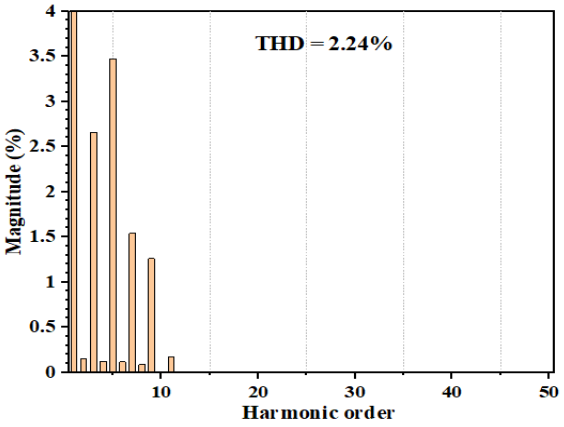

Fig. 4.6. Voltage harmonic for 400 Wm^{-2}

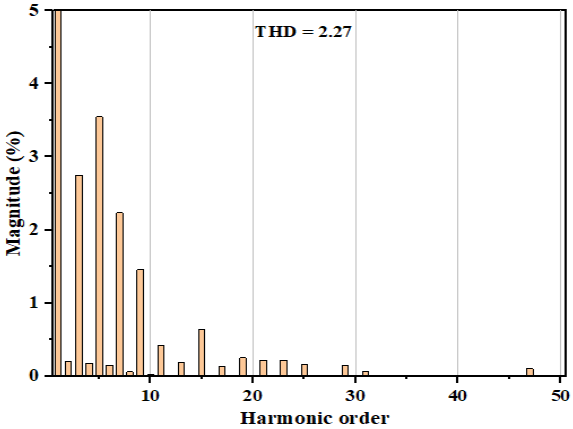

Fig. 4.7. Voltage harmonics for 1000 Wm^{-2}

4.1.1.4. Frequency

The frequency profile plays a very critical role with regards to the power quality of the grid. A minimal deviation from the prescribed standards has a negative impact on the quality, network synchronizability, stability, and reliability of the grid. Fig. 4.8 presents the frequency profiles for the solar simulator application. The maximum and minimum frequencies for the 400 Wm^{-2} were 50.028 Hz and 49.955 Hz. The measured frequency values did not present significant disparities, registering a standard deviation of 0.0125 Hz, indicating the closeness of the frequency during the entire period of experimentation with an average value of 49.994 Hz. The frequency profile of the 400 Wm^{-2} fell within the range of the standard by the EN 50160 (CENELEC, 2007; Dreidy et al., 2017), which specifies the frequency to be within ±1% of the

nominal frequency. The study with the 1000 Wm^{-2} irradiation recorded similar frequencies with the minimum and maximum frequencies being 49.629 Hz and 50.046 Hz, respectively. The average frequency and the standard deviations were 49.995 Hz and 0.017 Hz, respectively. The measured frequencies for the 1000 Wm^{-2} were within the acceptable range of ±1% prescribed by the EN 50160.

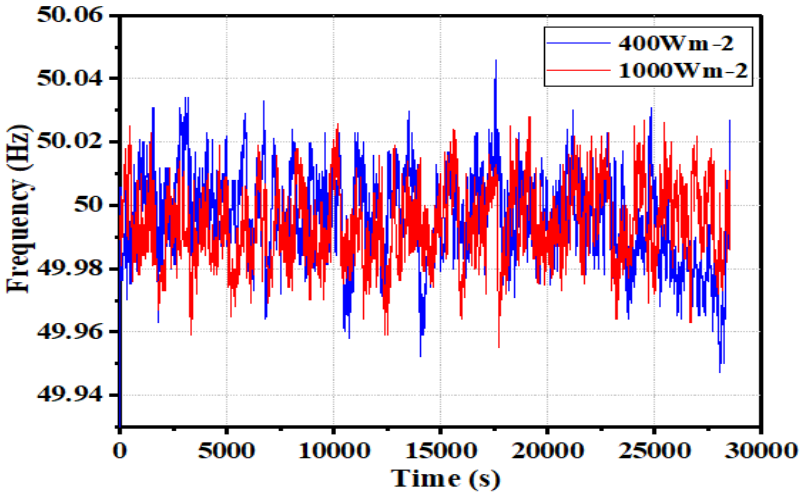

Fig. 4.8. Frequency profiles for the two scenarios of the solar simulator

4.1.1.5. Rapid voltage change

The Rapid voltage change (RVC), according to the IEC Standard 61000-4-30, defines RVC as a swift transition in the RMS voltage between two steady-state conditions, during which the voltage does not exceed the dip/swell thresholds (IEC Standard, 2015). Because the RVCs are events that occur swiftly, they are difficult to detect and track and thus, create serious quality issues for the management of the grid. Voltage events were recorded for both scenarios of 400 Wm^{-2} and 1000 Wm^{-2}. The recorded events were all below the nominal velocity, as shown in Fig. 4.9. There were about twenty, and eight voltage events for the 400 Wm^{-2} and the 1000 Wm^{-2}, respectively, as shown in Figs. 4a, and 4b. The maximum and minimum voltage changes for the 400 Wm^{-2} were -9.807 V and -4.79 V, respectively. These changes lasted for 0.11 s and 0.01 s, respectively, for the maximum and minimum changes. The highest duration RVC lasted for 0.111 s and recorded voltage sags of -8.65 V and -7.893 V. With the case of the 1000 Wm^{-2}, the maximum, and minimum RVC were -9.828 V and -5.481 V, respectively. These events lasted for 0.11 s and 0.01 s, respectively. The total duration for all the RVC recorded for the 1000 Wm^{-2} was 14 s, while it was 25.1 s for the 400 Wm^{-2} scenario. The most prolonged duration of the RVC for the radiation of 1000 Wm^{-2} was 0.12 s, and the voltage drop was -8.308 V. According to (Melhom et al., 2005), voltage deviations (sags and swells), rapid voltage changes (due to capacitor switching), harmonics and grounding are the most significant sources of power quality-related problems. Regarding the RVC, the numerous events recorded by the 400 Wm^{-2} scenario show the relatively higher issues of power quality compared with the higher irradiation generated by the solar simulator (1000 Wm^{-2}).

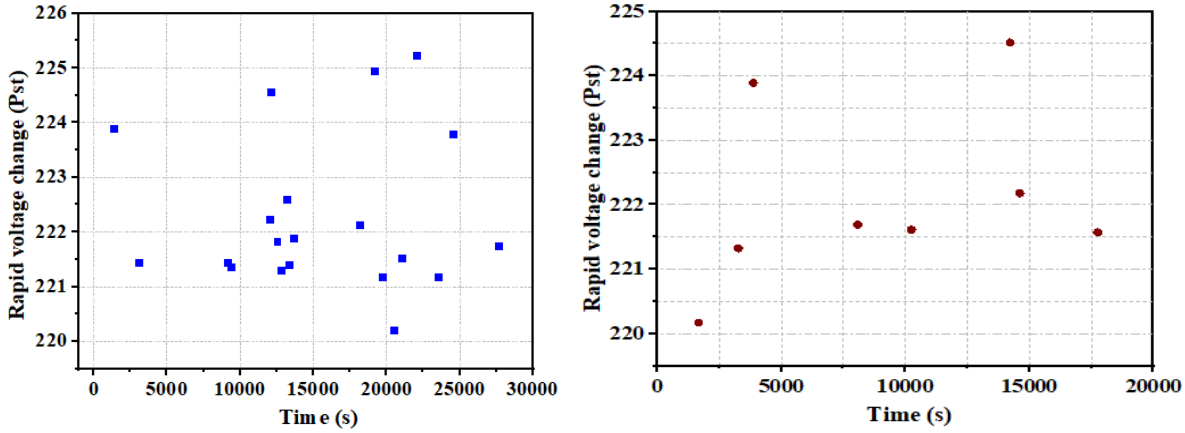

Fig. 4.9. Voltage events a) 400 Wm^{-2} scenario b) 1000 Wm^{-2} scenario

4.1.1.6. Power factor

The power factor (cos ϕ) (PF) shows the phase angle between the current and the voltage signals of the AC output. It is generally expressed as a decimal or in percentage. Per the IEEE 1547 standard, solar PV grid-connected inverters are to be designed to operate at power factors close to unity. To comply with the standards, inverters are designed to suppress the reactive power to zero to achieve the abovementioned characteristic. The studied microinverter showed the same properties when the solar simulator (non-intermittent PV source) was used. The technical regulations concerning power factor for most countries specify that the power factor range at the point of common coupling should be ≥ 0.95, whether leading or lagging (Al-Shetwi et al., 2020). Data were recorded at the time interval of 3 s. The maximum power factors were 0.99502 and 0.99627 for the 400 Wm^{-2} and 1000 $Wm^{-2,}$ and the minimum values were 0.9 and 0.9213 for 400 Wm^{-2} and 1000 Wm^{-2}, respectively. Throughout the study, the trend of power factor was within the standard range except for four points within the study where the power factors were outside the prescribed scope, which may be due to some sudden losses. These occurred for both cases of 400 Wm^{-2} and 1000 Wm^{-2}, but at different times, as shown in Fig. 4.10.

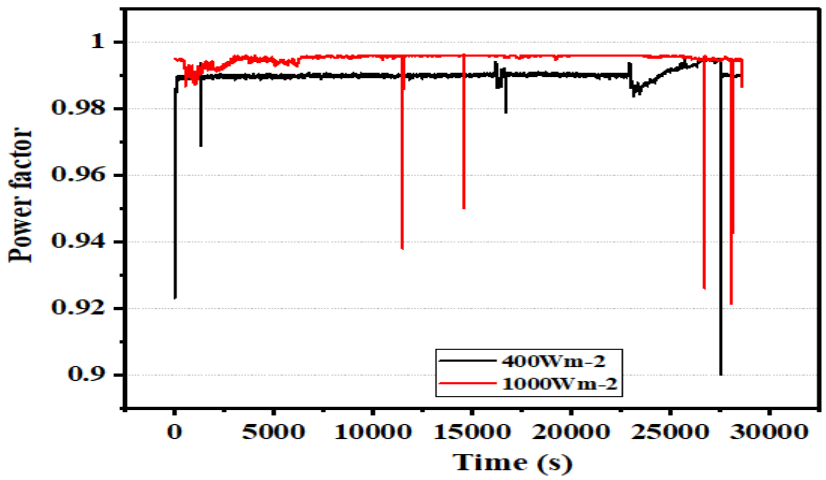

Fig. 4.10. Power factor for 400 Wm^{-2} and 1000 Wm^{-2}

4.1.2. Real modules with the experimental setup

In this section, the results obtained from the real modules under outdoor conditions using the GUNT setup are discussed, and comparisons made with the results that were got whiles using the solar PV simulator.

4.1.2.1. Frequency

Fig. 4.11 presents the frequency profiles for the three different solar modules studied with the microinverter. The interval for measurement was 6 s. Results show that all the profiles obtained were within limits provided by the referenced standards, EN 50160 (CENELEC, 2007). The three profiles showed similar trends, as seen in Fig 4.11. The minimum, maximum and average values for all the cases showed no significant differences. This was evident in the standard deviation of 0.014005 Hz, 0.014324 Hz and 0.014175 Hz, respectively, for Solarex, Dunasolar and Juta module setups. There was no significant difference between results under the solar simulator and those under the real outdoor operation.

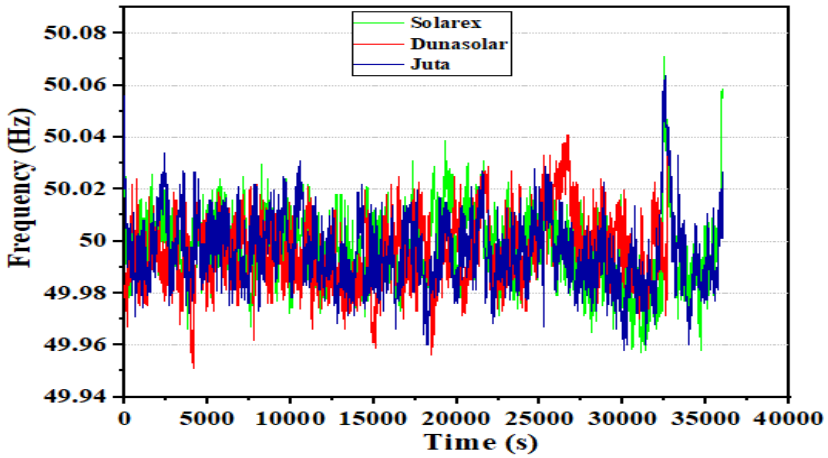

Fig. 4.11. Frequency profiles for Dunasolar, Solarex and Juta module setups

4.1.2.2. Phase voltage for the three different systems under outdoor conditions

The voltage profiles of the different technology solar PV modules studied under outdoor conditions using the GUNT and the 2E microinverter are presented in Fig. 4.12. According to the various standards EN 50160, IEC 61000-4-6 (IEC Standard, 2015; Markiewicz, H., Klajn, 2004), the voltage profiles observed under the studied modules were all within the prescribed voltage limits. The voltage profiles for the Solarex module and the Juta module recorded voltages that were all above the nominal voltage of 230 V. The Dunasolar had voltage values of less than 1% that were below the nominal value of 300 V. The maximum values recorded were 237 V, 238V, 235 V for Solarex, Juta and Dunasolar setups, respectively. The minimum voltages were 231 V, 231 V and 225 V for Solarex, Juta and Dunasolar, respectively. The average voltages were 234.6 V, 235 V and 231.7 V, respectively, for Solarex, Juta and Dunasolar modules. The glass-glass frameless module (Dunasolar) recorded the lowest range of voltage profile. The standard deviation was highest for the voltage profile of the Dunasolar (1.157 V) module compared to the pc-Si Solarex (0.727 V) and the mc-Si Juta modules (0.914 V). Comparing the voltage profiles recorded under the solar PV simulator with the results of

the real modules in outdoor operation, the 400 Wm^{-2} scenario under the solar simulator measurements had the highest voltage deviation, which was closely followed by the voltage profile of the Dunasolar module, even though both cases recorded a voltage variance of 10 V. The maximum voltages under both scenarios with the steady solar simulator were higher than all the studied cases with the real solar modules under outdoor operation. The deviations in the voltages recorded for the study under the solar simulator were higher than the standard deviations for the real solar modules under outdoor operation. However, both cases had the profiles within limits set by the various standards.

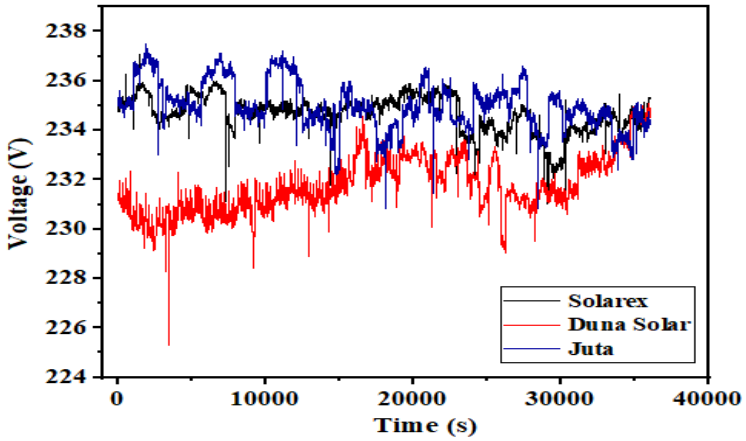

Fig. 4.12. Voltage profiles for Dunasolar, Solarex and Juta modules

4.1.2.3. Power factor

Figs. 4.13, 4.14 and 4.15 present the solar radiation profiles and the power factor (PF) profiles recorded for the different module setups used during the outdoor measurements to assess the performance of the microinverter. The power factor output depended significantly on the available irradiation as the power factor is derived from the values of the active power and the apparent power. This is an indication of the voltage and the current waveforms being out of phase. From the results, it can be seen that all the three cases produced high percentages of values that were outside the limits specified by the various standards for grid-connected solar PV systems, which should be ≥0.95, whether leading or lagging (Al-Shetwi et al., 2020). Except for the case of the Solarex modules, the power factors plunged into the negatives for the other cases with the lowest power factors reaching -1.49 and -1.33, respectively, for Dunasolar and Juta modules. Comparing the results of the outdoor measurements to the study under the steady PV simulator, the power factor profiles recorded for all the cases studied using the solar simulator were within the standard limits, whiles the profiles for all the cases for the outdoor study had values that were outside the set limits. This points to the fact that unsteady solar radiation has a significant impact on the power factor profile. This was evident in the trend and correlation of the measured irradiation with the power factor profiles, as shown in Figs. 4.13, 4.14 and 4.15. The trends were similar for all the three cases studied. The percentage of measured PF values below the standard limits for the cases studied was 67%, 54%, and 37% for Dunasolar, Juta, and Solarex module setups.

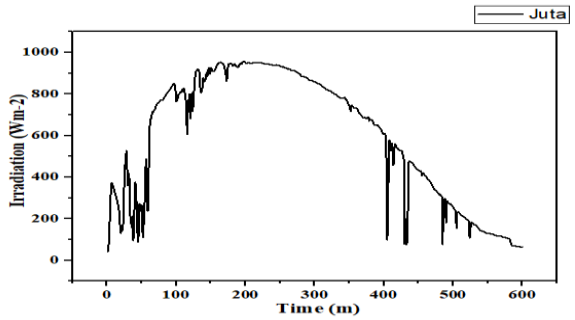

Fig 4.13a. Irradiation for the Juta setup

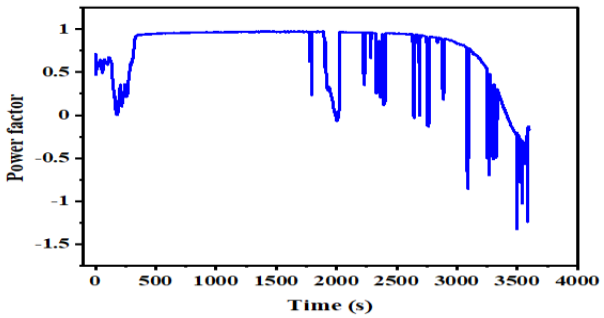

Fig. 4.13b. Power factor profile for the Juta module study

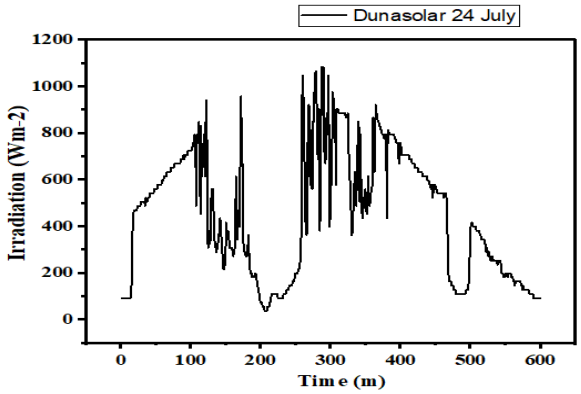

Fig 4.14a. Irradiation for the Dunasolar setup experiment

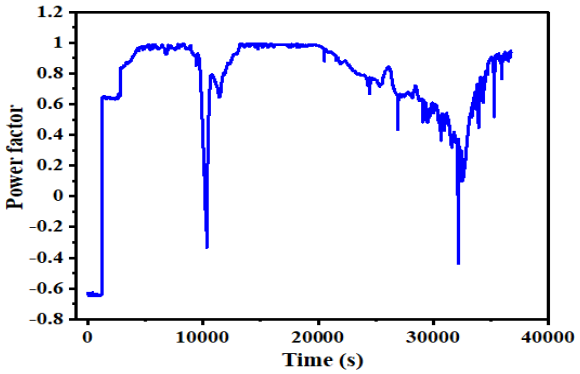

Fig. 4.14b. Power factor profile for the Dunasolar module study

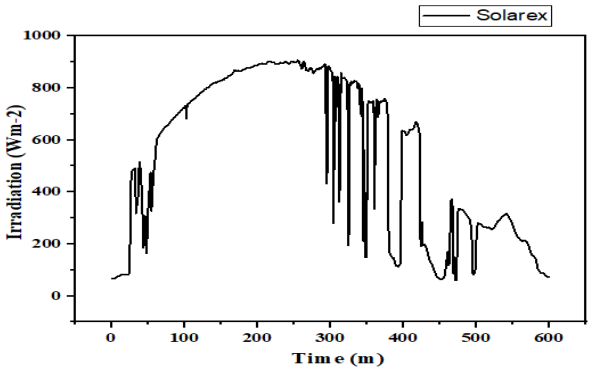

Fig 4.15a. Irradiation for the Solarex setup experiment

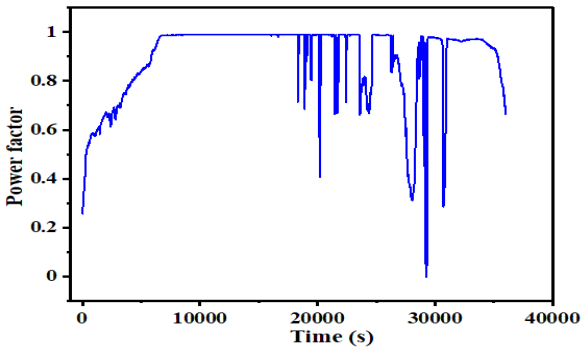

Fig. 4.15b. Power factor profile for the Solarex module study

4.1.2.4. Voltage events of rapid voltage change

The plots of rapid voltage changes with time for the different setups are presented in Fig. 4.16, Fig. 4.17, and Fig. 4.18. There were about 14 instances of voltage events occurring during the study with the Solarex module. The most prolonged duration of the RVC for the study with Solarex modules was 0.13 s with a dip of -11.212 V. The total time for the changes was 2.4 s. The least change was -5.966 V, which lasted for 0.1s. Results show that the study with the Juta module had the most voltage events of thirty-seven during the period of experimentation, while the study with the Dunasolar recorded twenty RVC. The recorded RVC for the outdoor study were negative events and were within limits prescribed by the various standards (IEC 61000-4-30). The greatest RVC for the Juta study was -11.32 V and had a duration of 0.04 s. The total

time for the RVC for the investigation with the Juta module was 2.29 s. There were 20 RVC for the Dunasolar study. The total time was 1.28 s, with the most significant change being -11.32 V, which lasted for 0.04 s. In terms of power quality disturbances with regards to RVC, it can be said that the study with the Juta module had a high-power quality disturbance. The RVC for the study with Solarex modules, Dunasolar modules and Juta modules are presented in Figs. 4.16 a, b and c, respectively.

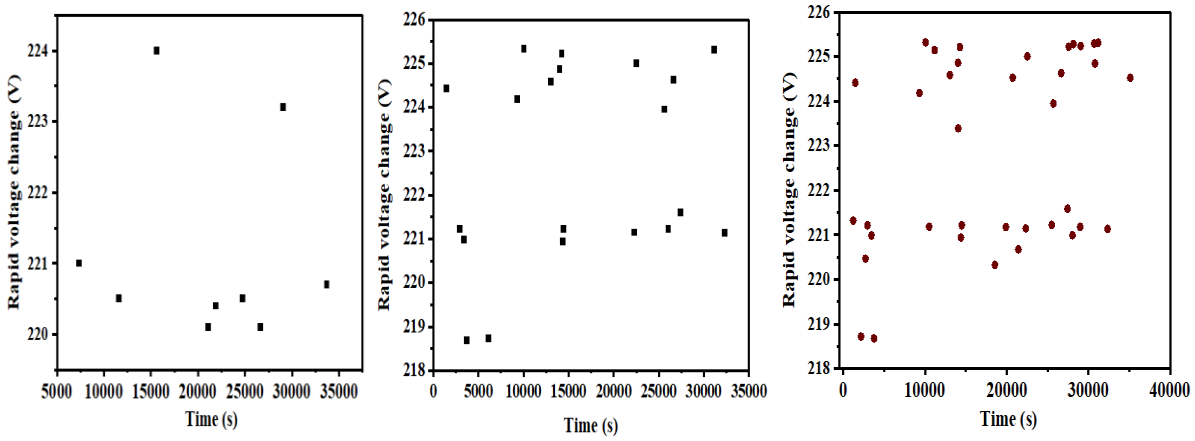

Fig. 4.16. RVC for the study with a) Solarex modules b) Dunasolar modules and c) Juta modules

4.1.2.5. Voltage short-term and long-term flicker

The results for the voltage flicker for the study in outdoor conditions are shown in Fig. 4.19. With reference to the standards for Pst at the PCC for grid-connected PV systems (EN 6100, IEEE 1547 and IEC 61000-3-3), Pst < 1.0 V and also between 0.6 and 0.9 pu for Plt and Pst, respectively (Basso et al., 2015). The percentage of the recorded voltage flicker that fell outside the regulations for the various cases of the study was 2.5% for both Juta and Solarex modules and 4% for Dunasolar modules. The most severe of the recorded short-term flickers were 1.5, 1.6 and 2.9 for the investigation with the Solarex module, Juta modules and the Dunasolar module, respectively. Studies have shown that the primary power quality issues caused by the intermittent PV power generation are voltage fluctuation and light flicker (Shivashankar et al., 2016; Zhao et al., 2013). A study by (Lim and Tang, 2014) concluded a positive correlation between the PV system and flicker severity. They inferred that flicker values were as a result of the fluctuation of PV power output. (Pakonen et al., 2016) demonstrated that intermittent PV power production generates significant levels of short-term flicker values. An empirical study by Rahman et al. also revealed a minimal correlation between varying PV power generation and short-term flickers (Rahman et al., 2018).

Comparing results of the outdoor study with the results of the cases with the solar simulator, the percentage of the flickers of all the three instances of the outdoor investigation that did not meet the standard requirements were all less than the results with the study with the solar simulator. Thus, the examination with the simulator had a higher severity of short-term flickers. It can be inferred that the intermittence of solar radiation (intermittent PV power generation) did not have a significant correlation with the measure of Pst in power output from the studied microinverter with the various setups.

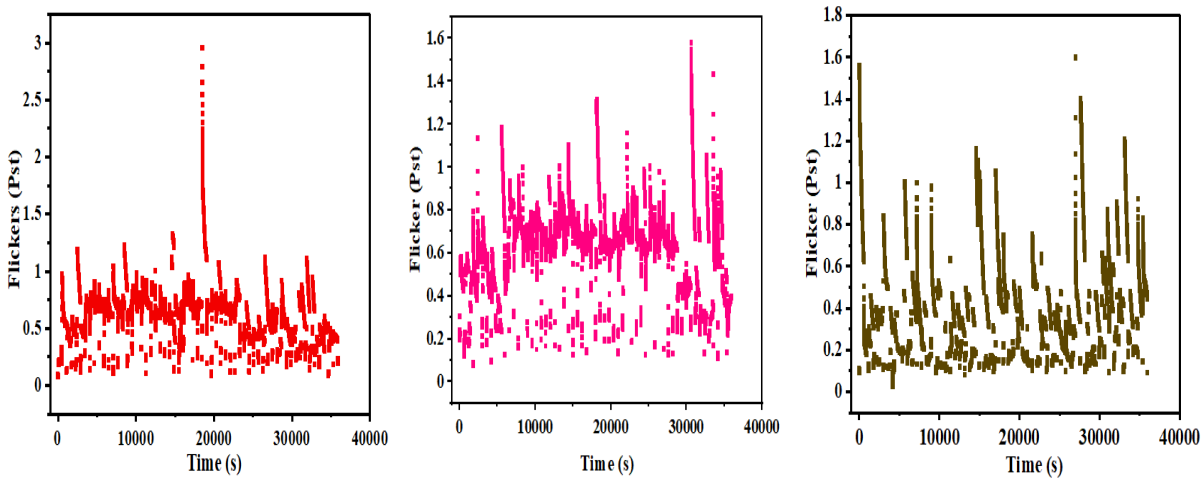

Fig. 4.19. Voltage flickers for a) Study with Dunasolar b) Study with Juta c) Study with Solarex

4.1.2.6. Current individual harmonic distortions

Figs. 4.22 presents the levels of harmonic distortions in the current output. Results revealed that the individual harmonic distortions for Juta, Dunasolar and Solarex scenarios were within the limit prescribed in IEEE 519 and the IEC 61000-3-2 standards. The individual harmonic distortions for all three cases were below 0.05%. However, the total harmonic distortions far exceeded the standard limit of 5% at the PCC for grid-connected PV systems. The CTHD for Juta, Dunasolar and Solarex were 27.43% and 33.6% and 14.28%. The study with the amorphous silicon glass module (Dunasolar) recorded the highest CTHD. It was evident that the CTHD increased with increasing time for all cases studied in the outdoor condition. The level of the harmonic content of the output signal is dependent on the carrier frequency and the switching function. At low irradiation levels or increased temperatures, solar PV systems produce low fundamental components; consequently, increasing the generation of total harmonic distortions at fixed switching frequencies (Jadeja et al., 2020).

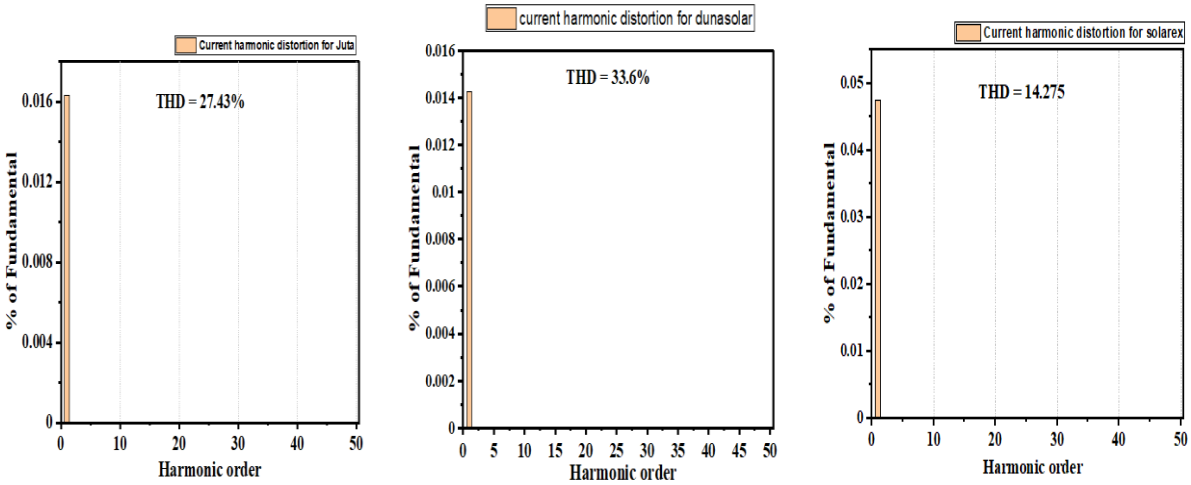

Fig. 4.22. Current harmonic distortions for a) Juta modules b) Dunasolar modules and c) Solarex modules

4.1.2.7. Current total harmonic distortion profiles

The results of the generated current THD for the studies with the solar simulator showed different trends compared to the results with the outdoor studies with the real solar modules, as presented in Fig. 4.23. It was observed that the CTHD output with the solar simulator (constant PV generation) was relatively steady with non-significant changes throughout the study. The CTHD generated in the outdoor studies with the microinverter had their minimum values at the start of the study at 8 am. However, the trend changed with time; it began to increase for all the three cases, even though the values were different for all the cases. The increase in the output for the Solarex, however, had a drastic upward change at about half past noon, after which it continued to increase linearly with time until the end of the study.

It was evident the strong correlation between the drastic change in the current THD of the Solarex module with the trend of irradiation for the day. It was apparent that at the time of change, there was an unstable solar radiation incident on the modules, as shown in Fig. 4.15, and this intermittence continued until the end of the experimentation. The CTHD output for the Solarex was also the least from the start of the investigation until the point of the drastic increase at about noon when it rose above the results for the solar simulator but not the above the results for the other outdoor investigations. The trend for the Dunasolar (a-Si frameless glass solar module) increased continuously from its minimum value at the start of the study. It showed a unique behaviour during low and unsteady irradiation values. The THD increased drastically during such periods of irradiations, with values reaching as high as 126%. However, during periods of fairly steady solar irradiations, the generated THD for the Dunasolar was relatively stable.

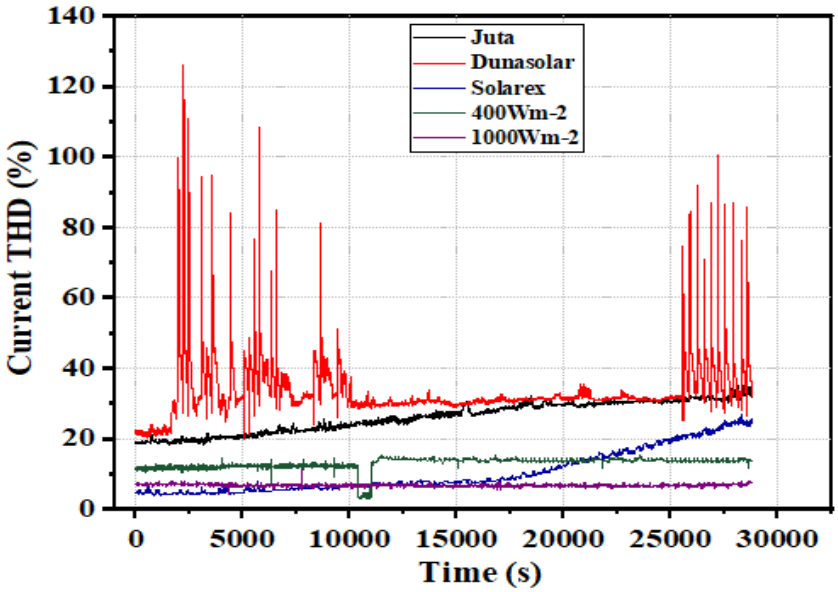

Fig. 4.23. Current THD for the studies with Juta, Dunasolar, Solarex, 400 Wm^{-2} and 1000 Wm^{-2}

4.1.2.8. Voltage individual harmonic distortion

The voltage harmonic contents for the outdoor measurements are presented in Figs. 426a, b, and c. The individual harmonic distortions and the total harmonic distortions recorded for all the cases studied in the outdoor conditions were within limits stated by the standards (IEEE 519, IEC 61000-3-2), as shown in Tables 2.5 – 2.7. The VTHDs were 1.94%, 1.968% and 2.03%, respectively, for Juta modules, Dunasolar module and Solarex modules. The 7^{th} harmonic order for the Dunasolar module had distortions that were above 3% but less than 5%. The other individual harmonic distortions for Dunasolar were below 3%. The individual harmonic distortions for Juta modules were all below 3%. The 5^{th} Harmonic order of the Solarex modules had distortions of 3.5%, apart from which the distortions for all the other harmonic orders were below 3%. The results (individual and total voltage harmonic distortions) for the outdoor study for all the scenarios were less than the values measured for the investigation with the steady irradiation source (solar simulator). It can be inferred that the intermittency of solar radiation has no significant correlation with the voltage harmonic content recorded for all the cases studied.

4.2. Power output quality of GMI 300 and Maysun-600W-B microinverters

This section presents the results and analyses the characteristic output of the different commercial PV grid-connected microinverters (GMI 300 (Holland) and Maysun-600W-B (China)) using different sets of modules of various technologies under varying conditions in outdoor operation.

4.2.1. Voltage profiles for the different setups

The voltage profiles recorded for the different set of modules connected to the Holland inverter are shown in Fig. 4.24a and b. Voltage measurements were taken at intervals of 200 ms. The EMC standards, EN 50160, EN 61000 stipulates that the voltage should be within the limits of ±10% for low voltage and medium voltage power systems (CENELEC, 2007). The results for the different sets of modules (Solarex and Juta) show that the profiles were within the limits specified by the various standards of ±10%. The maximum and minimum voltages recorded during the experimentation period were 238.9 V and 229.8 V, and 237.8 V and 232.3 V, respectively, for Juta and Solarex modules. The standard deviation of 0.8956 V and 1.1754 V for Solarex and Juta, respectively, indicates a lesser disparity in the voltage output for Solarex than the Juta modules. The average values were 235.0 V and 235.9 V for Juta and Solarex modules, respectively.

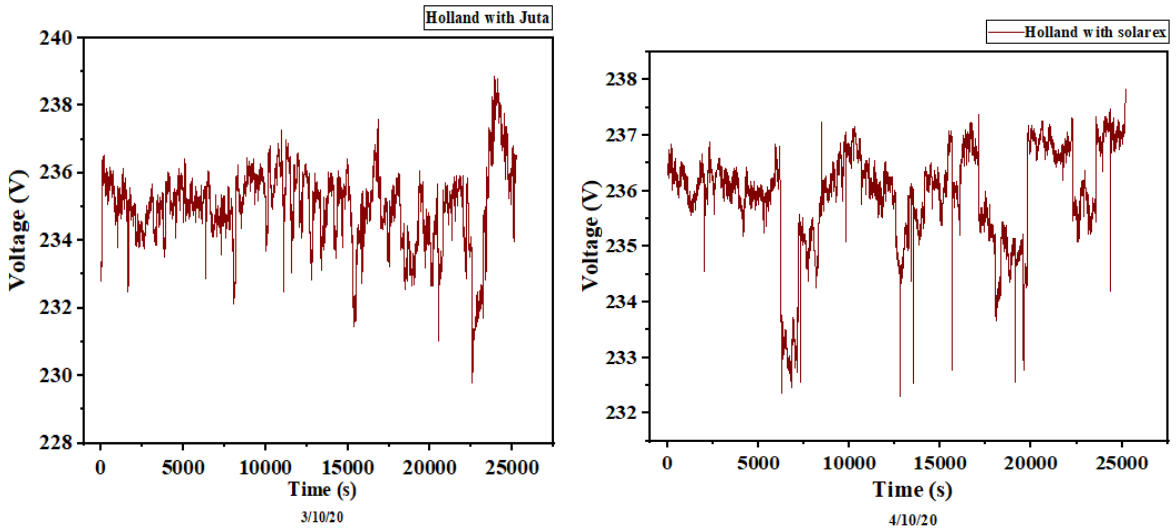

Fig. 4.24. Voltage profiles for Holland microinverter a) with Juta modules b) with Solarex modules

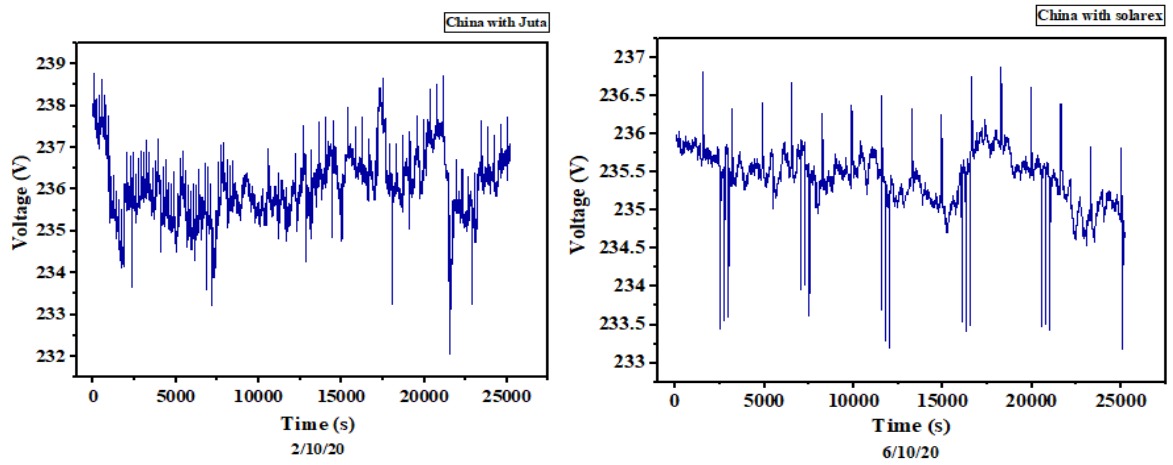

Fig. 4.25. Voltage profiles for China microinverter a) with Juta modules b) with Solarex modules

Results obtained for the China microinverter shows a similar voltage profile recorded by the Holland microinverter. The measured voltages for both sets of solar modules connected with the China microinverter were within the stipulated standards of ±10% of the nominal voltage. The voltages, however, were all above the nominal voltage of 230 V. The maximum and minimum voltages for the two cases were 238.8 V and 232.0 V, 236.9 V and 233.2 V for Juta and Solarex modules as shown in Fig. 4.25. The average voltages were 236.0 V and 235.4 V whiles the standard deviations were 0.748 and 0.395 for Juta and Solarex modules, respectively. It was observed that the recorded voltages for all the microinverters studied under the outdoor conditions with the different set of modules were all within the acceptable standards for grid-connected systems and had voltages that were all above the nominal voltage. The Holland microinverter had voltages with higher deviations than the China microinverter. Also, results with the Juta modules showed higher standard deviations than voltages recorded with the Solarex modules.

4.2.2. Power factor

According to the IEEE 1547 standard for power factor, solar PV grid-connected inverters are to be designed to operate at a power factor close to unity. The technical regulations concerning power factor for most countries specify that the range at the point of common coupling should be PF≥0.95, whether leading or lagging (Al-Shetwi et al., 2020). With reference to the specified standard, the Holland microinverter with the Juta modules recorded a power factor profile with all its values below the set standard. The maximum and the minimum values recorded were 0.98 and -1.06, respectively, as presented in Fig.4.26. The average power factor and the standard deviation were 0.796 and 0.14, respectively. However, the Holland microinverter with the Solarex set of modules had 0.398% of its power factor within the accepted range. The rest were below the 0.95 standards. The maximum and the minimum power factor were 0.98 and -1.056, respectively. The standard deviation was 0.3915 for the Holland inverter, and Solarex set of modules.

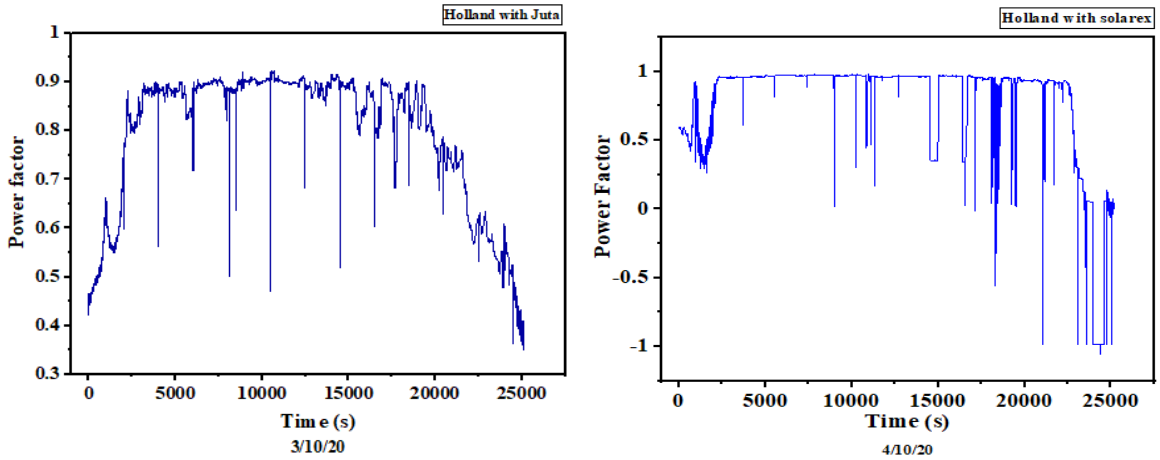

Fig. 4.26. Power factor profiles for Holland microinverter a) with Juta modules b) with Solarex modules

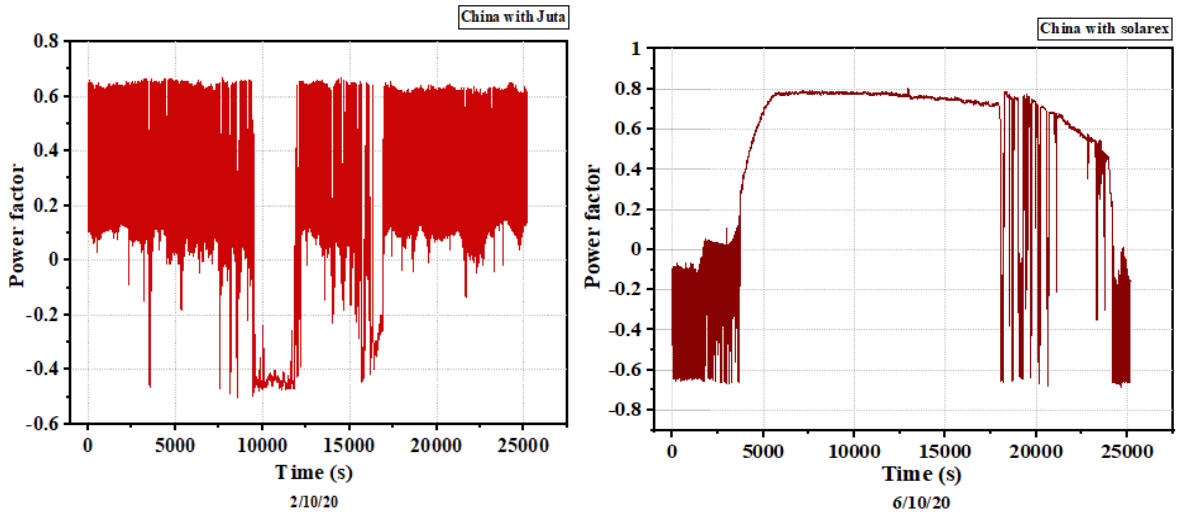

Fig. 4.27. Power factor profiles for China microinverter a) with Juta modules b) with Solarex modules

A unity power factor in an electrical system leads to the full use of the total energy supplied to the load. A lower power factor leads to an increase in the current flow through the lines, which causes the voltage to drop in the conductor. Consequently, lowering the voltage of various

equipment. A lower power factor causes a decline in the power of the distribution system. This may cause overload and overheat in different types of equipment. The low power factor indicates that the current is lagging the driving voltage. In a situation like this, the load consumes both the active and reactive power. As the consumption of reactive power is increased, the phase angle between the active power vector and the apparent power vector also increases, which causes the lowering of the power. The apparent power is also increased without any effect on the active power. However, a reduction in the reactive power to zero causes the phase angle to also decline to zero leading to a unity power factor (GSES, 2015).

The PF recorded by the China microinverter in the studies conducted with the various set of modules were below the specified standard, which should be ≥0.95. The maximum and minimum PF recorded for the China microinverter were 0.67 and -0.5, and 0.8 and -0.69 for Juta and Solarex modules, respectively, as shown in Fig. 4.27. The average power factor and the deviation in PF values for the two setups were 0.09 and 0.287, and 0.52 and 0.373 for Juta and Solarex, respectively.
It is evident from the results that there was higher production of reactive power, especially for the China inverter with the Juta setup, causing the power factor to remain low and violating the specified standard for the greater part of the experimentation. It was observed that the China microinverter is integrated with an MPPT algorithm which suffers from the disadvantage of being slow in tracking especially if solar radiation had not been high and stable for an extended time. Due to this, the active power recorded was extremely low mainly in the negatives. This was evident in the results for the setup for the China inverter with Juta modules. Kadri et al. (2011) mentioned that voltage-controlled MPPT could curtail the losses in power caused by dynamic tracking errors that would have occurred under intermittently changing solar radiation conditions (Kadri et al., 2011).

4.2.3. Current individual and total current harmonic distortions

The standards of reference of the acceptable range of current harmonic distortion are the IEC 61000-3-2, IEEE 1547, and AS 4777.2 standards listed in Tables 2.5-2.7. According to the standards for the odd harmonics of 33 < h, the acceptable least harmonic distortions are to be below 0.3%. The least for the even harmonics as specified by the referred standards is to be below 0.5%. Results for both microinverters (Holland and China) showed that the individual current harmonics were within the specified limits given the various standards. The highest recorded current harmonic distortions were for the first harmonics for all the four cases studied with the microinverters. The highest harmonic distortions were 0.0126% China with Juta, 0.196% for China with Solarex, 0.027% for Holland with Juta and 0.130 for Holland and Solarex. The China microinverter recorded current distortions for all odd harmonic orders up to the measured harmonics of 50.

The Holland microinverter recorded current distortions for only odd harmonics even though not for all the 50 harmonics. The CTHD for the two microinverters connected to the different set of modules studied under varying ambient conditions far exceeded the specified limit of <5% by the various standards, for both odd and even harmonics as stated in Tables 2.5 – 2.7. The CTHDs were 65.82%, 37.97%, 129.48% and 91.01% for Holland inverter with Juta modules, Holland inverter with Solarex modules, China inverter with Juta modules and China

inverter with Solarex modules, respectively. CTHD recorded for the test on the Juta modules (mc-Si) were higher than the results for the test on the Solarex (pc-Si) for both microinverters studied as presented in Fig. 4.28 and Fig. 4.29. Also, the THDs for the China microinverter were higher than the THDs for the Holland microinverter for the entire experimentation period for all the conditions studied. The Holland microinverter also recorded current THD that were beyond the limit for the Juta modules even though for the Solarex modules, except for 0.01% all the current THD recorded were also beyond the specified limits. It has been observed that the THDs for the Solarex (pc-Si) were more stable over a prolonged period during the measurement compared to the results for the Juta (mc-Si) modules.

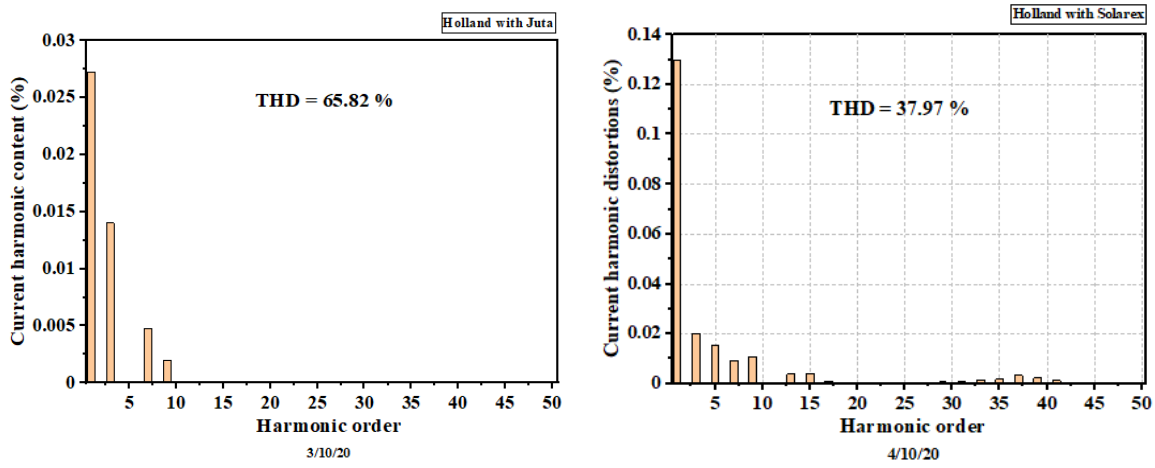

Fig. 4.28. Current harmonic distortions of Holland microinverter a) with Juta modules b) with Solarex modules

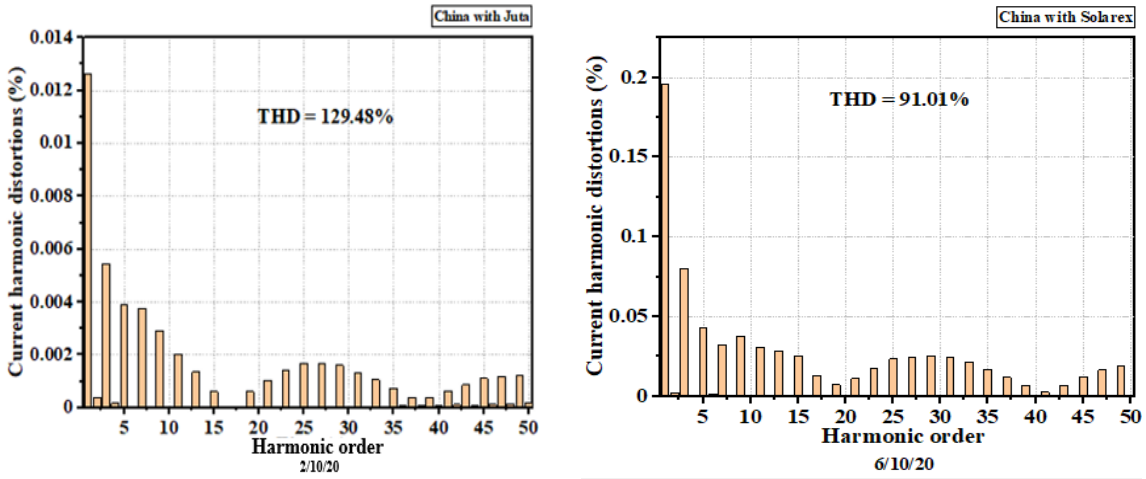

Fig. 4.29. Current harmonic distortions of China microinverter a) with Juta modules b) with Solarex modules

Results for the current total harmonic distortions for the various microinverters have been presented in Fig. 4.30. It has been observed that the total distortions for the China microinverter were all beyond the limit (THD<5%) specified by the various standards IEC 61000-3-2, IEEE 1547, AS 4777.2 listed in Tables 2.5 – 2.7. It was observed that the THDs for the Solarex (pc-Si) were more stable over a prolonged period during the measurement compared to the results

for the Juta (mc-Si) modules. The high CTHD observed may be due to the presence of non-linearity of some components within the microinverter, which increase the current harmonics injected at the PCC.

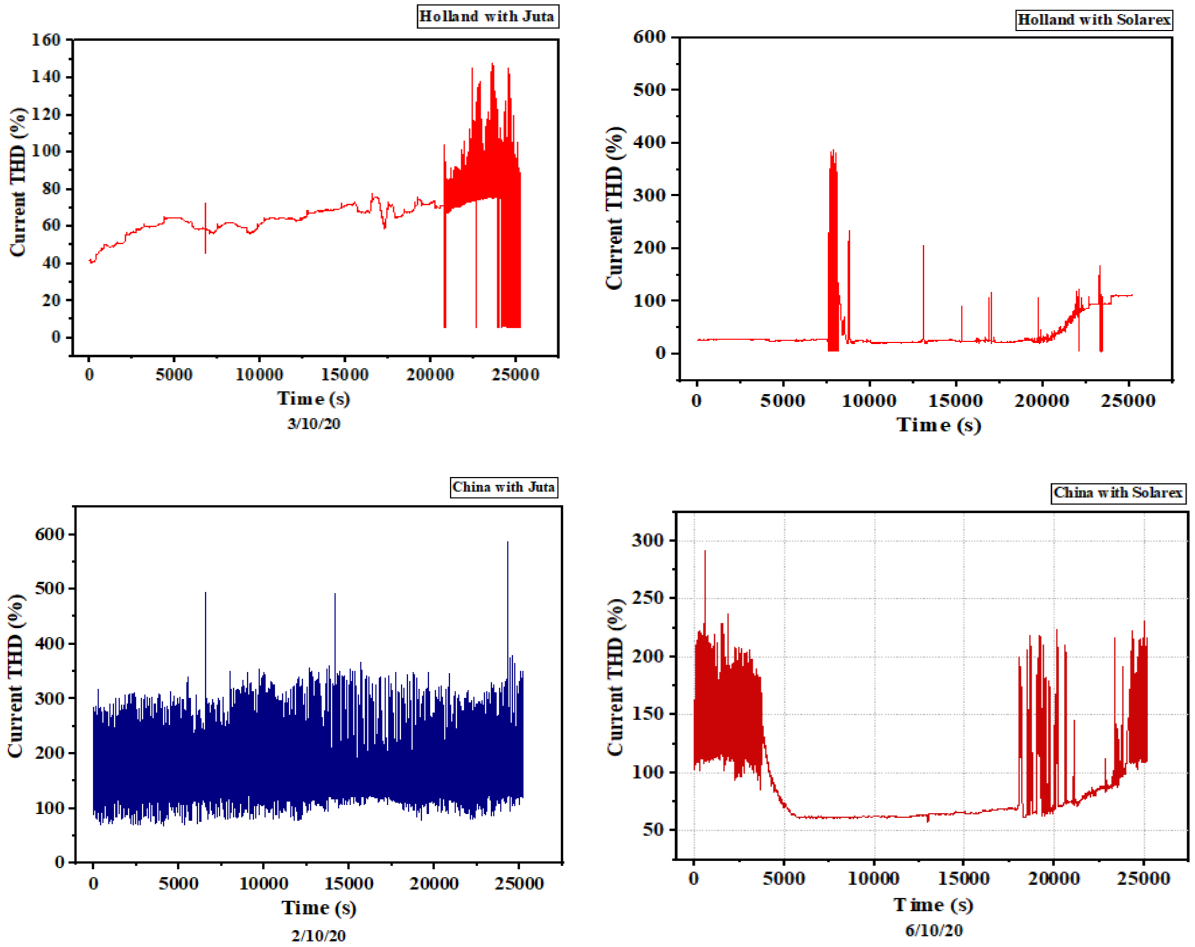

Fig. 4.30. Current total harmonic distortions a) Holland with Juta modules b) Holland with Solarex modules c) China with Juta d) China with Solarex modules

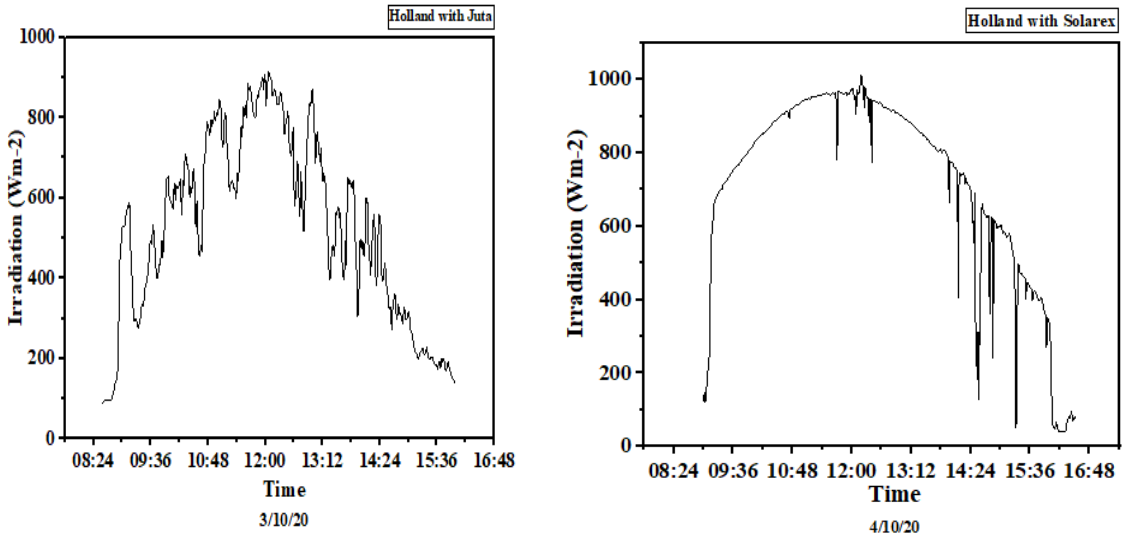

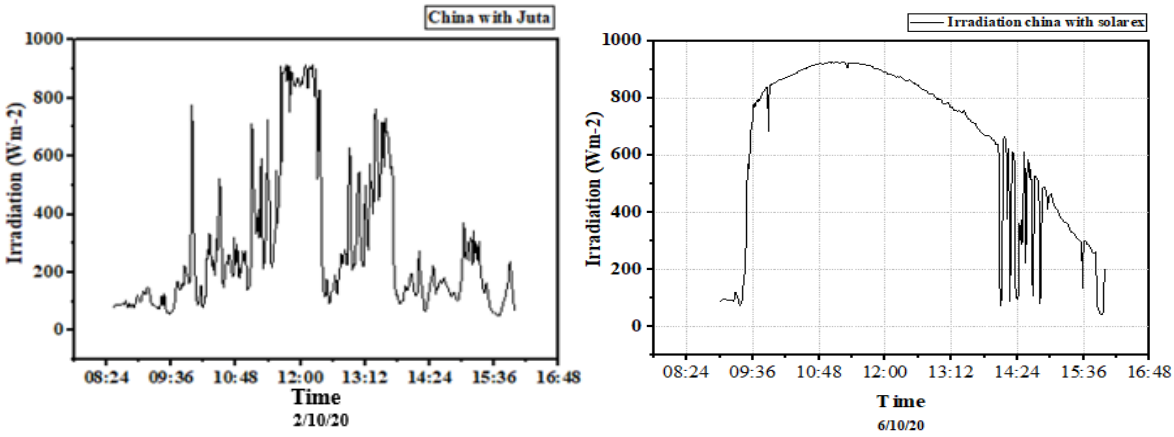

Fig. 4.31. Solar radiation for measurement days of a) Holland with Juta b) Holland with Solarex c) China with Juta d) China with Solarex

The maximum and minimum current THD recorded for the Holland microinverter for the different sets of solar modules were 387.69% and 4.55%, and 147.79% and 5.24%, respectively for Solarex and Juta modules. The average current THD and the disparity in the recorded values in terms of standard deviation were 37.84% and 31.05, 65.82% and 10.95, respectively, for Solarex Juta modules. For the china microinverter, the maximum and minimum current THD were 291.82% and 57.44%, and 586.75% and 66.68%, respectively for Solarex and Juta modules. The average CTHD and the standard deviations were 91.01% and 40.64, and 129.48% and 37.49, respectively for Solarex and Juta modules. It was observed that the Holland microinverter had lower deviations in CTHD compared with the China microinverter. The least variation of CTHD was however recorded for Holland microinverter with Juta module settings. It has been observed the correlation between stable solar radiation and a relative constant CTHD, as shown in Fig. 4.30 and Fig. 4.31. It is shown that the CTHD fluctuates correspondingly to the intermittence of the solar radiation. It was observed that the China microinverter suffered the disadvantage of slow tracking of the MPPT algorithm hence its inability to track the MPP at the instance of low solar radiation hence the widely unstable CTHD recorded for its measurement with the Juta modules. It was observed that low irradiation levels and thus the low current output of the inverter caused the CTHD to rise as exhibited in Fig. 4.30 and Fig. 4.31. With similar irradiation levels recorded for the Holland inverter with Solarex and China inverter with Solarex, it has been found that the China inverter recorded a higher CTHD at the same period of high and stable solar radiation compared to the Holland inverter. It has been mentioned that the higher the power factor recorded, the lower the current total harmonic distortion, as demonstrated in Eq. 4.2 (Grady, W M; Gilleskie, 1995). In the non-sinusoidal situations where voltages and currents contain harmonics. This equation provides an insight into the relationship between the true power factor and the CTHD. These two quantities are inversely proportional:

$$\mathrm{PF}_{\mathrm{true}} \leq \mathrm{PF}_{\mathrm{dist}} = \frac{1}{\sqrt{1+(\mathrm{THD_I}/100)^2}}, \tag{4.1}$$

where PF_{true} is the true power factor and PF_{dist} is the displacement power factor.

In other relationships between the PF and CTHD could be represented as Eq. 4.2.

$$PF \approx \frac{\cos\varphi_1}{\sqrt{1+THD_i^2}}. \quad (4.2)$$

This also reveals that the higher the CTHD, the lower the PF. When there is no harmonic present, the power factor is equal to $cos\varphi_1$ (Pinyol Ramon, 2015).

It was observed that the CTHD for the China microinverter presented a unique relationship with the power factor profile recorded for both sets of experiments with Juta and Solarex solar modules. The output curves for the power factor and the CTHD were exactly inverse in shape or a reflection of each other in the horizontal plane, as shown in Fig. 4.32. This observation confirms the essence of Eq. 4.1. However, the inverse relationship between the power factor and the CTHD observed for the China microinverter was not evident in the results for the Holland microinverter. The correlation between low solar irradiation and the total harmonic generated is apparent in the results for the China microinverter and the Juta setup, as shown in Fig. 4.32 and Fig. 4.33. It can, therefore, be said that the Eq. 4.1 does not hold for all the microinverters studied even under high irradiation levels.

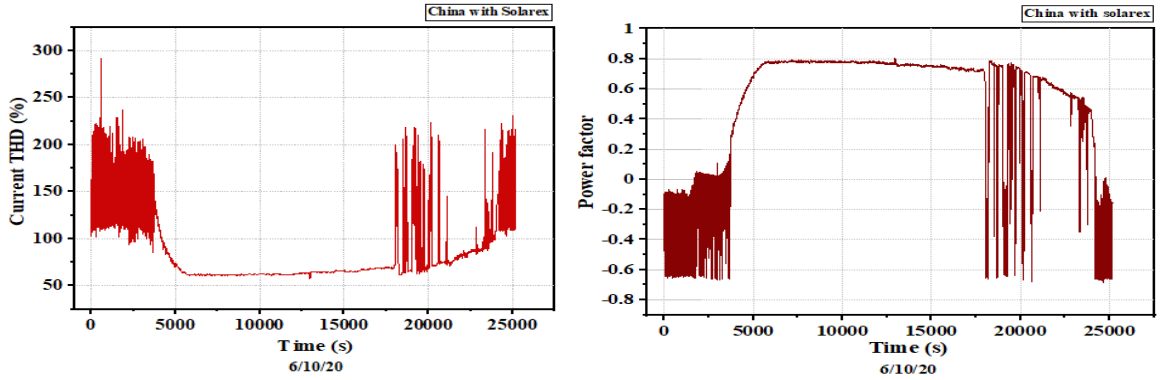

Fig. 4.32. Relationship between the power factor profile and the current total harmonic distortions of the China microinverter

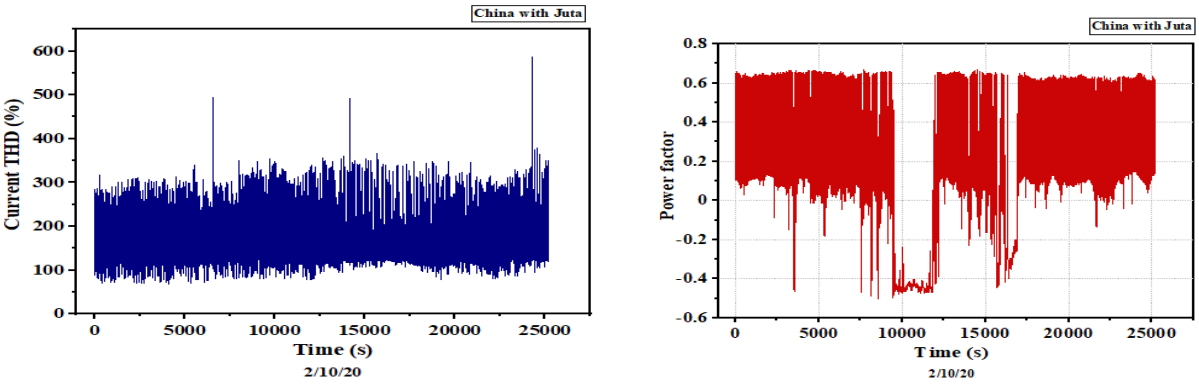

Fig. 4.33. Relationship between the power factor profile and the current total harmonic distortions of the China microinverter

4.2.4. Total voltage harmonic distortions

The voltage total harmonic distortions were recorded at the interval of 200 ms for each microinverter with the different sets of modules. The generated VTHD profiles were compared

with the specified standards for connecting PV systems with the power grid. As stated in Tables 2.5 – 2.7, the VTHD limits, according to the IEEE 519 and IEC 61000-3-2 standards are 8% and 5%, respectively. Results for all the microinverters studied were within the specified limits of 5%. The maximum VTHDs was 2.19%, 2.17%, 2.20% and 2.15% for Holland inverter with Juta, Holland inverter with Solarex Modules, China inverter with Juta modules and China inverter with Solarex modules, respectively. The minimum and average VTHDs for the various settings were 1.78 % and 1.95%, 1.67% and 1.85%, 1.53% and 1.90% and 1.79% and 2.04%, respectively for Holland inverter with Juta, Holland inverter with Solarex Modules, China inverter with Juta modules and China inverter with Solarex modules as shown in Fig. 4.34.

The standard deviations show that the China microinverter with Solarex modules recorded the least variation in the VTHD. The results for standard deviation were 0.1003, 0.111, 0.037 and 0.117, respectively for Holland inverter with Juta, Holland inverter with Solarex Modules, China inverter with Solarex modules and China inverter with Juta modules. A unique pattern in the VTHDs profile for the studied microinverters was observed. There were periodic rise and fall in the output profile. Even though the time span for the change was not according to any observed specific trend, the upper VTHDs at the rise lasted for a shorter period than the VTHDs at the fall. It was seen that for the Holland module, the linkage between the rise and fall of the VTHD was just a single point. However, for the Juta module, the change was gradual.

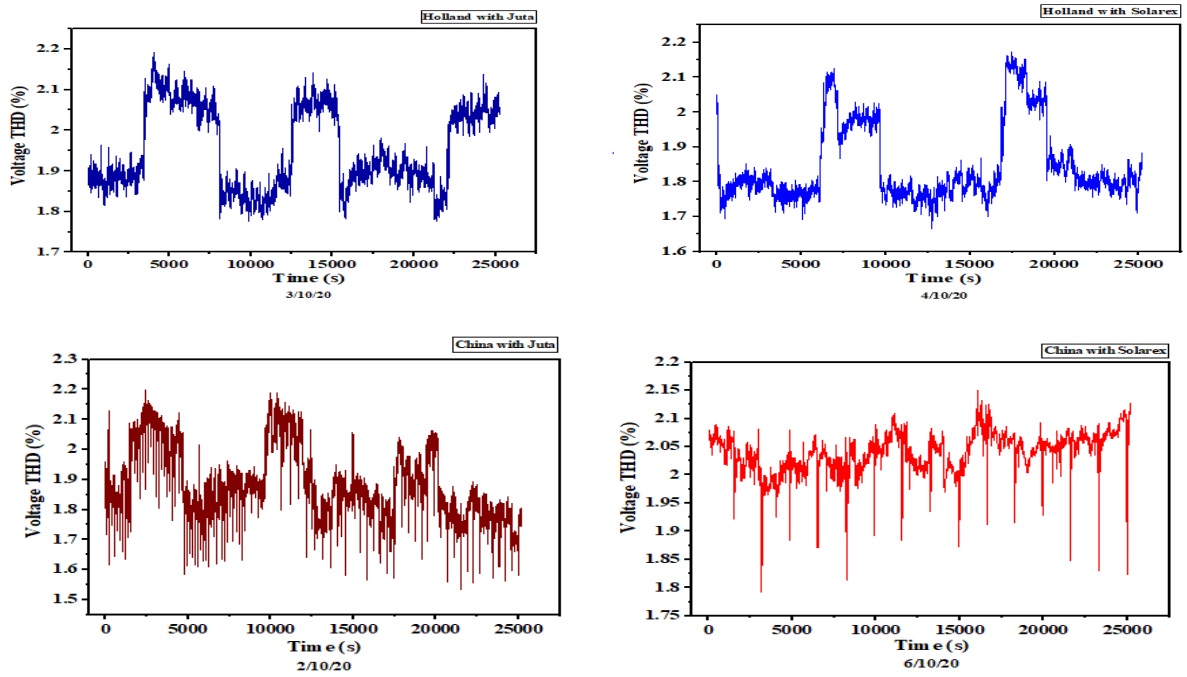

Fig. 4.34. Voltage total harmonic distortions a) Holland with Juta modules b) Holland with Solarex modules c) China with Juta modules d) China with Solarex modules

4.2.5. Voltage harmonic distortions

The voltage individual harmonic distortions for the different settings and microinverters are presented in Fig. 4.35. The 5th harmonic distortions for China microinverter for all studied modules were above 3% (3.14% and 3.18%). All the other individual harmonics for the China microinverter as well as the Holland microinverter were all below 3%. The THDs generated

for the period of experimentation was 1.95%, 1.85%, 1.89% and 2.04% for Holland microinverter with Juta, Holland microinverter with Solarex modules, China microinverter with Juta modules and China microinverter with Solarex modules, respectively. The results for all the microinverters studied were within the specified standards. The individual harmonic distortions for the even harmonics were negligibly low for all scenarios that were examined for the microinverters.

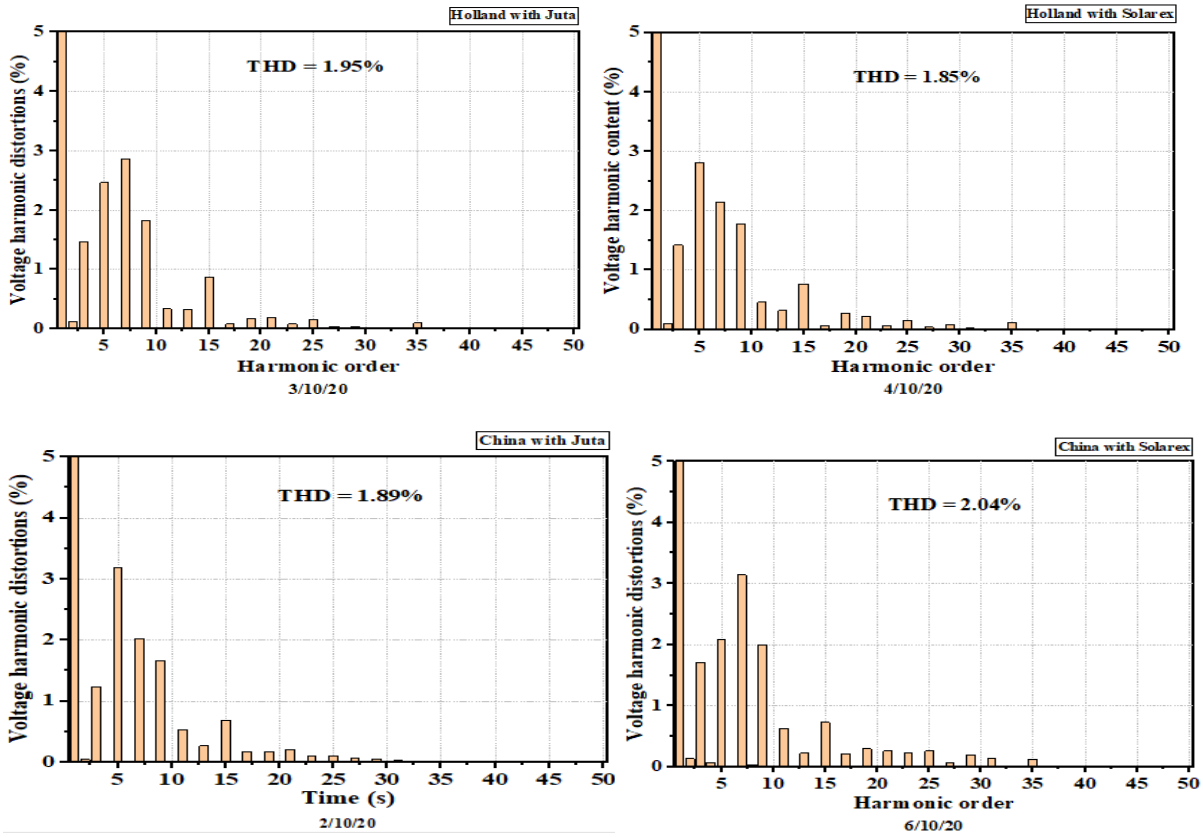

Fig. 4.35. Voltage harmonic distortions for a) Holland microinverter with Juta b) Holland microinverter with Solarex modules c) China microinverter with Juta modules and d) China microinverter with Solarex modules

4.2.6. Frequency profiles of the microinverters

The frequency profiles of the various scenarios of experimentation with the microinverters are presented in Fig. 4.36. The frequency profiles of the grid power output play a critical role in maintaining the grid's power quality, especially with a grid with distributed power generating sources as the distributed sources use the frequency to synchronise with the grid. The standard EN 50160 (CENELEC, 2007) specifies that the frequency should be within ±1% of the nominal frequency. The recorded frequency profile for the entire period was within limits sets by the different standards.

It was observed that the results from all the microinverters were very similar in magnitude. The maximum and minimum frequencies for the different scenarios were 50.05 Hz and 49.96 Hz, 50.05 Hz and 49.95 Hz, 50.06 Hz and 49.94 Hz and 50.08 Hz and 49.94 Hz, respectively for China microinverter with Juta, china microinverter with Solarex modules, Holland

microinverter with Juta and Holland microinverter with Solarex. The average frequencies and the standard deviations were determined as 50 Hz and 0.016, 50 Hz and 0.017, 50 Hz and 0.016 and 50 Hz and 0.021, respectively for China microinverter with Juta, china microinverter with Solarex modules, Holland microinverter with Juta and Holland microinverter with Solarex modules. The average frequencies show strict adherence to the specified limit and the nominal frequency of 50 Hz.

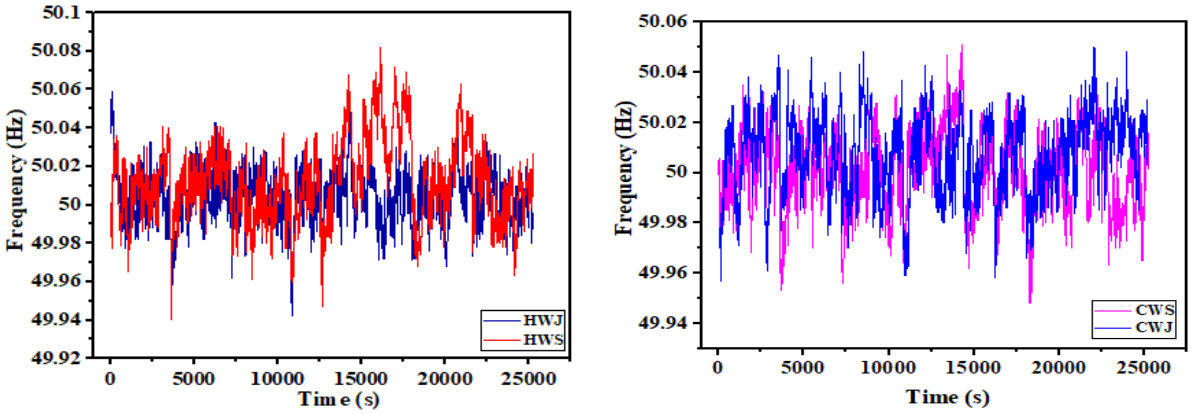

Fig. 4.36. Frequency profiles a) for the Holland microinverter with Juta modules (HWJ) and Solarex modules (HWS) b) for the China microinverter with Juta modules (CWJ) and Solarex modules (CWS)

4.2.7. Voltage flickers

The measured voltage flickers for the various microinverters of the different scenarios are presented in Fig. 4.37. There was no Plt recorded for any of the microinverters with the different modules. The specified reference standards for Pst at the point of common coupling for grid-connected PV systems as mentioned in EN 6100, IEEE 1547 and IEC 61000-3-3 are Pst < 1.0 V and also between 0.6 and 0.9 pu for Plt and Pst, respectively (Basso et al., 2015). Other studies have shown that the primary power quality issues caused by the intermittent PV power generation are voltage fluctuation and light flicker (Shivashankar et al., 2016; Zhao et al., 2013). A study by (Lim and Tang, 2014) revealed a positive correlation between the PV system and flicker severity. They concluded that the presence and magnitude of flickers resulted from the fluctuation of PV power output. (Pakonen et al., 2016) demonstrated that intermittent PV power production generates significant levels of short-term flicker values.

An empirical study by Rahman et al. also revealed a minimal correlation between varying PV power generation and short-term flickers (Rahman et al., 2018). The maximum Pst and most severe for the various scenarios were determined as 1.549, 1.542 1.678 and 1.285 for Holland microinverter with Juta modules, Holland microinverter with Solarex modules, China microinverter with Solarex modules and China microinverter with Juta modules, respectively. The percentages of Pst that were outside the specified limits by the various standards were 0.0069%, 0.001%, 0.0319% and 0.0092%, respectively for Holland microinverter with Juta modules, Holland microinverter with Solarex modules, China microinverter with Solarex modules and China microinverter with Juta modules. It has been shown that China microinverter with Solarex modules recorded the highest severity of short-term voltage flickers compared to the other scenarios investigated. For each experimental setting, short term flickers

were recorded from the start to the end of the process. It was observed from the results that the intermittency of solar radiation had no correlation with the trend of the measured short-term voltage flickers for all settings.

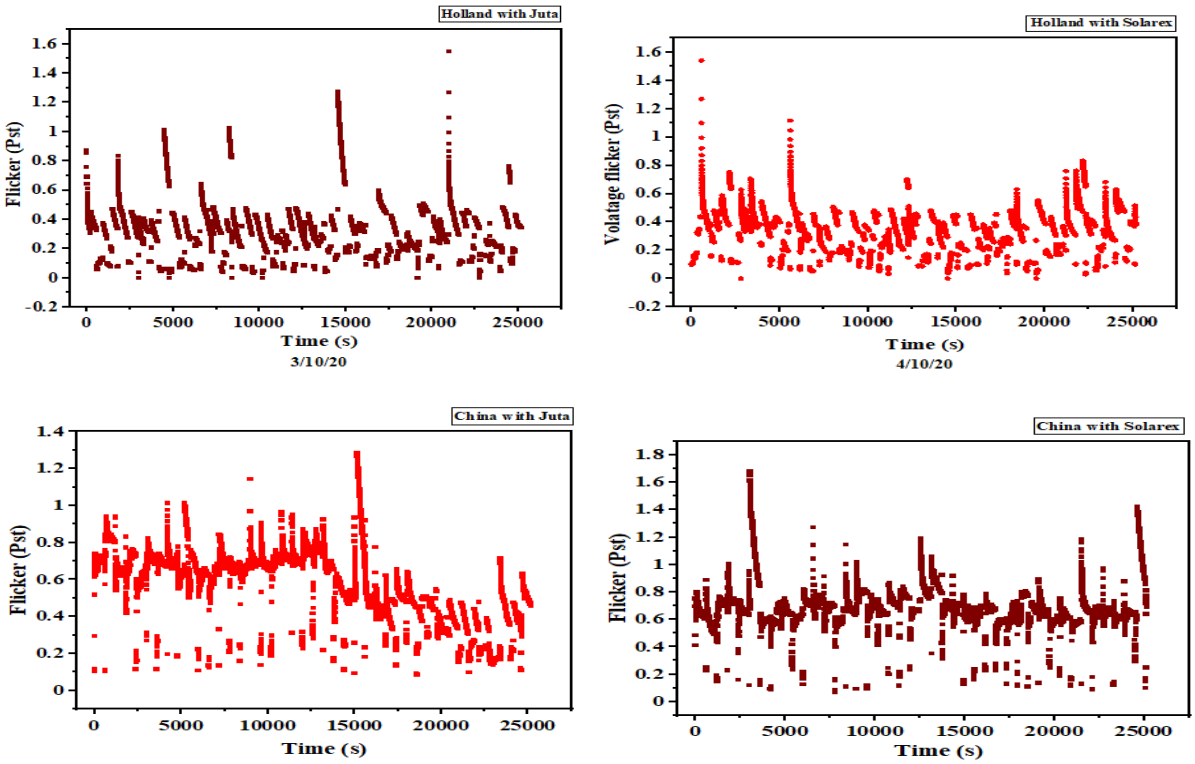

Fig. 4.37. Voltage flicker for a) Holland microinverter with Juta modules b) Holland microinverter with Solarex modules c) China inverter with Juta modules and d) China inverter with Solarex modules

4.2.8. Voltage over deviation

Voltage over deviations were recorded throughout the investigations on the microinverters. The maximum deviations were 3.85%, 3.81%, 3.41% and 2.99% for Holland microinverter with Juta module, China microinverter with Juta module, Holland microinverter with Solarex modules and China microinverter with Solarex modules, respectively. The maximum deviations for the different settings occurred at different times and conditions for each setup. The average deviation recorded for the different setups were 2.36%, 2.62%, 2.58% and 2.17%, respectively, for China microinverter with Solarex modules, China microinverter with Juta module, Holland microinverter with Solarex modules and Holland microinverter with Juta module. It could be inferred that averagely, the China inverter recorded the highest over deviation for the different modules studied compared with all the other setups. China microinverter with Solarex modules; however, recorded the highest average deviation of voltages as shown in Fig. 4.38.

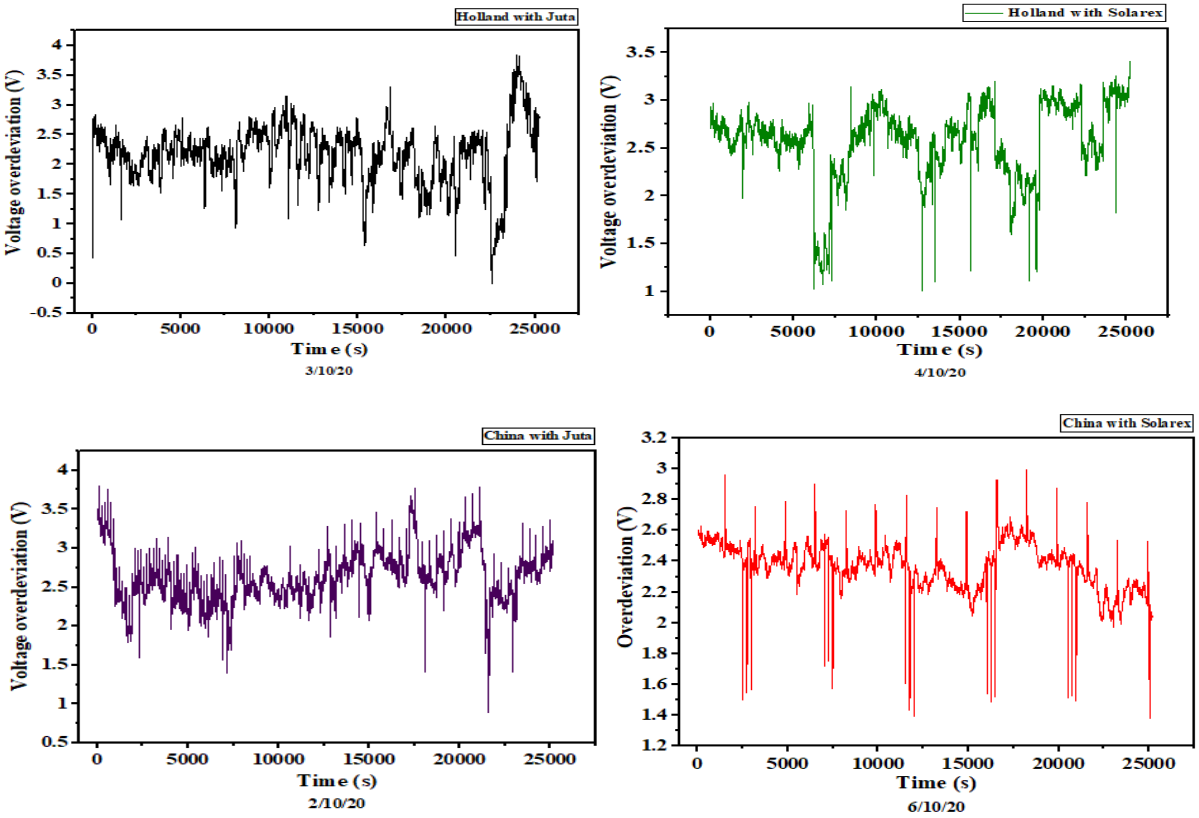

Fig. 4.38. Voltage deviation profiles for a) Holland microinverter with Juta modules b) Holland microinverter with Solarex modules c) China inverter with Juta modules and d) China inverter with Solarex modules

4.3. Power quality analysis of grid-connected PV systems with string inverters

4.3.1. Under conditions of relatively stable but intermittent solar irradiation

Performance analysis has been conducted on the three-phase grid-connected PV systems on the rooftop of the Szent Istvan University student hostel, Godollo – Hungary. In this section, the conditions of a relatively stable solar irradiation over a considerable period of the day after which there was a sudden drop (below 400 Wm^{-2}) in intensity at about 2 pm and beyond have been chosen. Each inverter has a single input point to represent one phase. This day among the other days of measurements was selected for comparison with other contrasting experimental conditions and to determine their influence on the performance of the various grid-connected PV systems. Solar radiation measured for the day and the phase current are presented in Fig. 4.39. The study was conducted for a period of seven hours (9 am to 4 pm). From the start of the task at 9 am, the level of solar radiation was fairly steady with some level of intermittency (in the range of 1- 200 Wm^{-2})

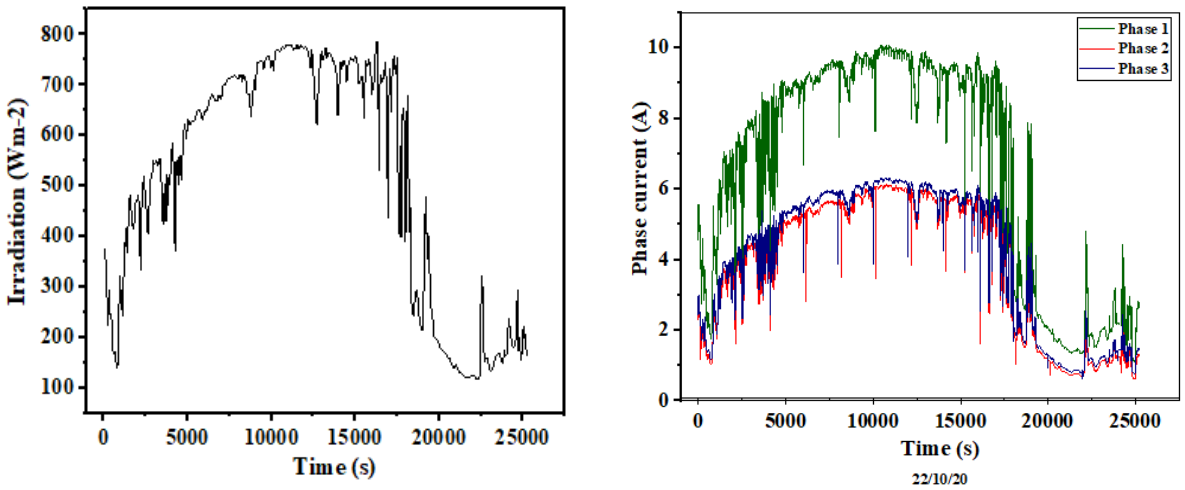

Fig. 4.39. a) Solar radiation profile for 22 October 2020 b) Phase currents for the different systems

4.3.1.1. Power factor

The power factor profiles of the studied grid-connected solar systems are presented in Fig. 4.40. A critical analysis of the power factor profiles vis-à-vis the recorded solar irradiation during the period of the study shows that beyond certain levels of a relatively stable solar radiation ($\geq$ 400 Wm^{-2}), the power factor remained nearly steady and very close to unity. Even though the change in the solar radiation intensity at certain times was about 200 Wm^{-2}, this did not affect the power factor as long as the irradiation was above 400 Wm^{-2}. It was observed that the power factor only decreased at irradiations below 400 Wm^{2}, as shown in Fig. 4.39 and Fig. 4.40. The periodic instantaneous decline (spikes) were observed for all the systems that were studied. The sudden drops were more significant for system 2 and least for system 1, as shown in Fig. 4.43. System 2 recorded the least power whiles system 1 recorded the highest power. These sudden drops occurred throughout the study and were more significant at the latter part of the study for all the grid inverters when the solar irradiation was extremely low. The time interval at which these considerable drops in the power factor were observed was about thirty-three (33) minutes for all the systems. The most significant drop in the power factor recorded for the different systems were 0.767, 0.693 and 0.796, for systems 1, 2 and 3. The power factor not being at unity shows the current and voltage not being in alignment. The average power factor recorded for the different systems were 0.994, 0.992 and 0.993, respectively for systems 1, 2 and 3. The standard deviations of the power factor were found to be 0.009, 0.011 and 0.012, respectively, for system 1, 2 and 3. This shows that system one recorded the power factor profile closest to unity and with the least deviation.

According to the IEEE 1547 standard for the power factor requirements in grid-connected PV systems, inverters are to be designed to operate at a power factor close to unity. The technical regulations concerning power factor for most countries specify that the power factor measured at the point of common coupling should be $\geq$0.95, whether leading or lagging (Al-Shetwi et al., 2020). With regards to the specified standard, it is observed that apart from the periodic instantaneous drops, the recorded power factor profiles were within the specified limits of

≥0.95. The percentage power factors below the specified standards were 0.0021%, 0.0017% and 0.0015%, respectively, for system 1, 2 and 3.

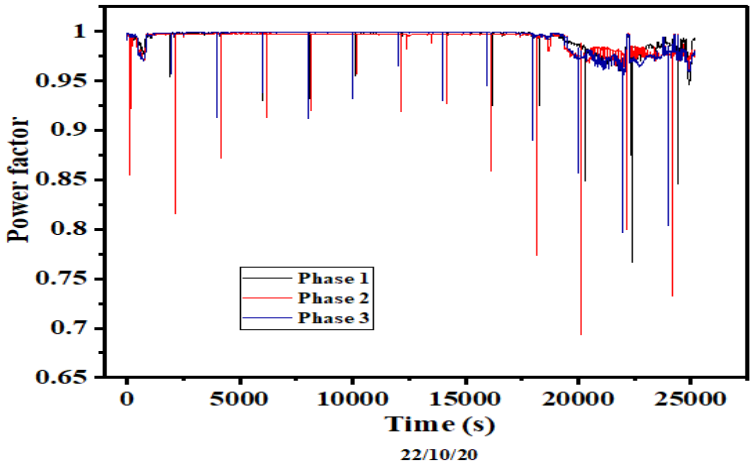

Fig. 4.40. Power factor profiles of the PV systems (22/10/20)

4.3.1.2. Line voltage

The phase voltage profiles for the studied systems are presented in Fig. 4.41. It has been observed that with reference to the standard operating range as specified by the EMC standards, EN 50160, EN 61000 as ±10% for low voltage and medium voltage power systems (CENELEC, 2007; Dreidy et al., 2017), the voltage profiles for all the systems were within the stated acceptable range. The recorded voltages for all the systems were below the nominal voltage of 230 V. The voltages recorded for subsystem three were higher than the other two subsystems' voltages throughout the study for that day. The voltage profiles for the three systems all followed the same trend throughout the study. Thus, the change in voltage per time was the same for all the systems until the latter stages of the study, at extremely low levels of irradiation that the changes in voltage with time varied for all the systems. The average voltages for the three systems are 225.20 V, 223.93 V and 222.73 V for system 3, 1 and 2, respectively.

The average voltages show that the line voltages of systems 2 and 3 were closer to each other than system 1, which has a different configuration and module technology. System 3 recorded voltages that were greater than the voltages of the other systems for the entire study period. System 2 also recorded voltages greater than voltages for system 1 from the start of the study until 3:35 pm when solar radiation figures were below 300 Wm^{-2}. The maximum voltages recorded by the various systems were 228.6 V, 226.9 V and 225.5 V, respectively, for system 3, 1 and 2. The minimum voltages and the standard deviations for the systems were 223.9 V and 1.2285, 222.7 V and 0.9206, and 225.2 V and 1.0862, respectively for systems 1, 2 and 3. The trend of the phase voltages recorded was a bit different compared to the line voltages. Line 1 voltages were lower than the voltages for the other lines throughout the measurement period for the day. Line 3-1 recorded voltages that were higher than line 2-3 until at the latter stages of the study, at about 3 pm, when the voltages of line 2-3 became higher than both lines 1-2 and 3-1. The possible reason for the disparity in the phase voltages may be the asymmetrical loading of the different phases. This causes the current to flow through the neutral, thereby making the phase voltages to vary.

The line voltages recorded for all the systems were within the limit restrictions specified by the standards. The average line voltages were 387.1 V, 389.3V and 389.5 V for line 1, 2 and 3, respectively. The standard deviations determined were 1.03, 0.84 and 0.72 for line 1, 2, and 3, respectively. The maximum, minimum, average, and phase voltage unbalance factors of the different systems are presented in Table 4.1.

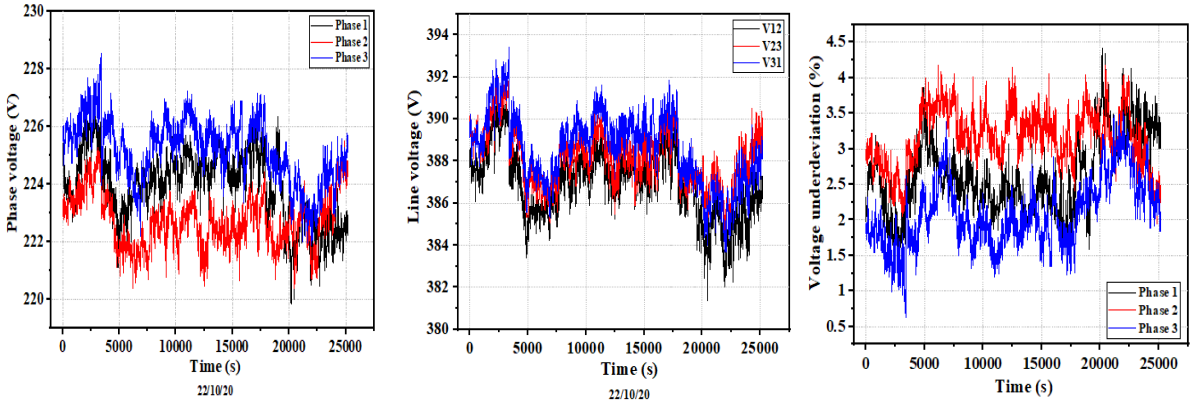

Fig. 4.41. a) The phase voltage b) Line voltage and c) voltage deviation profiles for system 1, 2 and 3 (22/10/20)

4.3.1.3. Line voltage unbalanced ratio and phase voltage unbalanced ratio

The measure of the voltage unbalance ratio (VUR) indicates the level of the quality of power fed into the grid by the distributed power source. Power utility managers are therefore critical about the VUR at the point of common coupling. Different countries, subregions and institutions have put in place standards concerning the limits of VUR permitted to be fed into the grid. The IEEE Standard (IEEE, 2014) specifies that the VUR does not exceed 3%. The IEC standard also restricts all distribution generators to limit the VUR to less than 2% (Cleveland and Member, 2008). Several countries such as Canada, China and Germany have their VUF standards limitation at 2% at the PCC (Wu et al., 2017) (China National Standards, 2012; CSA, 2015) (Yuan-Kang Wu, 2017). The PVUR determined for all the systems under the conditions of high and steady solar radiation were all within the reference standards' specifications. Results of the PVUR for the different systems show that system 1 had a higher phase voltage unbalance compared to system 2 and 3. The difference between the PVURs ranges from 0.1508 to 0.2788%, as shown in Table 4.1.

$$\%\ \mathrm{LVUR} = \frac{\text{max voltage deviation from the avg. line voltage}}{\text{avg. line voltage}} \tag{4.3}$$

$$\%\ \mathrm{PVUR} = \frac{\text{max voltage deviation from the avg. phase voltage}}{\text{avg. phase voltage}} \tag{4.4}$$

The phase angle is also omitted because the formula considers only the magnitudes. The assumption made for this expression is that the voltage is always equal to the rated line voltage for three-phase systems. The phase angle is not included because it considers only the magnitude (Generators, 1993; IEEE, 2017; Manyage and Pillay, 2001; Sonel, 2020) (Tagare, 2011) (IEEE, 2017). The IEC definition of voltage unbalance, the true voltage unbalance is

defined as the ratio of the negative sequence voltage component to the positive sequence voltage component (Dugan and McGranaghan, 1996).

$$\%\,VUF = \frac{negative\ sequence\ voltage\ component}{positive\ sequence\ voltage\ component} \times 100.$$

To determine the positive and negative sequence voltage components, the three-phase unbalanced line voltages Vab, Vbc, and Vca (or phase voltages) are resolved into two symmetrical components and V_n (of the line or phase voltages). The two balanced components are given by the balanced and unbalanced voltage vectors, as follows:

The following factors could contribute to voltage unbalance:

- When the source voltage from the electric utility is unbalanced or when the line or phase voltages differ from the standard nominal voltages,
- Unbalanced impedance of the three-phase distribution system,
- Unequal loading on the power factor correction capacitors (for instance a blown fuse on one phase),
- Unbalanced single-phase load distribution,
- Unbalanced loads on both single phase and three phases,
- Mismatched transformer taps (VoltageDisturbance, 2019).

The effects of voltage unbalance on the power grid include:

- Increased heating and reduced life of induction motors
  One of the most significantly affected devices is the induction motor. An induction motor supplied with unbalanced voltage causes 4-6 times current unbalance. This causes resistive losses leading to an increase in temperature, thus derating the motor insulation life.
- Reduced life of front-end-diodes and or bus capacitors.
- The load type determines the reduction in the voltage which could lead to increased current in one or more phases and hence increase losses (VoltageDisturbance, 2019).

Table 4.1. The maximum line voltage, minimum line voltage, standard deviation and the line unbalance factor of the different systems

	Line 1-2	**Line 2-3**	**Line 3-1**
Max	391.151	392.563	393.423
Min	381.366	384.334	383.638
Ave	386.8536	388.1394	388.5637
Stdev	1.619525	1.368742	1.688491
%LVUR	1.4185%	1.1397%	1.2677%

Table 4.2. The maximum and minimum phase voltages, and the standard deviation values for the different systems

	Phase 1	**Phase 2**	**Phase 3**
Max	226.898	225.514	228.557
Min	219.837	220.370	221.898
Ave	223.9251	222.7337	225.2008
Stdev	1.228536	0.92055	1.086221

4.3.1.4. Voltage flickers

Voltage flickers manifest in the sudden changes in lamps' brightness with the noticeable flicking of the lights (Ferdowsi et al., 2020). There were no long-term voltage flickers recorded for the studied systems. The low voltage power network standards, the EMC standard of EN 6100 specifies Pst to be < 1.0 and Plt to be < 0.8. The IEEE 1547, IEC 61000-3-3 standards also require that voltage flickers be between 0.6 and 0.9 pu for Plt and Pst, respectively (Tagare, 2011). The short-term voltage flickers for systems 1, 2, and 3 are presented in Figs. 4.45. Measurements of voltage flickers were made at the intervals of 3s. System 1 recorded the highest magnitude short term voltage flickers of 1.532, compared to system 2 and 3, which had the maximum Pst of 0.694 and 0.622, respectively. The Pst recorded for system 2 and 3 were all within the specified requirement of the standards considered. System 1, however, recorded some Pst that violated the standard requirements. 0.129% of the recorded Pst for system 1 were outside the limits stated by the standards. It can be deduced based on the probability flicker severity results that system 1 had a higher level of quality issues than the systems 2 and 3 under the experimental conditions as Pst as a parameter that demonstrates the degree of voltage fluctuation power networks.

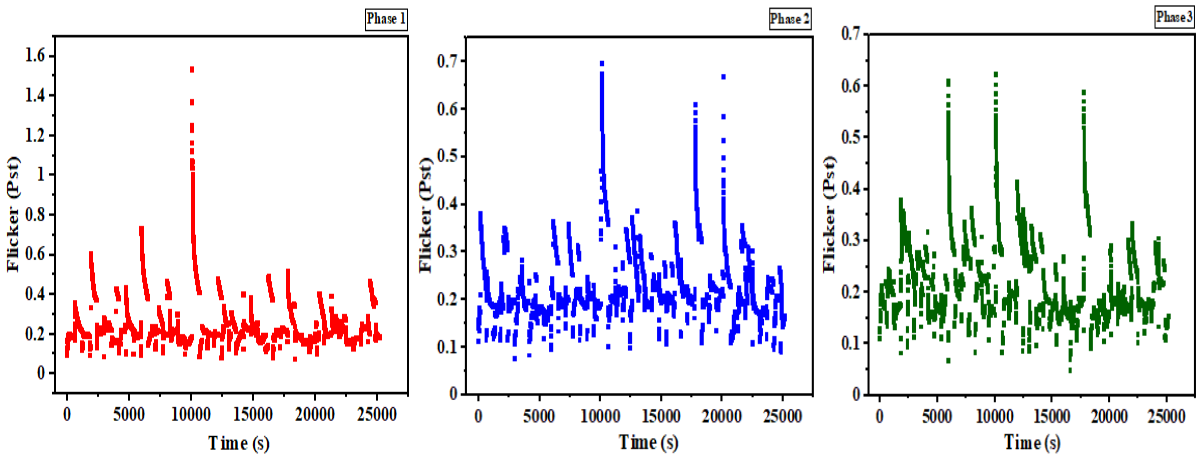

Fig. 4.42. Short term voltage flickers (Pst) for a) System 1, b) System 2, and c) System 3

The results showed that averagely, system 1 recorded the highest voltage deviations of 4.419 V from the nominal voltage followed by system 2 (4.187 V) and the least deviation of 3.523 V observed for system 3. Similar to the line voltage, the deviations for the various systems were not constant throughout the study time. This was evident in the results shown in Table 4.3.

System 1 exhibited the most significant deviation in voltages followed by system 3 and the least is system 2. The LVUR 1.826%, 1.49% and 1.28% for systems 1, 3 and 2, respectively.

The extent of the VUF indicates the severity of the power quality issues of the power fed into the grid by the distributed power source. Power utility managers are therefore critical about the VUF at the PCC. The IEEE Standard (IEEE, 2014) specifies that the VUF does not exceed 3%. Also, the IEC standard restricts all distributed generators to limit the VUF to less than 2% (Cleveland and Member, 2008). Several countries such as Canada, China and Germany have their VUF standards limitation at 2% at the PCC (China National Standards, 2012; CSA, 2015; Yuan-Kang Wu, 2017). Based on the results, it can be inferred that the severity of power quality issues in the different systems is in the decreasing order for system 1, system 3 and system 2.

Table 4.3. The minimum, maximum and LVUR of the various systems

Voltage under deviation			
	Phase 1	Phase 2	Phase 3
Max	4.419	4.187	3.523
Min	1.349	1.950	0.627
Average	2.641281	3.159263	2.086595
Stdev	0.534141	0.400236	0.472264
% **LVUR**	1.826%	1.28%	1.49%

4.3.1.5. Current total harmonic distortions

Results for the current total harmonic distortions for the different phases have been presented in Fig. 4.43. The permissible limit specified by the various standards IEC 61000-3-2, IEEE 1547, AS 4777.2 for current total harmonic distortion as listed in Tables 2.5 - 2.7 is (CTHD<5%). Results show few instances of relatively high instantaneous CTHDs that occurred at different times and irrespective of the irradiation levels for all the phases. For some of the systems, it happened in a condition of steady and high solar radiation levels and a relatively constant output of CTHD. The percentage difference in the deviation was as high as 800% for phase 1, 333% for phase 2 and 60% for phase 3.

The high CTHD observed may be as a result of the presence of non-linearity of some components within the microinverter, which increases the current harmonics injected at the PCC. System 1 recorded the highest average current total harmonic distortion of 6.54% over the period and a minimum CTHD of 1.801%. System 1 also recorded the highest standard deviation of 5.16, which indicates a high disparity in the measured CTHD for the system over the period compared to system 2 and 3. The maximum and minimum CTHDs for systems 2 and 3 are 5.58% and 2.94%, and 5.18% and 2.87%. The higher THDs observed for phase 1 could also be as a result of the excessive loading on phase 1 compared to phase 1 and phase 2. The standard deviations for systems 2 and 3 were 3.46 and 3.18, respectively, as shown in Table 4.4. This shows the level of power issues in the various systems.

The measured CTHDs for the different systems show a common correlation with the measured irradiation for the period. Above the irradiations of 400 Wm^{-2}, it was observed that relatively

steady CTHDs were measured for all the systems with similar values recorded for about 4 hours for all the systems. Below the irradiation values of 400 Wm^{-2}, the CTHDs increased and were irregular, as shown in Fig. 4.43. With reference to the acceptable limits specified by the related standards, it was observed that the percentage of the recorded CTHDs that did not violate the specifications were 64%, 66% and 69% for system 1, system 2 and system 3, respectively. This shows that with regards to the CTHDs, the severity of power quality issues recorded was greatest for system 1 compared to the results of the other systems. Comparably, system 3 recorded the least power quality issues in terms of the CTHDs.

Table 4.4. The maximum, average and minimum CTHDs for the various system

	System 1	**System 2**	**System 3**
Average	6.543686	5.575384	5.183166
Max	36.335	18.565	24.733
Min	1.801	2.938	2.864
Stdev	5.16032	3.461174	3.176348
% that conforms to the standard (<5%)	64%	66%	69%

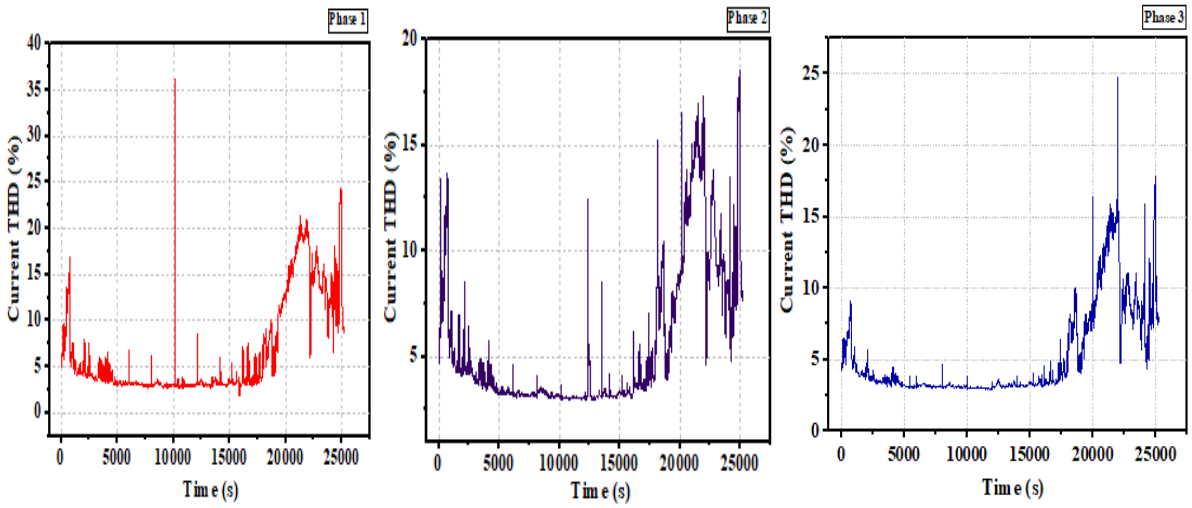

Fig. 4.43. Current total harmonic distortions for the different systems

4.3.1.6. Current individual harmonic distortions

The individual current harmonic distortions for the different systems are presented in Fig. 4.44. The acceptable range by the reference standards (IEC 61000-3-2, IEEE 1547, and AS 4777.2 standards) for current harmonic distortions are listed in Tables 2.5 -2.7. According to the standards for the odd harmonics for $33 < h$, the acceptable least harmonic distortions must be below 0.3%. The least acceptable harmonic distortion for the even harmonics which is for $10 \leq h \leq 32$ must be below 0.5% and < 0.225% for $15 \leq h \leq 39$ for the odd harmonics and < 0.345% for $8 \leq h \leq 40$ for the even harmonics, respectively, for IEC 61000-3-2 and IEEE 1547 standards.

All three systems generated individual current harmonic distortions that were within the specified limits given by the various standards considered. The highest recorded individual current harmonic distortions were 4.58%, 3.84% and 4.05%, respectively for system 1, 2 and 3, for the first harmonics. System one with the highest power generation capacity compared to system 2 and 3, and also the first phase, had the highest individual harmonic distortions throughout the study. System 1, thus recorded the most significant current THDs of 6.54% with systems 2 and 3, registering 5.58% and 5.18%, respectively.

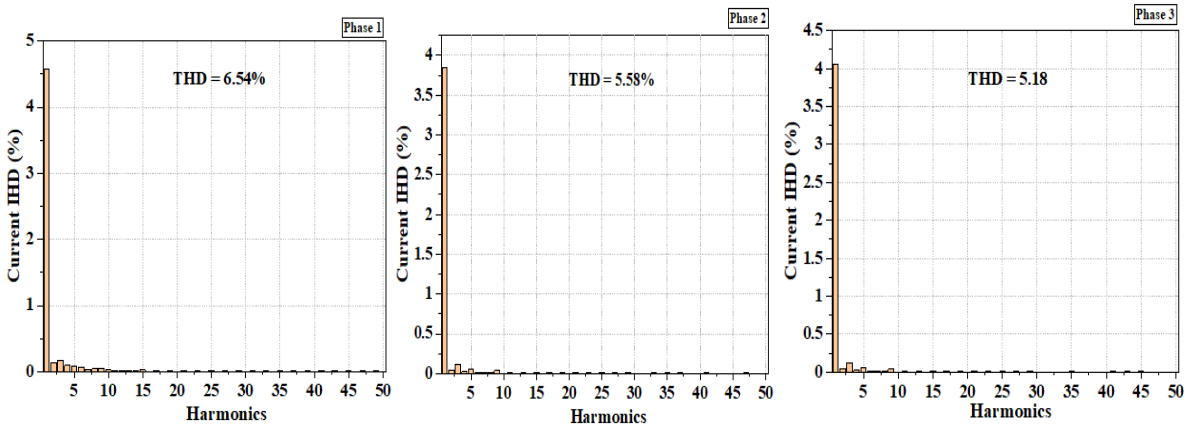

Fig. 4.44. Current individual harmonic distortions for systems 1, 2 and 3 (22 October 2020)

4.3.1.7. Voltage total harmonic distortions

The voltage total harmonic distortions for the different systems are presented in Fig. 4.45. The voltage THD measured for the three systems were all within the specified standards of the IEEE 519 standard for (V≤ 1) kV systems, which specifies individual harmonic distortions to be less than 5%, and the THD <8%. The VTHD for all three systems followed a similar trend. The VTHDs increased linearly for about two hours to their maximum values for all the systems and then decreased through the rest of the study period. The range of recorded VTHDs were 2.152% - 1.503%, 2.161% - 1.506% and 2.198% - 1.432%, respectively, for system 1, 2 and 3. The average VTHDs for the different systems show a close VTHD output for all three systems. The average VTHDs were 1.794%, 1.743% and 1.664%, respectively, for system 1, 2 and 3. The standard deviation in the VTHDs recorded for the different systems were 0.1039, 0.0727 and 0.0934, respectively, for systems 1, 2 and 3. Results also showed evidence of high instantaneous deviations that occurred severally in the form of spikes in the entire study period. This situation was more prevalent for system 2.

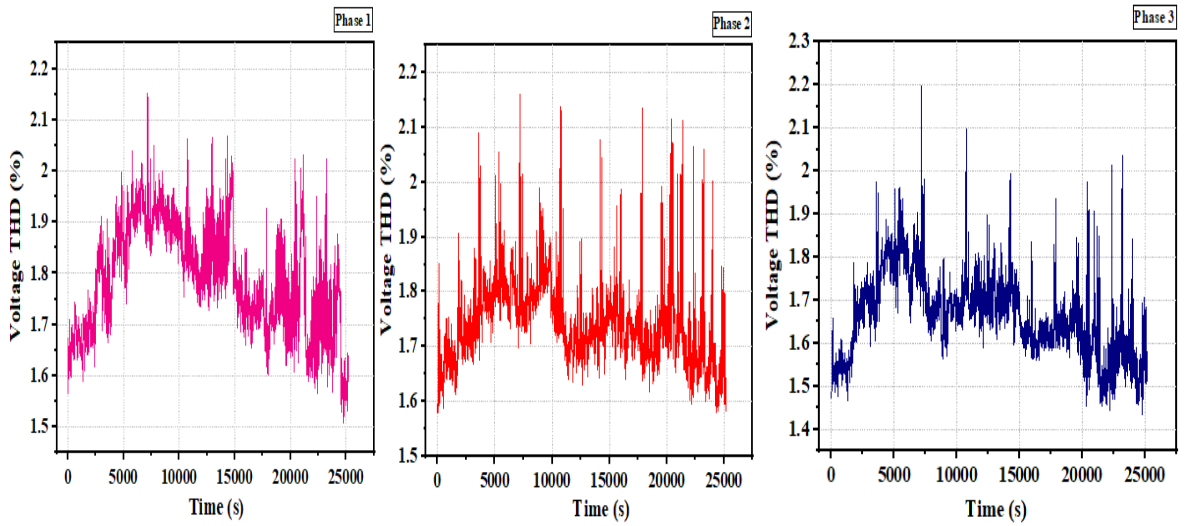

Fig. 4.45. Voltage total harmonic distortions for system 1, 2 and 3 (22 October 2020)

The voltage individual harmonic distortions for the different settings and inverters are presented in Fig. 4.46. The harmonic distortions for all the harmonic orders were within the specified range by the given standards in Tables 2.5 – 2.7. The highest individual voltage harmonic distortion was recorded for the 7th harmonic for system 2 and 3. However, for system 1, the highest individual harmonic distortion was recorded for the fifth harmonic order. The highest VIHDs for the different systems are 2.370%, 2.169% and 2.207%, respectively, for system 1, 2 and 3. The total harmonic distortions for the different systems throughout the study were 1.79%, 1.74% and 1.66% for system 1,2 and 3. The individual harmonic distortions for the even harmonics were negligibly low for all the systems examined.

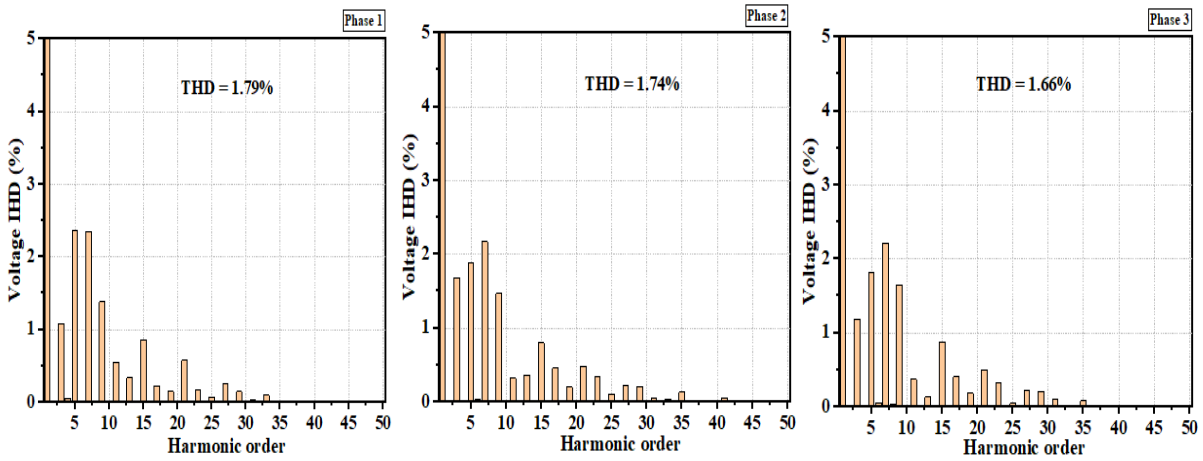

Fig. 4.46. Voltage individual harmonic distortions for system 1, 2 and 3 (22 October 2020)

4.3.2. Performance of string inverter systems under high and steady solar radiation

This section presents the results and discussions for the study of the power quality analysis of the rooftop grid-connected PV system on the student dormitory for a day of high, steady and unintermittent solar radiation. Measurements were conducted for 10 hours (8 am – 6 pm). The various quantities were recorded at intervals ranging from 200 ms to 6 s.

4.3.2.1. Power factor

The power factor (cos ϕ) (PF) indicates the phase angle between the current and the voltage signals of the AC signal output. The power factor for the different systems has been determined and their compliance with the grid regulations specified. The power factor profiles for the three subsystems are presented in Fig. 4.47. The standard for the power factor of grid-connected PV systems IEEE 1547 requires grid-connected inverters to operate at a power factor close to unity. The technical regulations concerning the power factor of grid-connected systems for most countries require that the power factor range at the point of common coupling should be ≥0.95, whether leading or lagging (Al-Shetwi et al., 2020). The percentage of the power factor profiles of the various systems that violated the standards was 3.44%, 3.12% and 3.45%, respectively, for system 1, system 2 and system 3. The percentage of the power factor outside the specified standard (>0.95) was measured mostly at the latter period of the study when the irradiation levels were below 400 Wm^{-2} and decreasing. At the initial stages of the study, even though the irradiation levels were below the 400 Wm-2, but rising, that did not cause the power factor of the systems to fall below the 0.95 marks. The range of values for the recorded power factor for the different systems were 0.652 – 0.999, 0.265 - 0.998, and 0.651 – 0.999, respectively, for system 1, 2 and 3. The average values were 0.994, 0.991 and 0.993 for system 1, 2 and 3, respectively.

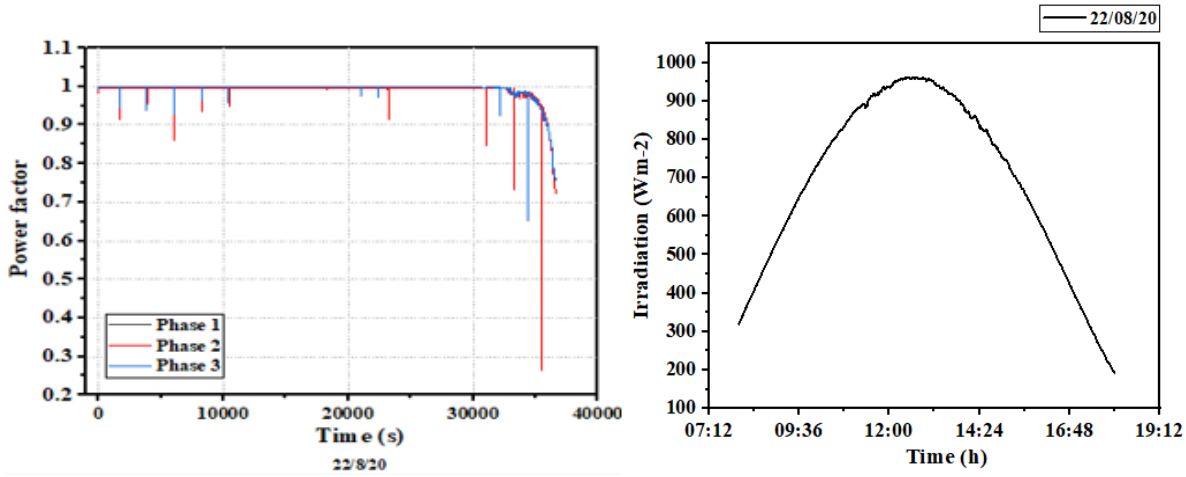

Fig. 4.47. a). Power factor profiles for the systems on the rooftop b). Solar radiation profiles for high and non-fluctuating radiation (22/8/20)

4.3.2.2. Frequency output profile

Fig. 4.48 presents the frequency profile for the grid systems on the 22nd of August 2020. The frequency profile plays a critical role in the maintenance of the power quality of the grid, especially with grids that are tied with distributed power generating sources. The standards EN 50160 (CENELEC, 2007) specifies that the frequency should be within ±1% of the nominal frequency. The recorded frequency profile for the entire period was within limits established by the different standards. The range of frequency values measured was 49.95 – 50.08 Hz. The average and the standard deviation values were 49. 9997 Hz, and 0.0145. The results showed the closeness of the frequency of the system to the nominal value.

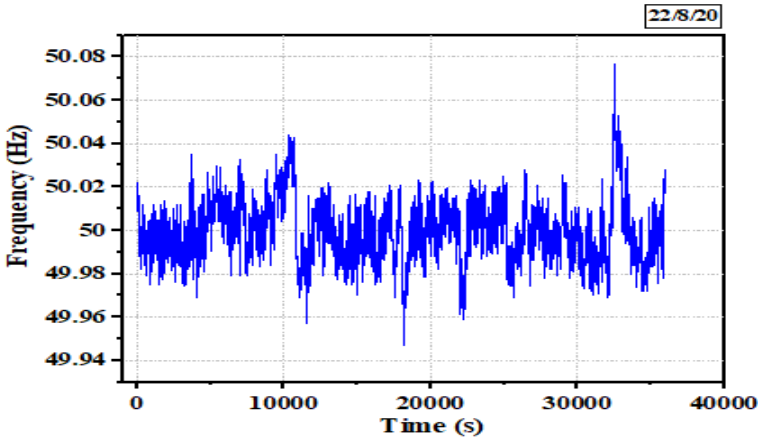

Fig. 4.48. Frequency profile generated by the grid system (22/8/20)

4.3.2.3. Phase and line voltage profiles

The phase voltage profiles for the three systems are presented in Fig. 4.49. The recorded voltages were all within the standard operating range specified by the EMC standards, EN 50160, EN 61000 as ±10% for low voltage and medium voltage power systems (CENELEC, 2007; Dreidy et al., 2017). For a balanced three-phase network, the phases are separated at an angle of 120 degrees, and the phase voltages (line to neutral) are the same for the three phases. If the above conditions are satisfied in a three-phase network, then the magnitude of the line voltages will be equal to 1.732 × Vp (Phase voltage).

The recorded voltages for the three systems were all below the nominal voltage of 230V. The voltages recorded for subsystem three were higher than the voltages of the other two subsystems throughout the study for that day. The difference at each instance was about 2 V. The average voltages for the three systems were 223.25 V, 223.29 V and 225.64 V for system 1, 2 and 3, respectively. The standard deviations showed that system 2 recorded voltages that were more uniform than the other two systems. The standard deviations were 1.124475, 0.953615 and 1.167674 for systems 1, 2 and 3, respectively. The phase voltages of system 1 and 2 instead showed close similarities. This was evident in the average values of 223.25 V and 223.29 V and 225.64, respectively, for system 1, 2 and 3.

The trends of the line voltages recorded were a bit different. Line 1-2 had lower voltages than the voltages of line 2-3 and line 3-1 throughout the measurement period for the day.

The line voltages recorded for line 2-3 and line 3-1 were similar to each other. The average line voltages were 386.91 V, 389.00 V and 388.25 V for line 1, 2 and 3, respectively. The standard deviations determined were 1.696, 1.659 and 2.231 for systems 1, 2, and 3, respectively. The line voltages recorded were within the limit restrictions of the grid standards. The possible reason for the disparity in the phase voltages may be the asymmetrical loading of the different phases. This causes the current to flow through the neutral, thereby making the phase voltages to vary (Sonel, 2020).

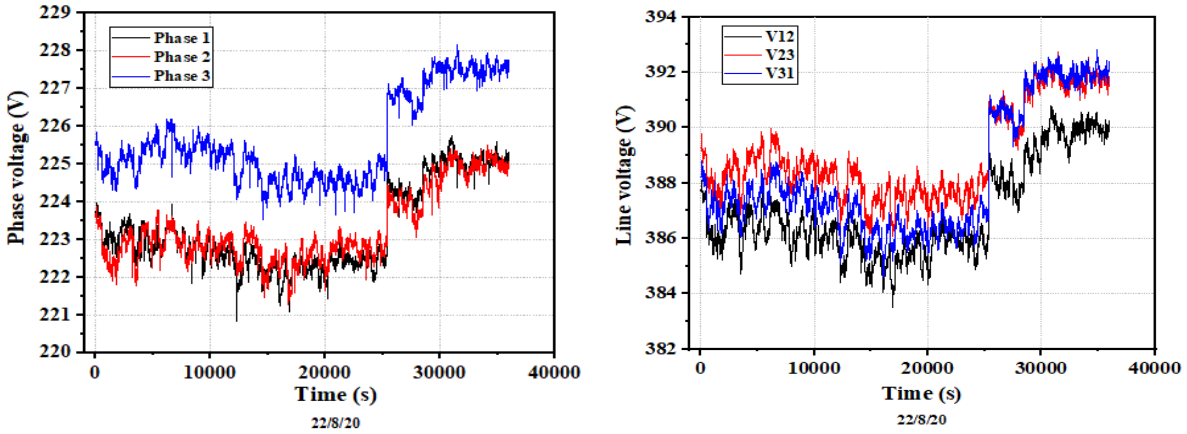

Fig. 4.49. Phase voltage and line voltage profiles for system 1, 2, and 3 of the rooftop grid-connected PV systems

4.3.2.4. Line voltage unbalanced ratio and phase voltage unbalanced ratio

The measure of the VUF is an indication of the level of the quality of power fed into the grid by the distributed power source. The requirements vary across the various countries and sub-regions as it is dependent on the grid infrastructure. The IEEE Standard (IEEE, 2014) specifies that the VUF does not exceed 3%. The IEC standard also restricts all distribution generators to limit the VUF to less than 2% (Cleveland and Member, 2008). Several countries such as Canada, China and Germany have their VUF standards limitation at 2% at the PCC (Wu et al., 2017)(China National Standards, 2012; CSA, 2015). The PVUR determined for all the systems under high non-intermittent solar radiation (22 of October 2020) were all within the referenced standards' specifications. Results of the PVUR for the different systems show that system 1 had a higher phase voltage unbalance compared to system 2 and 3. The difference between the PVURs ranges from 0.1508 to 0.2788%. System 3, however, had the highest LVUR compared to the other systems. The values were 1%, 0.96% and 1.18% for system1 system 2 and system 3, respectively.

4.3.2.5. Voltage underdeviation for system 1, system 2 and system 3

The voltage deviation profiles for the different subsystems are presented in Fig. 4.50. The voltage deviations for all the systems were below the nominal voltage. Even though system 2 and system 3 have the same system specifications different from system 1, the voltage deviation of system 1 and 2 followed the same trend and with very close to each other throughout the study. The percentage deviation for system 3 was lower than system 1 and 2 throughout the study. The difference in the deviation between system 3 and that of system 1 and 2 was average, 1% throughout the study. The maximum deviation of 4% was recorded for system 1, while the lowest deviation of 0.75% was recorded for system 3.

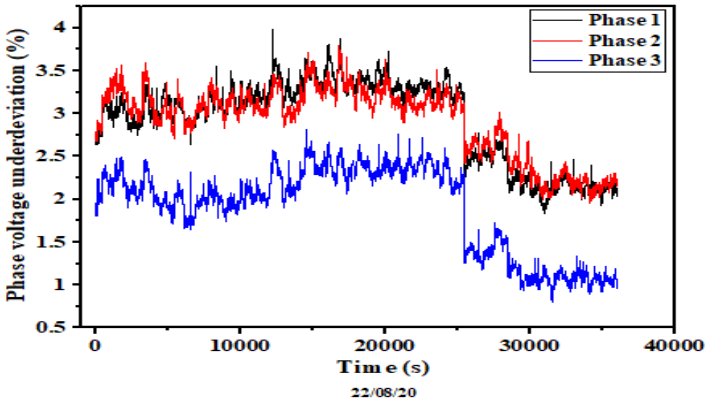

Fig. 4.50. Voltage underdeviation for system 1, system 2 and system 3

4.3.2.6. Current total and individual harmonic distortions

The current total harmonic distortions (CTHD) measurements for the different rooftop systems have been presented in Fig. 4.51. The permissible limit specified by the various standards IEC 61000-3-2, IEEE 1547, AS 4777.2 for current total harmonic distortion as listed in Tables 2.5 - 2.7 is (CTHD<5%). Results show few instances of relatively high instantaneous CTHDs spikes generated for all the phases that occurred at different times and were irrespective of the irradiation levels. For some of the systems, it happened at operating condition of steady and high solar radiation levels and a relatively constant output of CTHD. The percentage deviation of these instantaneously high CTHDs from the steady values was as high as 317% for phase 1, 480% for phase 2 and 640% for phase 3. The high CTHD observed maybe because of the presence of non-linearity of some components within the microinverter, which increases the current harmonics injected at the PCC.

System 2 recorded the highest average current total harmonic distortion of 7.9% over the period. System 2 also recorded the highest standard deviation of 3.228, which indicates a high disparity in the measured CTHD for the system over the period compared to system 1 and 3. The maximum and minimum CTHDs for systems 1 and 3 are 37.56% and 3.68%, and 32.09% and 4.33%, respectively. The standard deviations for the various systems were 2.751, 3.228 and 2.709, respectively, for system 1, 2, and 3, as shown in Table 4.5. The measured CTHDs for the different systems showed no correlation with the measured irradiation (whether low or high) for the period. The recorded CTHD profiles increased linearly from the lowest values at the start of the investigations to the highest values at the end of the study. With reference to the acceptable limits specified by the related standards, it was observed that the percentage of the recorded CTHDs that violated the requirements were 32.7%, 12.5% and 16.4% for system 1, system 2 and system 3, respectively. This shows that with reference to the CTHDs, the severity of power quality issues recorded was greatest for system 1 compared to the results of the other systems. Comparably, system 2 recorded the least power quality issues in terms of the CTHD.

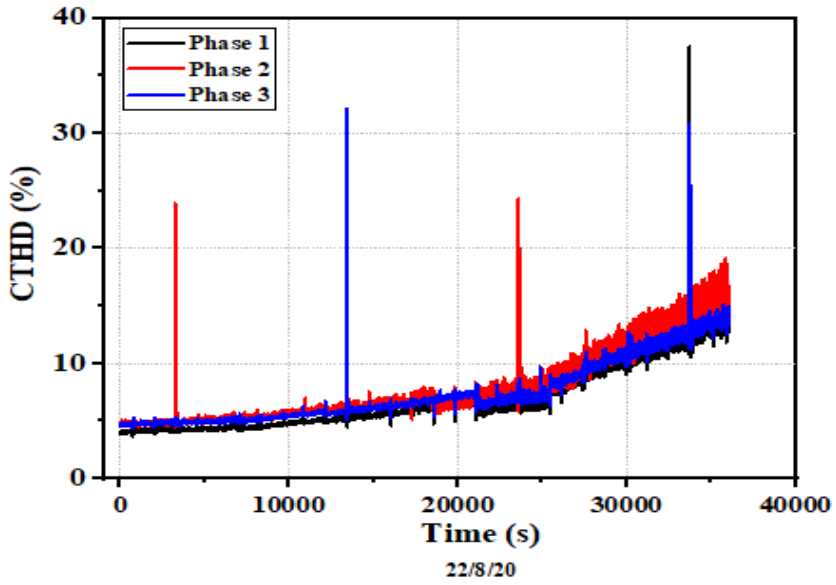

Fig. 4.51. Current total harmonic distortion for the three rooftop grid systems

Table 4.5. The maximum, minimum and standard deviation CTHD for the rooftop systems

	System 1	**System 2**	**System 3**
Max	37.557	24.295	32.088
Min	3.684	4.44	4.326
Av	6.794859	7.900591	7.427568
stdev	2.751306	3.228348	2.709481
% within limit	32.7%	12.5%	16.4%

The standards for reference of the acceptable range of current individual harmonic distortion are the IEC 61000-3-2, IEEE 1547, and AS 4777.2 standards listed in Tables 2.5 – 2.7. According to the standards for the odd harmonics 33 < h, the acceptable least harmonic distortions are to be below 0.3%. The least for the even harmonics specified by the referred standards is required to be below 0.5%. All the systems generated individual current harmonic distortions that were within the specified limits given by the various standards. The highest harmonic distortion was 1.95%, 1.58% and 1.68% for system 1, 2 and 3, respectively for the first harmonic. The THDs were 6.795%, 7.91%, and 7.44% and 91.01% for system 1, 2 and 3. The THDs for system 2 were higher than the THDs for the other systems for the entire experimentation period as shown in Fig. 4.52.

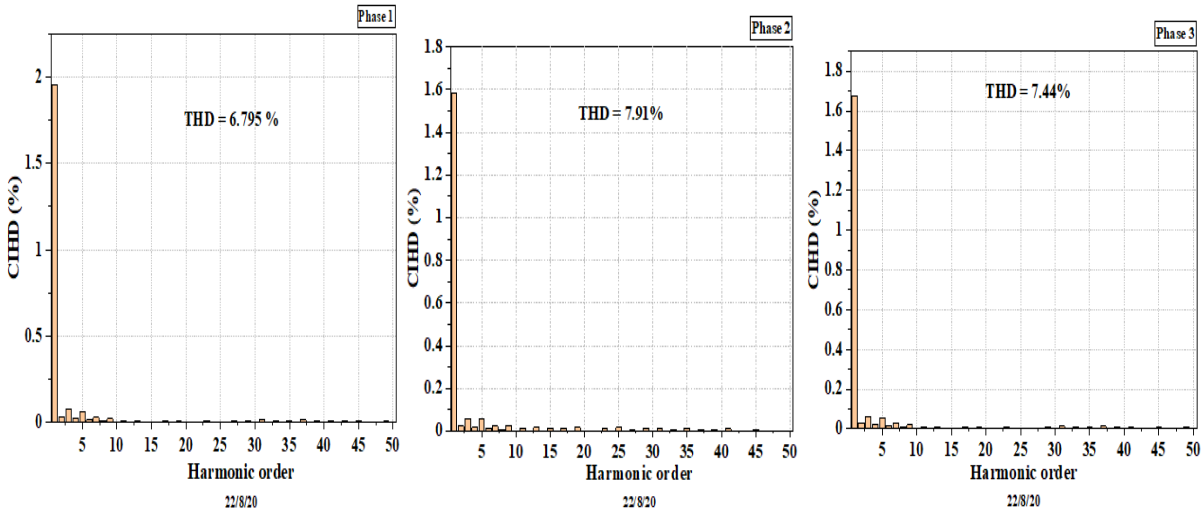

Fig 4.52. Individual current harmonic distortions for systems 1, 2 and 3

4.3.2.7. Voltage total and individual harmonic distortion

The voltage total harmonic distortions for the different systems are presented in Fig. 4.53. The voltage THD measured for the three systems were all within the specified standards of the IEEE 519 standard for (V≤ 1) kV systems, which specifies individual harmonic distortions to be less than 5%, and the THD <8%. The VTHD for all three systems followed a similar trend.

The VTHDs recorded for system 1 were higher than the values recorded for all the other systems studied. The VTHDs for system 2 was closer to each other than system 1 and 3 with the values ranging from 1.452% to 1.689%. The average VTHD and the standard deviation for system 2 were 1.556% and 0.02876, respectively. The VTHDs recorded for system 2 and 3 were quite similar to each other, which is evident in the average VTHD of 1.5559% and 1.5621% for system 2 and 3, respectively. When the profile is divided into three parts, the first one-third of the VTHD profile (the initial stages of the study) the VTHDs recorded for system 2 was fairly higher than the values recorded by system 3. At the mid-section of the profile, the VTHDs for system 2 and 3 were fairly the same. The latter section of the profile showed the profile of system 3 turn higher than the profile of system 2. It can be inferred that the VTHDs for the two systems (2 and 3) remained fairly the same at high and steady irradiation conditions. The range of VTHD for system 1 was 1.502% to 1.934%. The average VTHDs for systems 2 and 3 show a close output profile for the two systems. The average VTHDs were 1.676%, 1.556% and 1.562%, respectively, for system 1, 2 and 3. The standard deviation in the VTHDs recorded for the different systems were 0.04282, 0.02876 and 0.049125, respectively, for systems 1, 2 and 3.

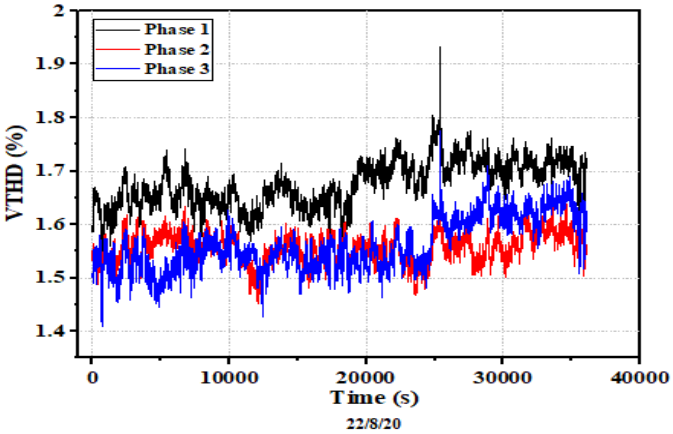

Fig. 4.53. Voltage total harmonic distortions for system 1, 2 and 3

The voltage individual harmonic distortions of 50 harmonic orders for the different systems are presented in Fig. 4.54. The harmonic distortions for all the harmonic orders fell within the specified range by the reference standards given in Tables 2.5 – 2.7. The highest individual voltage harmonic distortion was recorded for the 5th harmonic for all the systems studied. The highest VIHDs for the different systems were 2.803%, 2.192% and 2.371%, respectively, for system 1, 2 and 3. The 7th harmonic order had voltage distortions that were relatively close to the 5th harmonic distortions. The total harmonic distortions for the different systems throughout the study were 1.68%, 1.55% and 1.56% for system 1,2 and 3. The individual harmonic distortions for the even harmonics were negligibly low for all systems examined.

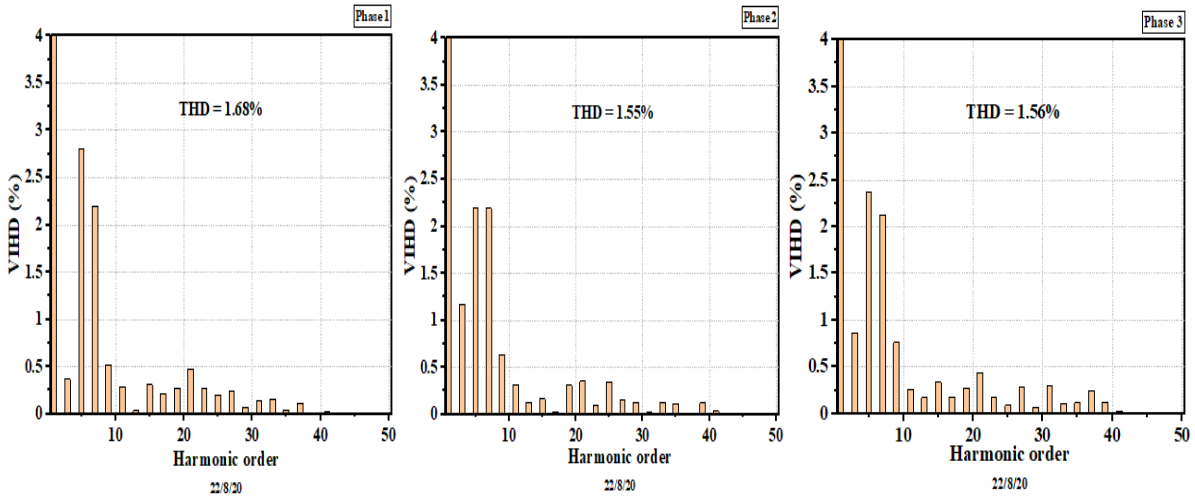

Fig. Fig. 4.54. Individual voltage harmonic distortions for systems 1, 2 and 3

4.3.2.8. Short-term and long-term voltage flickers

Voltage flickers are grouped into short-term probability flicker severity (Pst) and long-term probability flicker severity (Plt) to enable its proper control. Voltage flickers manifest in the sudden changes in the brightness of lamps with the noticeable flicking of the lights (Ferdowsi et al., 2020). The standards for low voltage power network, the EMC standard of EN 6100 specifies Pst to be < 1.0 and Plt to be < 0.8. The IEEE 1547, IEC 61000-3-3 standards also require that voltage flickers be between 0.6 and 0.9 pu for Plt and Pst, respectively (Tagare, 2011). The study under high unintermittent solar radiation shows that neither short-term voltage flicker (Pst) or long-term voltage flickers (Plt) were recorded for any of the three

systems throughout the study period. This could be due to the steady and high irradiation profiles registered for the day compared to the other days for the investigation. The source of voltage flickers results from power fluctuations or sharp changes in power output due to sporadic solar radiation and variations in rms voltage magnitude. Hence the absence of both Pst and Plt for the study under high and steady solar radiation. With reference to voltage flickers as a source of the level of power quality issues in grid-connected PV systems, it could be inferred that compared to the other days of the investigations, the experimental conditions of high steady solar radiation for the 22 August 2020 were more favourable for less or no power quality issues for Pst as a parameter that demonstrates the degree of voltage fluctuation in power networks.

4.3.2.9. Relationship between the harmonic current and harmonic voltage

Analysis of the harmonics generated by the various systems has been conducted to determine the relationship between the harmonic current and the harmonic voltages for each harmonic order and the similarities in the trends for the different systems. In the unique instance of the study conducted on 22 August 2020, a day on which solar radiation was steady and high for the period of study (1800 datasets). Three scenarios were assessed, in the first instance, data for the entire period of the study was used in the second instance, data for one hour (at the period of system power generation above half the nominal system capacity) was extracted and used for the study (3000 datasets). In the third instance, 100 datasets were applied. The simple linear regression analysis was applied by calculating the least square errors for each of the plots. The results of the analysis are presented in Fig. 4.55. The investigation was conducted for the odd harmonics (3^{rd} to 11^{th} harmonics), which severely impacted the grid output's quality performance.

Results for the first instance showed both negative and positive correlations for all the 3^{rd} to 11^{th} harmonic orders of the three systems. It was observed that the harmonic current of the various systems increased with increasing harmonic voltages for most of the harmonic orders presented. However, at least one of the harmonic orders for each system studied recorded a negative correlation with system 3, recording a negative correlation for two harmonic orders (3^{rd} and 11^{th}). The slopes of the regression analysis can be found in appendix 3. Thus, the correlation varied for each system. However, the 5th and 7th harmonics for all the systems recorded positive correlations. The negative correlations differed from harmonic order for the different systems, as shown in Fig. 4.55.

The negative slopes were not restricted to any particular harmonic order but occurred for lower and higher harmonic orders depending on the system analysed. Even though system 2 and 3 had the same inverter make and array specifications, they recorded varying trends of the relationship between the harmonic current and the system's harmonic voltage output. The inference is that the harmonic voltage present and the correlation with the harmonic current are system dependent and reliant on the system's conditions. The closest similarity among the results of the different systems was observed for the 5^{th} harmonic order with similar magnitudes of the slope. The 7^{th} harmonic also recorded a fairly close similarity in the slopes for the different systems. (Chicco et al., 2009) in their study, observed positive correlations for all the systems studied, except for the 3^{rd} harmonic of one of the systems that registered a negative

slope; thus, the current harmonic increasing whiles the voltage harmonic decreases. However, in the present study, it has been revealed that at least a negative slope and a maximum of two negative slopes for all the systems studied. Dress et al. (2005) mentioned in their research that individual harmonic currents demonstrate similarities in behaviour when the inverter's power output is more than 20% of the rated capacity (Dress et al., 2005), which is more significant for low harmonics orders, irrespective of system's characteristics. This, according to the present study, has been proven to be otherwise. Apart from the 5th harmonic order, which showed a positive correlation for all the systems and scenarios studied independent of the prevailing conditions, the rest of the harmonic orders demonstrated varying behaviours and correlations with the system's harmonic voltage.

The second scenario produced correlations not too different from the first scenarios except that most of the positive and the negative correlations for the various harmonic orders were different from the first scenario. However, it was observed that the 5th harmonic order of all the systems studied demonstrated a positive correlation for all scenarios studied. The 3rd harmonic order for the first system, the 9th harmonic order of systems 2 and 3, showed a positive correlation for both scenarios studied. However, the correlations for the rest of the harmonic orders were different from the first scenario, as shown in appendices 3 to 7.

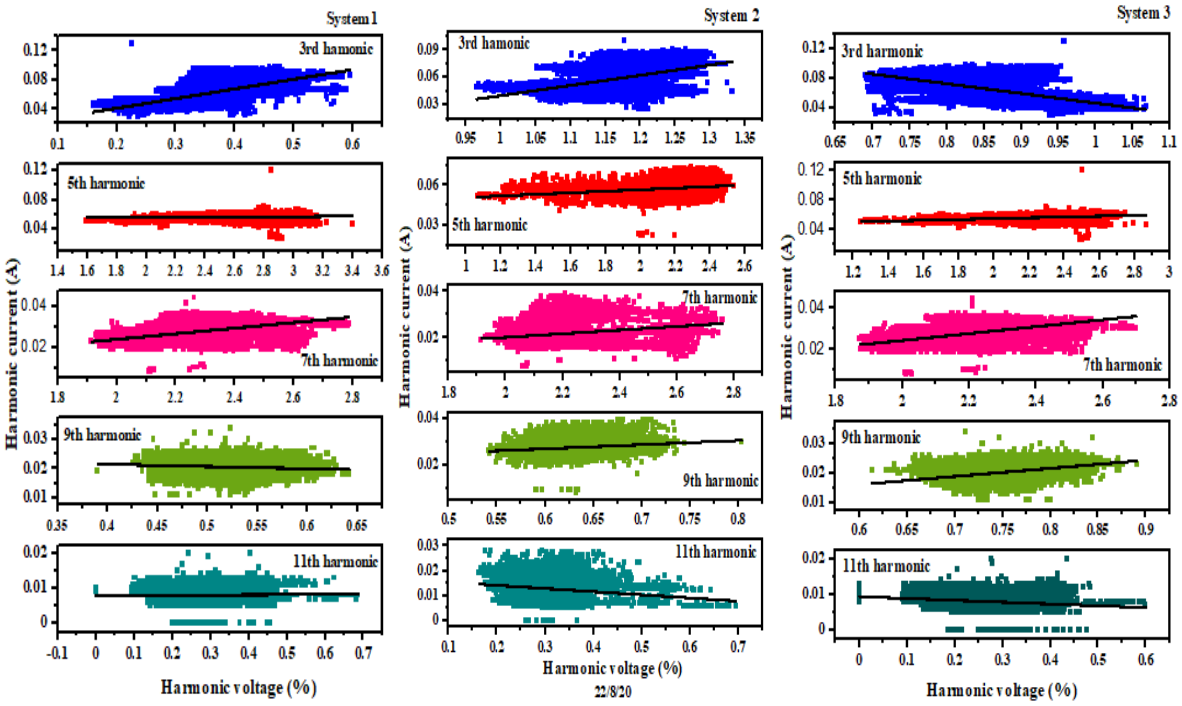

Fig. 4.55. Plots of harmonic current against system harmonic voltage for the rooftop grid systems (System 1, 2, and 3)

4.3.3. Under conditions of sporadically high and low solar radiation

This section presents the results and discussions for the study on the rooftop grid-connected PV system on the student dormitory for a day of sporadically high and low solar radiation (23 August 2020). Measurements were conducted for 10 hours (8 am – 6 pm). The various quantities were recorded at intervals ranging from 200ms to 6 s.

4.3.3.1. Power factor

Fig. 4.56 presents the irradiation measurements on the day and the power factor profiles for the three systems. The solar radiation shows a profile of sporadically high and low values of the first two-thirds and very low values at the last third. The power factor for the different systems has been determined and their compliance with the grid regulations specified. The standard for the power factor of grid-connected PV systems, IEEE 1547 requires grid-connected inverters to operate at a power factor close to unity. The technical regulations concerning the power factor of grid-connected systems for most countries require that the power factor at the point of common coupling should be ≥0.95, whether current leading or lagging (Al-Shetwi et al., 2020). The percentage of the power factor of the various systems that violated the standards was 1.4%, 1.18% and 1.48%, respectively, for system 1, system 2 and system 3. The percentage power factor outside the specified standard (0.95) was mostly measured at the latter period of the study when the irradiation levels were below 400 Wm^{-2} and decreasing. At the initial stages of the study, even though the irradiation levels were below 400 Wm^{-2}, it did not remain for long periods at the low value, which did not cause the systems' power factor to fall below the 0.95 marks. Also recorded were spikes of very low power factor that occurred sporadically for all the systems at different times from the start to the end of the study. The range of values for the recorded power factor for the different systems were 0.6000 – 0.9994, 0.5100 - 0.998, and 0.646 – 0.9993, respectively, for system 1, 2 and 3. The average values were 0.993, 0.991 and 0.992 for system 1, 2 and 3, respectively.

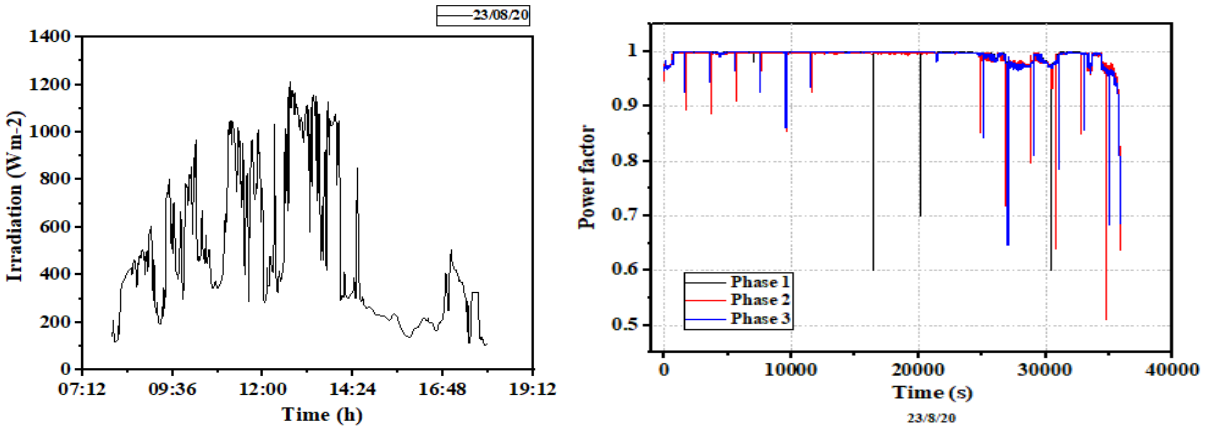

Fig. 4.56. Solar radiation and Power factor profiles for the different systems for a day of high but intermittent solar radiation

4.3.3.2. Phase and line voltage profiles for the three systems

The phase voltage profiles for the three systems are presented in Fig. 4.57. The recorded voltages were all in the standard operating range as prescribed by the EMC standards, EN 50160, EN 61000 as ±10% for low voltage and medium voltage power systems (CENELEC, 2007; Dreidy et al., 2017), even though all the recorded voltages for the three systems were lower than the 230 V nominal voltage. The phase voltages recorded for subsystem three were higher than the phase voltages of the other two subsystems throughout the study for that day. The difference at each instance was about 2 V. The average voltages for the three systems are 223.36 V, 223.72 V and 226.15 V for system 1, 2 and 3. The standard deviations show that system 3 had voltages that were more uniform than the other two systems. The standard

deviations were 0.6936, 0.5345 and 0.3900 for systems 1, 2 and 3. The line voltages of system 1 and 2 instead showed close similarities. This was evident in the average values of 221.31 V and 221.44 V for system 1 and 2. The trend of the phase voltages recorded was a bit different compared to the line voltages. Line 1 had voltages that were lower than other lines voltages throughout the measurement period for the day. Lines 2 and 3 recorded voltages that were similar to each other. The average line voltages were 387.1 V, 389.3 V and 389.5 V for lines 1-2, 2-3 and 3-1. The standard deviations determined were 1.03, 0.84 and 0.72 for line 1, 2, and 3, respectively. The line voltages recorded for all the phases were within the limit restrictions of the grid standards as shown in Fig. 4.57. The possible reason for the disparity in the phase voltages may be the asymmetrical loading of the different phases. This causes the current to flow through the neutral, thereby making the phase voltages to vary (Sonel, 2020).

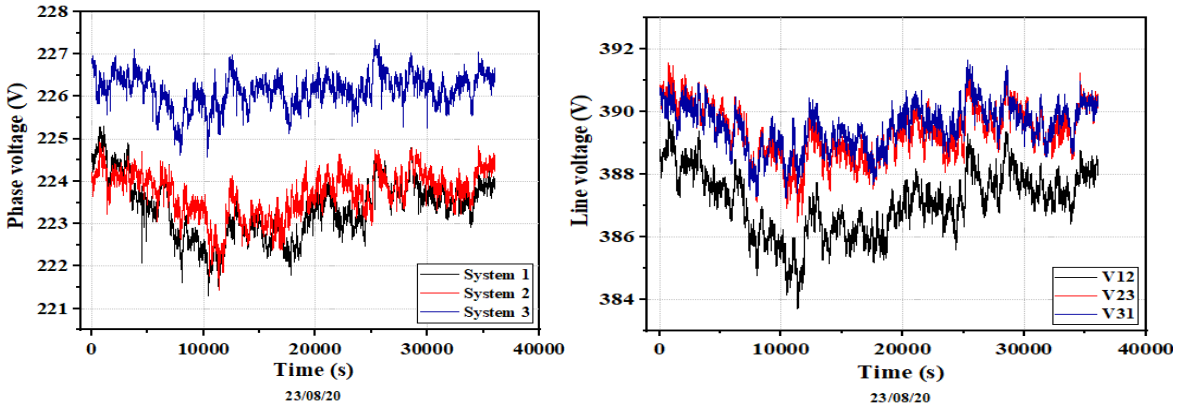

Fig. 4.57. Phase and line voltage profiles for the different systems

The reference voltages for the various systems were also recorded. The reference voltage is used to establish precision in the measurement. Thus, the reference voltage provides accurately set constant voltage, independent of load changes, temperature, input supply voltage and time. The reference voltage is usually independent of the power supply, the temperature, the processing variations, noise and interference (RSComponents, 2019).

As shown in Fig. 4.58, the reference voltage of system 3 was higher than the reference voltages of the other subsystems throughout the study period. The average values were 223.36 V, 223.71 V and 226.15 V for systems 1, 2 and 3. These values translate into the higher phase voltages recorded for system 3 compared to the other subsystems. The reference voltage system 2 was also higher than that of system one even though they were close, as was evident in the average values.

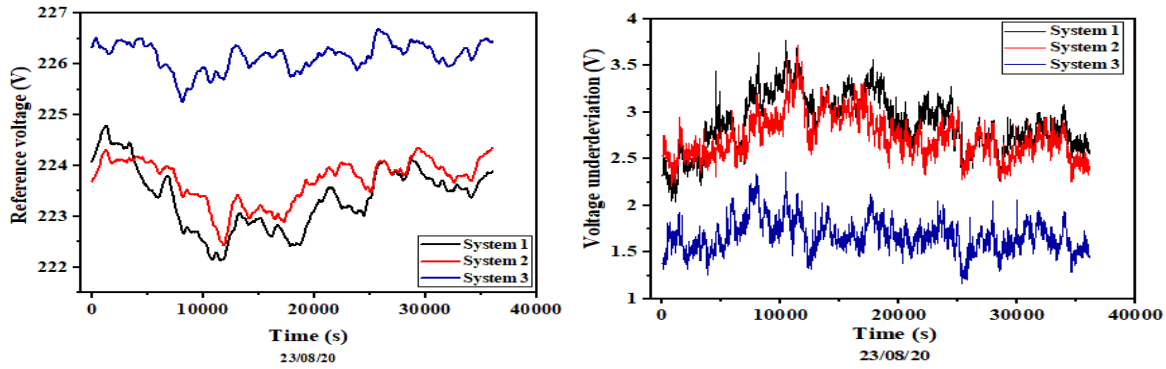

Fig. 4.58. The reference voltages and the voltage deviations of the various systems

4.3.3.3. Voltage deviation and voltage unbalance

Voltage deviation occurs when the power grid's voltage changes slowly (less than 1 % per second); thus, the is a difference in the measured voltage and nominal voltage. Factors such as power flow dispersion, transmission path, supply distance, voltage management, and reactive power control influence the grid's voltage deviation (Zhang et al., 2014). The voltage deviation can be determined by the expression in Eq. 4.5.

$$\text{Voltage deviation} = \frac{V_{measured} - V_n}{V_n} \times 100\%, \quad (4.5)$$

where V_n is the nominal voltage. The highest under deviation of 3.78 was recorded for the system, followed by system 2 with a deviation of 3.72. The least deviation of 1.16 was recorded by system 3 during the period of examination. The average deviation for the 3 systems were 2.89, 2.73 and 1.67, respectively, for systems 1, 2 and 3. The least deviation of system 3 shows its line and phase voltages' closeness to the nominal line and phase voltages compared to the other subsystems. There were no overdeviations recorded during the experimentation for that day. However, the phase VUF determined for the systems were 1.68%, 1.66% and 1.06%, respectively for systems 1, 2 and 3. The VUF for all three systems did not violate the set limits of the standards. The line VUF of the three systems also did not violate the standards considered. The calculated line VUF for the three systems were 0.97%, 0.96% and 0.61%, respectively, for systems 1, 2 and 3. This shows that the line voltages of the studied systems recorded lesser variations than the phase voltages.

4.3.3.4. Current total and individual harmonic distortions for the different systems

The current total and individual harmonic distortions recorded for the three subsystems on a day of sporadically low and high solar radiation are presented in Fig. 4.59 and Fig. 4.60. Even though system 2 and 3 have the same configuration (inverter and array), the phase current and the output power of system 3, exceeded that of system 2 by about 5% throughout the study period. This was not an issue of shading or one set of array receiving less sunlight than the other set of the array, since the trend of 5% difference was observed from sunrise to sunset. This observation could result from the malfunctioning of one or some components in the balance of system. The phase current for all the systems followed the solar radiation trend recorded as they are directly related. The current total harmonic distortion showed the opposite trend, as should be the case. The lower the irradiation levels (approximately below 400 Wm^{-2}) irrespective of the intermittency, the increasing the THD. This trend was evident in the three figures shown in Fig. 4.59. It could be seen that even though the intermittency was sporadic, at an intensity above 400 Wm^{-2}, the generated total harmonic distortions were relatively low and steady. The CTHD for system 3 was higher than system1 and 2 throughout the study for the day. The maximum CTHDs were 77.2%, 62.7% and 77.7% for system 1, 2 and 3. The extremely high values result from the instantaneously occurring spikes observed for all the systems at different times. At the start of the process, the CTHDs were the lowest for both systems at 4.2%, 4.1% and 4.7% for system 1, 2 and 3, respectively. The highest continuous CTHDs were observed at the latter stages of the study when the irradiation levels were constantly decreasing and extremely low. According to the standards, IEEE 1547, AS 4777.2, and IEC 61000-3-2, which specify that the CTHDs be less than 5%, it could be seen that for

system 3, only 2% of the recorded THD met the specified requirement. For system 1 and 2, 5.6% and 29.5% of the CTHD profile, respectively, were within the limits of the standards considered. The average CTHD and the standard deviation of the output for the different systems were 10.87% and 6.7 for system 1, 9.26% and 5.7 for system 2 and 11.4% and 6.4 for system 3.

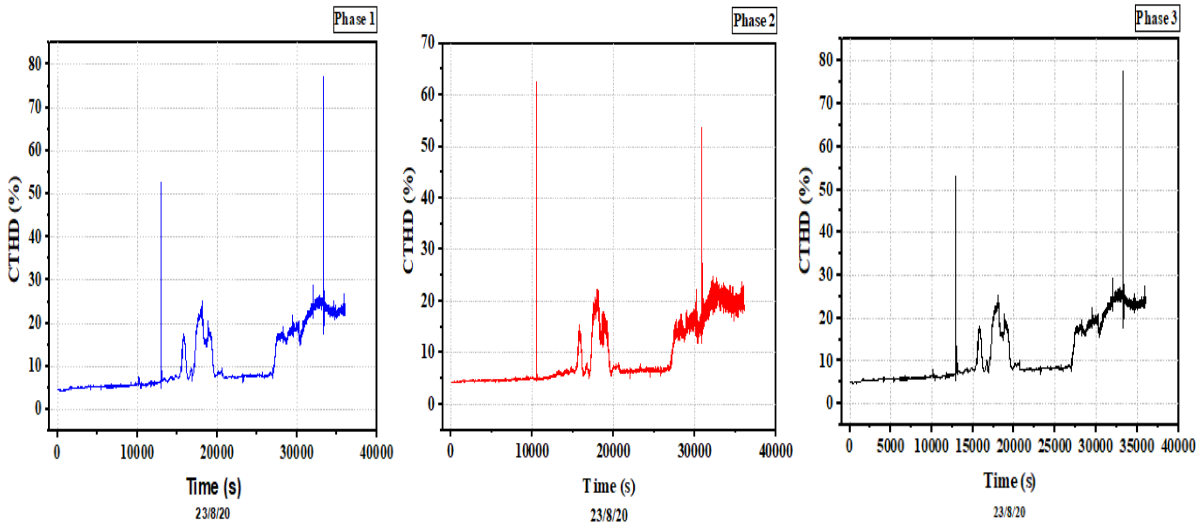

Fig. 4.59. Current total harmonic distortion for system 1, 2, and 3 on a day of high but intermittent solar radiation

The standards of reference for the acceptable range of current individual harmonic distortions are the IEC 61000-3-2, IEEE 1547, and AS 4777.2 standards listed in Tables 2.5 – 2.7. According to the standards for the odd harmonics 33 < h, the acceptable least harmonic distortions are to be below 0.3%. The least for the even harmonics as specified by the referred standards is to be below 0.5%. All the systems showed that the individual current harmonic distortions were within the various standards' specifications. The highest harmonic distortion was 1.805%, 1.725% and 1.812% for system 1, 2 and 3, respectively for the first harmonic. The THDs were 10.87%, 9.26%, and 11.37% for system 1, 2 and 3, respectively, as shown in Fig. 4.60. The THDs for system 3 were higher than the THDs for the other systems for the entire experimentation period.

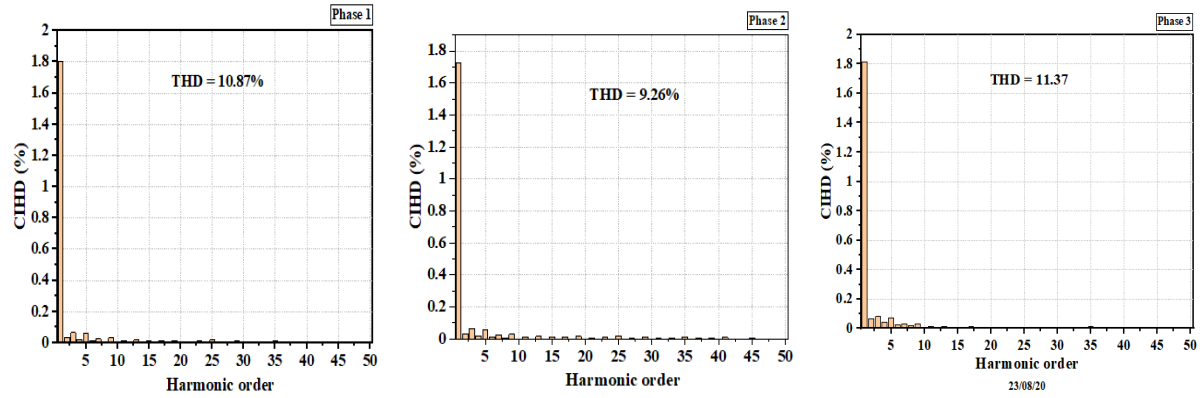

Fig. 4.60. The current individual harmonic distortions for system 1, 2 and 3 for a day of high but intermittent solar radiation

4.3.3.5. Voltage flickers

Voltage flickers manifest in the sudden changes in the brightness of lamps with the noticeable flicking of lights (Ferdowsi et al., 2020). The standards for low voltage power network, the EMC standard of EN 6100 specifies the Pst to be < 1.0 and Plt to be < 0.8. The IEEE 1547, IEC 61000-3-3 standards also require the voltage flickers to be between 0.6 and 0.9 pu for Plt and Pst, respectively (Tagare, 2011). Results show that there were no Plt recorded for any of the three systems throughout the study. The short-term voltage flickers for systems 1, 2, and 3 are presented in Fig. 4.61. Measurements of voltage flickers were taken at intervals of 3 s for the entire period. System 3 recorded the highest magnitude short term voltage flickers of 1.115, compared to system 1 and 2, which generated 0.866 and 0.744, respectively. The Pst recorded for system 1 and 2 were all within the standards considered. For system 3, however, 0.2% of the recorded Pst breached the limits specified in the referenced standards. These occurred with a 1-minute span at 16 minutes after midday. It can be deduced from the results of the probability flicker severity that system 3 had a higher level of quality issues compared to the systems 1 and 2 under the experimental conditions as Pst is a parameter that demonstrates the degree of voltage fluctuation in power networks. The average Pst determined for the different systems, however, showed system 2 having the highest average value of 0.1868. Whiles it is 0.1624 for system 1 and 0.1638 for system 3.

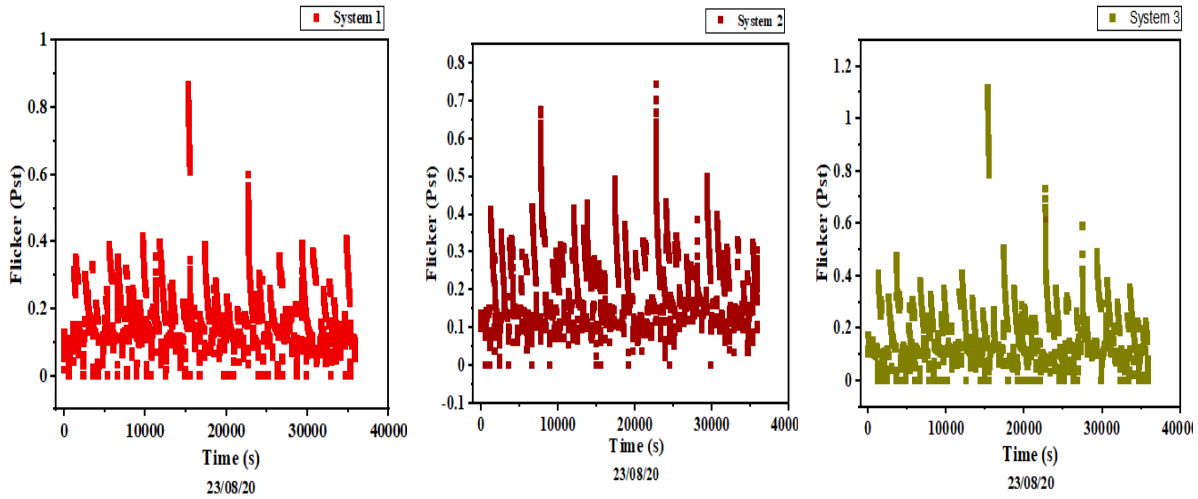

Fig. 4.61. Short term voltage flickers (Pst) for systems 1, 2 and 3

4.3.3.6. Voltage total and individual harmonic distortions for the different systems

Voltage total harmonic distortions for the three systems are presented in appendix 16. The voltage THD measured for the three systems were all within the specified standards of IEEE 519 for (V≤ 1) kV systems where individual harmonic distortions must not be beyond 5%, and the THD 8%. The THD for system 1 (the pc-Si modules) throughout the study was higher than subsystems 2 and 3 (a-Si systems) even though it had lower phase voltages than the two systems (system 2 and 3) throughout the study period. Systems 2 and 3 had relatively close values of VTHD from the start of the investigation until about midway. From midday until the end of the study, the THD of system 3 rose above that of system 2. The range of VTHDs recorded for the various systems were 1.53% - 1.81%, 1.41% - 1.68% and 1.4% - 1.79%, respectively, for system 1, 2 and 3. The average THDs were 1.69%, 1.59% and 1.56% for system 1, 3 and 2, respectively.

The voltage individual harmonic distortions for the different systems and inverters are presented in Fig. 4.62. The voltage individual harmonic distortions for the 50 harmonic orders for all the systems studied were within the specified range given by the standards provided in Tables 2.5 -2.7. The highest voltage individual voltage harmonic distortion was recorded for the 7th harmonic for system 2 and 3. However, for system 1, the highest individual harmonic distortion was recorded for the fifth harmonic order. The highest VIHDs for the different systems are 2.611%, 2.370% and 2.323%, respectively, for the 5th harmonic for system 1, 7th harmonic for system 2 and 7th harmonic for system 3. The total harmonic distortions for the different systems throughout the study were 1.69%, 1.56% and 1.59% for system 1, 2 and 3, respectively. The voltage individual harmonic distortions for the even harmonics were negligibly low for all systems examined.

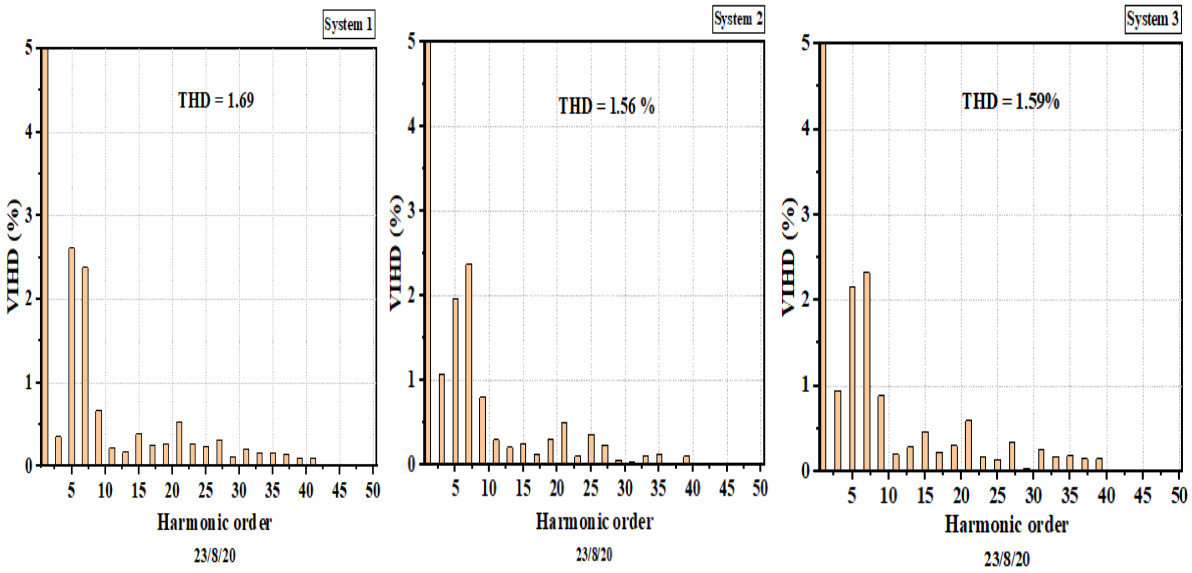

Fig. 4.62. Voltage individual harmonic distortion for system 1, 2 and 3 (23/08/20)

4.4. Power quality assessment of a single-phase grid-connected PV system

The results for the power quality investigation of the transparent glass monocrystalline solar modules system tied to a monophase grid inverter and the discussions are presented in this section. Three study days with contrasting climatic conditions out of the several days of examination have been chosen to analyse and describe the system's power output. The various quantities were recorded at intervals ranging from 200 ms to 6 s. The solar radiation profiles measured for the 1st, 6th and 7th of November are presented in Fig. 4.63. Measurements were taken from 9 am to 3:00 pm, from 9 am to 3:30 pm, and 9 am to 4 pm for 1st, 6th and 7th November. The period of measurement varied due to the sunset time for the various days. Nevertheless, the typical solar radiation characteristics were obtained. Solar radiation profiles for the three days were selected to present contrasting outputs for low, steady and intermittent solar radiation profiles. These solar radiation profiles have been chosen to assess their impact on the grid-connected PV system's power quality performance. Fig. 4.63 a) shows a solar radiation profile with an intermittent and low output for the first half of the measurement period and the other half with a steady solar radiation output. Fig. 4.63 b) presents a relatively stable

solar radiation output throughout the experimentation. Fig. 4.63 c) shows a relatively stable solar radiation output throughout the investigation.

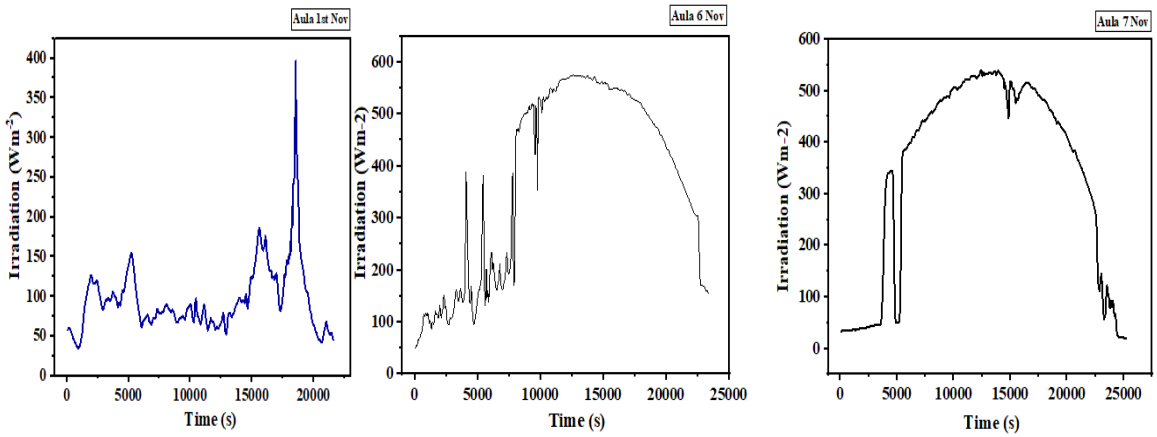

Fig. 4.63. Solar radiation data for the a) 1st November b) 6th November 2020 and c) 7th November 2020

4.4.1. Power factor profiles for the three scenarios

Power factor (cos ϕ) (PF) presents the phase angle between the current and the voltage signals of the system's AC signal output. According to the standard for power factor (IEEE 1547), solar PV grid-connected inverters are to be designed to operate at a power factor close to unity. The technical regulations concerning power factor for most countries specify that the power factor range at the point of common coupling should be ≥0.95 or ≤1, whether leading or lagging (Al-Shetwi et al., 2020). The proximity of the power factor to unity in an electrical system enhances the consumption of the total energy supplied to the load. Therefore, the deviation of the power factor from unity causes the current flow through the lines to increase, consequently rendering the voltage to drop.

The power factor profiles by the Aula PV system for the 1st Nov 6th Nov and 7th Nov 2020 are presented in Fig. 4.64. Since power factor is dependent on the active power output with respect to the apparent power, it is highly influenced by the availability of high levels of solar radiation, thus, high active power output. With reference to the stated standards, the PF for the 7th Nov recorded 10.5% of PF values outside the acceptable limits. The low values occurred at the start and the end of the study when the irradiation levels were very low. This is because of the steadily high irradiation figures that were measured on the day. The percentage of the PF below the 0.95 standard for the other days studied was 15% for the 6th of Nov 2020 and 92.3% for the 1st of Nov 2020. The low irradiations levels with an average of 96 Wm^{-2} for 1st Nov was translated into the low PF profile recorded for the day. The average power factor for the three selected days were 0.94, 0.98 and 0.84 for the 7th Nov, 6th Nov and 1st Nov, respectively. The minimum values were 0.26, 0.84 and 0.50 for the 7th Nov, 6th Nov and 1st Nov, respectively. The results show the deviation of the power factor values for the 7th of Nov compared to the rest of the days. The standard deviations were 0.1328, 0.0304 and 0.0983 for 7th Nov, 6th Nov and 1st Nov. The direct correlation between the power factor and the recorded solar radiation was evident in the results.

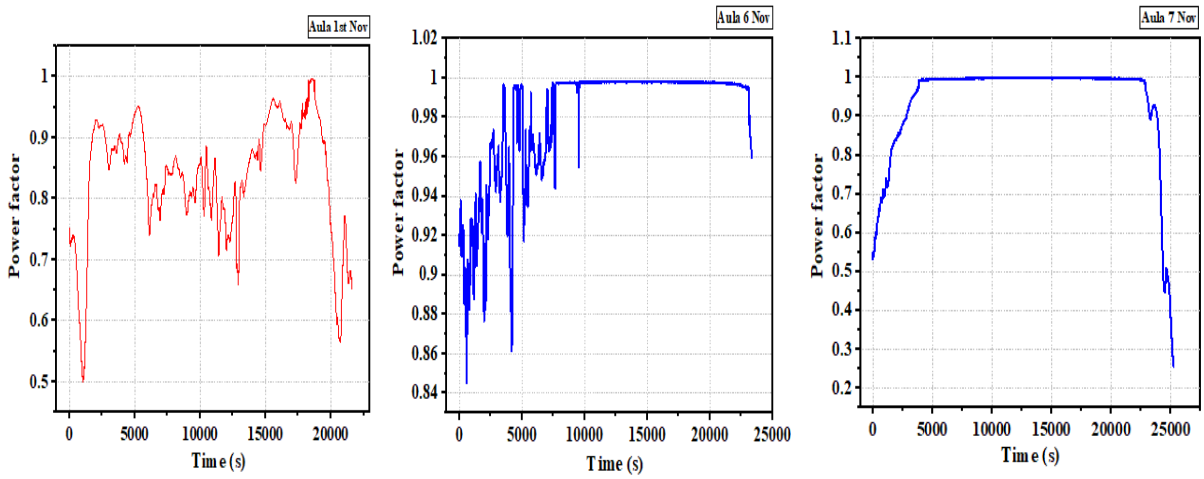

Fig. 4.64. Power factor profiles for the 1st Nov, 6th Nov and 7th Nov 2020

4.4.2. Voltage flickers

Voltage flickers are evident in the sudden changes that occur in the brightness of lamps with the noticeable flicking of the lights (Ferdowsi et al., 2020). The acceptable level of flickers for low voltage power network by the EMC standard (EN 6100) is Pst < 1.0 and the long-term voltage flickers (Plt) at < 0.8. The IEEE 1547, IEC 61000-3-3 standards also specify that voltage flickers be between 0.6 p.u and 0.9 p.u for Plt and Pst, respectively (Tagare, 2011). Results indicate that there was no Plt recorded for any of the scenarios throughout the experimentation for all the days. The short-term voltage flickers for the 1st, 6th and 7th Nov. 2020 are presented in Fig. 4.65. Measurements of voltage flickers were made at the intervals of 3 s. The measured Pst were all within limits specified for grid-connected PV systems by the various standards considered. The highest magnitude Pst of 0.899 for the system was recorded on the 7th of Nov. The highest Pst for the 1st and the 6th Nov were 0.656 and 0.551, respectively. However, the average Pst for the 7th (0.184) was less than that for the 6th (0.223). Even though the recorded Pst did not violate the specified standards, averagely, the occurrence of the Pst for the 6th Nov. was more severe than for the 1st and 7th Nov. Thus, based on the Pst, the system had recorded more quality issues on the 6th than on the 7th. The average Pst were 0.184, 0.20, and 0.223, respectively for the 7th, 1st and the 6th Nov.

The primary reason for the observation for the 6th Nov is that, as the solar radiation levels drop, inverters with their MPPTs will seek to extract the most of electricity that could be generated under the circumstance of dwindling irradiation levels. This initiates a nonlinear process that produces a considerable level of flicker**s**. The worst impact is experienced when sporadically fast-moving clouds occur and change at the same speeds. Several inverters respond to similar effects which result in the most significant generation and impact of voltage flickers. The generation of flickers depends on the occurrence of worst-case sporadic cloud cover and the number of inverters connected to the grid (Pterra, 2013).

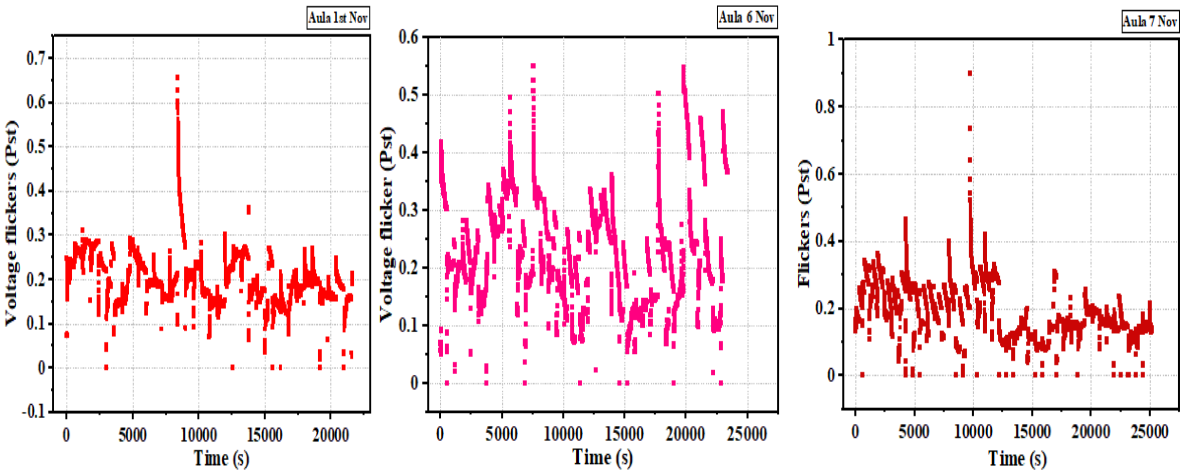

Fig. 4.65. Short term voltage flicker (Pst) for a) 1st November 2020 b) 6th November 2020 and c) 7th November 2020

4.4.3. Current total harmonic distortions

The results for the current total harmonic distortions for the Aula transparent PV module system for the different days and different weather conditions have been presented in Fig. 4.66. The permissible limit specified by the various standards IEC 61000-3-2, IEEE 1547, AS 4777.2 for current total harmonic distortion as listed in Tables 2.5 to 2.7 is (CTHD<5%). Results for all scenarios show similar increasing trends of CTHDs even though at different magnitudes for each of the days. The trend increased fairly linear from low values of CTHDs at the start of the investigations to the highest values at the end of the study. The CTHD profiles of all the scenarios studied with the Aula system did not correlate with the solar radiation recorded for the different days of the study. There was no occurrence of the randomly occurring high instantaneous spikes CTHDs recorded for the other large grid-connected string inverters studied.

The highest current total harmonic distortions were recorded on the day with the very low irradiation (1st Nov 2020). The maximum and the average values of CTHDs recorded for the various days were 30.25% - 20.10%, 6.58% - 4.51% and 5.76% - 4.65%, respectively for the 1st Nov, 7th Nov and the 6th Nov 2020. The minimum CTHDs were 5.147%, 4.51% and 4.17% for the 1st Nov, 7th Nov and 6th Nov, respectively. The average and the maximum values for the different days show that very low irradiation levels as recorded on the 1st Nov 2020, had a significant adverse influence on the occurrence of current distortions injected into the grid. Averagely, the CTHDs recorded on the 1st of Nov were five times greater than the CTHDs recorded for the 6th and 7th of Nov 2020. The intermittence of solar radiation recorded on the 6th of Nov did not show any correlation or influence on the current harmonic distortions. The distortions increased fairly linear irrespective of the change in the solar radiation intensity levels, as shown in Fig. 4.66.

The irradiation on the 7th of Nov was steady and high, with negligible intermittence compared to the other days. However, the trend of current harmonic distortions recorded for the day was similar to the other studied days. The current distortion output did not also correlate with the irradiation. With reference to the standards considered, the CTHDs recorded for the 1st of Nov

throughout the experimentation period were all beyond the specified limits set by the standards to be fed into the grid by a distributed power source. The average CTHD recorded on the 1st of Nov was four times (about 300%) greater than the maximum acceptable limit specified by the standards. However, this is not unexpected as at low power generations conditions (below 20% the rated capacity) of grid-connected PV systems, the maximum power point tracker and the controls for the factor are disabled. The startling observation is the increasing trend of the CTHD irrespective of the intensity and changing levels of the available solar radiation.

It is expected that at high solar irradiation levels, the current control systems within the grid inverter are re-established (Groß, 2005). Results showed that with regards to the acceptable limits specified by the standards that could be fed into the grid, the system met the requirement at the start of the measurements in the early hours of the day for the 7th of Nov and was extended for the 6th of Nov. The percentage of the CTHD that met the specified standards of <5% was 12.5% for the 7th of Nov, 85.8% for the 6th of Nov and 0% for the 1st of Nov. It could be seen that even though the profiles of the CTHD did not correlate with the solar radiation trends for the various days, the day with the least solar radiation recorded the highest CTHD which did not meet the set standards throughout the study period. The maximum, minimum and standard deviations of the CTHDs for the different days are presented in Table 4.6.

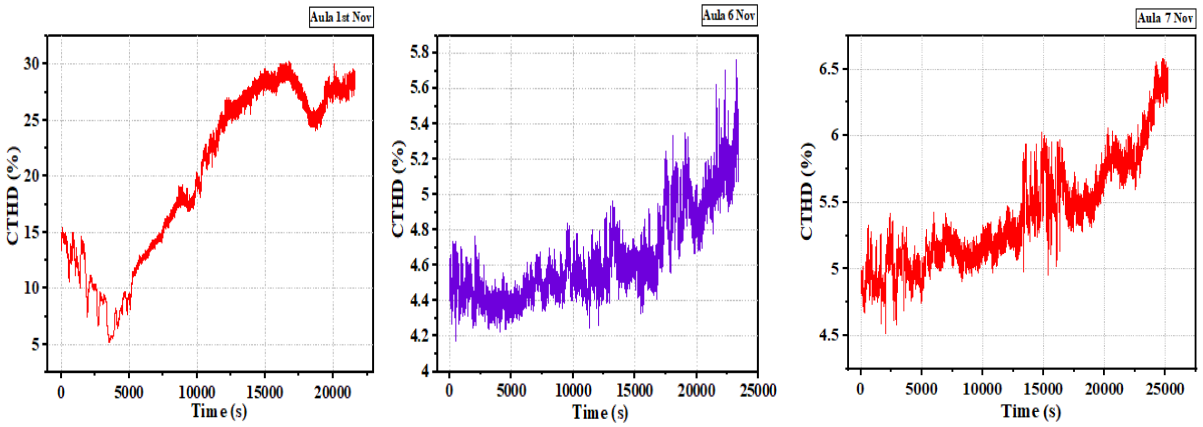

Fig. 4.66. The current total harmonic distortion profiles of the Aula grid-connected system for a) 1st November 2020 b) 6th November 2020 and c) 7th November 2020

Table 4.6. Maximum, minimum and the standard deviations of CTHDs for the different days

	1st Nov 2020	**6th Nov 2020**	**7th Nov 2020**
Max	30.25 %	5.76%	6.58%
Min	5.15 %	4.17%	4.51%
Ave	20.10 %	4.65%	5.40%
Stdev	7.59 %	0.27%	0.40%
% <5%	0	85.8%	12.5%

4.4.4. Current individual harmonic distortions

The individual current total harmonic distortions for the different days are presented in Fig. 4.67. The standards for reference of the acceptable range of current individual harmonic

distortion are the IEC 61000-3-2, IEEE 1547, and AS 4777.2 standards listed in Tables 2.5 – 2.7. According to the standards for the odd harmonics 33 < h, the acceptable least harmonic distortions are to be below 0.3%, and the least for the even harmonics as specified by the referenced standards is required to be below 0.5%. Results for the selected days showed that the individual current harmonics were within the specified limits given by the various standards. The highest recorded individual current harmonic distortions were for the first harmonics for all cases studied. The highest harmonic distortions were 0.127%, 0.425% and 0.392% for the 1st Nov 6th Nov and 7th Nov 2020. The current THD recorded for the different days for the system under study was 4.56%, 5.40% and 20.10% for the 6th Nov 7th Nov, and 1st Nov. The figures showed that apart from 6th Nov, the other selected days did not meet the power feed-in requirements by the relevant standards for current THD at the PCC for grid-connected solar PV systems. The current THD for the 1st of Nov was relatively very high because of the particularly low solar radiation levels for the day. However, the current THD for the 7th Nov was unexpected as the irradiation trend for the day was favourable to produce a low THD output with conditions similar to that of the 6th Nov 2020 except for the first half of the study as shown in Fig. 4.67. Harmonic distortions both for current and voltage generated at the PCC of PV systems with the grid result from the combined effect of the characteristics of the grid system and the line or power conditioning unit of the PV system being investigated (Vasanasong and Spooner, 2000). However, the system being investigated is not coupled with a transformer. The measurements took place when there was no power usage at the facility where the system is installed. This means that the quality issues observed are virtually emanating significantly from the installed PV system.

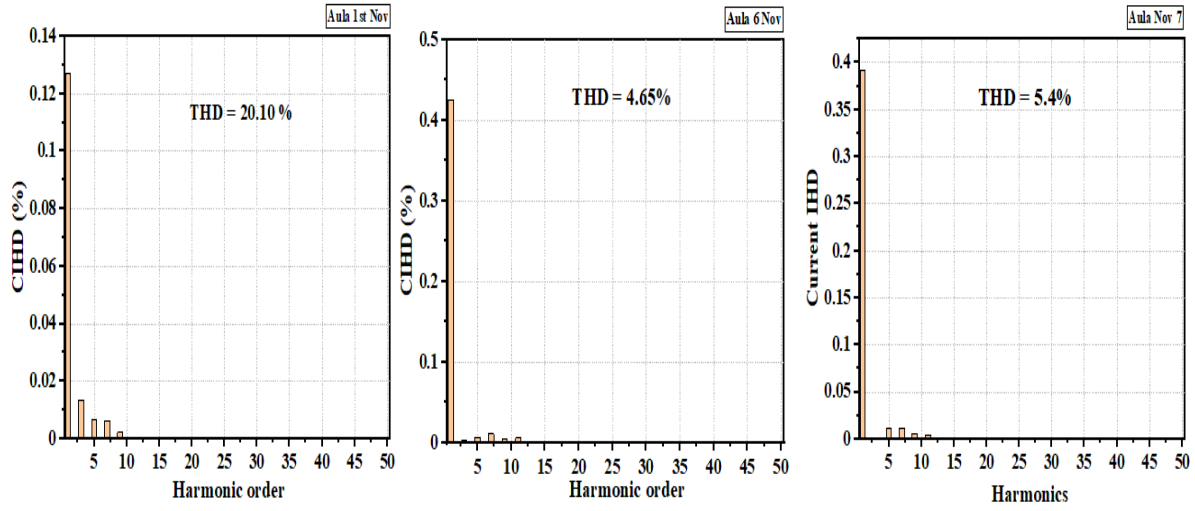

Fig. 4.67. The individual current harmonic distortions for a) 1st Nov 2020 b) 6th Nov 2020 and c) 7th Nov 2020

4.4.5. Voltage total and individual harmonic distortions

The voltage total harmonic distortions were recorded at the interval of 200ms for six hours, six and a half hours and seven hours for 1st Nov 6th Nov and 7th Nov 2020, respectively. The variation in the measurement duration is due to the different weather conditions (sunset hours) for the different days of the assessment. The recorded VTHD profiles were compared with the

specified standards for connecting PV systems with the power grid. As stated in Table 2.5 – 2.7, the VTHD limits, according to the IEEE 519 and IEC 61000-3-2 standards are 8% and 5%, respectively.

Results for all the scenarios studied were within the accepted limits of 5% and 8% specified by the referenced standards, as shown in Fig 4.72. The maximum VTHDs were 1.557%, 1.894% and 1.514% for the 1st Nov, 6th Nov and 7th Nov, respectively. The minimum and average VTHDs for the various scenarios were 1.267% and 1.415%, 1.051% and 1.188% and 1.152% and 1.269%, respectively. The VTHD profiles for the different days presented different unique trends. The VTHD for the 6th of Nov has the most significant fluctuations amongst the days of the studies. No established relationship was observed between the VTHD profile and the irradiation fluctuation. There was a periodic rise and fall in the output profile even though the time span for the change was not according to any observed specific trend. The trend in the profile of the VTHD for the 6th of Nov presented a relatively observable sequence apart from some high spikes of distortions that occurred momentarily. The VTHD started from a high value and decreased linearly for about one and a half hours and then restarted from the similarly high value of VTHD and dropped again for the same period. The least variation of the VTHDs amongst the studied days was observed for the 6th of Nov 2020. The standard deviation of the VTHDs were 0.0449, 0.0677 and 0.0400, respectively, for 1st, 6th and 7th Nov 2020 as shown in Fig. 4.68.

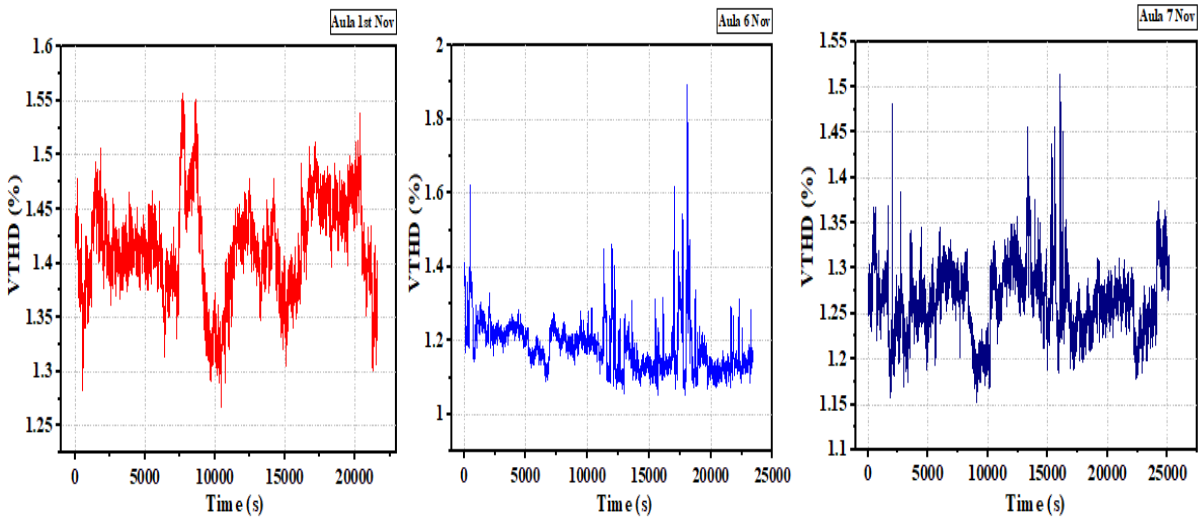

Fig. 4.68. The voltage total harmonic distortion profiles of the Aula grid-connected system for a) 1st November 2020 b) 6th November 2020 and c) 7th November 2020

The voltage individual harmonic emissions by the Aula system for the different days of study are presented in Fig. 4.69. Results show that the odd harmonics were the most pronounced for all the days of measurement. The specified limit for the individual harmonic voltage distortions for a PV system connected to a low voltage power grid is 5% for the IEEE 519 standard. As presented in Fig. 4.69, the highest voltage harmonic distortions emitted by the system into the grid at the PCC were for the 7th harmonic. The distortions for 7th harmonics for the different days were 2.044%, 1.956% and 1.901%, respectively, for 1st Nov 7th Nov and 6th Nov. The individual harmonics for the 1st of Nov were the highest as shown for the 5th and the 3rd harmonics with values of 2.009% and 1.188%, 1.469% and 1.164%, and 1.210% and 1.048%

for 1st, 7th and 6th Nov, respectively. The voltage harmonics emitted by the system for the days were all within the specified limits for the various standards. The individual harmonic distortions for the even harmonics were negligibly low for all scenarios that were examined for the microinverters.

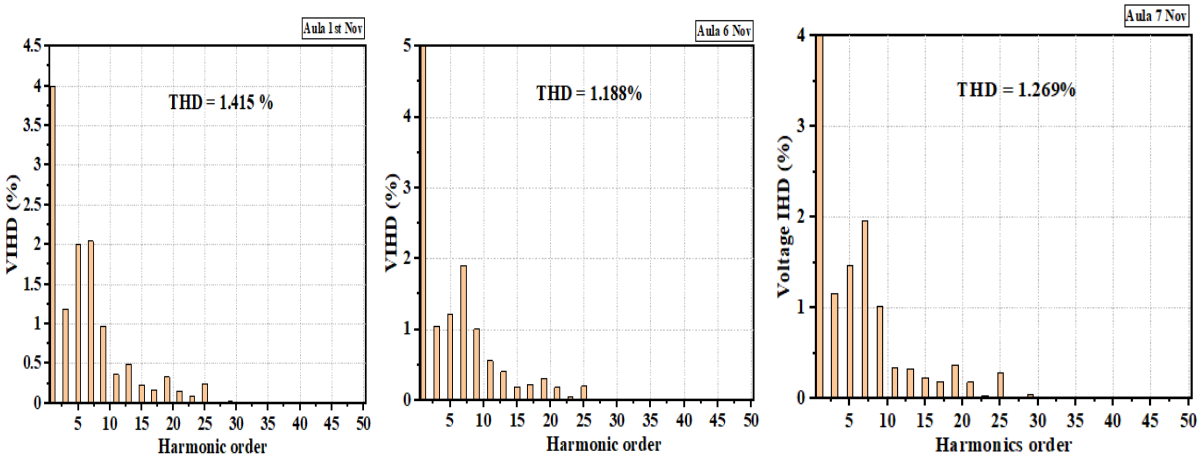

Fig. 4.69. Voltage individual harmonic distortions for a) 1st Nov 2020 b) 6th Nov 2020 and c) 7th Nov 2020

4.4.6. Phase voltage of the system for the different days of study

The phase voltage profiles for the three different days are presented in Fig. 4.70. The recorded voltages were all in the standard operating range as specified by the EMC standards, EN 50160, EN 61000 as ±10% for low voltage and medium voltage power systems (CENELEC, 2007; Dreidy et al., 2017), even though all the recorded voltages for the three systems were greater than the 230 V nominal voltage. The recorded voltages for the different days showed a similar trend where the initial voltages were the highest and then decreased gradually to the end of the study. However, the slopes were steeper for the 1st and the 7th Nov than the voltages for the 6th Nov. The 1st Nov profile also showed pronounced periodic rise and fall, which was not as evident for the 6th and 7th Nov. The average voltages for the three days are 238.08 V, 238.92 V and 238.69 V for system 1st, 6th, and 7th Nov. The highest voltage was recorded for the day with steady and high solar radiation. The standard deviations show that the voltages for 6th Nov were more uniform compared to the other days. The standard deviations were 0.6212, 0.4370 and 0.7225 for systems 1st, 6th, and 7th Nov.

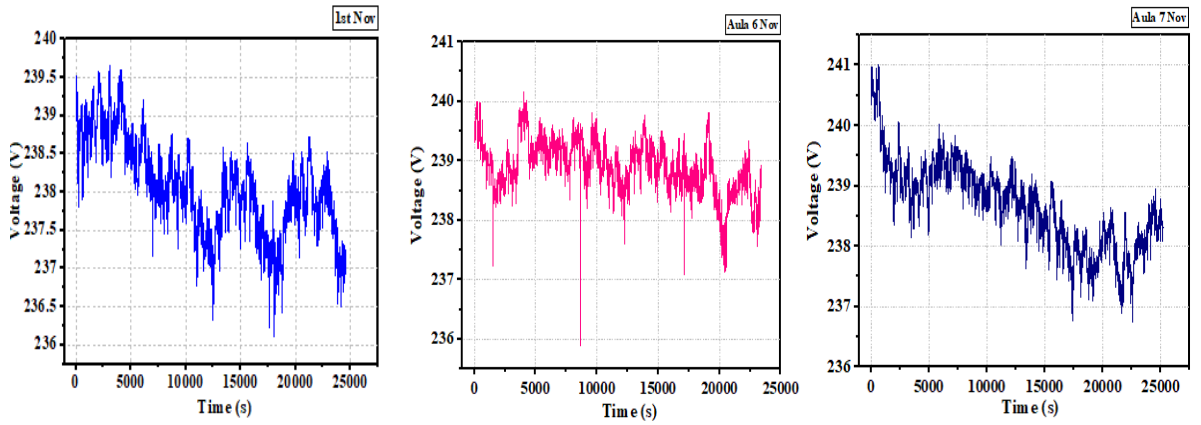

Fig. 4.70. Phase voltages for the different days of study

The voltage deviations for the different days of study were also determined. The results showed only over deviation for the whole period. The highest over deviation of 4.79% was recorded for the 7th Nov, followed by the measurement on the 6th Nov with a voltage deviation of 4.42%. The least deviation of 4.20% was recorded on the day with low solar radiation. The average deviations were 3.51%, 3.88% and 3.78% for the 1st, 6th and 7th Nov. The average deviation for the 6th Nov was the highest because of the recorded voltages' closeness compared to the other days. The average voltages were 238.08 V, 238.92 V and 238.69 V for 1st, 6th and 7th. The voltages range from 236.11 to 239.67 V, 235.88 to 240.16 V and 238.69 to 241.02 V for the 1st, 6th and 7th, respectively.

4.4.7. Frequency profiles for the different days

Fig. 4.71 presents the frequency profile for the different days of study. The related standards for grid frequency, EN 50160 (CENELEC, 2007), specifies that the frequency should be within ±1% of the nominal frequency (In the case of Hungary, 50Hz). The recorded frequency profiles for the days of study were within limits specified by the different standards. The ranges of the frequency measured were 49.95 – 50.05, 49.93 – 50.06 and 49.95 – 50.05 Hz for the 1st, 6th and 7th Nov. The average frequency was 50.00 Hz for all three days of study. This shows the efficiency of the system with regards to frequency. However, the standard deviations were 0.016, 0.017 and 0.014 for the 1st, 6th and 7th Nov.

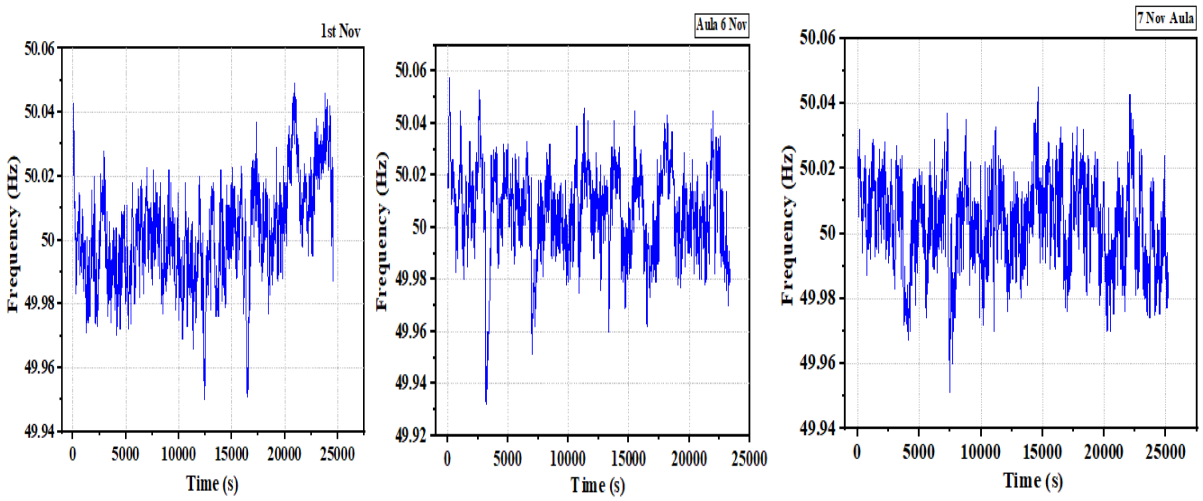

Fig. 4.71. Frequency profiles for the different days of study

4.5. Relationship between harmonic current and the system harmonic voltages

To ascertain each system's impact on the generation of harmonic voltage and the correlation with harmonic current, detailed investigations of the various systems were conducted. This section presents the discussions on the analysis. The plots and complete results are shown in appendices 4 to 15.

A study by Chicco et al., revealed a positive correlation for all the systems studied, except for the 3rd harmonic of one of the systems that registered a negative slope. Thus, according to their study, the harmonic current is directly proportional to the system harmonic voltage (Chicco et al., 2009). Dress et al. mentioned in their research that individual harmonic currents demonstrate similar behaviours when the inverter's loading or power output is more than 20%

of the rated capacity (Dress et al., 2005). Their observation was more significant for lower harmonics orders, irrespective of the system's characteristics.

Data for days with high and steady solar radiation were chosen for the study. The regression analysis was used to determine the relationship by applying the least square method. Data used for the analysis were extracted from the lot within the period when the PV system loading or PV power generation of more than half the nominal or rated capacity. Various scenarios with different datasets of 1000 and 3000 were applied. In a further study on the string inverters connected to the rooftop system, data for the entire period was again used to compare the results with the first scenario and determine the correlation between the harmonic current and the harmonic voltage.

The test on the solar PV simulator (2E microinverter) with solar radiation set at 400 Wm^{-2} showed negative correlations for the 3rd, and 7th harmonics while the 5th and the 9th harmonics recorded positive correlations. However, the test with irradiation fixed at 1000 Wm^{-2} recorded a negative correlation for only the 7th harmonic whiles the correlations for the other harmonics were positive. It could be seen that there were varying results recorded for the two scenarios under the constant irradiation conditions, as shown in appendices 11 and 12.

The test with the MaySun-600W-B (China) microinverter produced relationships that were either negative or positive. The 3rd and 5th harmonics showed a positive correlation for both tests with the different solar modules. The 7th and the 11th harmonics produced negative correlations for the test with the Juta and Solarex solar modules. Thus, the China microinverter showed similarities for different harmonic orders except for the 9th order, which showed different correlations for the different settings.

The GMI 300 (Holland) microinverter showed similar trends for the 5th and the 7th harmonics for both studies with the Juta and Solarex modules. The correlation for the 5th was positive whiles that for the 7th was negative. There were no harmonic values for the 7th harmonic order with the Juta modules and no values for the 11th harmonic for both scenarios for the study with the Holland inverter. The 3rd and 5th harmonics showed positive correlations 9th harmonics recorded positive correlations for the test with the Solarex modules. Details of the results presented in appendices 12 and 13. All the microinverters studied showed the same trend for the 5th and the 7th harmonic orders. Thus, a positive and negative correlation for the 5th and the 7th harmonic orders, respectively.

Results for the string inverters showed that regardless of the system studied, and the quantity of data used for the analysis, the correlation for the 5th harmonic remained positive as was realized for the microinverters. The usage of 1000 and 3000 measured values produced similar correlations for the 5th and the 7th harmonic orders for all the systems. The study with the 3000 data had correlations for three harmonic orders with the same trends for all the systems studied. Inferentially, it has been observed that the correlation is determined by the conditions prevailing and the harmonic order. Except for the 5th harmonic order, which showed a positive correlation for all the scenarios studied for both the string inverters and the microinverters, the other scenarios varied depending on the prevailing conditions. Details of the analysis are shown in appendices 6 to 9.

A linear model for the relationship between the harmonic current and the harmonic voltage for the 5th harmonic order of microinverter systems and string inverter systems employed in low voltage grid systems has been established out of the results of the regression analysis as

$$I_H = 0.03979 + 0.0064\ V_H,$$

where I_H is the harmonic current generated by the harmonic order and V_H is the harmonic voltage. The standard deviation was determined to be 0.0011.

Current harmonics are the main causes of voltage harmonics. The source of the voltage is distorted by current harmonics due to the source impedance (Rohouma et al., 2020). If the source impedance of the voltage source is small, current harmonics will cause proportionally small voltage harmonics. There are occasions where the increase of harmonic current correlate to an increase in harmonic voltage (Peterson et al., 2015). This can be explained by the lower values of energy being produced by the PV plant, and due to the changed relative impedance presented to the supply network, the contribution of 5th harmonic voltage by the supply system dominates (Peterson et al., 2015). Hence, the positive correlation observed for the 5th harmonic order irrespective of the system type and operating condition.

4.6. New scientific results

This section presents the new scientific findings from the research as follows:

1. Correlation between the power factor and the current total harmonic distortions

I have established that the inverse rule for the power factor and the current total harmonic distortions (CTHD):

$$PF_{true} \leq PF_{dist} = \frac{1}{\sqrt{1+(THD_I/100)^2}},$$

does not hold for all inverter systems under different operating conditions. It has also been determined that high power factor ≥ 0.95, within the acceptable standards depended on solar radiation values ≥400 Wm^{-2} or at ≥ 38% the solar PV system's nominal capacity power generation and non-intermittency. I have also proven that irradiation levels below 400 Wm^{-2} or PV power generation less than < 38% of the nominal PV system rated capacity has the most significant negative impact on the power quality of the solar PV systems.

2. Current harmonic distortions by PV systems

In the case of the current total harmonic distortions generated by the different systems, I have ascertained that the microinverter systems did not meet the specified standard requirement of <5% of CTHD injection for all scenarios and conditions studied. I have proven that microinverters under outdoor conditions, generate the highest CTHD ranging from 14.3% to 129.5%. Microinverters under indoor constant PV power generate CTHD ranging from 6.9% to 13%.

Furthermore, I have shown that the slope for the CTHD profiles for systems under constant PV power was zero whiles; it was positive (increased linearly) for the outdoor study.

It has also been established that the CTHD generated by string inverter systems was lower than that for the microinverters. It ranged between 4.5% to 20%.

I have shown that the CTHD profiles do not always correlate with the solar radiation profile; thus, the correlation between the CTHD and irradiation is not significant enough to determine its conformity with the grid codes.

3. Impact of system harmonic voltage on the harmonic current generation

I investigated the correlation between the generated harmonic current and the system harmonic voltage of grid-connected PV systems with microinverters and string inverters for varying data points and operating conditions. I have established that the generated harmonic current of the 5^{th} harmonic order for both microinverter systems and string inverter systems correlate positively with the system harmonic voltage of the studied systems irrespective of system type or operating condition in the low voltage grid systems.

I developed a linear model for the relationship between the harmonic current and the harmonic voltage for the 5^{th} harmonic order of microinverter systems and string inverter systems employed in low voltage grid systems as:

$$I_H = 0.03979 + 0.0064\ V_H,$$

where the standard deviation was determined to be 0.0011.

I have also ascertained the relationship between the harmonic current and the harmonic voltage for the 3^{rd}, 7^{th}, 9^{th} and the 11^{th} harmonic orders for both microinverter and string inverter systems connected to the low voltage power network followed no particular predictable trend but was dependent on the pertaining operating condition.

4. Voltage harmonic generation by micro and string inverter systems

Through the experimental results, I have proven that the VTHD, VIHD, the phase voltage, the line voltage and the frequency of the microinverter systems and string inverters are not significantly impacted by the solar radiation and the conditions of the PV system. It was found that the VTHD, VIHD, the phase voltage, the line voltage and the frequency of the microinverter systems and string inverters were within the specified requirement under the studied conditions.

Additionally, I have determined that the voltage harmonics generated by microinverter systems and string inverter systems in low voltage grid systems studied have no significant correlation with the solar radiation profile.

5. Voltage flicker generation

Based on the experimental results, I have established that the performance of microinverters under constant solar irradiation or PV power simulator generates higher severity of short-term flickers compared to their performance in outdoor conditions. It has been proven that the intermittence of solar radiation; hence, intermittent PV power generation does not have any significant correlation with the generation of short-term voltage flickers (Pst) in the power output of microinverters.

5. CONCLUSION AND SUGGESTIONS

In conclusion, experimental analysis has been conducted to determine the power quality performance and compliance with grid codes by different types and scenarios of solar PV grid-connected systems coupled with various microinverters and large string inverters. Power quality issues such as power factor deviation, voltage flickers, current and voltage harmonics distortions, voltage deviation, and voltage events associated with PV grid-connected systems have been studied under indoor steady PV source and varying outdoor operation conditions. The CTHDs measured for the studied microinverters under the outdoor conditions far exceeded that for the study with the PV simulator for all scenarios and microinverters. However, the voltage THD for the studies under outdoor conditions recorded lower VTHDs than the VTHDs generated with the investigations under the steady PV simulator. The recorded current THDs for the studies with all the microinverters under indoor and outdoor conditions flouted the limits specified by all the standards. The current THD profiles for the scenarios under constant simulated PV power showed a zero slope in the entire study period whiles the outdoor study with the microinverters showed positive slopes.

The voltage and current THD for the 400 Wm^{-2} and the 1000 Wm^{-2} scenarios under the steady solar radiation were 2.24%, 13%, and 2.27%, 6.93%, respectively. The voltage and current THDs for the outdoor study were 2.03% and 14.28% for Solarex (pc-Si module), 1.94% and 27.43% for Juta (mc-Si modules), and 1.97% and 33.6% for Dunasolar (a-Si glass module). Microinverters under outdoor conditions generated current total harmonic distortions ranging from 14.3% to 129.5%. However, under indoor conditions, the maximum of CTHD was 13%, and the minimum was 6.9% which were virtually constant throughout the entire measurement period. The string inverters comparably generated the lowest average CTHDs. Except for the SE 3500-ER-01-ITA single-phase string inverter, which generated an average value of 4.65% on one occasion, the recorded CTHDs were all above the 5% specified standard. The days with the highest and non-intermittent solar radiation did not produce the lowest CTHD. Thus, it is dependent on the cumulative interaction between the inverter components and the operating conditions available.

The measured power factors for the outdoor studies exhibited varying trends with compliance to the integration requirements. Under the PV simulator, the power factor was almost 100% in conformity with the standards. Thus, the power factor is strongly dependent on the steadiness of solar radiation and remains within the standard limit with irradiations above 400 Wm^{-2}, irrespective of intermittency. Except for the 5^{th} harmonic order, which showed a positive correlation between the generated harmonic current and the harmonic voltage, all other harmonic orders recorded varying trends for different inverters and systems studied. As a recommendation, further studies should be conducted to investigate the interaction of the various grid-connected PV systems and the distribution system during full equipment usage. Long periods of study on the various systems should be conducted and the cumulative effect of multiple systems on the grid investigated. Further work on the performance of other inverter types should be carried out.

6. SUMMARY

PERFORMANCE AND POWER QUALITY EVALUATION OF GRID-CONNECTED SOLAR PHOTOVOLTAIC SYSTEMS

The first section of this study dealt with the comprehensive analysis of microinverters' (2E microinverter) power output by employing a solar PV power simulator (GUNT equipment), and real modules of different technologies and make (structure) that meet the microinverter's kick start requirements under different operation conditions. The next was to investigate the power quality output of commercially available microinverters (MaySun-600W-B (China inverter) and the GMI 300 (Holland inverter) microinverters) by employing different modules under outdoor conditions. The was also conducted on large grid-connected single phase single input string inverters (SP 3100-600, SP 2800-550, SE 3500-ER-01-ITA) of different grid-connected systems with various solar modules and system capacities.

The results showed that microinverters' current THDs under the outdoor operating conditions far exceeded the current THDs for the study with the PV simulator for all scenarios and microinverters studied. However, the voltage THD for the investigations under outdoor conditions recorded lower voltage THDs than the studies with the PV simulator. The current THDs for the studies with all the microinverters under both indoor and outdoor conditions flouted the grid standards. The current THD profiles for the studies with the simulated PV power showed a zero slope for the entire study period, whiles it was positive for the studies under outdoor conditions for the microinverters.

Microinverters under real outdoor conditions generated the highest current total harmonic distortions ranging from 14.3% to 129.5%. However, under indoor conditions, the maximum CTHD was 13%, and a minimum was 6.9% were recorded. The string inverters comparable generated the lowest average CTHDs. However, except for the SE 3500-ER-01-ITA single-phase string inverter which generated an average value of 4.65 % on one occasion, the recorded CTHDs were all above the 5% specified standard. The days with the highest and non-intermittent solar radiation did not produce the lowest CTHD. Results showed that the inverse rule for the power factor and the CTHD did not hold for all inverters studied under different solar irradiation levels.

The measured power factors for the outdoor studies for both microinverters and string inverters exhibited varying trends with compliance to the integration requirements. Under the indoor study using the PV simulator, the power factor was virtually 100% in conformity with the standard. Thus, the power factor is strongly dependent on the steadiness of solar radiation and remains within the standard limit with solar irradiations above 400 Wm^{-2} or above 38% of the PV system's rated capacity. Except for the 5^{th} harmonic order, which presented a positive correlation between the generated harmonic current and the system harmonic voltage irrespective of system, inverter size or type, study conditions, the other harmonic orders showed different correlations for varying inverters and conditions. Thus, there is no one unique relationship between the generated harmonic current and the harmonic voltage for all the inverters and systems studied except for the 5^{th} harmonic.

7. ÖSSZEFOGLALÁS (SUMMARY IN HUNGARIAN)

HÁLÓZATRA KAPCSOLT FOTOVILLAMOS RENDSZEREK TELJESÍTMÉNYÉNEK ÉS VILLAMOS JELLEMZŐINEK MINŐSÉGE

A kutatás első része a mikroinverterek (2E mikroinverter) teljesítményének átfogó elemzésével foglalkozott a napelemes napenergia-szimulátor (GUNT egység), valamint különböző technológiájú és gyártmányú napelemes modulok felhasználásával. A munka része volt a kereskedelemben kapható mikroinverterek (MaySun-600W-B (kínai inverter) és a GMI 300 (Holland inverter) teljesítményminőségének vizsgálata, különféle modulok alkalmazásával kültéri körülmények között. Ezeket a méréseket nagy, hálózatra kapcsolt egyfázisú egybemenetű invertereken (SP 3100-600, SP 2800-550, SE 3500-ER-01-ITA) is elvégeztem, különféle napelemekkel és kapacitásokkal rendelkező valós rendszereken.

Az eredmények azt mutatják, hogy a mikroinverterek áramának teljes harmonikus disztorziója (THD) kültéri üzemi körülmények között messze meghaladta az áramerősség teljes harmonikus disztorzióját, a PV szimulátorral végzett vizsgálat során az összes menetrend és mikroinverter esetében. A kültéri körülmények között végzett vizsgálatok THD feszültsége azonban alacsonyabb feszültségű THD-ket rögzített, mint a PV-szimulátorral végzett vizsgálatok. Az összes mikroinverterrel mind beltéri, mind kültéri körülmények között végzett vizsgálatok jelenlegi THD-i nem felelnek meg a hálózat szabványainak. A mikroinverterek esetén a beltéri szimulátorral végzett vizsgálatok áramának THD profiljai nulla meredekséget mutattak a teljes időszak alatt, miközben ugyanez pozitív volt a kültéri körülmények között végzett vizsgálatok során.

A valódi kültéri körülmények között működő mikroinverterek a legnagyobb harmonikus torzítást eredményezték az áramerősségekre, 14,3% és 129,5% között. Beltéri körülmények között azonban a CTHD maximuma 13% volt, a minimum 6,9%. Összehasonlításképpen a hálózati inverterek eredményezték a legalacsonyabb átlagos CTHD-ket. Azonban az SE 3500-ER-01-ITA egyfázisú hálózati inverter kivételével, amely egy alkalommal átlagosan 4,65% -os értéket produkált, a rögzített CTHD-k mind meghaladták az 5%-ra meghatározott szabványt. A legalacsonyabb a CTHD nem a legnaposabb, stabil sugárzási viszonyú napokban volt. Az eredmények azt mutatták, hogy a teljesítménytényezőre és a CTHD-re vonatkozó inverz szabály nem érvényes minden vizsgált inverter esetében gyorsan változó napsugárzási értékek esetén.

A mikroinverterek és a hálózati inverterek kültéri vizsgálata során mért teljesítménytényezők változó tendenciákat mutattak,. A PV szimulátorral végzett beltéri vizsgálat során a teljesítménytényező 100%-ban megfelelt a szabványnak. Megállapítható volt, hogy a teljesítménytényező nagymértékben függ a napsugárzás állandóságától, és 400 W/m^2 feletti napsugárzás esetén vagy a PV rendszer névleges kapacitásának 38%-át meghaladó napsugárzás esetén a normál határon belül marad. Az 5. felharmonikus kivételével, amely pozitív korrelációt mutatott a rendszer harmonikus árama és feszültsége között, függetlenül a rendszertől, az inverter méretétől vagy típusától és a vizsgálati körülményektől. Így ennek kivételével nem állapítható meg egyetlen egyedi kapcsolat a generált harmonikus áram és feszültség között.

8. APPENDICES

A1: Bibliography

1. Ackermann, T., Andersson, G., and Söder, L. (2001): Distributed generation: A definition Electric Power Systems Research, 57(3), pp. 195–204. https://doi.org/10.1016/S0378-7796(01)00101-8
2. Agüero, J. R., Member, S., Steffel, S. J., and Member, S. (2011): Integration Challenges of Photovoltaic Distributed Generation on Power Distribution Systems 1–6
3. Ahmad, Z., and Singh, S. N. (2018): Improved modulation strategy for single phase grid connected transformerless PV inverter topologies with reactive power generation capability Solar Energy, 163, pp. 356–375. https://doi.org/10.1016/j.solener.2018.01.039
4. Aktas, A., Ozdemir, E., Karakaya, A., and Ucar, M. (2013): Operation and performance of grid-connected solar photovoltaic power system in Kocaeli university Journal of Optoelectronics and Advanced Materials, 15(5–6), pp. 559–564
5. Al-Shetwi, A. Q., Hannan, M. A., Jern, K. P., Alkahtani, A. A., and Abas, A. E. P. G. (2020): Power quality assessment of grid-connected PV system in compliance with the recent integration requirements Electronics (Switzerland), 9(2) https://doi.org/10.3390/electronics9020366
6. Alam, M. J. E., Muttaqi, K. M., and Sutanto, D. (2014): A novel approach for ramp-rate control of solar PV using energy storage to mitigate output fluctuations caused by cloud passing IEEE Transactions on Energy Conversion, 29(2), pp. 507–518. https://doi.org/10.1109/TEC.2014.2304951
7. Alexander, S. A. (2016): Development of solar photovoltaic inverter with reduced harmonic distortions suitable for Indian sub-continent In Renewable and Sustainable Energy Reviews, Vol. 56, pp. 694–704. https://doi.org/10.1016/j.rser.2015.11.092
8. Aliman, O., Daut, I., Isa, M., and Adzman, M. R. (2007): Simplification of sun tracking mode to gain high concentration solar energy American Journal of Applied Sciences, 4(3), pp. 171–175. https://doi.org/10.3844/ajassp.2007.171.175
9. Ankit, Sahoo, S. K., Sukchai, S., and Yanine, F. F. (2018): Review and comparative study of single-stage inverters for a PV system In Renewable and Sustainable Energy Reviews, Vol. 91, pp. 962–986. https://doi.org/10.1016/j.rser.2018.04.063
10. Araújo, S. V., Zacharias, P., and Sahan, B. (2008): Novel grid-connected non-isolated converters for photovoltaic systems with grounded generator PESC Record - IEEE Annual Power Electronics Specialists Conference, pp. 58–65. https://doi.org/10.1109/PESC.2008.4591897
11. Ausavanop, O., and Chaitusaney, S. (2011): Coordination of dispatchable distributed generation and voltage control devices for improving voltage profile by Tabu search ECTI-CON 2011 - 8th Electrical Engineering/ Electronics, Computer, Telecommunications and Information Technology (ECTI) Association of Thailand - Conference 2011, pp. 869–872. https://doi.org/10.1109/ECTICON.2011.5947978
12. Basso, T., Chakraborty, S., Hoke, A., and Coddington, M. (2015): IEEE 1547 Standards advancing grid modernization 2015 IEEE 42nd Photovoltaic Specialist Conference, PVSC 2015 https://doi.org/10.1109/PVSC.2015.7356267

13. Bellini, E. (2019): PV Magazine https://www.pv-magazine.com/2019/04/10/hungary-deployed-more-than-400-mw-of-solar-in-2018/ [Retrieved: 18/05/20]

14. Bertini, D., Falabretti, D., Moneta, D., Merlo, M., and Silvestri, A. (2011): Hosting Capacity of Italian Distribution Networks CIRED 21st International Conference on Electricity Distribution, 0930, 6–9 http://www.cired.net/publications/cired2011/part1/papers/CIRED2011_0930_final.pdf

15. Bollen, M., and Hassan, F. (2011): Integration of Distributed Generation in the Power System In Integration of Distributed Generation in the Power System, https://doi.org/10.1002/9781118029039

16. Braun, M., Stetz, T., Bründlinger, R., Mayr, C., Ogimoto, K., Hatta, H., Kobayashi, H., Kroposki, B., Mather, B., Coddington, M., Lynn, K., Graditi, G., Woyte, A., and MacGill, I. (2012): Is the distribution grid ready to accept large-scale photovoltaic deployment? State of the art, progress, and future prospects Progress in Photovoltaics: Research and Applications, 20(6), 681–697 https://doi.org/10.1002/pip.1204

17. Businesswire (2019a): Hungary's Solar Photovoltaic (PV) Power Market: Outlook 2018-2027 https://www.businesswire.com/news/home/20190924005834/en/Hungarys-Solar-Photovoltaic-PV-Power-Market-Outlook

18. Businesswire (2019b): Hungary's Solar Photovoltaic (PV) Power Market: Outlook 2018-2027 Report https://www.businesswire.com/news/home/20190924005834/en/Hungarys-Solar-Photovoltaic-PV-Power-Market-Outlook

19. Capitanescu, F., Ochoa, L. F., Margossian, H., and Hatziargyriou, N. D. (2015): Assessing the potential of network reconfiguration to improve distributed generation hosting capacity in active distribution systems IEEE Transactions on Power Systems, 30(1), pp. 346–356. https://doi.org/10.1109/TPWRS.2014.2320895

20. Cavalcanti, M. C., De Oliveira, K. C., De Farias, A. M., Neves, F. A. S., Azevedo, G. M. S., and Camboim, F. C. (2010): Modulation techniques to eliminate leakage currents in transformerless three-phase photovoltaic systems IEEE Transactions on Industrial Electronics, 57(4), pp. 1360–1368. https://doi.org/10.1109/TIE.2009.2029511

21. Çelik, Ö., Teke, A., and Tan, A. (2018): Overview of micro-inverters as a challenging technology in photovoltaic applications In Renewable and Sustainable Energy Reviews, Vol. 82, pp. 3191–3206. https://doi.org/10.1016/j.rser.2017.10.024

22. CENELEC (2007): En 50160 European Standard, 1–20 https://www.se.com/ww/library/SCHNEIDER_ELECTRIC/SE_LOCAL/APS/204836_1312/DraftStandard0026rev2-DraftEN501602005-05.pdf. [Retrieved: 10/02/20]

23. Chalmers, S. M., Hitt, M. M., Underhill, J. T., Anderson, P. M., Vogt, P. L., and Ingersoll, R. (1985): The effect of photovoltaic power generation on utility operation IEEE Transactions on Power Apparatus and Systems, PAS-104(3), pp. 524–530. https://doi.org/10.1109/TPAS.1985.318968

24. Chen, B., Gu, B., Zhang, L., Zahid, Z. U., Lai, J. S. J., Liao, Z., and Hao, R. (2015): A high-efficiency MOSFET transformerless inverter for nonisolated microinverter applications IEEE Transactions on Power Electronics, 30(7), pp. 3610–3622. https://doi.org/10.1109/TPEL.2014.2339320

25. Chicco, G., Schlabbach, J., and Spertino, F. (2009): Experimental assessment of the waveform distortion in grid-connected photovoltaic installations Solar Energy, 83(7), pp. 1026–1039. https://doi.org/10.1016/j.solener.2009.01.005

26. Chidi, M., Ipinnimo, O., Chowdhury, S., and Chowdhury, S. P. (2012): Investigation of impact of integrating on-grid home based solar power systems on voltage rise in the utility network IEEE Power and Energy Society General Meeting https://doi.org/10.1109/PESGM.2012.6344582

27. China National Standards (2012): Technical Rule for PV Power Station Connected to Power Grid; Chinese Enterprise Standards

28. Cleveland, F. M., and Member, I. S. (2008): IEC61850-7-420 Communications Standard for Distributed Energy Resources (DER) 5–8.

29. Cobben, S., Kling, W., and Myrzik, J. (2007): The making and purpose of harmonic fingerprints 19th International Conference on Electricity Distribution - CIRED, 1(0764), pp. 1–4

30. Conti, S. (2009): Analysis of distribution network protection issues in presence of dispersed generation Electric Power Systems Research, 79(1), pp. 49–56. https://doi.org/10.1016/j.epsr.2008.05.002

31. CSA, C. S. A. (2015): Interconnection of Distributed Resources and Electricity Supply Systems (No. 9-08-R2015; CSA C22.3) www.csagroup.org

32. Darvishi, A., Alimardani, A., and Hosseinian, S. H. (2011): Fuzzy multi-objective technique integrated with differential evolution method to optimise power factor and total harmonic distortion IET Generation, Transmission and Distribution, 5(9), pp. 921–929. https://doi.org/10.1049/iet-gtd.2010.0712

33. Dathu, K. P. M. Y. V., and Hariharan, R. (2020): Modelling of plug-in hybrid electric vehicle (PHEV) with multi source Materials Today: Proceedings https://doi.org/10.1016/j.matpr.2020.10.215

34. De La Rosa, F. C. (2006): Harmonics and Power Systems In Harmonics and Power Systems, (1st ed.). CRC Press. https://doi.org/10.1201/9781420004519

35. DeBlasio, R. (2009): IEEE Application Guide for IEEE Std 1547, IEEE Standard for Interconnecting Distributed Resources with Electric Power Systems (IEEE Standard 1547.2-2008)

36. Degner, T., Arnold, G., Reimann, T., Strauß, P., Breede, M., and Engel, B. (2011): Photovoltaic-system hosting capacity of low voltage distribution networks 30th ISES Biennial Solar World Congress 2011, SWC 2011, 2, pp. 1376–1385. https://doi.org/10.18086/swc.2011.10.04

37. Deline, C., Meydbray, J., and Donovan, M. (2012): Photovoltaic Shading Testbed for Module-level Power Electronics: 2014 update NREL Technical Report NREL/TP-5200-57991, May, 32 https://doi.org/NREL/TP-5200-54876

38. Dooner, M., and Wang, J. (2020): Compressed-air energy storage In Future Energy: Improved, Sustainable and Clean Options for Our Planet, pp. 279–312. https://doi.org/10.1016/B978-0-08-102886-5.00014-1

39. Dreidy, M., Mokhlis, H., and Mekhilef, S. (2017): Inertia response and frequency control techniques for renewable energy sources: A review In Renewable and Sustainable Energy Reviews, Vol. 69, pp. 144–155.

https://doi.org/10.1016/j.rser.2016.11.170

40. Dress, S., Kohn, A., and Schlabbach, J. (2005): Measurement of Harmonics generated by PV systems Elektrizitätswirtschaft (Ew), 104, pp. 68–71.
41. Dutta, S., Debnath, D., and Chatterjee, K. (2018): A Grid-Connected Single-Phase Transformerless Inverter Controlling Two Solar PV Arrays Operating under Different Atmospheric Conditions IEEE Transactions on Industrial Electronics, 65(1), pp. 374–385. https://doi.org/10.1109/TIE.2017.2711577
42. Fan, L., Miao, Z., and Domijan, A. (2010): Impact of unbalanced grid conditions on PV systems IEEE PES General Meeting, PES 2010 https://doi.org/10.1109/PES.2010.5589695
43. Faraji, F., Mousavi G., S. M., Hajirayat, A., Birjandi, A. A. M., and Al-Haddad, K. (2017): Single-stage single-phase three-level neutral-point-clamped transformerless grid-connected photovoltaic inverters: Topology review In Renewable and Sustainable Energy Reviews, Vol. 80, pp. 197–214. https://doi.org/10.1016/j.rser.2017.05.181
44. Fathabadi, H. (2018): Plug-In Hybrid Electric Vehicles: Replacing Internal Combustion Engine with Clean and Renewable Energy Based Auxiliary Power Sources IEEE Transactions on Power Electronics, 33(11), pp. 9611–9618. https://doi.org/10.1109/TPEL.2018.2797250
45. Fekete, K., Klaic, Z., and Majdandzic, L. (2012): Expansion of the residential photovoltaic systems and its harmonic impact on the distribution grid Renewable Energy, 43, pp. 140–148. https://doi.org/10.1016/j.renene.2011.11.026
46. Femin, V., Petra, M. I., Mathew, S., Hazra, J., and Ismail, H. (2016): Modeling the Temporal Variations in the Output of Large Solar PV Power Plants Energy Procedia, 95, pp. 294–301. https://doi.org/10.1016/j.egypro.2016.09.005
47. Ferdowsi, F., Mehraeen, S., and Upton, G. B. (2020): Assessing distribution network sensitivity to voltage rise and flicker under high penetration of behind-the-meter solar Renewable Energy, 152, pp. 1227–1240. https://doi.org/10.1016/j.renene.2019.12.124
48. Generators, M. (1993): ANSI/NEMA Standard MG1
49. Girgis, A., and Brahma, S. (2001): Effect of distributed generation on protective device coordination in distribution system LESCOPE 2001 - 2001 Large Engineering Systems Conference on Power Engineering: Powering Beyond 2001, Conference Proceedings, pp. 115–119. https://doi.org/10.1109/LESCPE.2001.941636
50. Goroohi Sardou, I., Zare, M., and Azad-Farsani, E. (2018): Robust energy management of a microgrid with photovoltaic inverters in VAR compensation mode International Journal of Electrical Power and Energy Systems, 98, pp. 118–132. https://doi.org/10.1016/j.ijepes.2017.11.037
51. Grady, W M; Gilleskie, R. J. (1995): Harmonics and how they relate to power factor (EPRI-TR-104581; CONF-9311343, TRN: 96:004684-0012)
52. Green Rhino Energy (n.d.): Solar energy Retrieved March 11, 2018, from http://www.greenrhinoenergy.com/renewable/solar.php
53. Groß, A. (2005): Measurement and assessment of harmonic current emission of PV inverters University of Applied Sciences Bielefeld, Germany
54. GSES (2015): Power Factor and Grid-Connected Photovoltaics

https://www.gses.com.au/wp-content/uploads/2016/03/GSES_powerfactor-110316.pdf

55. Hasan, R., Mekhilef, S., Seyedmahmoudian, M., and Horan, B. (2017): Grid-connected isolated PV microinverters : A review 67, pp. 1065–1080. https://doi.org/10.1016/j.rser.2016.09.082
56. Henner, D., and REN21 (2017): Ren21 https://abdn.pure.elsevier.com/en/en/researchoutput/ren21(5d1212f6-d863-45f7-8979-5f68a61e380e).html
57. Ho, W. S., Macchietto, S., Lim, J. S., Hashim, H., Muis, Z. A., and Liu, W. H. (2016): Optimal scheduling of energy storage for renewable energy distributed energy generation system In Renewable and Sustainable Energy Reviews, Vol. 58, pp. 1100–1107. https://doi.org/10.1016/j.rser.2015.12.097
58. Hossain, E., Kabalci, E., Bayindir, R., and Perez, R. (2014): Microgrid testbeds around the world: State of art Energy Conversion and Management, 86, pp. 132–153. https://doi.org/10.1016/j.enconman.2014.05.012
59. Hossain, M. A., Xu, Y., Peshek, T. J., Ji, L., Abramson, A. R., and French, R. H. (2015): Microinverter thermal performance in the real-world: Measurements and modeling PLoS ONE, 10(7) https://doi.org/10.1371/journal.pone.0131279
60. Huda, A. S. N., and Živanović, R. (2017): Large-scale integration of distributed generation into distribution networks: Study objectives, review of models and computational tools In Renewable and Sustainable Energy Reviews, Vol. 76, pp. 974–988. https://doi.org/10.1016/j.rser.2017.03.069
61. IAEA (2019): Country Nuclear Power Profiles https://www-pub.iaea.org/MTCD/publications/PDF/cnpp2019/countryprofiles/Hungary/Hungary.htm
62. IEC Standard (2015): IEC 61000-4-30 Corrigendum 1 - ELECTROMAGNETIC COMPATIBILITY (EMC) – Part 3-40: Testing and measurement techniques – Power quality measurement methods IEC Standard Corrigendum 1, pp. 2016–2017.
63. IEEE (2017): IEEE Standard Test Procedure for Polyphase Induction Motors and Generators In IEEE Std 112-2004 (Revision of IEEE Std 112-1996),
64. IEEE, 1547 (2014): IEEE Standard for Interconnecting Distributed Resources with Electric Power Systems1547 (No. 1547)
65. Ishaque, K., Salam, Z., Amjad, M., and Mekhilef, S. (2012): An improved particle swarm optimization (PSO)-based MPPT for PV with reduced steady-state oscillation IEEE Transactions on Power Electronics, 27(8), pp. 3627–3638. https://doi.org/10.1109/TPEL.2012.2185713
66. Ishikawa, T. (2002): Grid-connected photovoltaic power systems: survey of inverter and related protection equipments Httpwwwieapvpsorg http://www.iea-pvps.org/products/download/rep5_05.pdf
67. Islam, M., and Mekhilef, S. (2014): An improved transformerless grid connected photovoltaic inverter with reduced leakage current Energy Conversion and Management, 88, pp. 854–862. https://doi.org/10.1016/j.enconman.2014.09.014
68. Jadeja, R., Ved, A. D., Chauhan, S. K., and Trivedi, T. (2020): A random carrier frequency PWM technique with a narrowband for a grid-connected solar inverter

Electrical Engineering, 102(3), pp. 1755–1767. https://doi.org/10.1007/s00202-020-00989-6

69. Jana, J., Saha, H., and Bhattacharya, K. Das (2016): A review of inverter topologies for single-phase grid-connected photovoltaic systems Renewable and Sustainable Energy Reviews, August, 0–1 https://doi.org/10.1016/j.rser.2016.10.049
70. Jayasekara, N., Masoum, M. A. S., and Wolfs, P. J. (2016): Optimal operation of distributed energy storage systems to improve distribution network load and generation hosting capability IEEE Transactions on Sustainable Energy, 7(1), pp. 250–261. https://doi.org/10.1109/TSTE.2015.2487360
71. Jayasekara, N., and Wolfs, P. (2010): Analysis of power quality impact of high penetration PV in residential feeders AUPEC 2010 - 20th Australasian Universities Power Engineering Conference: "Power Quality for the 21st Century"
72. Jordan, D. C., Wohlgemuth, J. H., and Kurtz, S. R. (2012): Technology and climate trends in pv module degradation 27th European Photovoltaic Solar Energy Conference and Exhibition, October, pp. 3118–3124. https://doi.org/10.4229/27thEUPVSEC2012-4DO.5.1
73. Kabalci, E. (2017): Maximum power point tracking (MPPT) algorithms for photovoltaic systems Lecture Notes in Energy, 37, pp. 205–234. https://doi.org/10.1007/978-3-319-49875-1_8
74. Kabalcı, E. (2020): Review on novel single-phase grid-connected solar inverters: Circuits and control methods Solar Energy, 198(January), pp. 247–274. https://doi.org/10.1016/j.solener.2020.01.063
75. Kabemura, K., Yonekura, K., Tsukamoto, T., Hashimoto, K., and Hara, M. (2004): Application of a dispersed autonomous voltage control system to a real high-voltage distribution network Electrical Engineering in Japan (English Translation of Denki Gakkai Ronbunshi), 146(1), pp. 27–36. https://doi.org/10.1002/eej.10252
76. Kadri, R., Gaubert, J. P., and Champenois, G. (2011): An Improved maximum power point tracking for photovoltaic grid-connected inverter based on voltage-oriented control IEEE Transactions on Industrial Electronics, 58(1), pp. 66–75. https://doi.org/10.1109/TIE.2010.2044733
77. Katiraei, F., and Agüero, J. R. (2011): Solar PV integration challenges IEEE Power and Energy Magazine, 9(3), pp. 62–71. https://doi.org/10.1109/MPE.2011.940579
78. Kerekes, T., Teodorescu, R., Rodríguez, P., Vázquez, G., and Aldabas, E. (2011): A New high-efficiency single-phase transformerless PV inverter topology IEEE Transactions on Industrial Electronics, 58(1), pp. 184–191. https://doi.org/10.1109/TIE.2009.2024092
79. Khan, A., Ben-Brahim, L., Gastli, A., and Benammar, M. (2017): Review and simulation of leakage current in transformerless microinverters for PV applications In Renewable and Sustainable Energy Reviews, Vol. 74, pp. 1240–1256. https://doi.org/10.1016/j.rser.2017.02.053
80. Kjaer, S. B., Pedersen, J. K., and Blaabjerg, F. (2005): A review of single-phase grid-connected inverters for photovoltaic modules In IEEE Transactions on Industry Applications, Vol. 41, Issue 5, pp. 1292–1306. https://doi.org/10.1109/TIA.2005.853371

81. Kjaer, S. B., Pedersen, J. K., and Blaabjerg, F. (2002): Power inverter topologies for photovoltaic modules - A review Conference Record - IAS Annual Meeting (IEEE Industry Applications Society), 2, pp. 782–788. https://doi.org/10.1109/ias.2002.1042648

82. Kougias, I., and Szabó, S. (2017): Pumped hydroelectric storage utilization assessment: Forerunner of renewable energy integration or Trojan horse? Energy, 140, pp. 318–329. https://doi.org/10.1016/j.energy.2017.08.106

83. Kouro, S., Leon, J. I., Vinnikov, D., and Franquelo, L. G. (2015): Grid-connected photovoltaic systems: An overview of recent research and emerging PV converter technology IEEE Industrial Electronics Magazine, 9(1), pp. 47–61. https://doi.org/10.1109/MIE.2014.2376976

84. Kow, K. W., Wong, Y. W., Rajkumar, R. K., and Rajkumar, R. K. (2016): A review on performance of artificial intelligence and conventional method in mitigating PV grid-tied related power quality events In Renewable and Sustainable Energy Reviews, Vol. 56, pp. 334–346. https://doi.org/10.1016/j.rser.2015.11.064

85. Kundur, P., Paserba, J., Ajjarapu, V., Andersson, G., Bose, A., Canizares, C., Hatziargyriou, N., Hill, D., Stankovic, A., Taylor, C., Van Cursem, T., and Vittal, V. (2004): Definition and classification of power system stability IEEE Transactions on Power Systems, 19(3), pp. 1387–1401. https://doi.org/10.1109/TPWRS.2004.825981

86. Leal-Arcas, Rafael and Filis, Andrew and Peykova, Mariya and Greger, M. (2020): Towards a Carbon-Free, Decentralized, and Democratized System of Energy Generation Connecticut Journal of International Law, 35(1) https://ssrn.com/abstract=3460007

87. Li, X., Wen, H., Hu, Y., Jiang, L., and Xiao, W. (2018): Modified Beta Algorithm for GMPPT and Partial Shading Detection in Photovoltaic Systems IEEE Transactions on Power Electronics, 33(3), pp. 2172–2186. https://doi.org/10.1109/TPEL.2017.2697459

88. Lim, Y. S., and Tang, J. H. (2014): Experimental study on flicker emissions by photovoltaic systems on highly cloudy region: A case study in Malaysia Renewable Energy, 64, pp. 61–70. https://doi.org/10.1016/j.renene.2013.10.043

89. Linse, C., and Kuhn, R. (2015): Design of high-voltage battery packs for electric vehicles In Advances in Battery Technologies for Electric Vehicles, pp. 245–263. https://doi.org/10.1016/B978-1-78242-377-5.00010-8

90. Liu, Q., Tao, Y., Liu, X., Deng, Y., and He, X. (2014): Voltage unbalance and harmonics compensation for islanded microgrid inverters IET Power Electronics, 7(5), pp. 1055–1063. https://doi.org/10.1049/iet-pel.2013.0410

91. Liu, X., Aichhorn, A., Liu, L., and Li, H. (2012): Coordinated control of distributed energy storage system with tap changer transformers for voltage rise mitigation under high photovoltaic penetration IEEE Transactions on Smart Grid, 3(2), 897–906 https://doi.org/10.1109/TSG.2011.2177501

92. Madzonga, L. S., Munda, J. L., and Jimoh, A. A. (2009): Analysis of bus voltage regulation and OLTC performance on mismatched parallel-connected transformers IEEE AFRICON Conference https://doi.org/10.1109/AFRCON.2009.5308082

93. Mahela, O. P., and Shaik, A. G. (2017): Comprehensive overview of grid interfaced solar photovoltaic systems Renewable and Sustainable Energy Reviews, 68(September 2016), pp. 316–332. https://doi.org/10.1016/j.rser.2016.09.096

94. Mancarella, P., and Chicco, G. (2009): Global and local emission impact assessment of distributed cogeneration systems with partial-load models Applied Energy, 86(10), pp. 2096–2106. https://doi.org/10.1016/j.apenergy.2008.12.026

95. Manyage, P., and Pillay, M. (2001): Definitions of Voltage Unbalance IEEE Power Engineering Review, pp. 50–51. http://users.encs.concordia.ca/~pillay/16.pdf

96. Markiewicz, H., Klajn, A. (2004): Voltage Characteristics in Public Distribution Systems (Voltage Disturbances Standard EN 50160)

97. Martinez, J. A., De Léon, F., Mehrizi-Sani, A., Nehrir, M. H., Wang, C., and Dinavahi, V. (2011): Tools for analysis and design of distributed resources-Part II: Tools for planning, analysis and design of distribution networks with distributed resources IEEE Transactions on Power Delivery, 26(3), pp. 1653–1662. https://doi.org/10.1109/TPWRD.2011.2116046

98. Martinez, J. A., and Martin-Arnedo, J., (2011): Distribution load flow calculations using time driven and probabilistic approaches, 2011 IEEE Power and Energy Society General Meeting, Detroit, MI, USA, 2011, pp. 1-8. https://doi.org/10.1109/PES.2011.6039171

99. Mavir (2019): Data of the Hungarian electricity system for 2018 http://www.mszit.hu/uploads/media/MAVIR_VER_2018.pdf

100. MAVIR (2018): Data of the Hungarian Electricity System 2017 report http://www.mavir.hu/documents/10262/222691710/MAVIR_VER_2017_web_2.pdf/ 072248af-03f6-e6ed-9079- 767d2000c71b

101. McGranaghan, M. (2009): EPRI smart grid demonstration initiative-integrating DER with T&D operations In: Proceedings of the 20th International Conference and Exhibition on Electricity Distribution-Part 2

102. Meersman, B., Renders, B., Degroote, L., Vandoorn, T., and Vandevelde, L. (2011): Three-phase inverter-connected DG-units and voltage unbalance Electric Power Systems Research, 81(4), pp. 899–906. https://doi.org/10.1016/j.epsr.2010.11.024

103. Meinhardt, M., O'Donnell, T., Schneider, H., Flannery, J., O Mathuna, C., Zacharias, P., and Krieger, T. (1999): Miniaturized `low profile' Module Integrated Converter for photovoltaic applications with integrated magnetic components Conference Proceedings - IEEE Applied Power Electronics Conference and Exposition - APEC, 1, pp. 305–311. https://doi.org/10.1109/apec.1999.749656

104. Melhom, C. J., Maitra, A., Sunderman, W., Waclawiak, M., and Sundaram, A. (2005): Distribution system power quality assessment phase II: Voltage sag and interruption analysis Record of Conference Papers - Annual Petroleum and Chemical Industry Conference, pp. 113–120. https://doi.org/10.1109/PCICON.2005.1524546

105. Meneses, D., Blaabjerg, F., García, Ó., and Cobos, J. A. (2013): Review and comparison of step-up transformerless topologies for photovoltaic AC-module application IEEE Transactions on Power Electronics, 28(6), pp. 2649–2663. https://doi.org/10.1109/TPEL.2012.2227820

106. Mirhassani, S., Ong, H. C., Chong, W. T., and Leong, K. Y. (2015): Advances and challenges in grid tied photovoltaic systems In Renewable and Sustainable Energy Reviews, Vol. 49, pp. 121–131. https://doi.org/10.1016/j.rser.2015.04.064

107. Myrzik, J. M. A., and Calais, M. (2003): String and module integrated inverters for

single-phase grid connected photovoltaic systems - A review 2003 IEEE Bologna PowerTech - Conference Proceedings, 2, pp. 8–15. https://doi.org/10.1109/PTC.2003.1304589

108. Nghitevelekwa, K., and Bansal, R. C. (2018): A review of generation dispatch with large-scale photovoltaic systems In Renewable and Sustainable Energy Reviews, Vol. 81, pp. 615–624. https://doi.org/10.1016/j.rser.2017.08.035

109. Obi, M., and Bass, R. (2016): Trends and challenges of grid-connected photovoltaic systems - A review In Renewable and Sustainable Energy Reviews, Vol. 58, pp. 1082–1094 https://doi.org/10.1016/j.rser.2015.12.289

110. Olabi, A. G. (2017): Renewable energy and energy storage systems In Energy, Vol. 136, pp. 1–6. https://doi.org/10.1016/j.energy.2017.07.054

111. Oruganti, R. (2014): Photovoltaic (PV) systems – Characteristics of the utility interface (International Electrotechnical Commission; IEC 61727-2004)

112. Oshiro, M., Tanaka, K., Senjyu, T., Toma, S., Yona, A., Saber, A. Y., Funabashi, T., and Kim, C. H. (2011): Optimal voltage control in distribution systems using PV generators International Journal of Electrical Power and Energy Systems, 33(3), pp. 485–492. https://doi.org/10.1016/j.ijepes.2010.11.002

113. Öztürk, S., Poşpoş, P., Utalay, V., Koç, A., Ermiş, M., and Çadırcı, I. (2018): Operating principles and practical design aspects of all SiC DC/AC/DC converter for MPPT in grid-connected PV supplies, Solar Energy, 176, pp. 380–394. https://doi.org/10.1016/j.solener.2018.10.049

114. Paatero, J. V., and Lund, P. D. (2006): A model for generating household electricity load profiles International Journal of Energy Research, 30(5), pp. 273–290. https://doi.org/10.1002/er.1136

115. Pakonen, P., Hilden, A., Suntio, T., and Verho, P. (2016): Grid-connected PV power plant induced power quality problems - Experimental evidence 2016 18th European Conference on Power Electronics and Applications, EPE 2016 ECCE Europe, pp. 1–10. https://doi.org/10.1109/EPE.2016.7695656

116. Paliwal, P., Patidar, N. P., and Nema, R. K. (2014): Planning of grid integrated distributed generators: A review of technology, objectives and techniques In Renewable and Sustainable Energy Reviews, Vol. 40, pp. 557–570. https://doi.org/10.1016/j.rser.2014.07.200

117. Pandi, V. R., Zeineldin, H. H., Xiao, W., and Zobaa, A. F. (2013): Optimal penetration levels for inverter-based distributed generation considering harmonic limits Electric Power Systems Research, 97, pp. 68–75. https://doi.org/10.1016/j.epsr.2012.12.003

118. Patsalides, M., Evagorou, D., Makrides, G., Achillides, Z., Georghiou, G. E., Stavrou, A., Efthimiou, V., Zinsser, B., Schmitt, W., and Werner, J. H. (2007): The effect of solar irradiance on the power quality behaviour of grid connected photovoltaic systems Renewable Energy and Power Quality Journal, 1(5), pp. 323–330. https://doi.org/10.24084/repqj05.284

119. Peterson, B., Rens, J., Minnaar, U., Botha, G., and Desmet, J. (2015): A South African Review of Harmonic Emission Level Assessment As Per IEC61000-3-6 Cigre, pp. 1–9

120. Petinrin, J. O., and Shaaban, M. (2014): Voltage control in a smart distribution network

using demand response Conference Proceeding - 2014 IEEE International Conference on Power and Energy, PECon 2014, pp. 319–324. https://doi.org/10.1109/PECON.2014.7062464

121. Petinrin, J. O., and Shaabanb, M. (2016): Impact of renewable generation on voltage control in distribution systems In Renewable and Sustainable Energy Reviews, Vol. 65, pp. 770–783. https://doi.org/10.1016/j.rser.2016.06.073

122. Petreuş, D., Daraban, S., Ciocan, I., Patarau, T., Morel, C., and Machmoum, M. (2013): Low cost single stage micro-inverter with MPPT for grid connected applications Solar Energy, 92, pp. 241–255. https://doi.org/10.1016/j.solener.2013.03.016

123. Pinyol Ramon (2015): Harmonics : Causes , Effects and Minimization In Salicru White Papers, Salicru White Papers, Issue August https://www.salicru.com/files/pagina/72/278/jn004a01_whitepaper-armonics_.pdf

124. Pterra (2013): Flicker Trouble Ahead for Solar PV Inverters? https://www.pterra.com/photovoltaic-systems/flicker-trouble-ahead-for-solar-pv-inverters/

125. R.C. Dugan, M.F. McGranaghan, and H. W. B. (1996): Electrical Power Systems Quality McGraw-Hill.

126. Rahman, S., Moghaddami, M., Sarwat, A. I., Olowu, T., and Jafaritalarposhti, M. (2018): Flicker Estimation Associated with PV Integrated Distribution Network Conference Proceedings - IEEE Southeastcon, 2018-April https://doi.org/10.1109/SECON.2018.8479058

127. Rahmann, C., and Castillo, A. (2014): Fast frequency response capability of photovoltaic power plants: The necessity of new grid requirements and definitions Energies, 7(10), pp. 6306–6322. https://doi.org/10.3390/en7106306

128. Rizzoli, G., Mengoni, M., Zarri, L., Tani, A., Serra, G., and Casadei, D. (2016): Comparison of single-phase H4, H5, H6 inverters for transformerless photovoltaic applications IECON Proceedings (Industrial Electronics Conference), pp. 3038–3045. https://doi.org/10.1109/IECON.2016.7792984

129. Rohouma, W., Balog, R. S., Peerzada, A. A., and Begovic, M. M. (2020): D-STATCOM for harmonic mitigation in low voltage distribution network with high penetration of nonlinear loads Renewable Energy, 145, pp. 1449–1464. https://doi.org/10.1016/j.renene.2019.05.134

130. Romero-Cadaval, E., Spagnuolo, G., Franquelo, L. G., Ramos-Paja, C. A., Suntio, T., and Xiao, W. M. (2013): Grid-connected photovoltaic generation plants: Components and operation IEEE Industrial Electronics Magazine, 7(3), pp. 6–20. https://doi.org/10.1109/MIE.2013.2264540

131. RSComponents (2019): The Complete Guide to reference voltage https://www.encoding.com/widevine/. Retrieved November 15, 2018.

132. Sakar, S., Balci, M. E., Abdel Aleem, S. H. E., and Zobaa, A. F. (2018): Integration of large- scale PV plants in non-sinusoidal environments: Considerations on hosting capacity and harmonic distortion limits In Renewable and Sustainable Energy Reviews, Vol. 82, pp. 176–186. https://doi.org/10.1016/j.rser.2017.09.028

133. Salam, Z., Ahmed, J., and Merugu, B. S. (2013): The application of soft computing methods for MPPT of PV system : A technological and status review APPLIED

ENERGY, 107, pp. 135–148. https://doi.org/10.1016/j.apenergy.2013.02.008

134. Salas, V., Olías, E., Barrado, A., and Lázaro, A. (2006): Review of the maximum power point tracking algorithms for stand-alone photovoltaic systems In Solar Energy Materials and Solar Cells, https://doi.org/10.1016/j.solmat.2005.10.023

135. Sera, D., Mathe, L., Kerekes, T., Spataru, S. V., and Teodorescu, R. (2013): On the perturb-and-observe and incremental conductance mppt methods for PV systems IEEE Journal of Photovoltaics, 3(3), pp. 1070–1078. https://doi.org/10.1109/JPHOTOV.2013.2261118

136. Seres, I., and Farkas, I. (2007): Development of a 10 Kwp photovoltaic system - Efficiency analysis ISES Solar World Congress 2007, ISES 2007, 3, pp. 1652–1656. https://doi.org/10.1007/978-3-540-75997-3_339

137. Shahnia, F., Majumder, R., Ghosh, A., Ledwich, G., and Zare, F. (2011): Voltage imbalance analysis in residential low voltage distribution networks with rooftop PVs Electric Power Systems Research, 81(9), pp. 1805–1814. https://doi.org/10.1016/j.epsr.2011.05.001

138. Sher, H. A., and Addoweesh, K. E. (2012): Micro-inverters - Promising solutions in solar photovoltaics In Energy for Sustainable Development, Vol. 16, Issue 4, pp. 389–400. https://doi.org/10.1016/j.esd.2012.10.002

139. Shivashankar, S., Mekhilef, S., Mokhlis, H., and Karimi, M. (2016): Mitigating methods of power fluctuation of photovoltaic (PV) sources - A review In Renewable and Sustainable Energy Reviews, Vol. 59, pp. 1170–1184. https://doi.org/10.1016/j.rser.2016.01.059

140. Singh, S., and Singh, B. (2014): Optimized passive filter design using modified particle swarm optimization algorithm for a 12-pulse converter-fed LCI-synchronous motor drive IEEE Transactions on Industry Applications, 50(4), pp. 2681–2689. https://doi.org/10.1109/TIA.2013.2292991

141. Solargis (n.d.): No Title Retrieved October 20, 2019, from https://solargis.com/maps-and-gis-data/download/hungary

142. Sonel (2020): POWER QUALITY ANALYSIS https://www.sonel.pl/en/knowledge-centre/press-articles/power-quality-analysis/. Retrieved October 9, 2020

143. Stetz, T., and Braun, M. (2011): Dezentrale Verfahren zur Spannungshaltung in Niederspannungsnetzen - eine Fallstudie Elektrotechnik Und Informationstechnik, 128(4), pp. 105–109. https://doi.org/10.1007/s00502-011-0817-7

144. Stojkov, M., Trupinić, K., and Nikolovski, S. (2009): Procedure for determination of harmonic distortion along the distribution network Tehnicki Vjesnik, 16(4), pp. 19–26

145. Szabo, J. (2019): Legal sources of renewable energy. http://www.res-legal.eu/search-by-country/hungary/single/s/res-e/t/promotion/aid/feed-in-tariff-10/lastp/143. Retrieved August 20, 2019.

146. Tagare, D. M. (2011): Interconnecting Distributed Resources with Electric Power Systems In Electric Power Generation, pp. 301–313. https://doi.org/10.1002/9780470872659.ch15

147. Taha Attya, A. B., and Hartkopf, T. (2013): Control and quantification of kinetic energy released by wind farms during power system frequency drops IET Renewable Power Generation, 7(3), pp. 210–224. https://doi.org/10.1049/iet-rpg.2012.0163

148. Tang, Y., Yao, W., Loh, P. C., and Blaabjerg, F. (2016): Highly Reliable Transformerless Photovoltaic Inverters with Leakage Current and Pulsating Power Elimination IEEE Transactions on Industrial Electronics, 63(2), pp. 1016–1026. https://doi.org/10.1109/TIE.2015.2477802

149. Tengku Hashim, T. J., Mohamed, A., and Shareef, H. (2012): A review on voltage control methods for active distribution networks In Przeglad Elektrotechniczny, Vol. 88, Issue 6, pp. 304–312

150. Tofigh Azary, M., Sabahi, M., Babaei, E., and Abbasi Aghdam Meinagh, F. (2018): Modified Single-Phase Single-Stage Grid-Tied Flying Inductor Inverter With MPPT and Suppressed Leakage Current IEEE Transactions on Industrial Electronics, 65(1), pp. 221–231. https://doi.org/10.1109/TIE.2017.2719610

151. Turitsyn, K., Šulc, P., Backhaus, S., and Chertkov, M. (2010): Distributed control of reactive power flow in a radial distribution circuit with high photovoltaic penetration IEEE PES General Meeting, PES 2010 https://doi.org/10.1109/PES.2010.5589663

152. Vasanasong, E., and Spooner, E. D. (2000): The prediction of net harmonic currents produced by large numbers of residential PV inverters: Sydney Olympic Village case study Proceedings of International Conference on Harmonics and Quality of Power, ICHQP, 1, pp. 116–121. https://doi.org/10.1109/ICHQP.2000.897010

153. Velasco, D., Trujillo, C., Garcerá, G., and Figueres, E. (2011): An active anti-islanding method based on phase-PLL perturbation IEEE Transactions on Power Electronics, 26(4), pp. 1056–1066. https://doi.org/10.1109/TPEL.2010.2089643

154. Venkatesan, N., Solanki, J., and Solanki, S. K. (2012): Residential Demand Response model and impact on voltage profile and losses of an electric distribution network Applied Energy, 96, pp. 84–91. https://doi.org/10.1016/j.apenergy.2011.12.076

155. Viawan, F. A., Sannino, A., and Daalder, J. (2007): Voltage control with on-load tap changers in medium voltage feeders in presence of distributed generation Electric Power Systems Research, 77(10), pp. 1314–1322. https://doi.org/10.1016/j.epsr.2006.09.021

156. VoltageDisturbance (2019): VOLTAGE UNBALANCE Power Engineering Study Resource http://voltage-disturbance.com/voltage-quality/voltage-unbalance/

157. Von Jouanne, A., and Banerjee, B. (2001): Assessment of voltage unbalance IEEE Transactions on Power Delivery, 16(4), pp. 782–790. https://doi.org/10.1109/61.956770

158. Vovos, P. N., Kiprakis, A. E., Wallace, A. R., and Harrison, G. P. (2007): Centralized and distributed voltage control: Impact on distributed generation penetration IEEE Transactions on Power Systems, 22(1), pp. 476–483. https://doi.org/10.1109/TPWRS.2006.888982

159. Wong, J., Seng Lim, Y., and Morris, E. (2016): Distributed Energy Storage Systems with an Improved Fuzzy Controller for Mitigating Voltage Unbalance on Low-Voltage Networks Journal of Energy Engineering, 142(1), 04014058 https://doi.org/10.1061/(asce)ey.1943-7897.0000260

160. Xia, Y., Roy, J., and Ayyanar, R. (2017): A capacitance-minimized, doubly grounded transformer less photovoltaic inverter with inherent active-power decoupling IEEE Transactions on Power Electronics, 32(7), pp. 5188–5201. https://doi.org/10.1109/TPEL.2016.2606344

161. Xiao, H., Xie, S., Chen, Y., and Huang, R. (2011): An optimized transformerless photovoltaic grid-connected inverter IEEE Transactions on Industrial Electronics, 58(5), pp. 1887–1895. https://doi.org/10.1109/TIE.2010.2054056

162. Yang, Y., and Bollen, M. (2008): Power quality and reliability in distribution networks with increased levels of distributed generation March, 97 https://www.etde.org/etdeweb/details.jsp?osti_id=941924

163. Yuan-Kang Wu, J.-H. L. and H.-J. L. (2017): Standards and Guidelines for Grid-connected Photovoltaic Generation Systems : a Review and Comparison 9994(c) https://doi.org/10.1109/TIA.2017.2680409

164. Zeb, K., Uddin, W., Khan, M. A., Ali, Z., Ali, M. U., Christofides, N., and Kim, H. J. (2018): A comprehensive review on inverter topologies and control strategies for grid connected photovoltaic system Renewable and Sustainable Energy Reviews, 94(November 2017), pp. 1120–1141. https://doi.org/10.1016/j.rser.2018.06.053

165. Zhang, L., Sun, K., Xing, Y., and Xing, M. (2014): H6 transformerless full-bridge PV grid-tied inverters IEEE Transactions on Power Electronics, 29(3), pp. 1229–1238. https://doi.org/10.1109/TPEL.2013.2260178

166. Zhao, K., Ciufo, P., and Perera, S. (2013): Rectifier capacitor filter stress analysis when subject to regular voltage fluctuations IEEE Transactions on Power Electronics, 28(7), pp. 3627–3635. https://doi.org/10.1109/TPEL.2012.2228279

A2: Publications related to the dissertation

Refereed papers in foreign languages:

1. **Atsu, D.,** Seres, I., Farkas, I. (2021): The state of solar PV and performance analysis of different PV technologies Grid-connected installations in Hungary, Renewable and Sustainable Energy Reviews, Vol. 141, No. 110808, 2021, pp. 1-9. ISSN: 1364-0321, (IF: 12.110*).
2. **Atsu, D.,** Seres, I., Farkas, I. (2019): Comparison of efficiency for different photovoltaic modules, Acta Technologica Agriculturae, Vol. 22, No. 1, pp. 5-11. ISSN 1338-5267. doi: 10.2478/ata-2019-0002.
3. **Atsu, D.,** Seres, I., Farkas, I. (2020): Thermal behaviour analysis of different solar PV modules via thermographic imaging, Journal of Renewable and Sustainable Energy, Vol. 12, No. 1:013503, pp. 1-8., ISSN 1941-7012, doi.org/10.1063/1.5113763. (IF: 1.575*).
4. **Atsu, D.,** Dhaundiyal, A. (2019): Modeling of photovoltaic module using the Matlab, Journal of Natural Resources and Development, Vol. 9, pp. 59- 69. ISSN 0719-2452, doi: 10.5027/jnrd.v9i0.06.
5. **Atsu, D.,** Dhaundiyal, A. (2019): Effect of ambient parameters on the temperature distribution of photovoltaic (PV) modules, Resources, Vol. 8 (2), 107. ISSN 2079-9276, doi.org/10.3390/resources8020107.
6. Dhaundiyal, A., **Atsu, D.** (2020): The effect of wind on the temperature distribution of photovoltaic modules. Solar Energy, pp. Vol. 201, 259–267. ISSN: 0038-092X, doi: 10.1016/j.solener.2020.03.012 (IF = 4.608*).
7. **Atsu, D.,** Seres, I., Farkas, I. (2019): Degradation and performance evaluation of PV modules in the tropical climate, Mechanical Engineering Letters, Gödöllő, Hungary, Vol. 19, pp. 33-43., HU ISSN 2060-3789.
8. **Atsu, D.,** Seres, I., Farkas, I. (2019): Measurements of the grid quality for PV inverters, Mechanical Engineering Letters, Gödöllő, Hungary, Vol. 17, pp. 14-21. HU ISSN 2060-3789.
9. **Atsu, D.,** Seres, I., Aghaei, M., Farkas, I. (2020): Analysis of long-term performance and reliability of PV modules under tropical climatic conditions in sub-Saharan, Renewable Energy, Vol. 162, pp. 285-295. ISSN: 0960-1481, doi.org/10.1016/j.renene.2020.08.021 (IF: 6.274*).
10. Farkas I., **Atsu D**.: PEARL PV Hungary, PEARL PV Country Reports, COST Action CA16235, December 12, 2020, University of Twente, The Netherlands, pp. 108-115. ISBN 978-90-365-5107-6, doi: 10.3990/1.9789036551083.

Refereed papers in Hungarian language:

11. Seres, I., **Atsu, D**., Farkas, I. (2020): Fotovillamos modulok teljesítményének degradációja, Magyar energetika, 27: 3 pp. 15-20, 6 p.

International conference proceedings

12. **Atsu, D.,** Seres, I., Farkas, I. (2020): Performance evaluation of solar photovoltaic modules under real conditions, Conference proceedings. 13th International conference on solar energy for buildings and industry, Greece, 1-3 Sept. 2020.
13. **Atsu D.,** Seres I., Farkas I. (2020): Reliability assessment of PV modules, Proceedings of the Conference for Sustainable Energy (CSE), Chapter 8, Springer Proceedings in Energy, /ed. by I. Visa, A. Duta/, October 22-24, 2020, Brasov, Romania, pp. 111-124. ISBN 978-3-030-55756-0, doi:10.1007/978-3-030-55757-7.

International conference abstracts

14. **Atsu, D.,** Seres, I., Farkas, I. (2018): Analysis and characterisation of solar PV modules with different technologies, Book of Abstracts, 17th International Workshop for Young Scientists (BioPhys Spring 2018), Nitra, Slovakia, May 15-18, 2018, p. 11. ISBN 978- 83-89969-57-6.
15. **Atsu, D.,** Seres, I., Farkas, I. (2019): Reliability and degradation rate of ground-mounted solar modules in the tropical climate of the sub-Saharan, Book of abstracts, BioPhys Spring 2019, Gödöllő, Hungary, May 22-24, 2019, p. 8., ISBN: 978-963-269-823-6.
16. **Atsu, D.** (2019): Solar photovoltaic water pumping for irrigation: a sustainable option. Book of Abstracts, XII Spring Wind Conference – 2019, 3–5 May 2019, Debrecen ISBN 978-615-5586-42-2.
17. **Atsu, D.,** Seres, I., Farkas, I. (2017): Performance evaluation of solar photovoltaic modules under real conditions, Book of Abstracts, 23rd Workshop on Energy and Environment, Gödöllő, Hungary, November 30-December 1, 2017, p. 20, ISBN 978-963-9483-91-0.
18. **Atsu, D.,** Seres, I., Farkas, I. (2018): Investigation of the thermal behaviour of solar PV modules, Book of Abstracts, 24th Workshop on Energy and Environment, Gödöllő, Hungary, December 6-7, 2018, p. 23, ISBN 978-963-269-787-1.
19. **Atsu, D.,** Seres, I., Farkas, I. (2019): Performance analysis of grid-connected SI-poly and SI-amorphous photovoltaic systems, Book of Abstracts, 25th Workshop on Energy and Environment, Gödöllő, Hungary, November 28-29, 2019, p. 9., ISBN 978-963-9483- 95-8
20. Seres, I., **Atsu, D.,** Farkas, I. (2019): Voltage-time function measurements of inverters, Book of 73 Abstracts, 25th Workshop on Energy and Environment, Gödöllő, Hungary, November 28-29, 2019, p. 13., ISBN 978-963-9483-95-8.
21. **Atsu, D.,** Seres, I., Farkas, I. (2020): Performance assessment of long-term grid connected Si-Poly and Si-Amorphous photovoltaic systems, Book of abstracts, BioPhys Spring 2020, Prague, Czech Republic, May 19-21, 2020, p. 34., ISBN 978-83-89969-64-4.
22. **Atsu, D.,** Seres, I., Farkas, I. (2019): Degradation and performance evaluation of PV modules in the tropical climate. VI Synergy International Conference, Gödöllő, Hungary, November 4-6, 2019.
23. **Atsu, D.,** Seres, I., Farkas, I. (2020): Power quality assessment of microinverters for grid-connected PV systems in low voltage networks, Book of Abstracts, 26th Workshop on Energy and Environment, Gödöllő, Hungary, 10-11 December 2020, p. 8, ISBN 978-963-269-928-8.

A3: Details of harmonic current against harmonic voltage for different systems

Rooftop PV system on a day of high and non-fluctuating solar radiation (22/8/20- All data)					
System 1					
	3rd Harmonic	**5th Harmonic**	**7th Harmonic**	**9th Harmonic**	**11th Harmonic**
Intercept	0.01482± 3.92304E-4	0.05348 ± 4.34328E-4	-0.00342 ± 4.84639E-4	0.02456 ± 2.82979E-4	0.00805± 5.51199E-5
Slope	0.13255 ± 0.00104	0.00115 ± 1.54581E-4	0.01359± 2.2032E-4	-0.00759 ± 5.43539E-4	4.2142E-4 ± 1.8327E-4
R square	0.47334	0.00302	0.17433	0.01064	2.37764E-4
System 2					
	3rd Harmonic	**5th Harmonic**	**7th Harmonic**	**9th Harmonic**	**11th Harmonic**
Intercept	-0.07089 ± 0.0019	0.04523 ± 4.16644E-4	0.00465± 5.99698E-4	0.01635 ± 3.66237E-4	0.01669 ± 2.00613E-4
Slope	0.11117 ± 0.00162	0.0058 ± 1.8942E-4	0.0078 ± 2.73711E-4	0.0177 ± 5.72689E-4	-0.01267 ± 6.31854E-4
R square	0.20669	0.01003	0.04305	0.05034	0.02176
System 3					
	3rd Harmonic	**5th Harmonic**	**7th Harmonic**	**9th Harmonic**	**11th Harmonic**
Intercept	0.17692 ± 0.0011	0.04326 ± 3.60726E-4	-0.00881 ± 5.00728E-4	-3.28807E-4 ± 3.81429E-4	0.00953 ± 5.10729E-5
Slope	-0.1307 ± 0.00127	0.00567 ± 1.51701E-4	0.01655 ± 2.34868E-4	0.02744 ± 4.9925E-4	-0.00518 ± 1.8718E-4
R square	0.37109	0.0719	0.21601	0.14351	0.04075

A4: Harmonic current against harmonic voltage for rooftop systems
Using 3000 values

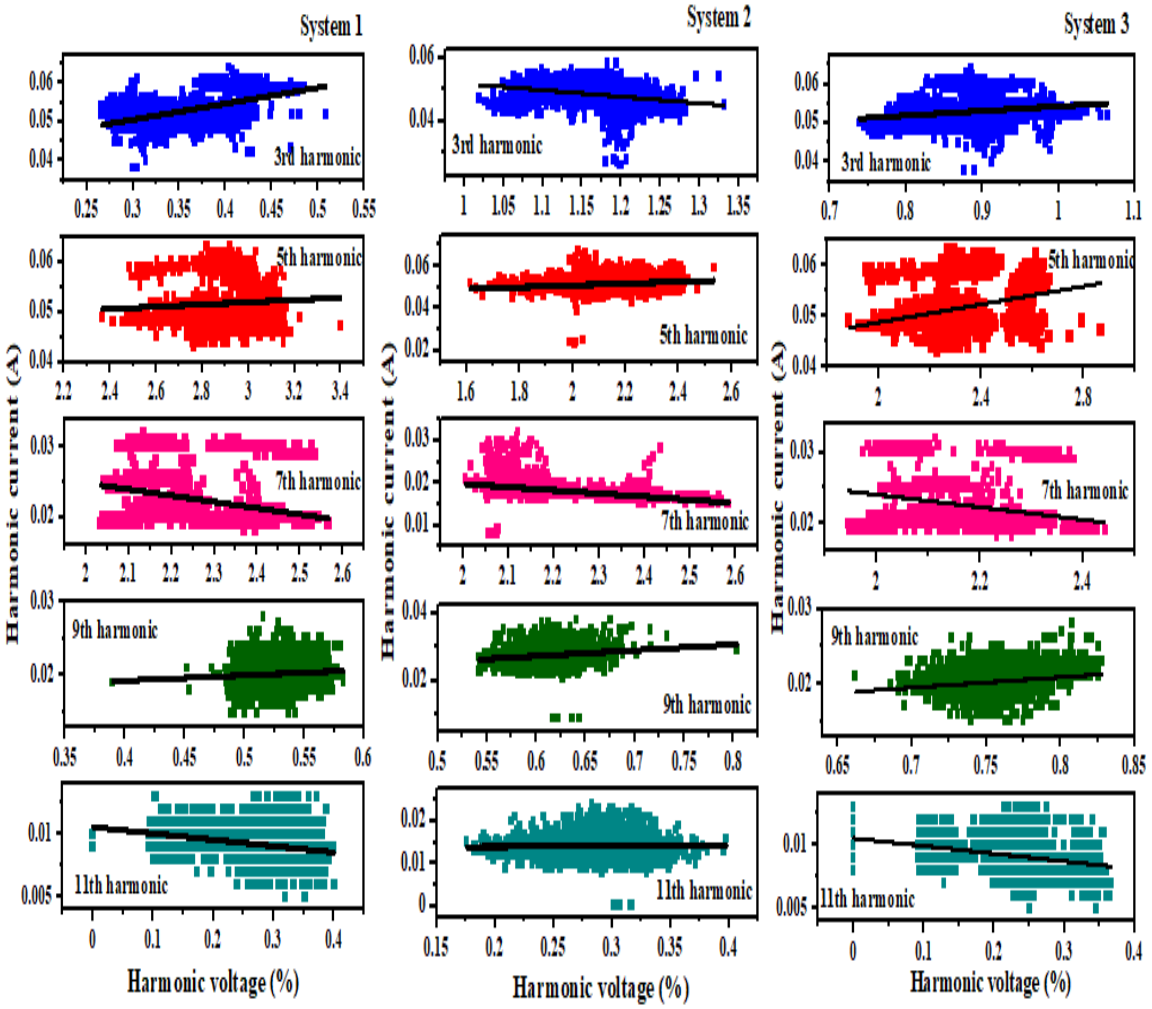

A5: Details of harmonic current against harmonic voltage using 3000 values

Rooftop system 3000 data points (22/8/20)					
System 1					
	3rd Harmonic	**5th Harmonic**	**7th Harmonic**	**9th Harmonic**	**11th Harmonic**
Intercept	0.03816 ± 4.69956E-4	0.04529 ± 0.00215	0.04283 ± 0.00151	0.0164 ± 8.13997E-4	0.01059 ± 8.00705E-5
Slope	0.04139 ± 0.00129	0.00222 ± 7.41894E-4	-0.009 ± 6.80336E-4	0.00729 ± 0.00153	-0.00504 ± 2.87165E-4
R square	0.25458	0.00265	0.05484	0.00715	0.09276
System 2					
	3rd Harmonic	**5th Harmonic**	**7th Harmonic**	**9th Harmonic**	**11th Harmonic**
Intercept	0.07238 ± 0.00121	0.04229 ± 8.48584E-4	0.03499 ± 6.68164E-4	0.01707 ± 0.00105	0.01397 ± 3.31654E-4
Slope	-0.02058 ± 0.00104	0.00437 ± 3.90859E-4	-0.00756 ± 3.05341E-4	0.01716 ± 0.0017	0.01665 ± 8.91918E-4
R square	0.1155	0.03972	0.16947	0.03263	0.25823
System 3					
	3rd Harmonic	**5th Harmonic**	**7th Harmonic**	**9th Harmonic**	**11th Harmonic**
Intercept	0.04251 ± 0.00108	0.03098 ± 0.0014	0.04182 ± 0.00157	0.0097 ± 9.94898E-4	0.01052 ± 6.22162E-5
Slope	0.01183 ± 0.0012	0.00886 ± 5.98976E-4	-0.00888 ± 7.38659E-4	0.01401 ± 0.00132	4.69172E-4 ± 0.00117
R square	0.03091	0.06774	0.04567	0.03596	0.13773

A6: Harmonic current against harmonic voltage for rooftop systems Using 1000 values

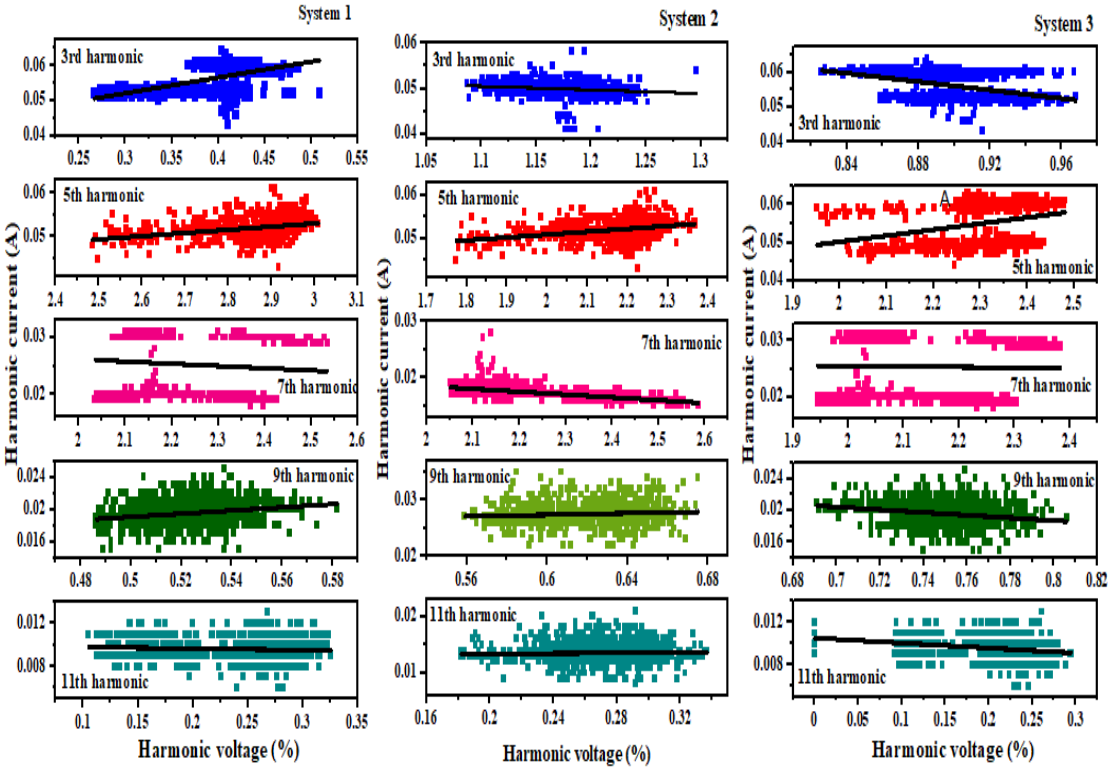

A7: Details of harmonic current against harmonic voltage using 1000 values

Rooftop system 1000 data points (22/8/20)					
System 1					
	3rd Harmonic	**5th Harmonic**	**7th Harmonic**	**9th Harmonic**	**11th Harmonic**
Intercept	0.03862± 7.72039E-4	0.03148 ± 0.00188	0.03409 ± 0.00343	0.0093 ± 0.00144	0.00995 ± 1.52137E-4
Slope	0.0449 ± 0.00195	0.0072 ± 6.57455E-4	-0.00395 ± 0.00156	0.01962 ± 0.00275	-0.00139 ± 6.07325E-4
R square	0.34592	0.10619	0.00537	0.04766	0.00424
System 2					
	3rd Harmonic	**5th Harmonic**	**7th Harmonic**	**9th Harmonic**	**11th Harmonic**
Intercept	0.05924± 0.00154	0.03765 ± 0.00135	0.02861± 5.91603E-4	0.02303 ± 0.00153	0.01314 ± 5.43024E-4
Slope	-0.00794 ± 0.00132	0.00665 ± 6.2047E-4	-0.00505 ± 2.68297E-4	0.00728 ± 0.00247	0.00154 ± 0.00201
R square	0.03413	0.10234	0.26088	0.00761	-4.13203E-4
System 3					
	3rd Harmonic	**5th Harmonic**	**7th Harmonic**	**9th Harmonic**	**11th Harmonic**
Intercept	0.1108± 0.00358	0.01841± 0.00393	0.02757± 0.00363	0.03245± 0.00177	0.01055± 1.09219E-4
Slope	-0.06068 ± 0.00398	0.01589± 0.00171	-0.00103 ± 0.00174	-0.01715± 0.00235	-0.00473 ± 5.2963E-4
R square	0.18761	0.07902	-6.52769E-4	0.04961	0.07305

A8: Harmonic current against system harmonic voltage for Aula grid system

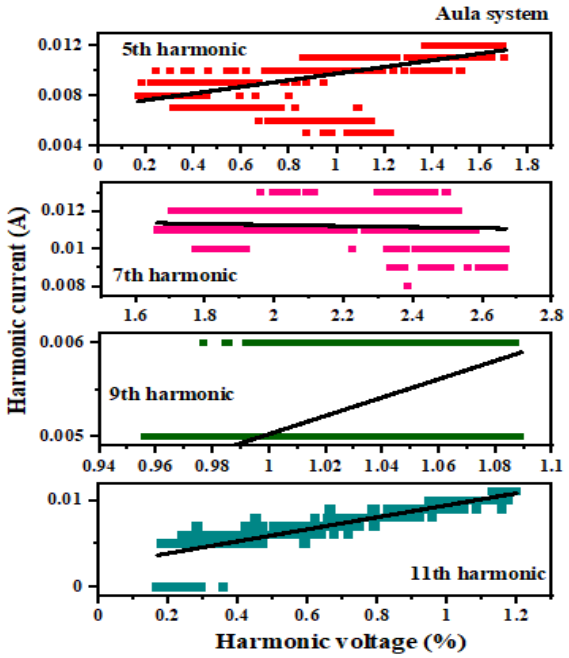

(07/11/20)

A9: Details of harmonic current against harmonic voltage for Aula grid system

Aula system with 3000 data points (07/11/20)				
	5th Harmonic	**7th Harmonic**	**9th Harmonic**	**11th harmonic**
Intercept	0.00713 ± 5.4414E-5	0.01188 ± 1.10859E-4	-0.00475 ± 2.94032E-4	0.00253± 4.19566E-5
Slope	0.00266 ± 4.09635E-5	-2.94054E-4 ± 5.43273E-5	0.00977 ± 2.85689E-4	0.00696 ± 9.65383E-5
R square	0.58494	0.00934	0.28051	0.63424

A10: Harmonic current against harmonic voltage by PV simulator

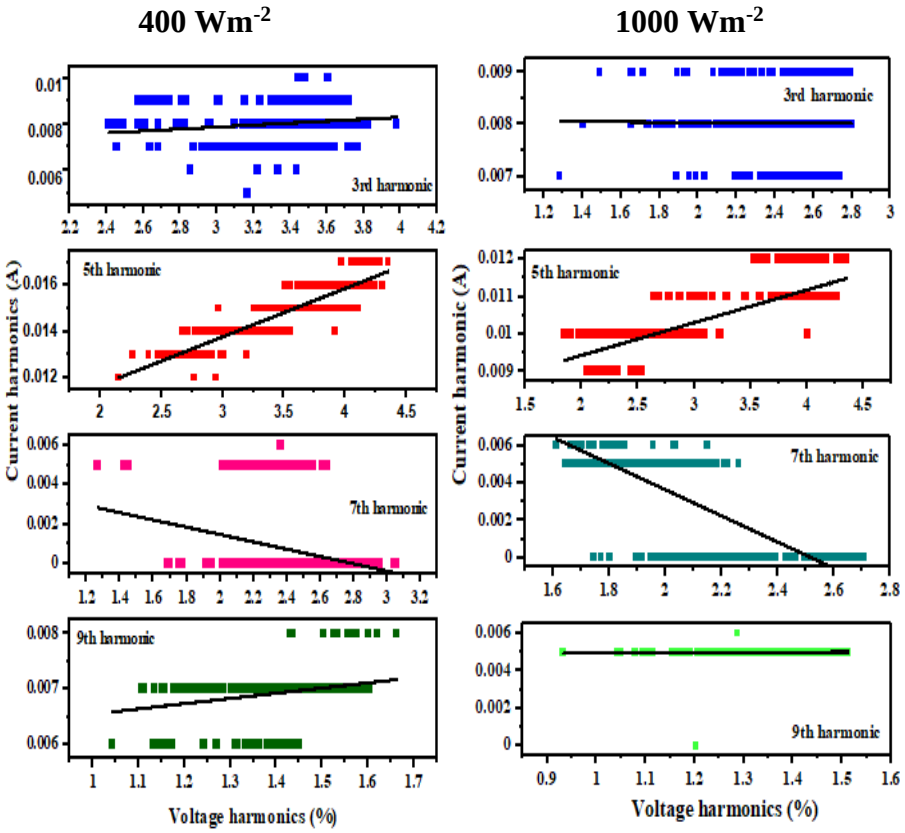

A11: Results of harmonic current against harmonic voltage by PV simulator

GUNT system 1000W				
	3rd Harmonic	**5th Harmonic**	**7th Harmonic**	**9th Harmonic**
Intercept	0.00658± 3.28917E-4	0.00749± 1.08022E-4	0.00519± 6.12445E-4	0.00561± 1.13969E-4
Slope	4.31119E-4± 9.52995E-5	0.0021± 2.83648E-5	-0.00185 ± 2.62827E-4	9.3829E-4± 7.76195E-5
R square	0.01913	0.84545	0.04636	0.12696
GUNT system 400W				
	3rd Harmonic	**5th Harmonic**	**7th Harmonic**	**9th Harmonic**
Intercept	0.00809 ± 1.46596E-4	0.00768± 7.19667E-5	0.01766± 3.83624E-4	0.00483 ± 9.1995E-5
Slope	-2.61399E-5 ± 5.81636E-5	8.73238E-4 ± 1.95825E-5	-0.00701 ± 1.9354E-4	1.23674E-4 ± 6.76696E-5
R square	-8.00261E-4	0.66572	0.56771	0.00234

A12: Harmonic current against harmonic voltage generated by HWJ and HWS

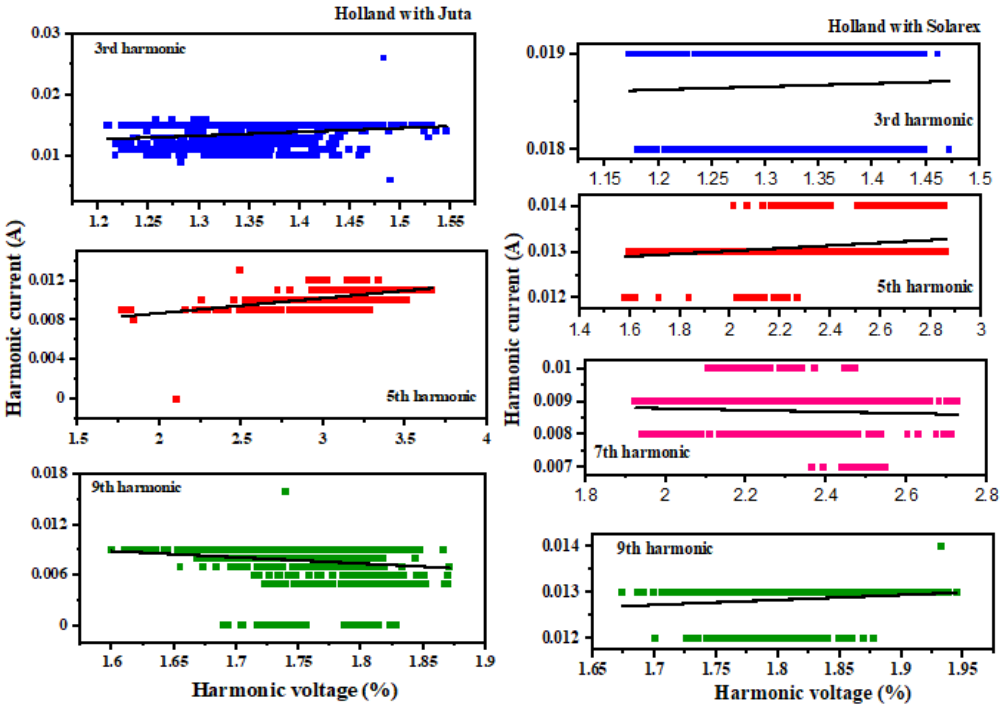

A13: Details of harmonic current against harmonic voltage by HWJ and HWS

Holland with Juta				
	3rd Harmonic	**5th Harmonic**	**7th Harmonic**	**9th Harmonic**
Intercept	0.00526 ± 0.00128	0.00568 ± 3.02408E-4		0.02078 ± 0.00263
Slope	0.00621 ± 9.53041E-4	0.00152 ± 9.60799E-5		-0.00741 ± 0.00149
R square	0.03982	0.1986		0.02311
Holland with Solarex				
	3rd Harmonic	**5th Harmonic**	**7th Harmonic**	**9th Harmonic**
Intercept	0.01824 ± 3.36811E-4	0.01243 ± 1.08961E-4	0.0093 ± 1.97853E-4	0.0109 ± 4.47283E-4
Slope	3.24813E-4 ± 2.53152E-4	2.9881E-4 ± 4.45595E-5	-2.50181E-4 ± 8.81296E-5	0.00108 ± 2.47154E-4
R square	6.45868E-4	0.04212	0.00701	0.01771

A14: Harmonic current against harmonic voltage by CWJ and CWS

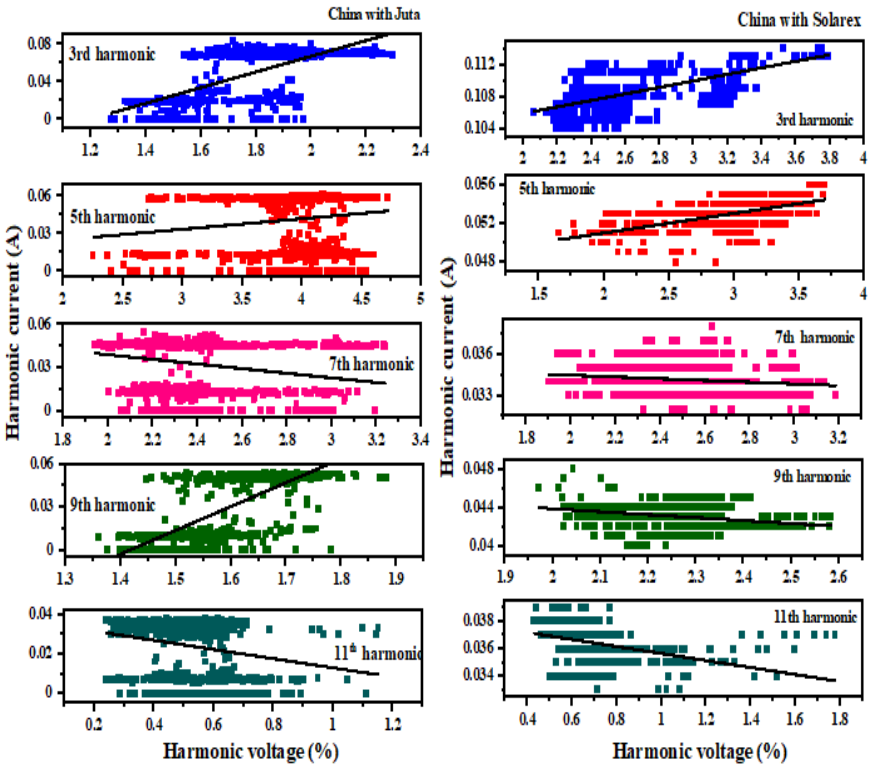

A15: Details of harmonic current against harmonic voltage by CWJ and CWS

China with Juta					
	3rd Harmonic	**5th Harmonic**	**7th Harmonic**	**9th Harmonic**	**11th Harmonic**
Intercept	-0.10006 ± 0.00514	0.00829 ± 0.00729	0.07142 ± 0.00474	-0.23352 ± 0.00727	0.03633 ± 0.00191
Slope	0.08378 ± 0.00284	0.00847 ± 0.00185	-0.01612 ± 0.002	0.1651 ± 0.00445	-0.02326 ± 0.00339
R square	0.46578	0.0195	0.06029	0.57898	0.04403
China with Solarex					
	3rd Harmonic	**5th Harmonic**	**7th Harmonic**	**9th Harmonic**	**11th Harmonic**
Intercept	0.09783 ± 4.58766E-4	0.04696 ± 2.86682E-4	0.03577 ± 3.1399E-4	0.05005 ± 7.59325E-4	0.03824± 1.40521E-4
Slope	0.00406 ± 1.74402E-4	0.00204 ± 9.46418E-5	-6.38072E-4 ± 1.27711E-4	-0.00307 ± 3.35859E-4	-0.00256± 1.9209E-4
R square	0.35137	0.31672	0.0234	0.0762	0.14983

A16: Voltage THD of the three systems under high intermittent solar radiation

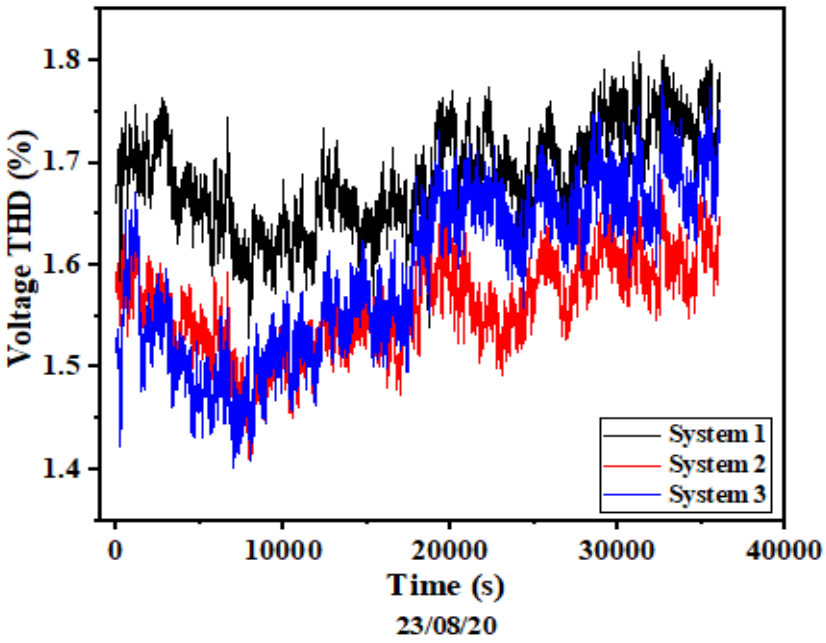

9. ACKNOWLEDGEMENT

This work was supported financially by the Stipendium Hungaricum Scholarship Program and the Mechanical Engineering Doctoral School at the Szent István University, Gödöllő, Hungary.

Foremost, I would like to say a big thank you to God almighty for His provisions, favour and guidance throughout the study period.

I would like to express my most profound appreciation to my supervisors Prof. Istvan Farkas and Dr Istvan Seres. They were like fathers to me during my stay in Hungary. Sirs, I am highly indebted to you, and words can not express how much I appreciate your support, guidance, and valuable pieces of advice throughout the four years stay at Szent Istvan University. I was indeed privileged to have been your supervisee. God bless you.

I am also thankful to Mr James Datsa, my brother in law and Mrs Lisa Kotoka Atsu, my wife, for their sacrifices. You had to endure so much to enable me attain this feat. Your support will never be forgotten. My most profound gratitude also goes to my family and friends.

Finally, I would like to thank the staff of the Doctoral School of Mechanical Engineering, Szent István University, for their diverse support; you are awesome people.

Gödöllő, March 2021

Divine Atsu